

REMOVAL OF ACID YELLOW-36 & DIRECT BLUE-86 USING PEANUT SHELL ACTIVATED CARBON FROM WASTEWATER

A THESIS

*Submitted in partial fulfilment of the
requirements for the award of the degree*

of

DOCTOR OF PHILOSOPHY

in

CHEMICAL ENGINEERING

by

DEEPAK GARG



**DEPARTMENT OF CHEMICAL ENGINEERING
INDIAN INSTITUTE OF TECHNOLOGY ROORKEE
ROORKEE-247 667 (INDIA)
FEBRUARY, 2020**

**©INDIAN INSTITUTE OF TECHNOLOGY ROORKEE, ROORKEE-2020
ALL RIGHTS RESERVED**





INDIAN INSTITUTE OF TECHNOLOGY ROORKEE

CANDIDATE'S DECLARATION

I hereby certify that the work presented in the thesis entitled "**REMOVAL OF ACID YELLOW-36 & DIRECT BLUE-86 USING PEANUT SHELL ACTIVATED CARBON FROM WASTEWATER**" is my own work carried out during a period from July, 2013 to September, 2019 under the supervisions of Dr. C.B. Majumder, Professor, and Late Dr. (Mrs.) Shashi, Professor, Department of Chemical Engineering, Indian Institute of Technology Roorkee, Roorkee, India.

The matter presented in the thesis has not been submitted for the award of any other degree of this or any other Institute.

Dated 14-02-2020

(DEEPAK GARG)

SUPERVISOR'S DECLARATION

This is to certify that the above mentioned work is carried out under our supervisions.

Dated 14-02-2020

(C.B. MAJUMDER)
Supervisor

The Ph.D Viva Voce Examination of Mr. Deepak Garg, Research Scholar, has been held on 14th February, 2020.

Chairman, SRC

Signature of External Examiner

This is to certify that the student has made all the corrections in the thesis.

Signature of Supervisor

Head of the Department

ABSTRACT

Water is an important component for existence of all living beings. Since the beginning of civilization, mankind flourished around the sources of water. With the skyrocketing growth in population, climatic changes and industrialization, availability of fresh water on earth is declining continuously, on the other hand demand is enlarging. After industrialization our water sources such as oceans, rivers started squeezing in quality, due to anthropogenic activities which have led to degradation of environment. Survival of living beings is threatened and earth's support system is endangered due to Pollution. Worldwide leading cause of diseases and deaths is due to water pollution.

Water is contaminated by numerous inorganic and organic substances such as industrial wastes, fertilizers, toxic chemicals, metals, dyes and its byproducts. Dyes are organic compounds used as colouring material in various industries mainly textiles. Dyes transmit colour to water and a small fraction is easily recognizable, which is aesthetically unacceptable. Due to complex structure, dyes are difficult to degrade. Abundant production of dyes have undesirable environmental effects. Despite the adverse effects caused by dyes to the environment, they are continuously being discharged in water bodies thus disturbing the water cycle. The condition can further intensify without strict remedial action. Thus, prioritizing wastewater treatment is essential to avert crippling water problems. Today world is becoming more eco sensitive which has given new impetus to waste water treatment. Researchers are in constant search of technically feasible and economically viable methods for removing dyes and its toxic effects from the environment. There are different methods that are used for the removal of dyes from wastewater amongst them adsorption has been found to be more advantageous and effective method. Adsorption is easy, reliable and versatile method for the removal of dyes. Over the past few years, trend of using ecofriendly, low cost adsorbent has increased.

Focus of this study is on the adsorptive removal of two anionic dyes: Acid Yellow-36 (AY-36) and Direct Blue-86 (DB-86) from aqueous solution using low cost activated carbon as adsorbent. So for present study, an agricultural waste, peanut shell was used as raw material for manufacturing peanut shell activated carbon (PnsAC) using H_3PO_4 as chemical activator. The pyrolysis is carried out under nitrogen environment at a ramp of $10\text{ }^\circ\text{C min}^{-1}$ upto a temperature of $650\text{ }^\circ\text{C}$ for 2 hr activation time.

To test the efficacy of PnsAC different characterization studies were performed. Thermal stability was analyzed using TGA technique. Surface morphology was studied by SEM images and elemental analysis was carried out using energy-dispersive X-ray spectroscopy (EDS). Variation in surface functional groups were interpreted by Fourier Transform Infrared spectroscopy (FTIR). Zero point charge for PnsAC was 2.3.

Investigations were done for studying the adsorption potential of PnsAC for the removal of anionic dye AY-36. Batch experiments were conducted to study the effects of pH (2 – 11), adsorbent dose (2 – 6 g L⁻¹), and initial AY-36 concentration (100 – 250 mg L⁻¹). The optimized condition obtained by varying the variables were obtained at temperature 35 °C, initial dye concentration 200 mg L⁻¹, pH 2, PnsAC dose 4 g L⁻¹ and equilibrium time 150 minutes. 98 % removal of AY-36 was achieved at optimized conditions. Equilibrium adsorption isotherms, kinetics, and thermodynamics were investigated. The experimental data were analyzed using different isotherm models: Langmuir, Freundlich, Redlich–Peterson, Sip, and Toth. The kinetics of adsorptive removal of dyes was studied with Pseudo first order, Pseudo second order and intra-particle diffusion model. Equilibrium study revealed that Freundlich isotherm model described best the experimental data. The kinetics of dye adsorption was found to confirm Pseudo second order kinetics with a correlation coefficient value of 0.999. Kinetic study results indicated that the chemisorption likely dominated the adsorption of AY-36 on peanut shell activated carbon (PnsAC). Thermodynamic study revealed that the adsorption process was feasible, endothermic and spontaneous.

Another dye DB-86 was adsorbed using PnsAC. Adsorbent dose of PnsAC was investigated through batch experiments at various initial pH and DB-86 concentration, to obtain maximum adsorption. This study showed that 78.6 % removal was obtained for 10 g L⁻¹ PnsAC dose in 150 minutes (equilibrium time) at pH 2, while temperature was maintained at 35 °C. Kinetic, equilibrium, and thermodynamic studies were carried out to validate the results from experiments. Kinetic study confirms that the adsorption phenomena follow the Pseudo second order rate equation. Isotherm study reveals that Freundlich, Redlich–Peterson, Sip, Radke–Prausnitz, Koble-Corrigan, and Fritz–Schlunder isotherm models well explained the experimental equilibrium data. Thermodynamic study showed a negative value of ΔG° which advocated that the process of adsorption was spontaneous. Positive values of ΔH° and ΔS° signified the endothermic and increased disorderness in the adsorption of DB-86, respectively.

Further, for effective adsorption, PnsAC was modified with alginate and used for the removal of DB-86 dye. The alginate encapsulated activated carbon (PnsAC-alginate), prepared from waste

peanut shell was used as an adsorbent. Alginate encapsulation was done by pouring homogenous mixture of sodium alginate and PnsAC into the bath of 1 % calcium chloride solution. The effects of temperature, equilibrium time, adsorbent dose, dye concentration and solution pH on the adsorption of DB-86 onto PnsAC-alginate were studied. To the best of our knowledge, no attempt have so far been made for optimization purpose using response surface methodology (RSM) in the adsorptive removal of DB-86. Central composite design coupled with RSM was used to optimize the adsorption feed conditions in order to achieve maximum dye removal efficiency. The statistical analysis revealed that for maximum dye removal efficiency, the optimal conditions were adsorbent dose of 24.65 g L^{-1} , DB-86 dye concentration of 125.5 mg L^{-1} and pH of 3.1. Under optimized conditions, experimental dye removal efficiency ($98.4 \pm 0.1\%$) agreed closely with the predicted results, thus indicating the suitability of RSM in optimizing the feed conditions. SEM, EDS, TEM, XRD, BET and FTIR analyses showed the surface morphology of the adsorbents and confirmed the adsorption of DB-86 onto PnsAC-alginate. Crystalline behavior of PnsAC-alginate were analyzed using X-Ray diffraction (XRD). Zero point charge for PnsAC-alginate was 7.8. The experimental results also showed that the dye removal efficiency was increased by 7 % compared to that with peanut shell activated carbon (PnsAC) as an adsorbent. The adsorption kinetics of DB-86 was well described by Pseudo second order kinetic model with intra-particle and film diffusion mechanisms. Langmuir isotherm model provided the best fit to the adsorption equilibrium data, obtaining maximum dye adsorption capacity of $21.6 \pm 0.9 \text{ mg g}^{-1}$. Estimation of thermodynamic parameters revealed that the adsorption process was feasible and was spontaneous and endothermic in nature. The present study has demonstrated that the use of positively charged PnsAC-alginate as an adsorbent is a cost effective and suitable alternative for the removal of anionic DB-86 dye from aqueous solutions.

From above study we can conclude that, low cost adsorbents PnsAC and PnsAC-alginate can be commercially converted into efficient adsorbents for the removal of AY-36 and DB-86 dyes from aqueous solutions by adsorption.

ACKNOWLEDGEMENT

It is a matter of pleasure for me to express my heartiest gratitude to my research supervisors **Dr. C. B. Majumder**, Professor and **Late Dr. (Mrs.) Shashi**, Professor, Department of Chemical Engineering, Indian Institute of Technology Roorkee, for their precious guidance, interest, stimulating suggestions and supervision at every level of this thesis. I am obliged forever for their kind inspiration, encouragement, useful criticism and constant support without which it was not possible to complete this work. I have gained enormous knowledge from them during my research work that would be immensely useful to me for all my future endeavors.

I owe a deep sense of gratitude to **Dr. Surendra Kumar**, Professor, Department of Chemical Engineering, Indian Institute of Technology Roorkee, for his continuous support, guidance and his keen interest on me at every stage of my research work. His prompt inspirations, timely suggestions with kindness, enthusiasm and dynamism have enabled me to complete my research work.

My sincere thanks are also due to student research committee (SRC) member Dr. Amit Dhiman, Associate Professor, Department of Chemical Engineering, Dr. Bijan Choudhury, Professor, Department of Biotechnology, Indian Institute of Technology Roorkee, for their time and invaluable input to my research.

My humble thanks to Head of the Department, all the technical and ministerial staff of the Department of Chemical Engineering for their assistance. I am sincerely grateful to Mr. Manga Ram, for his constant support.

I would like to express my gratitude to my lab mates and special thanks to my dear friends A.K.Jain, Dinesh Kumar and my Colleagues whose love and support had made me overcome the lows and highs of research tenure.

I thank profusely to Dr. Biswajit Sarkar, G.G.S.I.P.University, New Delhi, and Dr. Komal Sharma, for their invaluable help and support.

I would like to extend my deepest sincerest gratitude to all the people who helped there in any manner, who have shared the effort and knowledge in order to make this research a reality.

I am also thankful to the Head and Technical staffs of the Institute Instrumentation Centre for their help in the analysis of the samples.

I am profoundly thankful to All India Council of Technical Education, Government of India for providing financial assistance.

I would deeply appreciate my parents, parents in laws, brother and sister for their generous support, motivation and trust in me, without which it was not possible for me to complete my research work.

Last but not the least I would like to make a very special mention of my kids and my wife Preeti, who were the strongest force which encouraged me to complete my research work.

Above all, I thank 'Almighty God' for encouraging me in every possible way to reach this far.



LIST OF RESEARCH PUBLICATIONS

A. PAPERS IN REFEREED JOURNALS

PUBLISHED

- i. "Application of Waste Peanut Shells to form activated Carbon and its utilization for the removal of Acid Yellow 36 from Wastewater". Groundwater for Sustainable Development, **8** (2019) 512-519. <https://doi.org/10.1016/j.gsd.2019.01.010>
- ii. "Removal of Direct Blue-86 dye from aqueous solution using alginate encapsulated activated carbon (PnsAC-alginate) prepared from waste peanut shell". Journal of Environmental Chemical Engineering, **7** (2019). 103365, <https://doi.org/10.1016/j.jece.2019.103365>

COMMUNICATED

- iii. A paper entitled "Removal of Direct Blue-86 from waste water using Peanut shell Activated Carbon: Equilibrium, kinetic and Thermodynamic studies", Journal of Water Science and Engineering (Under review).

B. PAPER PRESENTED IN CONFERENCE

- i. "Adsorption of Acid Yellow-36 from Aqueous Solution Using Activated Carbon", Poster Presentation, CHEMCON 2016, Chennai, India, December 27-30 (2016).
- ii. "Comparative study for the removal of Acid Yellow-36 and Direct Blue-86 from aqueous solution by using peanut shell based Activated Carbon", MNIT, Jaipur, India, October 3-4 (2019).

TABLE OF CONTENTS

	Title	Page
	CANDIDATE'S DECLARATION	i
	ABSTRACT	ii
	ACKNOWLEDGEMENT	v
	LIST OF RESEARCH PUBLICATIONS	vii
	TABLE OF CONTENTS	viii
	LIST OF TABLES	xiii
	LIST OF FIGURES	xv
	NOMENCLATURE	xx
	ABBREVIATIONS	xxii
	CHAPTER-I : INTRODUCTION	01
1.0	PRELUDE	01
1.1	STATISTICS OF DYE PRODUCTION AND DISCHARGE	02
1.2	HARMFUL EFFECTS OF DYES	05
1.2.1	Acid Yellow-36 (AY-36)	06
1.2.2	Direct Blue-86 (DB-86)	07
1.3	TECHNIQUES AVAILABLE FOR WASTEWATER TREATMENT	07
1.3.1	Biological Methods	09
1.3.2	Chemical Methods	10
1.3.3	Physical Methods	11
1.4	RESEARCH OBJECTIVES	13
1.5	STRUCTURE OF THE THESIS	13

	Title	Page
	CHAPTER-II : LITERATURE REVIEW	16
2.0	DYES	16
2.1	CLASSIFICATION OF DYES	16
2.1.1	Classification on the basis of raw material	18
2.1.1.1	Natural Dyes	18
2.1.1.2	Synthetic Dyes	18
2.1.2	Classification on the basis of Chemical Structure	18
2.1.3	Classification on the basis of Nuclear Structure	19
2.1.3.1	Cationic Dyes	19
2.1.3.2	Anionic Dyes	19
2.1.4	Classification on the basis of Application of Dyes	19
2.2	ADSORPTION	21
2.3	FACTORS CONTROLLING ADSORPTION	22
2.3.1	pH of solution	22
2.3.2	Nature of adsorbent	22
2.3.3	Temperature	23
2.3.4	Contact Time	23
2.3.5	Initial Dye Concentration	23
2.3.6	Effect of adsorbent concentration	24
2.4	TYPES OF ADSORBENTS AND THEIR SELECTION	24
2.5	ACTIVATED CARBON	26
2.5.1	Peanut Shell Activated Carbon	28
2.6	ALGINATE	29
2.7	ADSORPTION STUDIES USING PEANUT SHELL ACTIVATED CARBON	31
2.8	ACID YELLOW-36 (AY-36) ADSORPTION STUDIES	34
2.9	DIRECT BLUE-86 (DB-86) ADSORPTION STUDIES	35
2.10	MOTIVATION FOR THE PROPOSED RESEARCH WORK	35

	Title	Page
	CHAPTER-III : MATERIALS AND METHODS	80
3.0	INTRODUCTION	80
3.1	EXPERIMENTAL STUDIES	80
3.1.1	Materials	80
3.1.1.1	Dyes	80
3.1.1.2	Raw Material For Adsorbent	83
3.1.1.3	Chemicals	84
3.1.1.4	Instruments	84
3.1.2	Methods	88
3.1.2.1	Adsorbent Preparation	88
3.1.2.1.1	PnsAC Preparation	88
3.1.2.1.2	Alginate Coated Activated Carbon (PnsAC- alginate) Preparation	88
3.1.2.2	Adsorbate Preparation	90
3.1.2.3	Characterization of PnsAC	90
3.1.2.4	Batch Adsorption Studies	91
3.2.	KINETICS AND ADSORPTION ISOTHERM MODELS	92
3.2.1	Adsorption Kinetic Models	92
3.2.2	Adsorption Isotherm Models	94
3.2.3	Optimization of feed conditions for adsorption of DB-86	97
3.2.4	Thermodynamic Study	98
3.2.5	Error Analysis	98
	CHAPTER-IV : ADSORPTION OF ACID YELLOW-36 DYE USING PEANUT SHELL ACTIVATED CARBON	99
4.0	INTRODUCTION	99
4.1	REMOVAL OF AY-36 FROM AQUEOUS SOLUTION USING PnsAC	99
4.1.1	Characterization of PnsAC	99
4.1.2	Adsorption Studies	106
4.1.2.1	Effect of Initial pH	106

	Title	Page
	4.1.2.2 Effect of Adsorbent dose	108
	4.1.2.3 Effect of Contact Time and Initial Concentration	109
4.1.3	Adsorption Equilibrium Isotherms	109
4.1.4	Adsorption Kinetics	112
4.1.5	Adsorption Thermodynamics	115
 CHAPTER-V : ADSORPTION OF DIRECT BLUE-86 DYE USING PEANUT SHELL ACTIVATED CARBON		 117
5.0	INTRODUCTION	117
5.1	REMOVAL OF DB-86 FROM AQUEOUS SOLUTION USING PnsAC	117
5.1.1	Characterization of PnsAC	117
5.1.2	Effect of Initial pH	123
5.1.3	Effect of Adsorbent dose	124
5.1.4	Effect of Initial DB-86 Concentration	125
5.1.5	Adsorption Equilibrium Isotherms	126
5.1.6	Adsorption Kinetics	129
5.1.7	Thermodynamic Study	131
 CHAPTER-VI : ADSORPTION OF DIRECT BLUE-86 DYE USING ALGINATE COATED PEANUT SHELL ACTIVATED CARBON		 133
6.0	INTRODUCTION	133
6.1	REMOVAL OF DB-86 FROM AQUEOUS SOLUTION USING PnsAC-ALGINATE	133
6.1.1	Characterization of PnsAC-alginate Adsorbent	133
6.1.2	Response Surface Methodology	142
6.1.2.1	Effect of Independent Variables on DB-86 Dye Removal Efficiency	145
6.1.2.2	Optimization of Feed Conditions and Validation of the Model	147

	Title	Page
6.1.3	Kinetic Studies	147
6.1.3.1	Effect of Adsorbent dose on Adsorption	148
6.1.3.2	Effect of Temperature on Adsorption	148
6.1.3.3	Effect of Solution pH on Adsorption	151
6.1.3.4	Modelling of Adsorption Kinetics	151
6.1.4	Isotherm Studies	158
6.1.5	Activation Energy and Thermodynamic Study	164
 CHAPTER-VII : CONCLUSIONS AND RECOMMENDATIONS		 167
7.0	INTRODUCTION	167
7.1	SUMMARY OF PRESENT WORK	167
7.1.1	REMOVAL OF AY-36 FROM AQUEOUS SOLUTION USING PnsAC	167
7.1.2	REMOVAL OF DB-86 FROM AQUEOUS SOLUTION USING PnsAC	168
7.1.3	REMOVAL OF DB-86 FROM AQUEOUS SOLUTION USING PnsAC-ALGINATE	170
7.2	CONCLUSIONS	171
7.3	RECOMMENDATIONS FOR FUTURE WORK	172
 REFERENCES		 173

LIST OF TABLES

Table	Title	Page
CHAPTER-I : INTRODUCTION		
1.1	An account of fixation and dye loss to effluent	03
1.2	Discharge limits of various countries	04
1.3	Techniques for dye removal from wastewater	08
CHAPTER-II : LITERATURE REVIEW		
2.1	Classification of Dyes on the basis of application	19
2.2	Comparative table of Physisorption and Chemisorption	21
2.3	Recent reported surface area S_{BET} ($m^2 g^{-1}$) for peanut shell activated carbon	29
2.4	Comparison of Adsorption Isotherms, Kinetic models and Adsorption capacities of PnsAC	37
2.5	Adsorption studies for removing AY-36 dye from wastewater	38
2.6	Adsorption studies for removing dyes from wastewater	39
2.7	Adsorption studies on the removal of dyes from wastewater using alginate and alginate composite as adsorbent	61
CHAPTER-III : MATERIALS AND METHODS		
3.1	Properties of dyes	80
3.2	Scientific Classification of peanut	83
CHAPTER-IV : ADSORPTION OF ACID YELLOW-36 DYE USING PEANUT SHELL ACTIVATED CARBON		
4.1	Adsorption equilibrium isotherm parameters of AY-36 on PnsAC	110
4.2	Comparison of monolayer adsorption capacities of AY-36 dye on various adsorbents	112
4.3	Kinetic parameters for AY-36 adsorption onto PnsAC	113

Table	Title	Page
4.4	Comparison of the Pseudo second order rate constant with various adsorbate on peanut shell based activated carbon adsorbents	114
4.5	Thermodynamic parameters for adsorption of AY-36 on PnsAC	115

CHAPTER-V : ADSORPTION OF DIRECT BLUE-86 USING PEANUT SHELL ACTIVATED CARBON

5.1	Adsorption equilibrium isotherm parameters of Direct Blue-86 on PnsAC (Temp: 35 °C; PnsAC: 10 g L ⁻¹ ; pH:2)	127
5.2	Kinetic parameters for DB-86 adsorption onto PnsAC at different initial dye concentration (Temp:35 °C; PnsAC:10 g L ⁻¹ ; pH:2)	130
5.3	Thermodynamic parameters for adsorption of DB-86 on PnsAC	132

CHAPTER-VI : ADSORPTION OF DIRECT BLUE-86 USING ALGINATE COATED PEANUT SHELL ACTIVATED CARBON

6.1	Central composite experimental design of five-levels and three-variables with their observed and predicted responses	143
6.2	Estimated regression coefficients for the polynomial model and the analysis of variance (ANOVA)	144
6.3	Kinetic data of DB-86 adsorption by PnsAC-alginate	157
6.4	Isotherm parameters for DB-86 adsorption at 35 °C	160
6.5	Adsorption capacity of different adsorbent	161
6.6	Thermodynamic parameters for Adsorption of DB-86 dye	165

LIST OF FIGURES

Figure	Title	Page
CHAPTER-I : INTRODUCTION		
1.1	Effects of dye effluents on the environment	05
1.2	Different wastewater treatment methods	08
1.3	Structure of the thesis	14
CHAPTER-II : LITERATURE REVIEW		
2.1	Classification of Dyes	17
2.2	Adsorbents used for different dyes removal	25
2.3	Structural features of alginates: (a) Monomers of alginate (b) Chain structure (c) Distribution of blocks	30
2.4	Formation of calcium alginate from sodium alginate	31
CHAPTER-III : MATERIALS AND METHODS		
3.1 (a)	Calibration curve for AY-36 dye	82
3.1 (b)	Calibration curve for DB-86 dye	82
3.2 (a)	Peanuts and Peanut Shells	83
3.2 (b)	Sodium alginate	83
3.3 (a)-(d)	Analytical instruments used in the study	85
3.4 (a)-(d)	Auxiliary equipment's used in the study	86
3.4 (e)-(g)	Auxiliary equipment's used in the study	87
3.5	Experimental setup for preparation for PnsAC	89
3.6	Peanut shell Activated Carbon (PnsAC)	89
3.7	Alginate Beads	89
CHAPTER-IV : ADSORPTION OF ACID YELLOW-36 DYE USING PEANUT SHELL ACTIVATED CARBON		

Figure	Title	Page
4.1	Thermogravimetric analysis of Peanut Shell at a heating rate of $10\text{ }^{\circ}\text{C min}^{-1}$	100
4.2 (a)	Micrograph of PnsAC at 2500X, before adsorption	101
4.2 (b)	Micrograph of PnsAC at 10000X, before adsorption	101
4.2 (c)	Micrograph of PnsAC at 2500X, after adsorption of AY-36	102
4.2 (d)	Micrograph of PnsAC at 10000X, after adsorption of AY-36	102
4.3 (a)	EDX spectra of PnsAC before Adsorption	103
4.3 (b)	EDX spectra of PnsAC after adsorption of AY-36	103
4.4 (a)	FTIR image of PnsAC	104
4.4 (b)	FTIR image of Pns used as precursor	105
4.5	The zero point charge of PnsAC	107
4.6	Effect of pH on dye removal using PnsAC at different time intervals (Temp: $35\text{ }^{\circ}\text{C}$; 200 mg L^{-1} ; PnsAC: 4 g L^{-1})	107
4.7	Effect of adsorbent dose on dye removal using PnsAC at different time intervals (Temp: $35\text{ }^{\circ}\text{C}$; C_0 : 200 mg L^{-1} ; pH: 2)	108
4.8	Effect of initial dye concentration on dye removal using PnsAC at different time intervals (Temp: $35\text{ }^{\circ}\text{C}$; PnsAC: 4 g L^{-1} ; pH: 2)	109
4.9	Comparison of experimental and calculated equilibrium adsorption capacity using several isotherm models for the adsorption of AY – 36 on PnsAC (Temp: $35\text{ }^{\circ}\text{C}$; PnsAC: 4 g L^{-1} ; pH: 2; C_0 : 200 mg L^{-1})	111
4.10	Pseudo second order kinetic plot (Temp: $35\text{ }^{\circ}\text{C}$; PnsAC: 4 g L^{-1} ; pH: 2; C_0 : 200 mg L^{-1})	114
4.11	Plot of ΔG° versus temperature for estimation of thermodynamic parameters (Temp: $35\text{ }^{\circ}\text{C}$; PnsAC: 4 g L^{-1} ; pH: 2; C_0 : 200 mg L^{-1})	116

CHAPTER-V : ADSORPTION OF DIRECT BLUE-86 DYE USING PEANUT SHELL ACTIVATED CARBON

5.1 (a)	Micrograph of PnsAC before adsorption at 10KX	118
5.1 (b)	Micrograph of PnsAC before adsorption at 5KX	118
5.1 (c)	Micrograph of PnsAC after adsorption of DB-86 at 10KX	119
5.1 (d)	Micrograph of PnsAC after adsorption of DB-86 at 5KX	119

Figure	Title	Page
5.2 (a)	EDX spectra before adsorption of DB-86	120
5.2 (b)	EDX spectra after adsorption of DB-86	120
5.2 (c)	FTIR of PnsAC before adsorption and after adsorption of DB-86	122
5.3	Effect of pH on dye removal using PnsAC at different time intervals (Temp: 35 °C; C ₀ : 100 mg L ⁻¹ ; PnsAC: 10 g L ⁻¹)	123
5.4	Effect of adsorbent dose on dye removal using PnsAC at different time intervals (Temp: 35 °C; C ₀ : 100 mg L ⁻¹ ; pH: 2)	124
5.5	Effect of initial dye concentration on dye removal using PnsAC at different time intervals (Temp: 35 °C; PnsAC: 10 g L ⁻¹ ; pH: 2)	125
5.6	Comparison of experimental and calculated equilibrium adsorption capacity using several isotherm models for the adsorption of DB-86 on PnsAC (Temp: 35 °C; PnsAC: 10 g L ⁻¹ ; pH: 2)	126
5.7	Pseudo second order kinetic plot (Temp: 35 °C; PnsAC: 10 g L ⁻¹ ; pH: 2; C ₀ : 100 mg L ⁻¹)	129
5.8	Effect of temperature on dye removal using PnsAC at different time intervals (C ₀ : 100 mg L ⁻¹ ; PnsAC: 10 g L ⁻¹ ; pH: 2).	131
5.9	A thermodynamic plot of ln K _d against 1/T for adsorption of DB-86 onto PnsAC (PnsAC: 10 g L ⁻¹ ; pH: 2; C ₀ : 100 mg L ⁻¹)	132

CHAPTER-VI : ADSORPTION OF DIRECT BLUE-86 DYE USING ALGINATE

COATED PEANUT SHELL ACTIVATED CARBON

6.1 (a)	Scanning Electron Micrographs (SEM) image of PnsAC-alginate adsorbent at 10 KX before adsorption	134
6.1 (b)	Scanning Electron Micrographs (SEM) image of PnsAC-alginate adsorbent at 2 KX before adsorption	134
6.1 (c)	Scanning Electron Micrographs (SEM) image of PnsAC-alginate adsorbent at 10 KX after adsorption of DB-86	135
6.1 (d)	Scanning Electron Micrographs (SEM) image of PnsAC-alginate adsorbent at 2 KX after adsorption of DB-86	135
6.1 (e)	EDX spectra before adsorption of DB-86	136
6.1 (f)	EDX spectra after adsorption of DB-86	136
6.2 (a)	N ₂ adsorption-desorption isotherm PnsAC and PnsAC-alginate	138

Figure	Title	Page
6.2 (b)	Pore size distribution (calculated using BJH method) of PnsAC and PnsAC-alginate	138
6.2 (c)	XRD patterns of PnsAC and PnsAC-alginate	139
6.2 (d)	HRTEM micrograph of PnsAC and PnsAC-alginate	139
6.3 (a)	FTIR of PnsAC-alginate before adsorption and after adsorption of DB-86	141
6.3 (b)	Zero point charge of PnsAC and PnsAC-alginate	142
6.4 (a)	Three-dimensional response surface plot for the effect of adsorbent and initial DB-86 dye concentration during adsorption onto PnsAC-alginate	146
6.4 (b)	Three-dimensional response surface plot for the effect of adsorbent and solution pH on DB-86 dye removal efficiency during adsorption onto PnsAC-alginate	146
6.5 (a)	q_t vs t plot for different adsorbent dose at pH 3.5 and 308 K	149
6.5 (b)	q_t vs t plot for different pH at 20 g L ⁻¹ adsorbent dose and 308 K	149
6.5 (c)	q_t vs t plot for different temperature at 20 g L ⁻¹ adsorbent dose and at pH 3.5	150
6.5 (d)	UV-visible absorbance spectra of DB-86 in the residual solution at different time intervals for optimum dose	150
6.6 (a)	Pseudo first order kinetic model under optimal conditions	154
6.6 (b)	Pseudo second order kinetic model under optimal conditions	154
6.6 (c)	Intra-particle diffusion model under optimal conditions	155
6.6 (d)	Boyd model under optimal conditions	155
6.6 (e)	Liquid film diffusion model under optimal conditions	156
6.6 (f)	The plot of $\ln K_2$ Vs $1/T$	156
6.7 (a)	The plot of q_e Vs C_e , (Adsorption isotherm of DB-86 at 24.65 g L ⁻¹ adsorbent, 3.1 pH and 308 K)	162
6.7 (b)	The linearized plot of Langmuir isotherm (Adsorption isotherm of DB-86 at 24.65 g L ⁻¹ adsorbent, 3.1 pH and 308 K)	162
6.7 (c)	The linearized plot of Freundlich isotherm (Adsorption isotherm of DB-86 at 24.65 g L ⁻¹ adsorbent, 3.1 pH and 308 K)	163
6.7 (d)	The linearized plot of Temkin isotherm (Adsorption isotherm of DB-86 at 24.65 g L ⁻¹ adsorbent, 3.1 pH and 308 K)	163

Figure	Title	Page
6.8	The plot of ΔG° vs T for DB-86 adsorption	166
6.9	Possible adsorption Mechanism of DB-86 by PnsAC-alginate	166



NOMENCLATURE

SYMBOLS

A	Koble-Corrigan isotherm constant ($L^n \text{ mg}^{1-n} \text{ g}^{-1})^n$
a	Radke-Prausnitz isotherm model constant ()
a_R	Redlich-Peterson isotherm constant ($L \text{ mg}^{-1}$)
a_T	Toth isotherm constant (mg L^{-1})
B	Koble-Corrigan isotherm constant ($L \text{ mg}^{-1})^n$
b	Langmuir isotherm constant ($L \text{ mg}^{-1}$)
b_o	This constant relates heat of adsorption (J mol^{-1})
B_t	Mathematical function of F
C_+	Concentration at time $t = t$
C_e	Equilibrium Concentration
C_o	Initial Concentration
f	Fraction of solute adsorbed ($f = \frac{q_e}{q_t}$)
k_1	Pseudo first order rate constant (min^{-1})
K_f	Freundlich isotherm constant [$(\text{mg g}^{-1})(L \text{ mg}^{-1})^{(1/n)}$]
k_{id}	Intra-particle diffusion rate constant ($\text{mg g}^{-1} \text{ min}^{-0.5}$)
K_{LF}	Sips adsorption isotherm constant ($L \text{ mg}^{-1}$)
K_R	Redlich-Peterson isotherm constant ($L \text{ g}^{-1}$)
K_T	Toth isotherm constant (mg g^{-1})
m	Mass of adsorbent (g)
n	Sips adsorption isotherm exponent, Koble-Corrigan isotherm exponent, Radke-Prausnitz isotherm exponent
q_e	Adsorption capacity (mg g^{-1})
$q_e(\text{exp})$	Experimental q_e (mg g^{-1})
$q_e(\text{pred})$	Predicted q_e (mg g^{-1})
q_m	Maximum monolayer adsorption capacity (mg g^{-1})
q_t	Adsorption capacity (mg g^{-1}) at time $t = t$
r	Radke-Prausnitz isotherm model constant
R	Universal gas constant ($\text{J mol}^{-1} \text{ K}^{-1}$)
R_L	Dimensionless separation factor

t Dimensionless Toth exponent

GREEK SYMBOLS

α	Temkin isotherm equilibrium binding constant (L mg^{-1})
α_1	Fritz-Schlunder isotherm model constant ($\text{mg}^{1-\beta_1} \text{g}^{-1} \text{L}^{\beta_1}$)
α_2	Fritz-Schlunder isotherm model constant ($\text{mg g}^{-1})^{-\beta_2}$
β	Redlich-Peterson isotherm exponent
$\beta_1\beta_2$	Exponent in Fritz-Schlunder isotherm
ΔG°	Gibbs free energy (kJ mol^{-1})
ΔH°	Enthalpy change (kJ mol^{-1})
ΔS°	Entropy change ($\text{kJ mol}^{-1}\text{K}^{-1}$)



ABBREVIATIONS

AATCC	American Association of Textile Chemists and Colourists
AC	Activated Carbon
ACF	Activated Carbon Fibers
AY-36	Acid Yellow-36
BET	Brunauer-Emmett-Teller
BJH	Barrett-Joiner-Halenda
BOD	Biochemical Oxygen Demand
COD	Chemical Oxygen Demand
CP	Conventional Pyrolysis
DB-38	Direct Black-38
DB-86	Direct Blue-86 (Direct Fast Turquoise Blue GL)
EDS	Energy-Dispersive X-ray spectroscopy
FTIR	Fourier Transform Infrared Spectrometer
GAC	Granulated Activated Carbon
IC	Impregnated Carbon
MPSAC	Magnetic Peanut Shell based Activated Carbon
MWP	Microwave Irradiation followed by Pyrolysis
PAC	Powdered Activated Carbon
PHC	Peanut Husk Carbon
PnsAC	Peanut Shell Activated Carbon
RR-141	Reactive Red-141
SEM	Scanning Electron Microscope
TGA	Thermo gravimetric Analysis
XRD	X-Ray Diffraction
ZPC	Zero Point Charge

CHAPTER I

INTRODUCTION

1.0 PRELUDE

Water is one of the most crucial renewable natural resources available on earth (Outline, 2013), and is vital for life (Liu et al., 2013). Water plays a critical role in survival of each and every organism on earth. Water being a universal solvent is susceptible to pollution. Our ecosystem is jeopardized due to increase in water pollution globally. Advancement in technology and rapid industrialization over the last decades have resulted in the growth of pollutants which have led to immutable damage to ecosystem (He et al., 2018) and ultimately to human health. Anthropogenic influence has degraded the quality of water (Reddy, 2008). Huge amount of trash, plastic waste, oil spills and toxic chemicals are dumped in rivers, seas and lakes. About 71% of earth's surface is covered with water but less than 2 % of the total available water on earth is drinkable. Worldwide usage of water has increased by 1 % annually and as expected the demand will continue at same rate till 2050 which will lead to rise in water consumption by 20 to 30% above current level (Nations, 2019). Scarcity of water will be faced by 50 % of world's population by the year 2025 (kirk othmer, 2017). Hazardous effects of pollution and shortage of water have already impacted humanity. Global scarcity of water can cause poor access to billions of people. 1.8 billion people are using contaminated drinking water, since 80% of untreated wastewater flows back to the ecosystem (Nations, 2019). Out of ten, three people worldwide do not have access to drinkable water (Nations, 2019). To avert water crisis, replenishing water and sustainable designs have to be developed. Improvising wastewater management and lowering pollution level is the major solution for the challenge of providing safe and sufficient water supplies to everyone.

India is the major contributors of wastewater in South Asia. Industries have a key role in producing wastewater and textile industry is leading among them. India is one of the major producer of textiles, its share in global trade is approximately 7 % ("Year End Review 2018: Ministry of Textiles," n.d.). In India, though the textile industry ranks among the top ten water

consuming industry but the amount of pollution generated by them is much larger and have contaminated a vast amount of water resources (Raja et al., 2019). Wastewater from textile industries can be characterized by organic pollutants, inorganic pollutants, dyes, heavy metals etc. The presence of organic pollutants provides toxic characteristics in real effluents. Treatment of wastewater from textile industries is vitally important which enables its reuse and brings down the consumption of water in textile industry (Núñez et al., 2019). Among the wide variety of pollutants found in wastewater, dyes are a serious threat to the environment (Chiou and Chuang, 2006; Sharma et al., 2017a). Colour is the first indicator of pollutants in wastewater which is due to the residual dyes obtained from different sources including textile industries, pharmaceutical industries, paper, dye and bleaching industries etc. (Samal et al., 2018). These industries discharge a huge amount of coloured wastewater. Extensive use of dyes poses problems, as coloured wastewater is generated which requires treatment prior to its disposal into mainstream. Concentrations of dyes present in dye-house effluents range from 0.01 g L^{-1} to 0.25 g L^{-1} , depending on the type of dyes and processes used for dyeing (Faria et al., 2009) (Dalai et al., 2018), but the durability of dyes in wastewater is mainly responsible for the pollution caused by them. Numerous reports indicate that our ecology is affected by the toxic effects caused by dye effluents. Hence an effective and versatile technology which can decolourize the dye effluents needs to be developed. Researchers have shown interest in the process of adsorption and it has been found suitable, considering its higher efficiency for removing a wide variety of metals and dyes. Although, activated carbon is an efficient adsorbent but its high cost restricts its use. Various investigators have attempted to produce activated carbon from agriculture and industrial wastes. Therefore, in the present study our emphasis is on the preparation of activated carbon from low cost material and its application in removing dyes.

1.1 STATISTICS OF DYE PRODUCTION AND DISCHARGE

The rising demand of dyes from industries such as textiles, paints, food, printing inks etc. has witnessed a remarkable growth in global market. The expected annual growth of dye industry is 2-3 % in near future (“Chemical Economics Handbook,” n.d.). The global production of dyes is 800,000 tons annually (Hassaan and Nemr, 2017). More than 10,000 types of dyes are used for manufacturing of textiles only (Hassaan and Nemr, 2017). Out of the total dyes produced worldwide, azo dyes constitute 70 % (Heibati et al., 2014; Ruiz et al., 2011). In 2011 for acid dyes, global export and import market was 680,000 tons and for direct dyes it was 181,998 tons (Ghaly et al., 2014).

Worldwide major producers and exporters of dyes are China and India (“Global Dyes Market,” n.d.). Major textile producer is China and it accounts for 40 – 45 % of world dye consumption (“Chemical Economics Handbook,” n.d.). In India, the production of dyes and pigments during fiscal year 2018 was almost 367,000 tons (“India - dyes and pigments production volume 2018,” n.d.) and annual growth rate in fiscal year 2019 was 6.73 % (“India - dyes and pigments production growth rate 2019,” n.d.).

A huge amount of liquid waste is produced by textile industries which contain inorganic and organic compounds. During dyeing process all the dyes applied, does not get attached to the fabric, instead a small amount of dyes gets separated from the fabric and are washed out. Textile effluents contain high concentration of these unfixed dyes (Hassaan and Nemr, 2017). The dyeing material that is discharged annually in the environment is 5000 tons (Pirkarami and Olya, 2017). An account of fixation and dye loss to effluent is shown in Table 1.1. In the production of textiles, industries utilize a huge amount of water and chemicals. For producing 1 kg of fabric, water consumed is about 0.08 - 0.15 m³. It was estimated that per day after processing 12-20 tons of textiles around 1000 - 3000 m³ of water is released (Ghaly et al., 2014). During the forecast period (2019-2024), CAGR (compound annual growth rate) of 5.46 % is anticipated for dyes and pigment market (Markets, n.d.).

Table 1.1 : An account of fixation and dye loss to effluent (Neill et al., 1999)

Type of Dye	Fibre	Degree Of Fixation (%)	Loss of Effluent (%)
Acid	Polyamide	89 ± 95	5 ± 20
Basic	Acrylic	95 ± 100	0 ± 5
Direct	Cellulose	70 ± 95	5 ± 30
Disperse	Polyester	90 ± 100	0 ± 10
Metal-complex	Wool	90 ± 98	2 ± 10
Reactive	Cellulose	50 ± 90	10 ± 50
Sulfur	Cellulose	60 ± 90	10 ± 40
Vat	Cellulose	80 ± 95	10 ± 40

Globally environment protection agencies have imposed some limits on disposing the wastewater into the environment, for safeguarding human health and environment from pollution caused by industries. Discharge limits of various countries have been shown in Table1.2

Table 1.2 : Discharge limits of various countries (Ghaly et al., 2014)

Parameters	BIS	CCME	China	FEPA	Mexico	SL
pH	5.5 - 9	6.5 - 8.5	6-9	6 – 9	6 - 8.5	6 - 8.5
Temperature (°C)	50	30	-	40	-	40
Colour (Pt - Co)	None	100	80	7(Lovibond)	-	30
TDS (mg L ⁻¹)	2100	2000	-	2000	-	2100
TSS (mg L ⁻¹)	100	40	150	30	-	500
Sulphide (µg L ⁻¹)	2000	200	1000	200	-	2000
Free Chlorine (µg L ⁻¹)	1000	1000	-	1000	-	-
COD (mg L ⁻¹)	250	80	200	80	< 125	600
BOD5 (mg L ⁻¹)	30	50	60	50	< 30	200
Oil & Grease (mg L ⁻¹)	10	-	-	10	-	30
Dissolved Oxygen (µg L ⁻¹)	-	1000	-	-	-	-
Nitrate (µg L ⁻¹)	10000	13000	-	20000	10000	45000
Ammonia (µg L ⁻¹)	-	0.1	-	0.2	-	60
Phosphate (µg L ⁻¹)	5000	<4000	1000	5000	-	2000
Calcium (µg L ⁻¹)	-	-	-	200000	-	240000
Magnesium (µg L ⁻¹)	-	200000	-	200000	-	150000
Chromium (µg L ⁻¹)	100	1	-	<100	50	50
Aluminium (µg L ⁻¹)	-	5	-	<1000	5000	-
Copper (µg L ⁻¹)	3000	<1000	1000	<1000	1000	3000
Manganese (µg L ⁻¹)	2000	5	2000	5.0	200	500
Iron (µg L ⁻¹)	3000	300	-	20000	1000	10
Zinc (µg L ⁻¹)	5000	30	5000	<10000	10000	10000
Mercury (µg L ⁻¹)	0.01	0.026	-	0.05	-	1

CCME Canadian Council of Ministers of the Environment

BIS Bureau of Indian Standards

FEPA Federal Environmental Protection Agency (United States)

SL Sri Lanka

1.2 HARMFUL EFFECTS OF DYES

Wastewater discharged from dye industries carry a variety of chemicals. Colour in wastewater is highly noticeable and it occurs due to the presence of dye. Effluents containing dyes are not only polluting water but are aesthetically displeasing (Sharma et al., 2017a). Dyes are harmful as the dye effluents pose direct as well as indirect effects on the environment as shown in Fig.1.1.

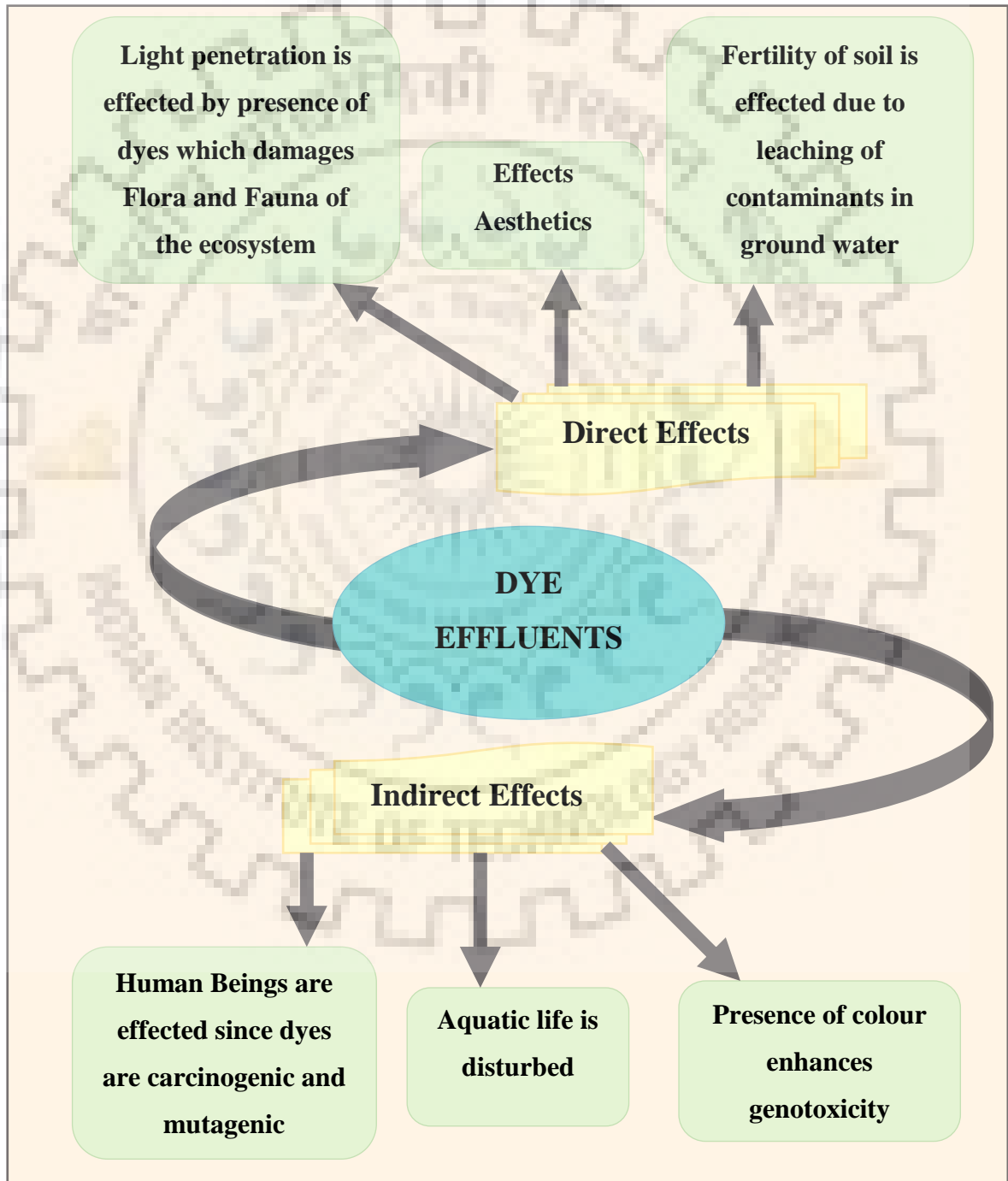


Fig. 1.1 : Effects of dye effluents on the environment

Most of the dyes are resistant to photo-oxidation and non-biodegradable in nature. Coloured water traps sunlight which in turn curbs photosynthesis in aquatic plants thus disturbing the flora and fauna of aquatic life. Moreover, the fertility of soil is also affected due to leaching of dyes in ground water. Wastewater containing dyes is difficult to treat as the dye molecules are defiant which show resistance towards aerobic digestion and are stable to oxidizing agents, heat and light (Hassaan et al., 2017). Removing colour from wastewater is extremely crucial as even a small amount of dye (less than 1 ppm) causes wastewater colouration (Abd El-Rehim et al., 2012). Textile industry effluents have a harmful impact on environment since during treatment process a huge amount of energy is consumed and later hazardous waste in the form of sludge remains which needs safe disposal. Synthetic dyes are poisonous because they are highly soluble in water due to which they are considered to be a common water pollutant.

Dyes are posing detrimental threats on human health and environment due to their carcinogenic and mutagenic nature (Dahri et al., 2014). Stringent legislations are imposed on various parameters of industrial discharge in recent years. Globally synthetic dyes are getting replaced by organic dyes or natural dyes since synthetic dyes contain hazardous chemicals. Awareness is rising among end product users due to escalating pollution levels and environmental issues. Thus, removal of dyes is of paramount importance.

1.2.1 Acid Yellow – 36 (AY - 36)

Acid Yellow 36 (AY-36), also known as Metanil Yellow with IUPAC name 3-(4-anilinophenylazo) benzenesulfonic acid sodium salt (Mittal et al., 2008), is an azo dye. Azo dyes, containing $-N=N-$ as a chromophore are used in textile, leather, plastic, food, and pharmaceutical industries (Ahmad et al., 2010) and are the most crucial class of dyes. These dye molecules are stable and non-degradable that can produce toxic aromatic amines (Abd El-Rehim et al., 2012).

AY-36 raises high environmental concern because of its high solubility in water. It is used in soap colours, shoe polish, spirit, lacquer, cosmetic products, leather dyes, pigment manufacturing, coloured-water fast ink, and textile industry and is thus released in the wastewater of these industries. Though it is not permitted to be used as a food colour, it is found in various types of food such as sweet meat, ice cream, and beverages. It is used as turmeric coating due to its orange–yellow colour (Mittal et al., 2008). Furthermore, AY-36 with the pH range of 1.2 – 2.3 is used to estimate H^+ ion concentration (Mittal et al., 2008). The oral consumption of AY-36 can cause methaemoglobinaemia, cyanosis, tumour, and intestinal and enzymic disorders in human body (Anjaneya et al., 2011). Upon contact with skin, AY-36 may have adverse effects

and cause dermatitis. Thus removing AY-36 from wastewater is necessary because of its many hazardous effects.

1.2.2 Direct Blue – 86 (DB - 86)

Direct dyes are water soluble and anionic in nature and are widely used in dyeing industries due to their easy application and economic factor. Direct dyes are generally applied in an aqueous bath having electrolytes within a temperature range of 75 - 95 °C. These dyes are not colour fast since they are unable to form strong bond with fibre molecules (Ghaly et al., 2014). Direct Blue-86 (DB-86), a phthalocyanine direct dye, are brilliant greenish blue or turquoise in shades (Othmer, n.d.). DB-86 (Nemr et al., 2009), is commercially used for dyeing of cellulosic fibers like cotton, flax, viscose rayon, acetate, jute and applicable on leather and paper colouration.

1.3 TECHNIQUES AVAILABLE FOR WASTEWATER TREATMENT

Wastewater is the used water containing a large number of pollutants which originates from domestic, industrial and agricultural activities. These pollutants contain organic and inorganic compounds that are responsible for disturbing the water cycle. Their removal can be simple or complex depending upon the nature of the contaminants and their toxicity level. Wastewater treatment is not only crucial for environment but also for making it reusable.

In recent years, textile waste is gaining attention due to the large amount of effluents generated which is disposed untreated in sources of water. Treatment of wastewater containing dyes is a big challenge due to the complex and diverse structure of dyes (Arumugam et al., 2018). Moreover energy consumption is high for the treatment of wastewater containing dyes. Major problem faced is the removal of colour from the effluents which is due to the residual dyes.

There are many factors such as economic feasibility, residual by products and effluent required, that are considered while selecting the method to be employed for wastewater treatment, further quality of water source and usage of treated water are most critical determinants for selecting the process (Crittenden et al., 2012). The techniques for wastewater treatment may also be chosen depending upon the volume and size of wastewater. Various methods of wastewater treatment are shown in Fig.1.2.



Fig.1.2 : Different wastewater treatment methods

A lot of research have been conducted for treating wastewater from industries and efficient methods have been explored for decolourization of effluents from industries such as physical, chemical and biological methods. For each and every technique advantages and disadvantages are extensively reviewed as shown in Table 1.3. Due to the presence of variety of contaminants in various effluents, a combination of two or more treatment methods may be employed for better results.

Table 1.3 : Techniques for dye removal from wastewater (Robinson et al., 2001)

Physical / chemical / biological methods	Advantages	Disadvantages
Adsorption using Activated carbon	Simple and easy operation, good removal for variety of dyes.	Expensive, Ineffective for vat and disperse dyes, regeneration is tedious.
Electrochemical destruction	Breakdown compounds are non-hazardous.	High cost of electricity.
Electrokinetic coagulation	Economically feasible.	High sludge production and disposal problem.

Physical / chemical / biological methods	Advantages	Disadvantages
Fenton's reagent	Effective decolourisation of both soluble and insoluble dyes.	Sludge generation, economically unfeasible, formation of undesirable intermediates.
Ion exchange	Regeneration: no adsorbent loss.	Not effective for disperse dyes, Economically not viable.
Membrane filtration	Removes all dye types.	Expensive, Concentrated sludge production, it cannot handle large volume.
Ozonation	Applied in gaseous state: no alteration of volume	Short half-life (20 minutes), ineffective for disperse dyes, COD removal is less and Cost of Ozone is high.
Photochemical	No sludge production	Formation of harmful intermediate products.
Aerobic Process	All types of dyes can be removed	Cost of supplying oxygen to microorganism is high. Maintenance cost is high.

1.3.1 Biological Methods

It is the most economical method as compared to physical and chemical methods. Bacteria, fungi, yeast and other microorganism degrade and accumulate the pollutants, thus industrial effluents are treated by using different biodegradation methods like adsorption by microbial biomass, fungal decolourization, bioremediation method, microbial degradation (Sahu and Singh, 2019). Biological treatment involves aerobic and anaerobic process.

In aerobic process bacteria converts sludge into CO₂ and biomass in the presence of oxygen or air and in anaerobic process, anaerobic bacteria degrades the sludge into CO₂, biomass and methane in the absence of oxygen (Ghaly et al., 2014). Colour of azo dyes can be removed by

reducing the azo bond (-N=N-) under reducing conditions. During reduction amines are produced which are reluctant to degradation under anaerobic conditions, though these amines are colourless. So by this process colour is somehow reduced on the cost of toxicity. Main advantage of anaerobic process is the production of biogas which can be utilized in providing power and energy (Robinson et al., 2001).

Bioaugmentation and bioremediation methods are used to decolourize dye wastewater using enzymes such as lignin peroxidases, manganese peroxidases and laccases (Freeman and Reife, 2003). Although enzymes have proved to be effective for decolouring organic dyes but they have certain disadvantages:

- If temperature and pH are not in optimum range, the rate of reaction will be slow.
- Lignin peroxidases and manganese peroxidases which are most effective enzymes for dye degradation, are not commercially available.

In biological methods there is ease of operation and flexibility in the process but complicated dyes are defiant because of their synthetic organic origin and complex structure. Thus, these cannot be degraded by biological process. Many of the synthetic dyes are harmful to some microorganisms besides that time taken in this process is much higher and also large area is required for the process and the process is further effected by diurnal variations and toxicity of various chemicals (Sahu and Singh, 2019). Biological method is not found to be suitable in removing colour from wastewater (Kharub, 2012).

1.3.2 Chemical Methods

Treatment of effluents from industries by chemical methods involves a number of processes such as Fenton's reagent, Ozonation, Electrochemical destruction etc. These are efficient methods for removing dyes but the high cost and large amount of chemical consumption restricts their use.

Fenton's Reagent ($\text{Fe}^{2+}/\text{H}_2\text{O}_2$)

It is one of the advanced oxidation process which can oxidise and decolourize effluents containing azo, reactive and anthraquinone dyes. Fenton's reagent is a mixture of ferrous iron and H_2O_2 . Rate of Fenton's reagent is limited by the rate of OH ion generated. Removal study of Reactive Black 5 and Reactive Blue 19 dyes are carried out using Fenton's reagent (Freeman and Reife, 2003). Ferrous ions of Fenton's reagent react with hydrogen peroxide, producing hydroxyl radicals. These hydroxyl radicals transform big organic molecules in the presence of UV light

into mineral acid, small molecules of SO₂ and water. This process oxidises in a very short time but the major drawback of this process is sludge generation (Robinson et al., 2001).

Ozonation

Ozone is one of the most powerful oxidising agent. The oxidation potential of ozone is 2.08 eV. The disinfectant power of ozone has been known from last 100 years but its use for ozonation have started from last three decades only. Ozone has low solubility and is highly reactive. In Advanced Oxidation Process (A.O.P.), ozone and hydroxyl radicals oxidise the organic and inorganic pollutant in presence of UV light.

Oxidation of organic species is carried out by the combination of reactions with ozone and hydroxyl radicals. Ozone molecules is selective and attacks preferentially the unsaturated bond of chromophores. Chromophore are organic molecules with conjugated double bonds that can be broken by ozone forming intermediate radicals and finally smaller molecules that decreases the effluent colour (Shriram and Kanmani, 2014). Major drawback of this process is the cost of ozone, which is high. Moreover, the process is having short half-life (20 minutes) (Robinson et al., 2001).

Chemical and Biological methods are effective methods of wastewater treatment containing dyes. However, they need specialized equipment and are energy guzzlers. Further, they create huge amount of chemical intermediates which require safe disposal (Sahu and Singh, 2019).

1.3.3 Physical Methods

There are a wide number of physical methods used for wastewater treatment such as membrane filtration (Reverse osmosis, nanofiltration), ion exchange, and various adsorption techniques. These methods are briefly described below.

Membrane Filtration

This is a separation process that is pressure driven. In this technique membrane acts as a physical barrier for particles of specific size to pass through it. Membrane filtration technique can be classified as reverse osmosis, nanofiltration and ultrafiltration based on the particle size to be retained. This process is used for effluent treatment of various industries such as textile, dye, electrochemical, chemical, paper, and many others.

In Reverse osmosis and Nanofiltration, wastewater is passed through a semipermeable membrane by using pressure and thus solids are left on one side of the membrane. In reverse osmosis pore

size is in the range of 0.5 nm and operating pressure is between 7 and 100 bar and in Nanofiltration the pore size is between 0.5 and 2 nm and operating pressure is between 5 to 40 bar. The reverse osmosis membranes can remove organic, inorganic substances, colour, hardness, bacteria and viruses from water. By using this process for acid dyes the colour removal was found to be 97.2% (Abid et al., 2012).

Major advantage of this technique is that it produces less waste and the wastewater can be reused moreover the efficiency of the process is high. But this is an expensive procedure and it cannot work on high concentration of dyes, also there is a high probability of membrane fouling.

Ion Exchange

This process is effectively used in the treatment of wastewater from textile industries. Ion exchange is a reversible process in which wastewater containing dyes are passed through the bed of cationic and anionic exchange resins and ions are exchanged between solid (resin) and liquid (wastewater). Cations are removed by passing through cation exchange resins and the resins are recharged by hydrogen ions making it acidic. Anions are removed by passing through anion exchange resins and these resins are recharged by hydroxyl ions (Ghaly et al., 2014). In this method no loss of adsorbent is there, however, it is an expensive process as well as it cannot treat wide range of dyes.

Adsorption

In the adsorption process, the matter is extracted from one phase and concentrated on the surface of another phase (Interface accumulation). In compliance with the abundant literature available on adsorption, it is the most preferred process pertaining to its ease of operation, simplicity, reliability, high potential for colour removal. The pollutants that are too stable to be removed by other conventional methods can be removed efficiently by adsorption process due to which it is gaining importance (Robinson et al., 2001). However, the high cost of adsorbent makes it an expensive process.

Adsorbent plays a pivotal role in the adsorption process. It is an insoluble material which has the capacity to contain a definite amount of solids and liquids in its pores and cavities. The performance of adsorbent depends upon the surface area and porosity, more the surface area more will be the adsorption. A wide range of adsorbents are available, amongst them activated carbon (AC) is the most widely used adsorbent. To overcome the high cost of commercially available AC, a large number of industrial, agricultural and domestic wastes such as sugarcane, orange peel, coconut shell, rice husk, fly ash (Singh et al., 2008) and others are utilized to prepare low

cost AC. In recent trends these developed adsorbents were utilized efficaciously in the removal of dyes from wastewater (Malik, 2004).

1.4 RESEARCH OBJECTIVES

Based on the detailed literature review presented in the Chapter II, objectives of the present study have been formulated. In the present study, efficacy of Peanut shell Activated Carbon (PnsAC) for the adsorption of AY-36 and DB-86 from aqueous solution have been studied. RSM was used for the optimization of adsorption parameters. Main objectives of this research can be summarized as follows :

- i. To synthesize Peanut shell Activated Carbon (PnsAC) (in a single step) using H_3PO_4 followed by pyrolysis from waste peanut shell.
- ii. To characterize PnsAC by SEM analysis to find surface morphology of PnsAC, EDS analysis to find the chemical composition of PnsAC, FTIR analysis to confirm surface functional group.
- iii. To study the effect of different parameters like pH, initial dye concentration, PnsAC dosage, contact time and temperature on the removal of dyes.
- iv. To examine the kinetics, equilibrium isotherm and thermodynamics of AY-36 and DB-86 dye for the above adsorption process.
- v. To synthesize the immobilized Peanut shell Activated Carbon (PnsAC-alginate).
- vi. To characterize the PnsAC-alginate by SEM, EDS, TEM, FTIR, BET surface area and pH_{ZPC} .
- vii. To analyze kinetic and isotherm data using various isotherm and kinetic models and to evaluate suitability of this PnsAC-alginate for the removal of DB-86 dye from wastewater.

1.5 STRUCTURE OF THE THESIS

The present work has been divided in seven chapters as shown in Fig.1.3. A brief record of these chapters has been given below.

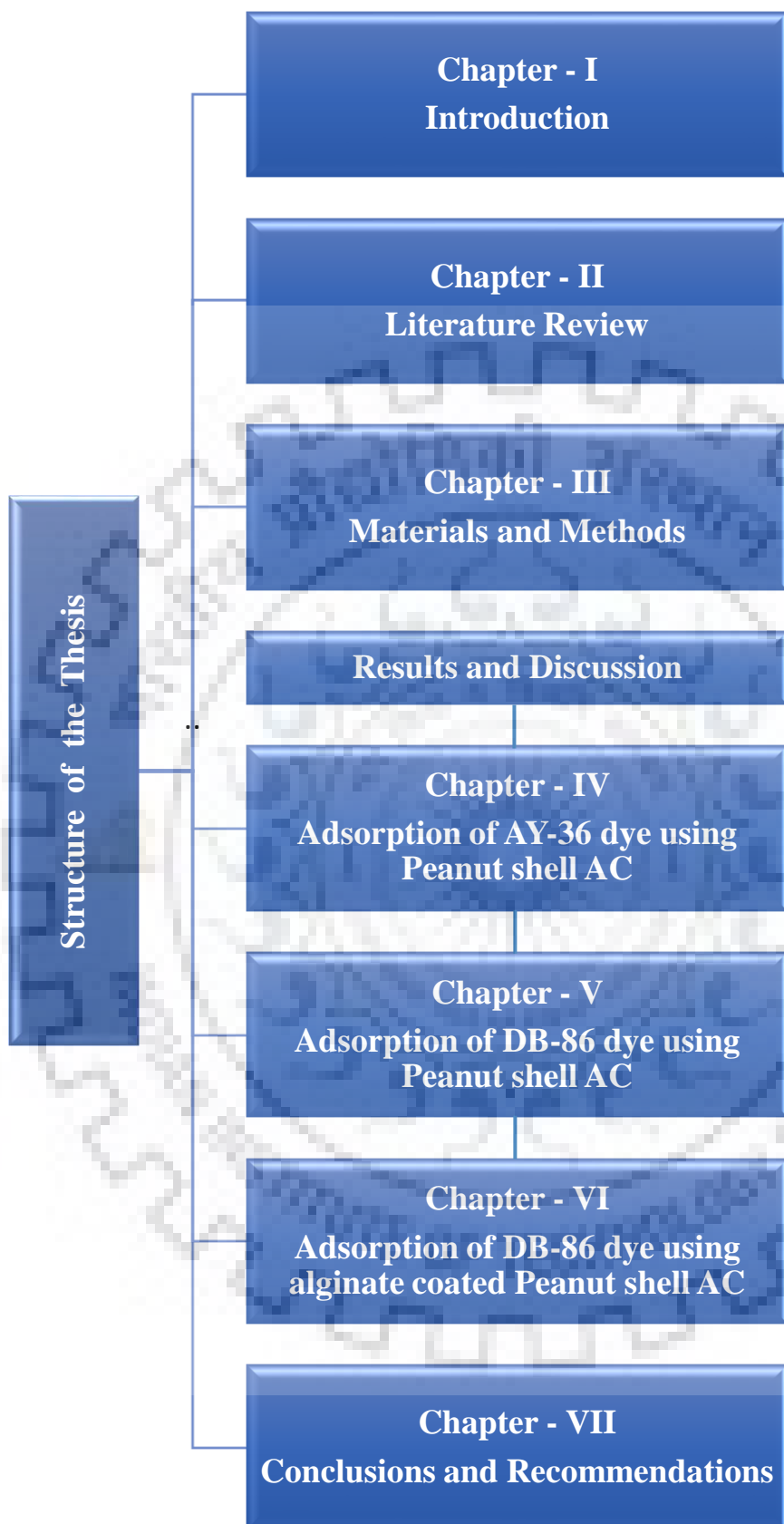


Fig. 1.3 : Structure of the thesis

Chapter I gives a brief introduction to the importance of water, harmful effects of dye discharge in water bodies and the effect of effluents on environment. Different techniques available for wastewater treatment has also been discussed. Research objectives were extracted from the inadequacy of literature.

Chapter II presents the classification of dyes and pollution effects, arising due to the presence of dyes. Physisorption and chemisorption were explained. Furthermore, various factors like pH, contact time, initial dye concentration, adsorbent dose, temperature effects were explained.

Chapter III consists of various chemicals and their use with the synthesis process of Peanut shell Activated Carbon (PnsAC). The use of various equipments and analytical instruments were also summarized. A brief methodology of characterization, kinetic and isotherm models, thermodynamic study were given. Detailed procedure of batch adsorption study has been given.

Chapter IV explains the characterization of PnsAC and effect of different parameters like effect of initial pH, adsorbent dose, contact time, equilibrium isotherm, kinetic and thermodynamic study of AY-36 dye.

Chapter V contains the adsorption study of DB-86 on indigenously developed activated carbon and effect of various parameters like initial pH, dye concentration, amount of PnsAC, temperature. Kinetic, isotherm and thermodynamic studies were also carried out.

Chapter VI consists of alginate coated Activated Carbon for the removal of DB-86 dye from synthetic wastewater. Response surface methodology was used to optimise the process variables like adsorbent dose, adsorbate dose and pH. Kinetic, isotherm and thermodynamic studies were also carried out.

Chapter VII provides important outcomes, conclusions and further recommendations for the study.

LITERATURE REVIEW

2.0 DYES

Mankind have always been fascinated towards colour aesthetically and socially. From the onset of civilization, colours appealed humans as is evident from fabrics found in Egyptian tombs (Stothers, n.d.). Dyes used were of natural origin (plants and animals) and people used it for colouring their clothes, surroundings. These natural dyes were exclusively used till 1850's. Synthetic dye was first discovered in 1856, by William Henry Perkin and was named mauve. Industrial revolution led to the growth of textile industry demanding for economic and readily available dyes. Thus by 1900, markets were dominated by synthetic dyes (Stothers, n.d.).

Dyes are organic solvents, which on applying to the substrate, in an aqueous solution chemically bonds to it. Some additives are used to improve and vary the colours of dyed materials, these additives are commonly known as Mordant.

Dye molecule contains two important constituents namely Chromophore and Auxochrome (colour helper). The function of chromophore is to give colour to dye molecule and auxochromes function is to regulate intensity of colour, e.g. amino group, aldehyde group, hydroxyl group. Auxochromes are usually electron donating and chromophores are electron withdrawing. In dye structure chromophores and auxochrome are attached by a conjugated system ("Chemistry of dyes," n.d.)

2.1 CLASSIFICATION OF DYES

Dyes are classified in different ways. Internationally a system used for classification of dyes is Colour Index. It is the most authentic reference database of colours which provide detailed information such as manufacturers, properties, preparation, uses. Colour index international is maintained by Society of Dyers and Colourists and the American Association of Textile Chemists and Colourists (AATCC) (Othmer, n.d.).

In colour index, dyes are grouped using dual classification in which Generic name is assigned first and then CI Constitution number on the basis of chemical structure is assigned. No single parameter can classify all types of dyes due to their various variants (Ajmal et al., 2014). Fig.2.1 shows the classification of dyes.

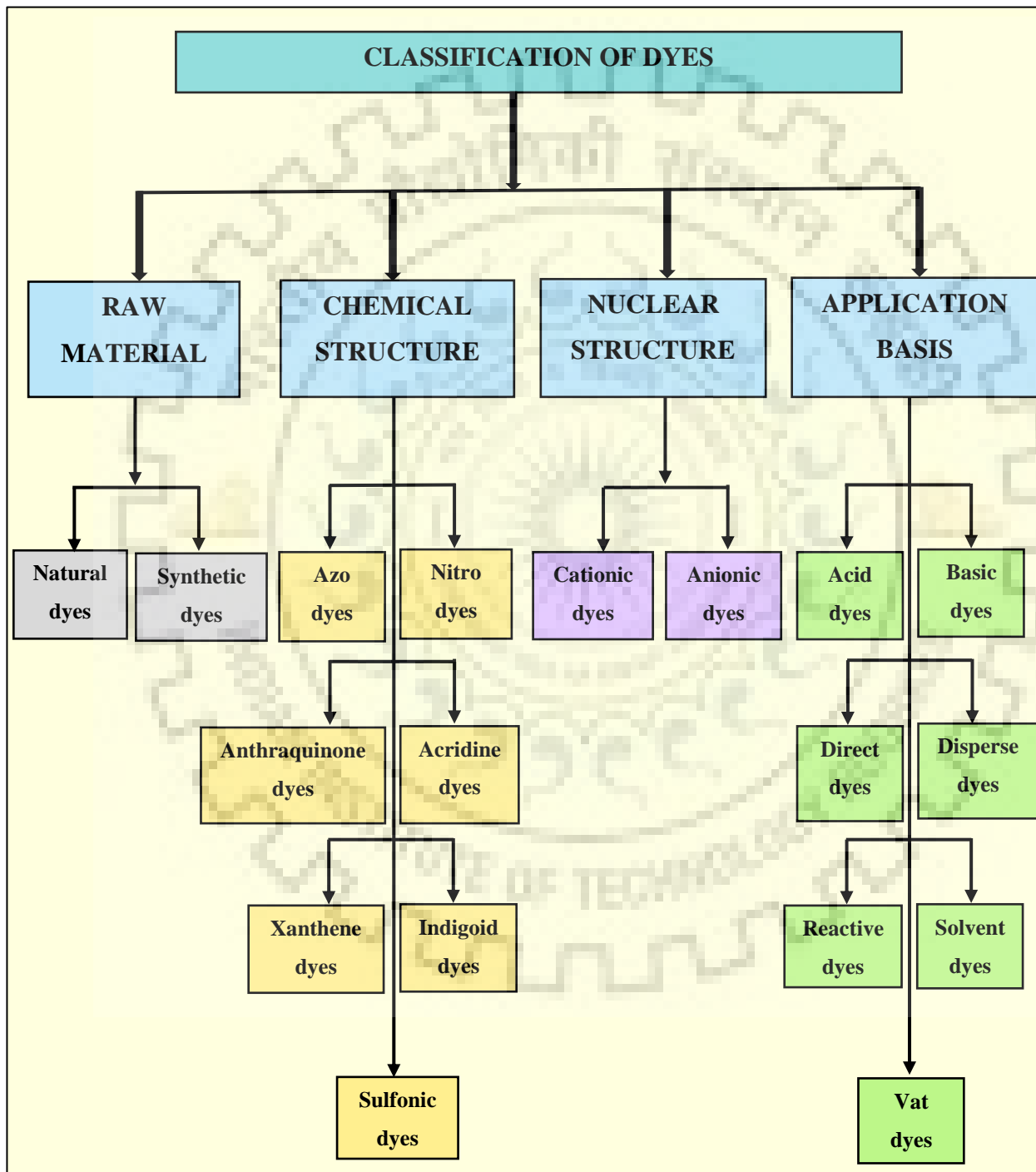


Fig. 2.1 : Classification of dyes

2.1.1 Classification on the Basis of Raw Material

Dyes are basically classified as Natural and Synthetic, on the basis of source from which it is obtained.

2.1.1.1 Natural Dyes

Natural dyes are the earliest known dyes which originated from plants, animals and minerals. Major variety of these dyes are vegetable dyes obtained from plants.

Plants : Indigo is known as the oldest dye obtained from indigo plant in Asia. Alizarin dye is extracted from the roots of madder plant. Natural dye logwood obtained from trees is used on silk and nylon black.

Animals : Cochineal dye is obtained from coccus cacti an insect. It gives red and orange colour onto silk and wool fabrics. Tyrian purple dye is obtained from shell fish.

Minerals : Iron Buff, Chrome Yellow, Chrome orange etc. are some dyes produced from mineral resources.

2.1.1.2 Synthetic Dyes

Whatever colour we see today is due to synthetic dye. These dyes are produced from inorganic and organic molecules. Azo dyes are those synthetic dyes that have chromophoric azo group ($-N=N-$). Natural dyes do not possess this chromophore. Commercially, azo dyes are available in abundance. These dyes are economic, easy to apply, colour fast. Generally azo dyes have one azo group, two groups may be present which are known as diazo, three groups known as triazo and so on (Heibati et al., 2014).

Synthetic dyes find its application in diversified fields. Many industries like textile, food, cosmetics, pharmaceuticals, paper printing etc. are using these dyes excessively. There are many categories of these dyes : acid, basic, direct, reactive, vat, disperse, mordant and sulphur etc. (Hassaan and Nemr, 2017).

2.1.2 Classification on the Basis of Chemical Structure

Dyes can be categorized on the basis of chromophores present in the structure such as Acridine dyes derivative of acridine, Anthraquinone dyes derivative of anthraquinone, Azo dyes, Nitro dyes, Xanthene dyes etc.

Azo Dyes- e.g. aniline yellow, butter yellow, Congo red, disperse red, Bismarck brown, chrysoidine, Methylorange, orange-II, resorcin yellow, parared, etc.

Sulfated azo dye- e.g. acid red 66, direct red 28, Reactive red 35, reactive black 5, reactive violet 5 etc.

Anthraquinoid Dye- e.g. Alizarin etc.

Indigoid and Thioindigoid- e.g. Indigo, thioindigo, tyrian purple etc.

Sulfonic Dyes- e.g. acid fuchsin, Thymol blue etc.

Xanthene Dyes- e.g. rhodamines, Fluorescein etc. (Ali et al., 2017; Othmer, n.d.)

2.1.3 Classification on the Basis of Nuclear Structure

2.1.3.1 Cationic Dyes

Basic dyes are cationic dyes as chromophore of basic dyes contains positive charge. These dyes are soluble in water. Cationic dyes show good affinity towards acrylic, silk and wool but show no affinity for cellulose. These dyes are economical, available in wide range of shades and have good brightness but are poor light fast, e.g. Methylene Blue

2.1.3.2 Anionic Dyes

Acid dyes or anionic dyes are negatively charged dyes. These consists of salt of carboxylic, sulphuric or phenolic group. Azo groups (-N=N-) are present in the center of some acid dyes (Ghaly et al., 2014). Anionic dyes are easily soluble in water and can be applied to wool, nylon, silk and acrylic fibres. E.g. acid yellow-36, direct blue-86.

2.1.4 Classification on the Basis of Application of dyes

Various dyes are classified in Table 2.1 according to their application, chemicals present and their properties.

Table 2.1 : Classification of dyes on the basis of application (Neill et al., 1999)

Class	Principal Substrate	Chemical type	Properties
Acid	Wool, Nylon, silk, paper, leather and ink.	Azo, azine, anthraquinone, nitro, nitroso,	Anionic, Water Soluble.

Class	Principal Substrate	Chemical type	Properties
		triphenylmethane and xanthenes.	
Basic	Paper, polyester, polyacrylonitrile modified nylon and inks.	Azo, azine, acridine, anthraquinone, Cyanine, hemicyanine, diphenylmethane, diazahemicyanine, triarylmethane, xanthenes and oxazine.	Cationic, Water Soluble.
Direct	Rayon, nylon, cotton, leather and paper.	Azo, phthalocyanine and oxazine.	Anionic, Water Soluble.
Disperse	Acrylic, acetate, plastic, polyamide and polyester.	Azo, anthraquinone, nitro, styryl and benzodifuranone.	Water insoluble and non-ionic dyes used to dye hydrophobic fibres.
Reactive	Nylon, silk, wool and cotton.	Azo, anthraquinone, basic, oxazine, phthalocyanine and formazan.	Dyes form covalent bond with fibre.
Solvent	Plastics, gasoline, varnishes, fats, inks, stains, oils and waxes.	Anthraquinone, Azo, triphenylmethane and phthalocyanine.	Water insoluble and solvent soluble.
Vat	Cotton, wool and rayon.	Anthraquinone and indigoids.	Water insoluble.

2.2 ADSORPTION

Adsorption was discovered in 1785 by Lowitz and applied for decolourization of sugar during refining. Later in 19th century inactivated charcoal was used in water treatment plant of America. In 1929 at Hamm, Germany, first granular activated carbon units were used for water supply treatment. 1930, municipal corporation of New Jersey, first used powdered activated carbon for water treatment (Crittenden et al., 2012).

Adsorption is a surface phenomenon. When one component is accumulated on the surface of another component, the phenomenon is known as Adsorption. The component that gets accumulated (adsorbed) is adsorbate and the surface on which it gets accumulated is adsorbent. The adsorbate molecules are transported into micro and macro pores of adsorbent. Adsorption can also be defined as the process of mass transfer in which, physical or chemical interactions, bound a substance and transfers it from liquid phase to surface of a solid. Higher adsorption capacity is achieved by larger surface area (Rashed, 2013). Adsorption may be categorised into two, based on adsorbent and adsorbates nature of attraction.

- i. If dissolved species are concentrated on solid surface by chemical reaction then the process is known by **Chemisorption** (Chemical Adsorption).
- ii. If the dissolved species are accumulated on solid surface by physical attraction then the process is known as **Physisorption** (Physical Adsorption).

Table 2.2 shows difference between physical adsorption and chemical adsorption for various adsorption properties.

Table 2.2 : Comparative table of Physisorption and Chemisorption

Physical adsorption	Chemical adsorption
Low temperature process.	High temperature process.
Prominent forces are Vander Waal's forces.	Chemical bonding exists.
Reversible process.	Irreversible process.
Low heat of adsorption(4–40 kJ mol ⁻¹)	High heat of adsorption (>200 kJ mol ⁻¹)
Forms multi molecular layer.	Forms mono molecular layer.

Physical adsorption	Chemical adsorption
Nonspecific process (extent of adsorption depends upon properties of adsorbent).	Highly specific process (extent of adsorption depends upon both adsorbate and adsorbent).
Activation energy is not required.	Requires activation energy.
Quantity adsorbed per unit mass is high (entire surface is participating).	Quantity adsorbed per unit mass is low (only active surface sites are important).

Among the various techniques applied to wastewaters, adsorption has fascinated the researchers owing to its accuracy, easy operation, insensitivity to toxic substances and ability to treat concentrated coloured solution.

2.3 FACTORS CONTROLLING ADSORPTION

Adsorption is influenced by factors like pH of solution, nature of adsorbent, temperature, contact time, initial concentration and effect of adsorbent concentration.

2.3.1 pH of solution

pH is the prominent factor in the study of adsorption. Activity of functional group present in the AC effect the solution chemistry. pH_{zpc} is defined as zero point charge. It is the pH at which surface has no charge or the surface is neutral.

If $pH < pH_{zpc}$, the surface of AC becomes positively charged and it will attract anionic dye. If $pH > pH_{zpc}$, the surface of AC becomes negatively charged and it will attract cationic dye. Thus, there exists strong electrostatic force of attraction.

2.3.2 Nature of Adsorbent

Adsorption process is dependent on the nature of the adsorbent. For removing organic / inorganic compounds from aqueous solution various types of porous adsorbents are used. Activated Carbon (AC), activated alumina, silica gel, zeolites etc. are some of the adsorbents which are generally used in industries. Biomass can be used as precursor for manufacturing AC, which can be utilized for the removal of dyes from wastewater. Pores of AC provides surface area for adsorption of dye. Adsorption capacity is proportional to the surface exposed, since adsorption is a surface phenomenon.

In the adsorption process, particle size of an adsorbent has a significant role. Under comparable conditions, adsorbents with large particle size will have low surface area on the contrary the adsorbents with smaller particle size will be having greater relative surface area (Y. Zhang et al., 2015). For non-porous adsorbents, the capacity of adsorption is inversely proportional to the particle diameter on the other hand for porous adsorbents it is independent of particle size. However, the particle size of porous substances affects the rate of adsorption. Smaller particle size of adsorbent ensures larger surface area, therefore the rate of adsorption is generally higher.

2.3.3 Temperature

Temperature is the key parameter in the adsorption process. Adsorption is generally exothermic in nature. According to Le Chatelier's principle, the process will shift in the direction where it can eliminate the generated stress. If endothermic adsorption is there, then the adsorption will shift in the direction where temperature is more.

The Vander Waal's forces are prominent in physisorption process which occurs at low temperature. But in chemisorption process, the reaction requires activation energy which is provided by high temperature. The adsorption will initially increase with increase in temperature since:

- i. Mobility of adsorbate is increased.
- ii. Number of adsorbent site increases owing to breakage of internal bonds at the edge.

2.3.4 Contact Time

Contact time affects the adsorption capacity. Contact time of the adsorption process depends on the vacant sites and nature of adsorbent. Contact time of physical adsorption is less but of chemical adsorption is more due to chemical bond formation between adsorbent and adsorbate. Initially adsorption is high because a lot of adsorption sites are empty. Thereafter the adsorption becomes slower and finally it becomes constant due to repulsion between solute molecules adsorbed on the surface.

2.3.5 Initial dye concentration

Adsorption capacity is affected by the initial dye concentration. Initially the adsorption capacity increases when initial concentration of dye is increased due to the presence of many dye molecules in the solution. The initial driving force (max. because of the max. concentration of

dye solution in dye bath) overcome the mass transfer resistance by dye molecules between the solid phase and aqueous phase.

2.3.6 Effect of Adsorbent Concentration

When the quantity of adsorbent is increased in the solution, the number of active sites increases thus adsorption also increases. However, percentage removal at equilibrium is not affected by increasing the amount of dose on prevailing condition of experiments.

2.4 TYPES OF ADSORBENTS AND THEIR SELECTION

Adsorbent is the most crucial substance which defines the success or failure of adsorption process. An adsorbent having high BET surface area, good adsorption capacity and has macropores and micropores for adsorption is considered good. Porous material are categorized by their size as per International Union of Pure and Applied Chemistry (IUPAC) as follows :

- Microporous Materials: pore dia less than 2 nm.
- Mesoporous Materials: pore dia between 2nm and 50 nm.
- Macroporous Materials: pore dia greater than 50nm.

Fig.2.2 show various adsorbents used for dye removal.

There exists four major kinds of adsorbents namely silica gel, activated alumina, zeolites and activated carbon (Yang, 2003).

Silica gel have high surface area ($800 \text{ m}^2 \text{ g}^{-1}$) due to which it quickly adsorbs water, making it a good desiccant. Silica gel is harmful for respiratory tract, digestive tract and irritates eyes and skin (Scientific, 1997).

Activated alumina is made from aluminium hydroxide. It is having surface area around $200 \text{ m}^2 \text{ g}^{-1}$. It can be used in desiccator. Activated alumina acts as a good adsorbent and is used for removing arsenic, fluoride and sulphur (Wikipedia activated alumina, n.d.) .

Zeolite have huge pores and high specific properties which makes it attractive to be utilized in gas separation, for purification of water, for removal of water, carbon dioxide and sulphur dioxide from low grade natural gas.

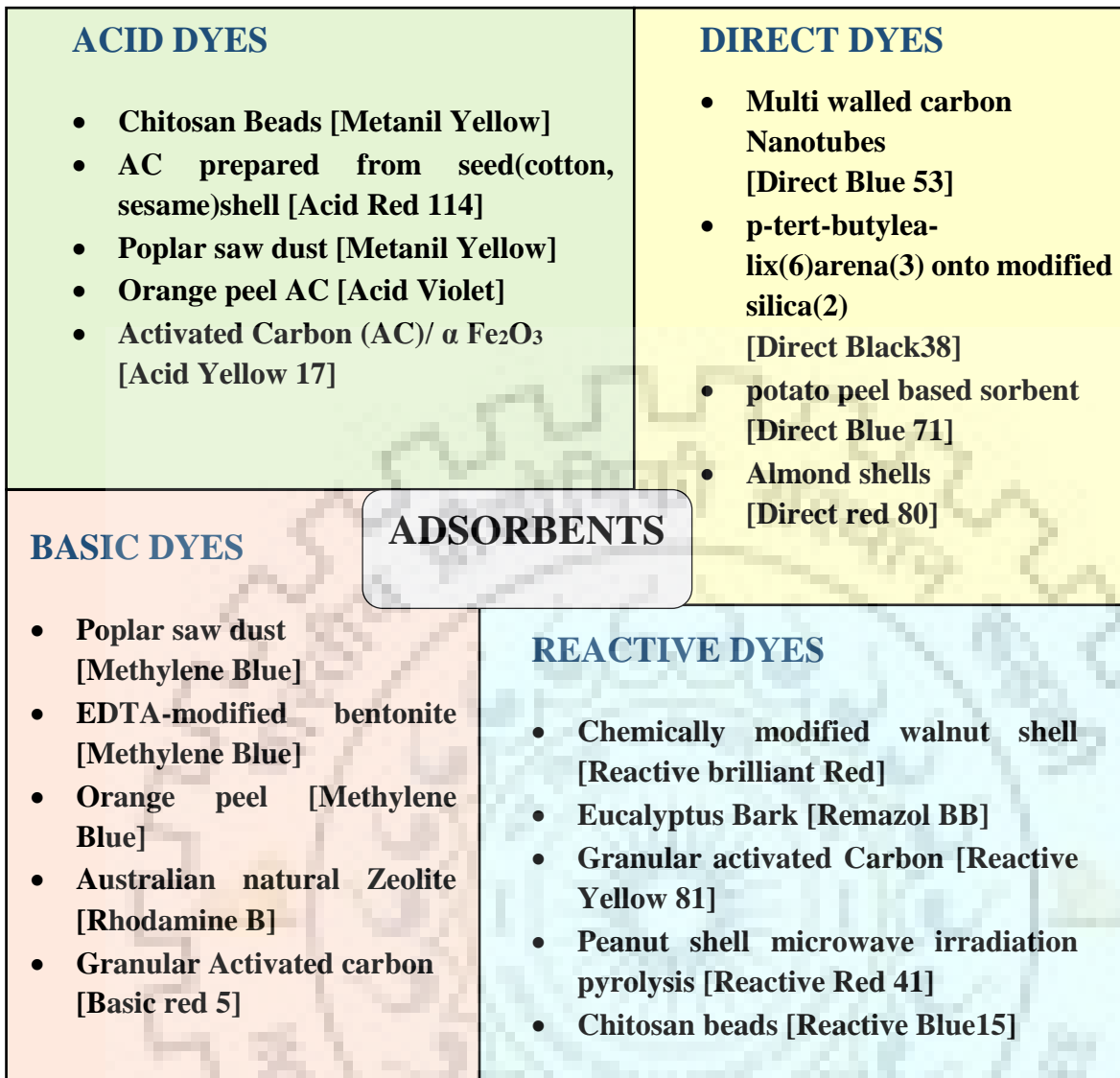


Fig. 2.2 : Adsorbents used for different dyes removal

Activated carbon (AC) is one of the best adsorbent to remove colour from wastewater. It shows high adsorption efficiency due to its high porosity, large surface area, and thermal stability. Adsorptive removal using activated carbon was a widely accepted method due to availability of its large surface area (Sharma et al., 2017b). The size of carbon pore opening is greater than that of pollutant molecules, and hence these molecules are adsorbed as they can easily pass into carbon pores (Malik, 2003). Furthermore, the attraction force of carbon is stronger than the force by which pollutants are dissolved in the solution. Therefore, the pollutants are adsorbed on the surface of the AC. Surface of AC have wide variety of functional groups. Even though, AC is widely used as an effective commercial adsorbent for the treatment of wastewater but it is

expensive due to its high manufacturing cost, which restrains its application most of the time. This has led to search for cheaper, easily available, and efficient raw material for the preparation of AC. Initially when AC was developed, the finest raw material used for manufacturing AC was coal because it was rich in carbon. Since coal is non-renewable natural resource, with limited supply, the focus shifted towards renewable resources for the production of AC. The renewable agricultural waste is considered to be the best option for precursor material as it has high carbon content and sufficient structural strength (Danish and Ahmad, 2018). Although a variety of agricultural waste biomass has been used for the preparation of AC such as agricultural peel (Anastopoulos and Kyzas, 2014), wood biomass (Danish and Ahmad, 2018), lignocellulosic precursors (Reviews, 2018) etc., there is still a need for development of cost-effective, locally available and efficient adsorbents for removal of dyes from wastewater. Various lignocellulosic precursors were used for manufacturing AC.

Stem- date palm, grape (Saeed et al., 2010), oil palm (Rashidi and Yusup, 2017), wheat (Robinson et al., 2002; Zhang et al., 2014) etc.

Shells- almond (Deniz, 2013), coconut (Dias et al., 2007), peanut (Garg et al., 2019), pistachio nut (Dias et al., 2007), pomegranate (Amin, 2009), walnut (Miyah et al., 2018) etc.

Peels- Orange (Fernandez et al., 2014), Banana (Temesgen et al., 2018), lemon (Aichour et al., 2018), sweet lemon etc.

Husks- Rice (Isoda et al., 2014), Barley, Rye etc.

Wastes- Apple pulp, Potato waste, pineapple, Parthenium hysterophorus (Venugopal and Mohanty, 2011), Tea, Soyabean oil cake, Bagasse (Kumari and Das, 2015) etc.

Woods- Pine (Dias et al., 2007), Almond tree, Tamarind (Danish and Ahmad, 2018), Jatropha wood, Eucalyptus (Danish and Ahmad, 2018) etc.

2.5 ACTIVATED CARBON

Activated carbon was used as a purification material since ancient times. In ancient India, drinking water was filtered using activated carbon. Later in early 19th century sugar refining industry in Europe started using it. Today activated carbon is used for removing contaminants in various residential, commercial and industrial applications (“Oxbow Activated Carbon,”)

Production : Activated Carbon production generally involves two processes i.e. carbonization and activation. Activated Carbon is a highly porous carbon which is prepared by chemical or physical activation of a carbon rich material such as wood, coal, lignite etc.

Continuous attempts are made for manufacturing AC from low cost renewable materials. Utilizing agricultural wastes / plant residues as raw material for AC production is a good alternative to commercial AC as activated carbon is expensive since it is made of costly material like coal (Oubagaranadin and Murthy, 2012).

Physical Activation : of AC is done by following processes :

Carbonization : Carbon rich material is pyrolyzed at 600 - 900 °C temperature range in inert atmosphere. Carbonization creates initial porosity as carbon content is enriched.

Activation / Oxidation : After pyrolysis, the carbonized material is heated in the temperature range of 600 - 1200 °C using oxidizing gases like oxygen, steam, CO₂. Porous structure of AC is enhanced which increases the capacity of adsorption (Ahmida et al., 2015).

Chemical Activation : takes place in two steps

- Heating
- Chemical treatment

Heating is usually done in the temperature range of 450 - 900 °C in a furnace, thus less heat is required as compared to physical activation.

Chemical treatment of AC material is done to increase the surface area in which chemicals like acids (HCl, H₂SO₄, H₃PO₄), bases (KOH, NaOH) and other salts (ZnCl₂) are added.

Chemical activation is favoured more than physical activation process due to its shorter activation time, lower temperature, good thermal stability, porous volume and larger surface area.

Classification: AC can be widely classified. A broad classification based on physical characteristics is made as Powdered AC, Granulated AC, AC Fibers, and Impregnated AC.

i. Powdered Activated Carbon (PAC)

The AC below the size of 1.0 mm and physically in powdered form is known as PAC. As per ASTM (American Society for testing and Materials) the particle size of PAC must be less than 0.177 mm or 80 mesh sieve, so they have large surface to volume ratio. PAC cannot be used in column studies because being a fine particle it closely packs the column due to which pressure

drops very large (Kwiatkowski, 2012). Pollutants from all the three phases (solid, aqueous and gas) can be efficiently removed by using PAC.

ii. Granulated Activated Carbon (GAC)

The particle size of GAC is relatively larger than PAC and thus have smaller external surface. 90% of GAC is retained by 80 mesh sieve (180 μm). It is used for column adsorption. Organic compounds, lead, chromium and dyes such as C.I. Reactive black can be removed from water using GAC (Kwiatkowski, 2012).

iii. Activated Carbon Fibers (ACF)

ACF is the latest form of AC. It is used as cloth and felt. As compared to GAC, adsorption capacity of ACF is relatively high. ACF have mostly micropores due to which it has high surface area. Various organic and inorganic contaminants have been removed by using ACF from aqueous and gaseous phases (Kwiatkowski, 2012).

iv. Impregnated Carbon (IC)

To increase the surface activity of AC, doping is carried out with metal, organic or inorganic substances which enhances the adsorption capacity and surface properties. Examples of IC are copper impregnated AC, zinc chloride impregnated AC etc. (Kwiatkowski, 2012).

2.5.1 Peanut Shell Activated Carbon

Peanut, commonly known as groundnut, is a legume crop grown for its edible seeds, which is grown in tropic and subtropical regions. India is the second largest peanut producer after China, with a production of 54.80 lakh tons. Thus, peanuts are abundantly available at an extremely low cost. Peanuts can be used as cattle feed and fuel (Han et al., 2016).

Peanut shell is an agricultural waste and an effective ingredient for preparing activated carbon (Girgis et al., 2002). Peanut shells, are excellent source of cellulose, hemicellulose and lignin (Adeosun et al., 2016) with high liquidity absorbency, chemical inertness and biodegradability. Table 2.3 show the reported surface area of PnsAC.

Peanut shells have high volume and low density (AL-Othman et al., 2012). They are extremely flammable, and thus can be used for producing fireplace logs. They are a good source of fibre and do not contain any harmful material. Scientists have studied methods to produce hydrogen as a fuel by using peanut shells; it is an eco-friendly alternative to various products, such as mulch, for manufacturing biodegradable dish soap and plywood.

Table 2.3 : Recent reported surface area S_{BET} ($m^2 g^{-1}$) for Peanut shell Activated Carbon.

Reference	Adsorbent	S_{BET} ($m^2 g^{-1}$)
(Girgis et al., 2002)	PnsAC	228 - 1177
(Lochananon and Chatsiriwech, 2008)	PnsAC	1000
(AL-Othman et al., 2012)	PnsAC	88.85 - 95.51
(Li et al., 2015)	PnsAC	1195 - 1871
(Wu et al., 2015)	PnsAC	1277
(Xu and Liu, 2008)	PnsAC	807 - 1019
(Georgin et al., 2016a)	PnsAC	370.1 - 395.8
(Zhong et al., 2012)	PnsAC	952.6
(Wu et al., 2013)	PnsAC	1060
(Wilson et al., 2006)	PnsAC	542 - 726
(Zhang et al., 2015)	PnsAC	717 - 1322
(Zhang et al., 2016)	PnsAC	494 - 1533
(Han et al., 2016)	Peanut shell biochar	145.25
(Ahmad et al., 2012)	Peanut shell biochar	3 - 448
(Ricordel et al., 2001)	PnsAC	485

2.6 ALGINATE

Alginate was discovered in 1881 by a British chemist, E.C.C. Stanford. Alginate is a natural polymer occurring in the cell walls of brown seaweeds, in the form of gel which contain calcium, sodium, barium and strontium ions. From various researches, alginate was found to be the best gelling polysaccharide. Alginate is abundantly used in various industries like textile, printing, food, dyeing, pharmaceuticals etc. due to its properties such as gelling, stabilizing, ability to be viscous and water retention capability (Draget, 2009). For the forecast period of 2017 - 2025, the consumption of the product in Asia Pacific is expected to rise at a rate of 5.9% and this forecast is limited to U.S., UK, Canada, France, China, Germany, Japan, India, Brazil ("Global Alginate Industry Trends," n.d.). Variations in physical and chemical properties of alginate are observed due to different sources of species (Draget and Taylor, 2011). There are a wide variety of species from which alginate is extracted amongst them the important species are Laminaria, Macrocystis and Ascophyllum (McHugh, n.d).

Alginate is composed of homopolymeric blocks of (1→4) linked β -D-mannuronate (M) and α -L-guluronate (G) residues, having different sequences and composition of blocks (Ai et al., 2011). Fig.2.3 shows the structural characteristics of alginates, Fig.2.3(a) monomers of alginate are shown, Fig.2.3(b) represents the polymeric chain structure. A molecule of alginate is a block copolymer which has three different blocks G, M and MG having different proportions depending on the source of seaweeds. Alginate have irregular pattern of blocks so the structure of alginate polymer cannot be judged by the knowledge of monomer. Fig.2.3(c) shows the combination of different blocks of alginate. These blocks differ in their properties like G blocks formed by adding calcium ions, are responsible for gel formation. Higher the amount of G blocks greater will be the gel strength. Similarly alginates solubility in acid, is determined by the quantity of MG blocks (McHugh, n.d.).

Alginate can be conveniently altered by physical and chemical methods for improvising its properties, structure and function for utilising in various applications. Properties of alginate can be determined by the composition of guluronic acid and mannuronic acid. Solution to gel transition of alginate takes place in presence of divalent cations (eg. Ca^{2+}).

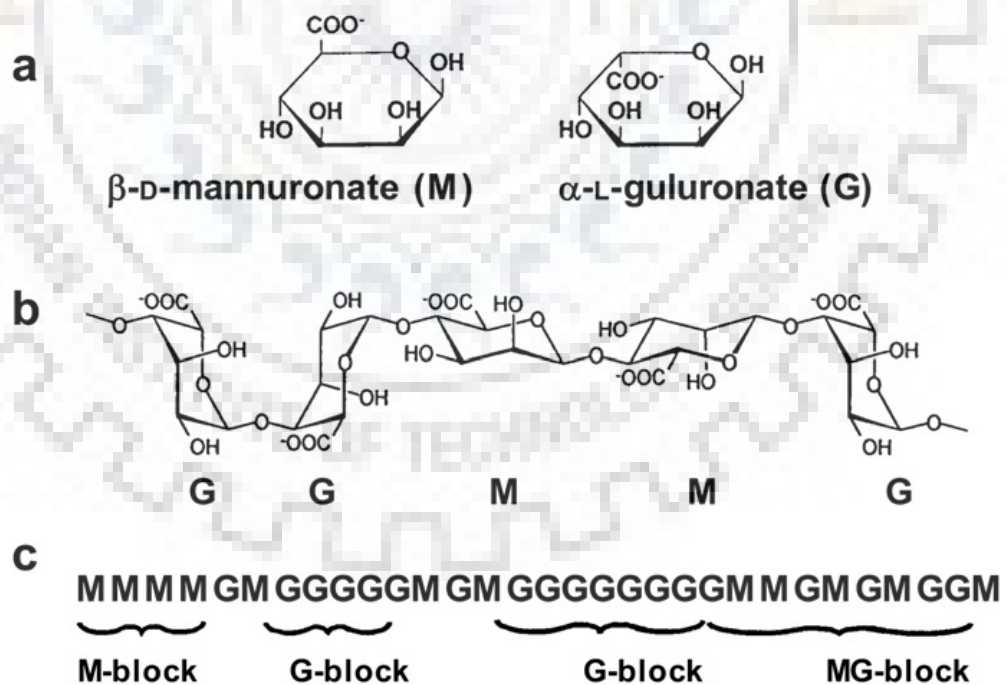


Fig.2.3 : Structural features of alginates: (a) Monomers of alginate, (b) chain Structure, (c) Distribution of blocks (Draget and Taylor, 2011)

Water soluble sodium alginate is converted into calcium alginate by adding sodium alginate solution, drop wise into the bath of calcium chloride solution (Fig.2.4). The key feature of alginate is, preferential ionic interaction with divalent ions which converts it into hydrogel thus forming egg box structure. The cross linked structure of alginate makes it favourable to be used as an immobilization matrix for adsorbent impregnation. Therefore it may be used as a natural and economic adsorbent (Ai et al., 2011).

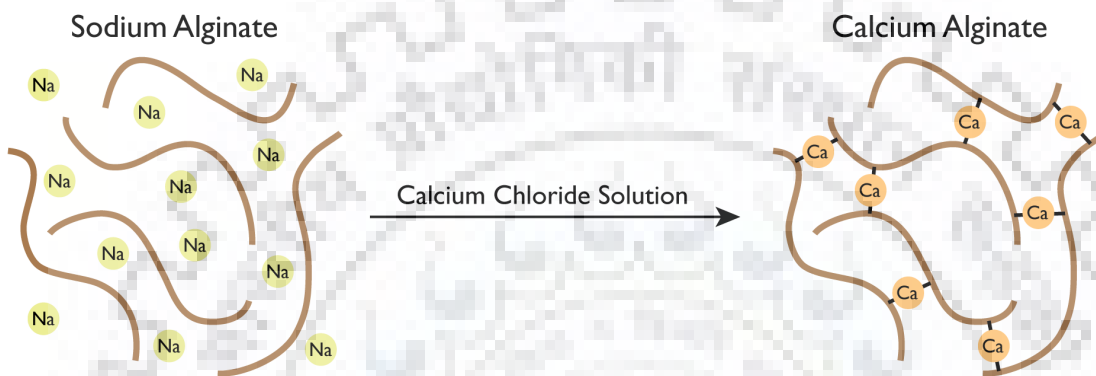


Fig.2.4 : Formation of calcium alginate from sodium alginate

2.7 ADSORPTION STUDIES USING PEANUT SHELL ACTIVATED CARBON

Girgis et al. (2002) manufactured the AC from peanut hull, activated by phosphoric acid, zinc chloride, potassium hydroxide (Girgis et al., 2002). In this study, they carbonized the precursor at 700 – 900 °C then carried out steam pyrolysis at a temperature of 600 °C thus mesopores were generated. With increase in impregnation ratio, porosity also increased. BET surface area of 1177 m² g⁻¹ was found at H₃PO₄/ precursor ratio of 1 with pyrolysis for 3h at 500 °C. BET surface area of 420 m² g⁻¹ was reported with impregnation of 50 % ZnCl₂ and pyrolyzed for 6h at 300 °C. BET surface area of 228 m² g⁻¹ was obtained for 1:1 KOH impregnation, followed by 3h pyrolysis at 500 °C.

Lochananon and Chatsiriwech (2008) produced activated carbon using peanut shell using (10-60 wt %) H₃PO₄ solution at 200 °C temperature for 2h (Lochananon and Chatsiriwech, 2008). The yield of reaction decreased from 60 % to 45 % while the BET surface area increased upto

100 m² g⁻¹ by increasing H₃PO₄ acid concentration from 10 - 60 wt %. Increase in surface area is proportional to increase in adsorptive properties.

Othman *et al.* (2012) prepared AC by chemical activation of peanut shell with KOH and removed hexavalent chromium (AL-Othman *et al.*, 2012). The reported BET surface area was 88.85 to 95.51 m² g⁻¹ for oxidized and unoxidized sample. Kinetic study showed that Pseudo first order and second order model followed appropriately. Equilibrium data concludes that Langmuir and Freundlich models were most suitable. The estimated Langmuir monolayer adsorption capacity was 16.26 mg g⁻¹. Negative value of ΔG° revealed that the process was spontaneous. ΔG° value decreased with increase in temperature. Positive value of ΔS° represents disorderness within the system.

Wu *et al.* (2015) prepared peanut shell activated carbon by using KOH as activator under microwave heating (Wu *et al.*, 2015). If KOH / peanut shell mass ratio was 1 and 600 W microwave power was utilized for 8 minutes, the surface area (S_{BET}) was found to be 1277 m² g⁻¹. An efficient and simple approach for the preparation of low cost AC was found by microwave heating of peanut shell, activated by KOH.

XU and LIU (2008) studied the effect of heavy metal ion Pb²⁺ (Xu and Liu, 2008). 58 % phosphoric acid was used in 1:1 mass ratio (peanut shell : H₃PO₄), heated upto 550 °C for 2h in nitrogen atmosphere to prepare AC. PnsAC was treated with HNO₃ (5 %, 20 % and 50 %) to improve the properties. FTIR confirmed that more number of groups are attached after the treatment. Carboxyl groups, carbonaceous phosphor compound, phosphate ester etc. were found. Monolayer Langmuir adsorption capacity of PnsAC was 24.02 mg g⁻¹. The increase in adsorption capacity was due to pore widening.

Georgin *et al.* (2016) prepared PnsAC by conventional pyrolysis (CP) and they further prepared AC by using microwave irradiation and pyrolysis (MWP) (Georgin *et al.*, 2016a). In above two types of preparation the second preparation was found to be more appropriate in removing Direct Black-38 (DB-38) and Reactive Red-141 (RR-141) dyes from synthetic wastewater. BET surface area of CP sample, MWP sample was 370.10 and 395.80 m² g⁻¹ respectively. FTIR study revealed the presence of –OH stretching, C-H stretching, C-C stretching, -C=C stretching and C=C of aromatic group etc. C-O group in carboxylic and alcoholic groups corresponded to lignin which was due to peanut shell. Adsorption was found maximum at pH 2.5. Pseudo second order kinetic model and Sips isotherm model were found fit. Maximum monolayer adsorption capacity was found to be 141.3 for DB-38 and 307.5 for RR-141 dye.

Zhong et al. (2012) utilized peanut shell for production of AC through microwave induced phosphoric acid activation (Zhong et al., 2012). Different process variables such as radiation time, input power and H₃PO₄ concentration were optimized by RSM. The optimum conditions were 33.04 volume % of H₃PO₄, 500.07 W microwave power and 9.8 minute radiation time and under these conditions the yield was 42.12 %. BET surface area of PnsAC was 952.60 m² g⁻¹ having pore volume 0.8807 cm³ g⁻¹. Langmuir monolayer adsorption capacity of AC was 149.25. The process followed Pseudo second order kinetics and intra-particle diffusion model.

Wu et al. (2013) prepared PnsAC in fluidised bed reactor kept at high temperature, by carbon dioxide activation (Wu et al., 2013). 225.8 mg g⁻¹ of MB was produced at optimized condition of 900 °C activation temperature and 5h activation time. Phenazone uptake yield was 26.157 %. The BET surface area was 1060 m² g⁻¹ and the pore volume 0.8021 cm³ g⁻¹ under optimized condition. FTIR showed -COOH, -OH and -R functional groups. The ionisable groups (carboxyl and hydroxyl) were able to interact with positive dye ions. So adsorption does not depend only on surface area but functional group present on surface adsorption will also be responsible for adsorption. Kinetic data was found fit to Pseudo second order model. The quality of AC was as per the British Pharmacopoeia and the United States Pharmacopoeia Standards for AC. Hence the developed PnsAC can be used commercially for medical use.

Wilson et al. (2006) prepared PnsAC from peanut shell by pyrolysis in N₂ environment for the adsorption of Cd²⁺, Cu²⁺, Pb²⁺, Ni²⁺ and Zn²⁺ (Wilson et al., 2006). Author compared three commercial type of AC (DARCO 12x20, NORIT C GRAN and MINOTAUR) with the prepared PnsAC. Surface area of prepared PnsAC and other commercial activated carbon were 542 – 815 m² g⁻¹. In house produced PnsAC (800 °C activation temperature, 4h activation time and non-crushed) was found best and subsequently NORTI C GRAN, for removing various metal ions.

Zhang et al. (2015) prepared magnetic MPSAC via single step procedure in presence of potassium carbonate and ferric oxide (S. Zhang et al., 2015). The samples were first carbonized at 300 °C for 1h duration then activated at 650 – 800 °C for 0.5 - 3h. The surface area was dependent on activation time and activation temperature. The Maximum surface area of MPSAC was 1322 m² g⁻¹ at 650 °C activation temperature when activated for 3h. The Fe was converted into Fe₃C.

Zhang et al. (2016) prepared magnetic peanut shell activated carbon (MPSAC) to observe the impact of K₂CO₃ and Fe₃O₄ on the porosity development (Zhang et al., 2016). During impregnation potassium carbonate underwent anionic hydrolysis. Formation of KOH broke the

key ester linkages among lignin and carbohydrates and one part of lignin was removed. Weight loss peak was shifted from 350 °C to 255 °C by the addition of K₂CO₃ during pre-carbonization. During activation stage various compounds were formed like K₂CO₃, 15 H₂O, K₂O and K. These compounds developed micropores in MPSAC. Fe₃O₄ acted as the source of Fe and activation promoting agent which formed Fe₃C.

Han et al. (2016) made magnetic char from peanut hull using FeCl₃ and pyrolyzed at (450 – 650 °C). Cr(VI) was adsorbed using the magnetic char (Han et al., 2016). Langmuir monolayer adsorption capacity was 77.54 mg g⁻¹. The coefficient of determination (R²) is maximum for Elovich and Pseudo second order model. BET surface area for magnetic biochar pyrolysed at 650 °C, was 145.25 m² g⁻¹. However economic feasibility must be studied before commercial production of magnetically recoverable biochar.

Ricordel et al. (2001) peanut husks (PHC) was used for manufacturing activated carbon for the removal of Pb²⁺, Zn²⁺, Ni²⁺ and Cd²⁺ (Ricordel et al., 2001). The calculated surface area of PHC was 485 m² g⁻¹. FTIR study revealed carboxyl group, phenolic hydroxyl groups and carbonyl groups. At equilibrium, the metal ions adsorbed were in the order of Cadmium < Nickel < Zinc < Lead. Langmuir adsorption isotherm model (R²=0.999) was found fit for the metal ion removal study using PHC.

2.8 ACID YELLOW – 36 (AY-36) ADSORPTION STUDIES

Mittal et al. (2008) removed AY-36 from aqueous solution by using De-oiled soya and bottom ash (Mittal et al., 2008). Batch and column studies were performed for lethal dye removal. Langmuir and Freundlich represented the isotherm data well. The adsorption followed Pseudo first order reaction. Film diffusion mechanism was observed in the process. The process was spontaneous since the value of ΔG^o was negative. De-oiled soya and Bottom ash can be used commercially for removing AY-36 from wastewater.

Pekkuz et al. (2008) investigated the adsorption of AY-36 by poplar saw dust, a low cost adsorbent (Pekkuz et al., 2008). Cationic dyestuffs were more adsorbed than anionic dyestuffs. Kinetic models and intra-particle diffusion model were studied for three different temperatures, 293 K, 313 K and 333 K. Langmuir isotherm was found fit (R²>0.98). The calculated monolayer adsorption capacity was 3.57×10⁻³ mol g⁻¹. Thermodynamic parameters (ΔG^o, ΔH^o and ΔS^o) were estimated.

Chiou and Chuang (2006) studied the adsorption of anionic dye using chitosan beads which were chemically cross-linked (Chiou and Chuang, 2006). The adsorption capacities was 1334 mg g⁻¹ for AY-36. Langmuir model was found fit with adsorption data ($R^2 > 0.996$). First order reaction was followed at lower concentration and second order reaction was followed at higher concentration. Adsorption was found to be maximum at lower pH. The competitive adsorption favoured the AY-36 adsorption.

2.9 DIRECT BLUE – 86 (DB-86) ADSORPTION STUDIES

Dutta et al. (2012) studied adsorption of DB-86 through fixed bed column (Dutta et al., 2012). The adsorbent was made from composite of alumina and AC (using microwave). For batch adsorption, Langmuir ($R^2 = 0.98$), Temkin ($R^2 = 0.96$) and Freundlich ($R^2 = 0.93$) were found fit. Estimated monolayer Langmuir adsorption capacity was 500.16 mg g⁻¹. The AC bed height in the column was (5.04 - 10.16) cm. The bed capacity was estimated to be 142.67 mg L⁻¹.

Nemr et al. (2009) investigated orange peel activated carbon for the treatment of DB-86 (Direct Fast Turquoise Blue GL) dye from synthetic wastewater (Nemr et al., 2009). Percentage dye adsorption is proportional to adsorbent dose. Optimum pH value was 2. Adsorption rate was maximum in first 30 minutes. Pseudo second order kinetics ($R^2 > 0.99$) was the best model to represent the kinetic data. Langmuir monolayer adsorption capacity was 33.78 mg g⁻¹. Langmuir, Temkin, Dubinin-Radushkevich (D-R) isotherm models were found better fit than Redlich-Peterson and Freundlich model. The optimum conditions were 100 mg L⁻¹ dye concentration at pH 2 with 6 g L⁻¹ adsorbent dose. At room temperature maximum removal was 92 %. Orange peel AC can be used commercially in the treatment of DB-86 dye.

2.10 MOTIVATION FOR THE PROPOSED RESEARCH WORK

On the basis of literature review, following observations have been made:

- i. Peanut shells were used to prepare AC in the past and PnsAC (Peanut shell Activated Carbon) thus prepared was used in adsorption process for removing dyes and heavy metals from wastewater. However it was not used for the removal of AY-36 and DB-86 dye from wastewater.

- ii. There are very few studies, available for the adsorption of dye using immobilized beads of alginate coated Peanut shell Activated Carbon (PnsAC-alginate). To our Knowledge, there is no single study reported on the adsorption of DB-86 dye using PnsAC-alginate.

In view of the above observations, objectives of the present research work as stated in the Chapter I, have been formulated and pursued in the thesis.



Table 2.4 : Comparison of Adsorption Isotherms, Kinetic models and Adsorption capacities of PnsAC

S.No.	Adsorbate	pH	Temp. (°C)	Initial adsorbent concentration	Adsorption capacity (mg g ⁻¹)	Isotherm	Kinetic model proposed	Reference
1	Cr(VI)	2 -10	20, 30, 40	1 g L ⁻¹	16.26	Langmuir, Freundlich	Pseudo First order, Pseudo Second order	(AL-Othman et al., 2012)
2	Pb ²⁺	2.5	25	10 g L ⁻¹	35.46	Langmuir, Freundlich	-	(Xu and Liu, 2008)
3	Direct black	2.5	25	0.3 g L ⁻¹	110.6	Langmuir, Freundlich, Redlich Peterson and Sips	Pseudo First order, Pseudo Second order	(Georgin et al., 2016a)
4	Reactive red	2.5	25		284.5			
5	Remazol brilliant blue R	-	20	1.6 g L ⁻¹	149.25	Langmuir, Freundlich, Temkin	Pseudo First order, Pseudo Second order	(Zhong et al., 2012)
6	Phenazore	-	25	6.67 g L ⁻¹	421.5	-	Pseudo First order, Pseudo Second order	(Wu et al., 2013)
7	Methylene blue	-	25		225.8	-		
8	Cd ²⁺ , Cu ²⁺ , Pb ²⁺ , Ni ²⁺ , Zn ²⁺	4.8	-	10 g L ⁻¹	37.43, 66.66, 240.55, 34.63, 38.31	Langmuir	-	(Wilson et al., 2006)
9	Trichloroethylene	7	25	0.3 g L ⁻¹	50.01	Langmuir, Freundlich	-	(Ahmad et al., 2012)
10	Se(IV)	1.5 - 7	-	-	42.96	Langmuir	First order rate expression	(El-Shafey, 2007)

Table 2.5 : Adsorption studies for removing AY-36 dye from wastewater

S.No.	Adsorbent	pH	Temp. (°C)	Initial dye concentration	Adsorption capacity (mg g ⁻¹)	Isotherm	Kinetic model proposed	Reference
1	Cross linked Chitosan beads	4	30	2.77 g L ⁻¹	1334	Langmuir	First order, Second order	(Chiou and Chuang, 2006)
2	Sawdust	6.23	25, 35, 45	0.0093 g L ⁻¹	1.310	Langmuir	Pseudo First order, Pseudo Second order, Intraparticle diffusion model	(Pekkuz et al., 2008)
3	Bottom ash, Deoiled soya	2	30, 40, 50	0.037 g L ⁻¹	-	Langmuir, Freundlich	First order	(Mittal et al., 2008)
4	Graphene oxide	7	25, 35, 45	(80 - 800) mg L ⁻¹	71.62	Langmuir, Henry, Temkin, Freundlich, Dubinin-Radushkevich	Pseudo First order, Pseudo Second order	(Guo et al., 2013)
5	Grape industrial processing activated carbon	6.23	30	(200 - 900) mg L ⁻¹	386	Langmuir, Freundlich	-	(Saygılı et al., 2015)

Table 2.6 : Adsorption studies for removing dyes from wastewater

S.No.	Reference	Adsorbent	Adsorbate / Object of study	Operating Mode	Inference
1.	(Suteu et al., 2017)	waste seashell powder	brilliant Red HE-3B reactive dye	Batch	<ul style="list-style-type: none"> The maximum monolayer adsorption capacity was 294.1 mg g⁻¹ at 60 °C. Maximum removal was obtained in seven hours' time. Langmuir, Freundlich and Dubinin-Radushkevich models were used to analyse the isotherm data. Kinetic data found to follow pseudo second order model with R² > 0.99.
2.	(Leah et al., 2018)	EDTA-modified bentonite	methylene Blue (MB) and Cu(II) ions	Batch	<ul style="list-style-type: none"> The observed Langmuir monolayer adsorption capacity was 160 and 27 mg g⁻¹ for MB and Cu(II) respectively. pH_{ZPC} of EDTA modified bentonite was found to be 2.3 Langmuir, Freundlich, Temkin and D-R models were applied on the isotherm data. The negative value of E_a for MB and Cu(II) were -10 and -41 KJ mol⁻¹ which denotes exothermic adsorption and process to be more effective at lower temperature.

S.No.	Reference	Adsorbent	Adsorbate / Object of study	Operating Mode	Inference
3.	(Fernandez et al., 2014)	orange peel activated carbon	methylene blue and rhodamine B	Batch	<ul style="list-style-type: none"> Activated carbon was made from orange peel using H_3PO_4 as activator. BET surface area was $1090 \text{ m}^2 \text{ g}^{-1}$ Kinetic data was best presented by Pseudo second order with R^2 value 0.971 and 0.998 for methylene blue and rhodamine B.
4.	(Prola et al., 2013)	multi-walled carbon nanotubes (MWCNT) and powder activated carbon (PAC)	direct blue 53	Batch	<ul style="list-style-type: none"> Effect of initial pH, time of contact and temperature were studied. The optimum pH was 2 for MWCNT and PAC. Time to achieve equilibrium was 3h and 4h for MWCNT and PAC. The maximum adsorption capacity was 409.4 and 135.2 mg g^{-1} for MWCNT and PAC respectively. Synthetic simulated dye house effluent containing five dyes was used. The observed pH_{ZPC} was 7.00 and 7.80 for MWCNT and PAC.

S.No.	Reference	Adsorbent	Adsorbate / Object of study	Operating Mode	Inference
5.	(Cao et al., 2014)	chem-modified walnut shell (MWNS)	reactive brilliant red K-2BP	Batch	<ul style="list-style-type: none"> The monolayer Langmuir adsorption capacity was found to be 568.18 mg g⁻¹. Langmuir adsorption isotherm was most suitable isotherm model as R² > 0.999. Separation factor R_L was less than 1. As R² > 0.999, the Pseudo second kinetics was most suitable kinetic model.
6.	(Ranjithkumar et al., 2014)	activated carbon/ α -Fe ₂ O ₃	acid yellow 17	Batch	<ul style="list-style-type: none"> Langmuir monolayer adsorption capacity was estimated to be 333.30. Pseudo-second order rate constant for AC and modified AC was R² > 0.98 and q_e exp. was very close to q_e cal. Freundlich, Langmuir and Temkin models were applied on the isotherm data.
7.	(Kamboh et al., 2014)	p-tert-butylcalix[6]arene (3) onto	direct black-38	Batch	<ul style="list-style-type: none"> FTIR, SEM and TGA study confirmed the synthesis of new adsorbent. Maximum adsorption was 91 % at pH 9.0

S.No.	Reference	Adsorbent	Adsorbate / Object of study	Operating Mode	Inference
		modified silica (2)			
8.	(Mittal et al., 2010)	bottom ash (BA), de-oiled soya (DOS)	crystal violet	Batch/Column	<ul style="list-style-type: none"> • If pH was increased from 2-4 there is sharp increase in adsorption. • 4h time was required to achieve saturation. • Regression coefficient was 1 for Pseudo second order model.
9.	(Dil et al., 2017)	zinc (II) oxide nanorods loaded on activated carbon (ZnO-NRs-AC) to	Cd ²⁺ , Co ²⁺ , methylene blue (MB) and crystal violet (CV)		<ul style="list-style-type: none"> • Langmuir isotherm was found suitable isotherm model with monolayer adsorption capacity of 97.1, 92.6, 83.9 and 81.6 mg g⁻¹ for cadmium, cobalt, methylene blue and crystal violet respectively. • The optimum dose predicted by RSM was 25, 24, 18 and 14 mg L⁻¹ for cadmium, cobalt, methylene blue and crystal violet respectively. • Artificial neural network (ANN) was applied with 14 neurons. • Pseudo second order and intra-particle diffusion model were suitable kinetic model.

S.No.	Reference	Adsorbent	Adsorbate / Object of study	Operating Mode	Inference
10.	(Khani et al., 2018)	γ -Fe ₂ O ₃ -2-HEAS	direct Blue 71	Batch	<ul style="list-style-type: none"> Langmuir adsorption capacity was 47.60 mg g⁻¹. New activated carbon γ-Fe₂O₃-2-HEAS was developed. Freundlich isotherm model was found to be most suitable as R² > 0.98. Pseudo first order and Pseudo second order kinetic model were found suitable as R² > 0.99.
11.	(Maleki et al., 2016)	potato peel-based sorbent	direct blue 71	Batch	<ul style="list-style-type: none"> Taguchi method was used for experimental design. Maximum adsorption capacity was 448 mg g⁻¹. The ANN model was having five neurons input layers.
12.	(Saygılı et al., 2015)	grape waste activated carbon	methylene blue and Metanil yellow	Batch	<ul style="list-style-type: none"> Maximum surface area was obtained at 6 :1 impregnation ratio, 600 °C activation temperature, 60 minutes of activation time. The yield of activated carbon was 44.15 % and the observed surface area was 1455 m² g⁻¹. The monolayer adsorption capacity for Methylene blue was 417 mg g⁻¹ and 386 mg g⁻¹ for Metanil yellow.
13.	(Jain et al., 2010)	AC and activated	naphthol yellow S	Batch	<ul style="list-style-type: none"> BET surface area was 929.7 and 326.5 for AC and ADM respectively.

S.No.	Reference	Adsorbent	Adsorbate / Object of study	Operating Mode	Inference
		de-oiled mustard (ADM)			<ul style="list-style-type: none"> • pH_{ZPC} for ADM was 8.2. • Maximum adsorption was at 50 °C for AC, it followed the order 30 °C < 40 °C < 50 °C. Adsorption by ADM was exothermic in nature. • Pseudo first order kinetic model agreed well.
14.	(Mall et al., 2006)	fertilizer plant waste carbon (WC)	auramine-O (AR), congo red (CR), orange-G (OG), and methyl violet (MV)	Batch	<ul style="list-style-type: none"> • The BET surface area of low cost fertilizer plant waste carbon (WC) was 357 m² g⁻¹. • The polar group attached on the surface of AC gave cation exchange capacity to it. • The optimum pH was 7.0. • The adsorption kinetics followed Pseudo second order kinetics. • pH_{ZPC} value was 7.2.
15.	(Sarkar et al., 2014)	amylopectin and poly(acrylic acid) (AP-g-PAA)	malachite green	Batch	<ul style="list-style-type: none"> • Synthesized graft copolymer (adsorbent) was biodegradable. • pH_{ZPC} for (AP-g-PAA) was 5.51. • Pseudo second order model was having higher correlation coefficient and lower error value.

S.No.	Reference	Adsorbent	Adsorbate / Object of study	Operating Mode	Inference
					<ul style="list-style-type: none"> Monolayer adsorption capacity has been found to be 352.11 mg g⁻¹.
16.	(Othman et al., 2018)	magnetic graphene oxide (MGO)	methylene blue	Batch	<ul style="list-style-type: none"> Langmuir and Freundlich represented the isotherm data with R² > 0.97. Pseudo second order kinetics was found to be most suitable. Langmuir monolayer adsorption capacity was 1666.67 mg g⁻¹.
17.	(Liao et al., 2012)	microwave (MW) modified bamboo charcoal (BC)	methylene blue (MB) and acid orange 7 (AO7)	Batch/Column	<ul style="list-style-type: none"> Removal of MB and AO7 was studied on MW modified BC. Freundlich and Dubinin-Radushkevich model were found suitable. Adsorption was suitable at pH below 5 and below 3 for MB and AO7 respectively. Thermodynamic analysis revealed the process to be spontaneous and endothermic.
18.	(Luo et al., 2018)	cucurbiturils (CB[8]s)	acidic blue 25 (AB25)		<ul style="list-style-type: none"> Langmuir and Freundlich represented the isotherm data. Maximum monolayer adsorption capacity was 434.8 mg g⁻¹. Kinetic data was represented by Pseudo second order model with R² > 0.99.

S.No.	Reference	Adsorbent	Adsorbate / Object of study	Operating Mode	Inference
					<ul style="list-style-type: none"> BET surface area of CB [8] was $3.7\text{m}^2\text{ g}^{-1}$. Thermodynamic data revealed the process to be spontaneous and exothermic.
19.	(Humelnicu et al., 2017)	zeolite tuff	basic Blue 41	Batch	<ul style="list-style-type: none"> The kinetics study showed that Pseudo second order model follows the adsorption data. Maximum adsorption was 95.7 % at pH 8. Langmuir monolayer adsorption capacity was 192.31mg g^{-1} at $50\text{ }^\circ\text{C}$ and pH 5. Langmuir isotherm best described the equilibrium data. Temperature increase from $8\text{ }^\circ\text{C}$ to $50\text{ }^\circ\text{C}$ favoured the adsorption. The data of Thermodynamic study revealed the process to be spontaneous and endothermic.
20.	(Gong et al., 2005)	powdered peanut hull	amaranth (Am), sunset yellow (SY) and fast green FCF (FG).		<ul style="list-style-type: none"> All three dyes were removed efficiently at pH = 2. Monolayer adsorption capacity was 14.90, 13.99 and 15.60 mg g^{-1} for Amaranth, sunset yellow and fast green FCF. Pseudo first order rate kinetics fits the kinetic data. Isotherm data followed Langmuir and Freundlich model.

S.No.	Reference	Adsorbent	Adsorbate / Object of study	Operating Mode	Inference
21.	(Zhao et al., 2017)	cationic surfactant-modified peanut husk	light green anionic dye	Batch	<ul style="list-style-type: none"> • Adsorption is favoured at pH 2 - 4. • Pseudo first order kinetic equation describes the kinetic data. • Langmuir isotherm was found suitable with monolayer adsorption capacity of 146.2 mg g⁻¹ at 303 K. • Thermodynamic study showed the adsorption process to be spontaneous and exothermic.
22	(Auta and Hameed, 2011)	waste tea activated carbon (WTAC)	acid blue 25 (AB25)	Batch	<ul style="list-style-type: none"> • For Batch studies of Acid blue 25 dye, initial concentration (50 - 350 mg L⁻¹), initial pH (2-12), temperature (30 °, 40 °, 50 °C) were taken. • Langmuir adsorption isotherm was most suitable equilibrium isotherm with monolayer adsorption capacity of 203.34 mg g⁻¹. • The calculated pH_{ZPC} was 7.2. • Maximum adsorption was at pH 2. • Positive value of entropy ΔS° indicates the increase in randomness at solid-liquid interface. • BET surface area was 820 m² g⁻¹.

S.No.	Reference	Adsorbent	Adsorbate / Object of study	Operating Mode	Inference
23	(Doulati Ardejani et al., 2008)	almond shells	direct red 80 (DR 80)	Batch	<ul style="list-style-type: none"> • Concentration of Direct Red was taken (50 - 150) mg L⁻¹ at pH 2 and 97 % removal was obtained. • Maximum adsorption capacity was found to be 22.422 mg g⁻¹ • The time required to achieve equilibrium was 300 minutes. • Langmuir, Freundlich and BET isotherm equilibrium were applied on adsorption isotherm data and R² > 0.8639 was obtained. • BET surface area was 10.5 m² g⁻¹. • For Pseudo second order kinetic model, R² varies from 0.9986 to 1.
24	(Hussain et al., 2018)	nitrogen-enriched carbon sheet (NECS)	methyl blue dye		<ul style="list-style-type: none"> • Nitrogen enriched carbon sheet (NECS) was prepared from sodium gluconate (as a carbon source). • High surface area 604 m² g⁻¹. • Langmuir adsorption isotherm represents the adsorption process with the adsorption capacity of 847 mg g⁻¹. • NECS shows increase in adsorption capacity from 34 to 701 mg g⁻¹ when the pH was decreased from 10 to 2.

S.No.	Reference	Adsorbent	Adsorbate / Object of study	Operating Mode	Inference
					<ul style="list-style-type: none"> Upto five adsorption desorption cycles, no loss in efficiency was observed.
25	(El Ashtoukhy, 2009)	loofa egyptiaca activated carbon (LE),	direct blue 106	Batch	<ul style="list-style-type: none"> Loofa egyptiaca (LE) was used for manufacturing three different types of adsorbents namely LE and two low cost activated carbon (LE_{C1} and LE_{C2}). Experimental data were examined by Langmuir, Freundlich and Temkin isotherms with $R^2 > 0.965$. The value of dimensionless equilibrium parameter R_L was less than 1. Kinetic data confirms Pseudo first order and Pseudo second order models with $R^2 > 0.97$.
26	(Wang and Zhu, 2006)	an australian natural zeolite	rhodamine B methylene blue	Batch	<ul style="list-style-type: none"> Kinetic studies showed that Pseudo second order kinetic model fits the data with R^2 close to 0.999. Langmuir and Freundlich models were found to be most suitable models. Process is spontaneous as ΔG° was found to be negative. Positive value of ΔS° showed disorder at the solid-solution interface.

S.No.	Reference	Adsorbent	Adsorbate / Object of study	Operating Mode	Inference
					<ul style="list-style-type: none"> BET surface area was $16.0 \text{ m}^2 \text{ g}^{-1}$.
27	(Belaid et al., 2013)	granular activated carbon	acid blue 113 (AB), basic red 5 (BR) and reactive yellow 81 (RY)	Batch	<ul style="list-style-type: none"> The estimated equilibrium time was $\leq 1\text{h}$ for RY and 4h for AB and BR. Kinetic data was perfectly fitted to Pseudo second order with $R^2 > 0.98$. Surface area was $1100 \text{ m}^2 \text{ g}^{-1}$ for GAC. Elovich model very well describes the experimental results.
28	(De Castro et al., 2018)	modified bentonite	methylene blue dye (MB) and copper ions (Cu(II))	Batch	<ul style="list-style-type: none"> Ethylene diamine tetra acetic acid modified Phillippine bentonite, a low cost material for the removal of Methylene Blue (MB) and Cu(II). Pseudo second order kinetics was found to fit the kinetic data with $R^2 > 0.99$. Thermodynamic study reveals the process to be spontaneous as ΔG° value was negative.
29	(Sandoval et al., 2017)	TNT	methylene blue dye		<ul style="list-style-type: none"> BET surface area was found to be $206 - 239 \text{ m}^2 \text{ g}^{-1}$.

S.No.	Reference	Adsorbent	Adsorbate / Object of study	Operating Mode	Inference
30	(Khaled et al., 2009)	activated carbon from orange peel	direct N blue-106 (DNB)	Batch	<ul style="list-style-type: none"> • Direct Navy Blue (DNB) was removed from wastewater using adsorption. • Langmuir and Freundlich model reasonably represents the equilibrium adsorption data ($R^2 > 0.97$) so adsorption process is heterogenous. • The maximum adsorption capacity was 107.53 mg g^{-1} for 150 mg L^{-1} DNB and 2 g L^{-1} of AC. • Pseudo second order was found fit with $R^2 > 0.99$.
31	(He et al., 2018)	paddle wheel ligand, $\text{H}_3[\text{Mn}_3\text{O}_3(\text{BTB})]$ (Mn-BTB, HBTB=1,3,5-tris(4-carboxyph	cationic dyes (methylene blue (MB) and rhodamine B (RhB)) and an anionic dye (methyl orange (MO))		<ul style="list-style-type: none"> • Metal organic framework based on manganous (II) ions and a paddle wheel ligand, $\text{H}_3[\text{Mn}_3\text{O}_3(\text{BTB})]$ (Mn-BTB, HBTB=1,3,5-tris(4-carboxyphenyl) benzene acid) was synthesized. • 120 minutes time was required to achieve equilibrium. • The BET surface area and pore volume of Mn-BTB were $5.089 \text{ m}^2 \text{ g}^{-1}$ and $0.04175 \text{ cm}^3 \text{ g}^{-1}$.

S.No.	Reference	Adsorbent	Adsorbate / Object of study	Operating Mode	Inference
		nyl)benzene acid)			
32	(Kumar and Ahmad, 2011)		crystal violet (CV)		<ul style="list-style-type: none"> The maximum monolayer adsorption capacity was 64.93, 227.27 and 277.7 mg g⁻¹ at 30°, 40° and 50° C respectively. The estimated equilibrium time was 150 minutes. ΔG° was found to be (-ve) which indicated feasibility of reaction.
33	(Angela et al., 2018)		acetaminophen or acetyl-para-aminophenol (APAP) methylene blue (MB)		<ul style="list-style-type: none"> Kinetic data was found fit by first order kinetics (0.986-0.987) and Pseudo second order kinetics (0.998). ΔG° value obtained was negative indicating spontaneity of the reaction. ΔH° values were 16.5 and 74.7KJ mol⁻¹. pH_{ZPC} was found to be 10. The surface functional group –OH and –COOH were found.
34	(Sham and Notley, 2018)	graphene exfoliated	cationic methylene blue		<ul style="list-style-type: none"> The maximum adsorption capacity was 782.3 mg g⁻¹ at 20 °C. Adsorption data was modelled by Langmuir and Freundlich adsorption isotherm.

S.No.	Reference	Adsorbent	Adsorbate / Object of study	Operating Mode	Inference
					<ul style="list-style-type: none"> Pseudo second order model was found fit for the kinetic data.
35	(Ghaedi et al., 2013)	zinc oxide nanoparticle s loaded on activated carbon (ZNO-NP-AC)	brilliant green (BG) solid		<ul style="list-style-type: none"> The entropy was $136.59 \text{ J mol}^{-1} \text{ K}^{-1}$. Langmuir isotherm model show high correlation coefficients ($R^2 = 0.994$). The monolayer adsorption capacity was 142.9 mg g^{-1}. The calculated ΔG° value were -3026 to $-8942.8 \text{ J mol}^{-1}$ which indicated the spontaneity of the reaction. Positive ΔH° value indicated endothermic nature of adsorption. ΔS° is positive so adsorption was random.
36	(Senthil Kumar et al., 2010)	cashew nut shell (CNS)	congo red (CR) dye		<ul style="list-style-type: none"> The equilibrium time was 90 minutes. The maximum removal was obtained at $\text{pH} \leq 3$ (due to electrostatic attraction). ΔG° was negative, values lies between -30317 to -10.576. Redlich-Peterson, Koble-Corrigan model, Sips and Toth model represented the isotherm data with $R^2 > 0.999$.
37	(Dogan et al., 2007)	sepiolite	methyl violet (MV) and		<ul style="list-style-type: none"> Equilibrium was attained in 3 hours.

S.No.	Reference	Adsorbent	Adsorbate / Object of study	Operating Mode	Inference
			methylene blue (MB)		<ul style="list-style-type: none"> The adsorption kinetics was best described by Pseudo second order model with $R^2 > 0.99$. Surface area of Sepiolite was $342 \text{ m}^2 \text{ g}^{-1}$.
38	(Inyang et al., 2014)	carbon nano tubes (CNT)	methylene blue (MB)	Batch	<ul style="list-style-type: none"> MB sorption capacity was 6.2 mg g^{-1}. Electrostatic attraction was dominant mechanism for the sorption of MB. Thermo stability of the biochars were increased by the addition of carbon nano tubes (CNT). Langmuir model fits the adsorption isotherm data with $R^2 = 0.93$. Elovich model fits the kinetic model with $R^2=0.978$.
39	(M. Saban Tanyildizi, 2011)	peanut hull	reactive black 5 (RB5)	Batch	<ul style="list-style-type: none"> Analysis of variance (ANOVA) showed $R^2 = 0.95$. The interaction between RB5 and peanut hull was very significant ($P < 0.05$) for RB5 adsorption. Effect of temperature studied was $20 \text{ }^\circ\text{C}$ to $60 \text{ }^\circ\text{C}$. Monolayer adsorption capacity was 55.55 mg g^{-1}. Pseudo second order with $R^2 = 0.99$ fits the adsorption data.

S.No.	Reference	Adsorbent	Adsorbate / Object of study	Operating Mode	Inference
					<ul style="list-style-type: none"> The negative value of ΔG° confirms the spontaneous adsorption.
40	(Temesgen et al., 2018)	banana and orange peels	red reactive dye	Batch	<ul style="list-style-type: none"> The maximum removal efficiency was 89.4 % and 70.2 % at pH = 4, adsorbent dosage 1 g in 100 mL, pH = 4 at 30 °C on the activated surface of orange and banana peels respectively. The surface area of orange and banana peel were 21.456 and 336.224 m² g⁻¹. The value of dimensionless separation factor was found to be favourable and its value was less than 1. The monolayer adsorption capacity for banana peel and orange peel were 0.323 and 1.690 mg g⁻¹ respectively.
41	(Muntean et al., 2012)		a symmetrical disazo dye (OD), an asymmetrical disazo dye (RD), and a trisazo dye (GD)		<ul style="list-style-type: none"> The Monolayer adsorption capacity was 143.40 mg g⁻¹. Langmuir isotherms fits the equilibrium data. ΔG° was negative indicating spontaneous adsorption.

S.No.	Reference	Adsorbent	Adsorbate / Object of study	Operating Mode	Inference
42	(Sadaf and Bhatti, 2014)	peanut husk biomass	indosol yellow BG dye	Batch and Column studies	<ul style="list-style-type: none"> Acetic acid treated immobilized peanut husk biomass was used as adsorbent. Maximum Indosol Yellow BG dye removal efficiency was obtained at pH 2, with 0.05 g /50 mL adsorbent dose. The adsorption process was exothermic in nature. Maximum adsorption capacity was 79.7 mg g⁻¹ pH_{ZPC} of native, acetic acid treated and immobilized peanut husk biomass was 7.4, 6.3 and 5.9 respectively. Kinetic data followed Pseudo second order model with R² = 0.999. Langmuir model was found to fit the equilibrium data with maximum monolayer adsorption capacity of 84.74 mg g⁻¹ for acetic acid treated peanut shell husk.
43	(Nuithitikul et al., 2010)	activated carbon derived from durian peel	basic green 4 dye, acid blue 11, direct blue 80		<ul style="list-style-type: none"> The maximum BET surface area was 951, 1015 and 549 for H₂O treated HCl treated and NaOH treated respectively. Pseudo second order kinetics was better fit for the kinetic data with R² > 0.99.

S.No.	Reference	Adsorbent	Adsorbate / Object of study	Operating Mode	Inference
					<ul style="list-style-type: none"> Langmuir isotherm model was better fit than Freundlich isotherm model. The dimensionless constant R_L value lies between (0-1) for both the activated carbon. The maximum monolayer adsorption capacity was 312.5 mg g^{-1}.
44	(Noorimotlagh et al., 2014)	activated carbon from milk vetch and	acid orange 7 (AO7)	Batch	<ul style="list-style-type: none"> SEM analysis confirmed the pore size distribution of AC was lower than 100 nm. Increasing adsorbent dose from 0.5 to 1.5 g L^{-1} increased the removal efficiency from 59.96 to 89.40 % respectively. Pseudo second order kinetic model was found to be most suitable kinetic model with $R^2 = 0.9865$. Langmuir adsorption isotherm model fits the equilibrium data with $R^2 = 0.9907$. The maximum monolayer adsorption capacity was 99 mg g^{-1}.

S.No.	Reference	Adsorbent	Adsorbate / Object of study	Operating Mode	Inference
45	(Khani et al., 2018)	γ -Fe ₂ O ₃ nanoparticle	triazole dye direct blue 71	Batch	<ul style="list-style-type: none"> • γ-Fe₂O₃ nanoparticle has removed 98.2 % of triazole dye Direct Blue 71. • Pseudo first order fits the kinetic data with $R^2 = 0.99$. • Monolayer adsorption capacity was 47.6 mg g⁻¹. • Dimensionless parameter R_L was found to be (0.23 - 0.64) which favours the adsorption process.
46	(Belaid et al., 2013)	commercially available granular activated carbon (GAC)	acid blue 113 (AB), basic red 5 (BR) and reactive yellow 81 (RY)	Batch	<ul style="list-style-type: none"> • The equilibrium time for batch adsorption was ≤ 1h for RY and AB and ≈ 4h for BR. • Adsorption results perfectly fitted Pseudo second order kinetics with $R^2 > 0.98$ for all the three dyes. • Fitting of Elovich equation confirms that the process was chemisorption.
47	(Georgin et al., 2018)	Para chestnut husk (Bertholleti)	cationic dyes crystal violet (CV) and methylene blue (MB)	Batch	<ul style="list-style-type: none"> • A low cost adsorbent, Para chestnut husk (PCH) was used to remove cationic dyes crystal violet (CV) and Methylene Blue (MB) from aqueous solution. • PCH had amorphous structure containing carboxylic acids, esters, ketones and aldehydes.

S.No.	Reference	Adsorbent	Adsorbate / Object of study	Operating Mode	Inference
		a excelsa) (PCH)			<ul style="list-style-type: none"> • For both the dyes, adsorption was favoured by acidic condition. • The maximum biosorption capacities were 83.6 and 83.8 mg g⁻¹ for CV and MB respectively. • 90 % colour removal was observed.
48	(Deniz, 2013)	almond shell residues	methyl orange dye	Batch	<ul style="list-style-type: none"> • Pseudo second order kinetics fits the adsorption data. • The equilibrium data was found to best fit the Langmuir isotherm model with R² = 1.0. • Maximum monolayer capacity was 40.650 mg g⁻¹. • The dimensionless parameter R_L value lies between 0.0235 - 0.0255, which was less than 1.0 so it favoured the process.
49	(Cao et al., 2014)	chem-modified walnut shell (MWNS)	reactive brilliant red K-2BP	Batch	<ul style="list-style-type: none"> • Modified walnut shell was used to treat anionic dye reactive brilliant red K-2BP. • Maximum adsorption capacity was 568.18 mg g⁻¹ at 313 K. The above stated value was 10 fold to the initial value. • Kinetic data well fitted the Pseudo second order model. • Langmuir isotherm model was found to fit equilibrium data with R² > 0.99.

S.No.	Reference	Adsorbent	Adsorbate / Object of study	Operating Mode	Inference
50	(Sandoval et al., 2017)	titanate nanotubes	methylene blue (MB)	Batch	<ul style="list-style-type: none"> • Titanate nanotubes were used to study the combined effect of adsorption and photo catalysis. • Generated OH radicals degrade the MB dye. • Degussa P-25 was used as a photo catalyst.
51	(Pekkuz et al., 2008)	poplar sawdust	metanil yellow (MY) (acidic) and methylene blue (MB) (basic)		<ul style="list-style-type: none"> • Pseudo second order with $R^2 > 0.99$ fits the kinetic data. • E_a was 14.93 KJ mol⁻¹ and 10.41 for KJ mol⁻¹ MY and MB respectively. • BET surface area was 3.80 m⁻¹ g for sawdust. • Langmuir adsorption isotherm fits the equilibrium data with $R^2 > 0.98$. • Negative value of ΔG° indicates spontaneous adsorption. • ΔS° value is positive, therefore it indicates increased randomness.

Table 2.7 : Adsorption studies on the removal of dyes from wastewater using alginate and alginate composite as adsorbent

S.No.	Reference	Adsorbent	Adsorbate / Object of study	Operating Mode	Inference
1.	(Ai et al., 2011)	activated carbon /cobalt ferrite /alginate composite beads	methylene blue (MB)	Batch	<ul style="list-style-type: none"> • Ionic polymerization technique was applied for synthesis of magnetic alginate composite beads. • Pseudo second order was found suitable for the kinetic data with $R^2 > 0.999$. • Equilibrium data was found to follow Langmuir ($R^2 = 0.973$) and the Freundlich model ($R^2 = 0.979$). • The value of dimensionless constant separation factor R_L lies between 0 and 1. • The negative value of ΔG° indicates spontaneous adsorption.
2	(Ma et al., 2019)	gelatin/calcium alginate (GA) composite nanofiber membranes	methylene blue (MB)	Batch	<ul style="list-style-type: none"> • Monolayer adsorption capacity was 2046 mg g^{-1} and 1937 mg g^{-1} for calcium alginate membrane (CA) and gelatin/ calcium alginate composite (GA). • The value of dimensionless constant separation factor R_L lies between (0.044-0.546) for CA and (0.051-0.585) for GA.

S.No.	Reference	Adsorbent	Adsorbate / Object of study	Operating Mode	Inference
					<ul style="list-style-type: none"> Equilibrium data was found to follow Langmuir ($R^2 = 0.996$ and $R^2 = 0.994$) and Freundlich model ($R^2 = 0.958$ and $R^2 = 0.943$) for CA and GA respectively.
3	(Mohammed et al., 2016)	cellulose nanocrystals alginate (CNC-ALG)	methylene blue (MB)		<ul style="list-style-type: none"> The maximum adsorption capacity of the column was 255.5 mg g⁻¹. Breakthrough curve revealed that dramatic increase followed by a gradual decrease to a plateau at saturation.
4	(Oussalah et al., 2019)	hybrid beads were prepared from natural bentonite and alginate	methylene blue (MB) and congo red (CR)		<ul style="list-style-type: none"> The monolayer adsorption capacity for methylene blue onto adsorbents was 385.25 to 1309.5 mg g⁻¹ and $R^2 > 0.97$ for Langmuir adsorption isotherm model. The monolayer adsorption capacity for Congo red dye onto adsorbents was from 12.25 to 353.73 mg g⁻¹ and $R^2 > 0.98$. Pseudo second order was found to fit kinetic data with $R^2 > 0.95$. Thermodynamic parameter ΔG° was found negative which indicates spontaneous nature of adsorption.

S.No.	Reference	Adsorbent	Adsorbate / Object of study	Operating Mode	Inference
5	(Pawar et al., 2018)	mesoporous synthetic hectorite (MSH) MSH-alginate beads (MSH-AB)	methylene blue (MB)	Batch	<ul style="list-style-type: none"> The surface area of Mesoporous synthetic hectorite (MSH) and Mesoporous synthetic hectorite-alginate beads (MSH-AB) were $468 \text{ m}^2 \text{ g}^{-1}$, $205 \text{ m}^2 \text{ g}^{-1}$ and pore volume $0.34 \text{ cm}^3 \text{ g}^{-1}$, $0.29 \text{ cm}^3 \text{ g}^{-1}$ respectively. Langmuir monolayer adsorption capacity for: <ul style="list-style-type: none"> MSH-AB -wet(W) $785.45 \text{ mg MB g}^{-1}$ MSH-AB -dry(D) $357.14 \text{ mg MB g}^{-1}$ Powdered MSH $196.00 \text{ mg MB g}^{-1}$. Kinetic data represented the Pseudo second order model for MSH and the Pseudo first order model for MSH-AB. Langmuir isotherm model was followed by MSH with $R^2 = 0.997$.
6	(Fabryanty et al., 2017)	bentonite – alginate composite	crystal violet (CV)	Batch	<ul style="list-style-type: none"> The pH_{ZPC} value for acid activated bentonite was 3.88, sodium alginate was 7.07 and bentonite-alginate composite was 5 to 6. Kinetic data was found to fit Pseudo second order model with R^2 (0.92 to 0.99)

S.No.	Reference	Adsorbent	Adsorbate / Object of study	Operating Mode	Inference
					<ul style="list-style-type: none"> Langmuir and Freundlich isotherm model were found fit. Maximum monolayer adsorption capacity was 462.60, 555.81 and 601.93 at 30 °C, 50 °C and 70 °C respectively. Thermodynamics parameter ΔG° was negative which indicated spontaneous adsorption. The positive value of ΔH° indicated endothermic process. The positive value of ΔS° reflects increased randomness between adsorbate and adsorbent.
7	(Jabli and Hassine, 2018)	synthesis of [sodiumalginate/4-methyl-2-(naphthalen-2-yl)-N-propylpentanamide-function-alizedethoxy-silica]	methylene blue and acid blue 25	Batch	<ul style="list-style-type: none"> pH_{ZPC} were equal to 6.3 and 6.6 for alginate gel beads(AGB) and Composite gel beads (CGB) respectively. Contact time was varied up to 150 minutes. AGB group present was COO^- amino (-NH-) and carbohydrate(COO^-) group in the chemical structure of CGB. Pseudo second order was found fit for the kinetic data with $R^2 > 0.97$. Maximum monolayer adsorption capacity was 12.98 for AGB and 9.26 for methylene blue.

S.No.	Reference	Adsorbent	Adsorbate / Object of study	Operating Mode	Inference
		composite gel beads			
8	(Ravi and Pandey, 2019)	bentonite and alginate beads	methylene blue		<ul style="list-style-type: none"> • Maximum monolayer adsorption capacity was 2024 mg g⁻¹. • Kinetic data is best presented by Pseudo second order with R² > 0.97. • Separation factor R_L value lies between 0.78 and 0.33, which indicated feasibility of the process. • Value of ΔG° was negative which indicated spontaneous adsorption. • ΔS° value was positive which indicated enhancement of randomness between adsorbate and adsorbent.
9	(Uyar et al., 2016)	alginate–montmorillonite composite beads	methylene blue	Batch	<ul style="list-style-type: none"> • A novel cryogelation process was developed by deep-freezing the alginate beads at –21 °C. • The drug encapsulation of calcium alginate beads was improved, using montmorillonite (MMT) clay . • Maximum monolayer adsorption capacity was 181.8mg g⁻¹.

S.No.	Reference	Adsorbent	Adsorbate / Object of study	Operating Mode	Inference
					<ul style="list-style-type: none"> • Equilibrium data was explained by Freundlich isotherm model with $R^2 > 0.99$. • Pseudo second order kinetic model explains the kinetic data much better than any other kinetic model having $R^2 > 0.99$. • ΔG° was found negative which indicated spontaneous adsorption. • Adsorption was endothermic since value of ΔH° was positive. • ΔS° was positive which indicated increased randomness.
10	(Aichour et al., 2018)	lemon peels activated with phosphoric acid (ALP) and encapsulated with alginate (ALP/A beads)	methylene blue (MB)	Batch	<ul style="list-style-type: none"> • pH_{ZPC} of ALP/A 1/1 beads was 8.1. • 100 mg L^{-1} of methylene blue dye was adsorbed 91 %, 94 % and 99 % by ALP/A 4/1, ALP/A 2/1 and ALP/A 1/1 respectively. • Spontaneous adsorption was indicated by negative value of ΔG°. • Positive value of entropy show increased randomness between ALP/A 1/1 and methylene blue.

S.No.	Reference	Adsorbent	Adsorbate / Object of study	Operating Mode	Inference
					<ul style="list-style-type: none"> • Monolayer adsorption capacity of ALP/A 1/1, was 841.37 mg g⁻¹. • Langmuir adsorption isotherm model was found to fit equilibrium data with R² = 0.991. • Pseudo first order and Pseudo second order fits the kinetic data.
11	(Jung et al., 2016)	entrapping activated carbon powder derived from spent coffee grounds into calcium-alginate beads (SCG-GAC)	acid orange 7 and methylene blue	Batch	<ul style="list-style-type: none"> • Spent coffee grounds was used to make activated carbon. This activated carbon was used to make alginate beads. • pH of solution for Acid orange 7(AO-7) and methylene blue are 3.0 and 11.0 respectively. • The BET surface area and pore volume were 704.23 m² g⁻¹ and 0.2926 cm³ g⁻¹ respectively for SCG-GAC. • Monolayer adsorption capacity of AO-7 and methylene blue were 665.9 and 986.8 mg g⁻¹ for SCG-GAC. • Sips isotherm model was found suitable as value of R² is close to unity and has lowest value of error function.

S.No.	Reference	Adsorbent	Adsorbate / Object of study	Operating Mode	Inference
12	(Kwak et al., 2018)	sericin-derived activated carbon (S-AC)/Alg beads	methylene blue	Batch	<ul style="list-style-type: none"> • Silk sericin (a secondary protein of the sericulture industry) and alginate (Alg) were used to make a matrix, which was used as adsorbent. • Sericin-derived activated carbon (S-AC) was prepared by using NaOH as chemical activator and has a BET surface area of $2150.1 \text{ m}^2 \text{ g}^{-1}$. • S-AC/Alg bead has surface area of $1215.4 \text{ m}^2 \text{ g}^{-1}$. • Monolayer adsorption capacity of methylene blue by the S-AC/Alg beads was 841.37 mg g^{-1}. • Equilibrium data was best represented by Freundlich isotherm with $R^2 = 0.997$. • Pseudo second order fits the kinetic data with $R^2=0.999$. • Negative value of ΔG° indicated spontaneous adsorption. • Positive ΔS° value indicated enhanced randomness between S-AC/Alg bead and methylene blue.
13	(Wang et al., 2018)	carboxyl functionalized	methylene blue		<ul style="list-style-type: none"> • Monolayer adsorption capacity of CA-MWCNT-COOH was 1189 mg g^{-1} and for calcium alginate it was 1144.7 mg g^{-1}.

S.No.	Reference	Adsorbent	Adsorbate / Object of study	Operating Mode	Inference
		multiwall carbon nanotubes (MWCNT-COOH) impregnated into calcium-alginate (CA) beads (CA-MWCNT-COOH)	(MB)		<ul style="list-style-type: none"> • In 5 minutes 92.8 % adsorption of MB was found by MWCNT- COOH . • With $R^2 > 0.97$, Langmuir adsorption isotherm model was found to fit best.
14	(Zou et al., 2019)	a novel polyacrylamide (PAM) / PAM/SA mi- crospheres	methylene blue (MB)	Batch	<ul style="list-style-type: none"> • Polyacrylamide (PAM) and Sodium alginate were used to form PAM / SA composite through polymerization. • Pore size was in the range of 0 - 200 nm and the mesoporous structure is uniform. • Particle size was in the range of 1 - 10 μm. • Maximum monolayer adsorption capacity of composite was 1070.54 mg g^{-1}. • Pseudo first order was found to be most suitable kinetic model with $R^2 > 0.999$.

S.No.	Reference	Adsorbent	Adsorbate / Object of study	Operating Mode	Inference									
					<ul style="list-style-type: none"> Langmuir adsorption isotherm model was found fit with $R^2 > 0.99$. Negative value of ΔG° confirmed spontaneous adsorption. 									
15	(Wang et al., 2019)	three kind of water insoluble membrane were made by crosslinking of calcium chloride (CaCl_2), glutaraldehyde vapour (GA), and trifluoroacetic acid (TFA), respectively.	methylene blue (MB)	Batch	<ul style="list-style-type: none"> Three kind of water insoluble alginate membrane were prepared by electrospinning and crosslinking with calcium chloride (CaCl_2), glutaraldehyde vapour (GA), and trifluoroacetic acid (TFA), respectively. The monolayer maximum adsorption capacity was $2357.87 \text{ mg g}^{-1}$ for MB removal using SA nanofiber membrane. Negative value of ΔG° confirmed the process to be spontaneous. <table border="1"> <thead> <tr> <th></th> <th><u>Surface Area</u> (BET) ($\text{m}^2 \text{g}^{-1}$)</th> <th><u>Pore Volume</u> ($\text{cm}^3 \text{g}^{-1}$)</th> </tr> </thead> <tbody> <tr> <td>Non cross linked</td> <td>13.97</td> <td>0.0256</td> </tr> <tr> <td>CaCl_2 Cross linked</td> <td>13.56</td> <td>0.0450</td> </tr> </tbody> </table>		<u>Surface Area</u> (BET) ($\text{m}^2 \text{g}^{-1}$)	<u>Pore Volume</u> ($\text{cm}^3 \text{g}^{-1}$)	Non cross linked	13.97	0.0256	CaCl_2 Cross linked	13.56	0.0450
	<u>Surface Area</u> (BET) ($\text{m}^2 \text{g}^{-1}$)	<u>Pore Volume</u> ($\text{cm}^3 \text{g}^{-1}$)												
Non cross linked	13.97	0.0256												
CaCl_2 Cross linked	13.56	0.0450												

S.No.	Reference	Adsorbent	Adsorbate / Object of study	Operating Mode	Inference
					GA Vapour cross linked 11.86 0.0185 TFA Cross linked 15.26 0.0455
16	(Bayat et al., 2018)	synthesized magnetic nanocomposite of zeolite /nickel ferrite through co-precipitation method and modify its surface by sodium alginate	methylene blue dye		<ul style="list-style-type: none"> • Synthesized magnetic nanocomposite of nickel ferrite, zeolite and sodium alginate to enhance the removal of MB. • Response surface methodology was used for optimization with $R^2 = 0.977$. • Under optimal conditions adsorption capacity of 69.61 mg g^{-1} was estimated (pH = 8, 0.01 adsorbent amount and initial concentration of 50 mg L^{-1} are the optimal conditions). • Langmuir isotherm model was most suitable model with $R^2 = 0.99$. The dimensionless parameter R_L was between 0.01-0.07. • Pseudo second order kinetic model was found most suitable as $R^2 = 1$. • Adsorption was spontaneous as the value of ΔG° was negative.

S.No.	Reference	Adsorbent	Adsorbate / Object of study	Operating Mode	Inference
17	(Boukhalifa et al., 2019)	magnetic beads (AO- γ -Fe ₂ O ₃) of alginate (A) impregnated with citrate coated maghemite nanoparticles (γ -Fe ₂ O ₃) and oxidized multiwalled carbon nanotubes (OMWCNTs) were synthesized.	methylene blue		<ul style="list-style-type: none"> • Special magnetic bead with γ-Fe₂O₃ and alginate were synthesized. • Maximum monolayer adsorption capacity was 905.5 mg g⁻¹. • Freundlich adsorption isotherm model was found most suitable model for the adsorption data with R² = 0.98. • Thermodynamic parameter revealed adsorption process was spontaneous and endothermic in nature,
18	(Talbot et al., 2018)	magnetic alginate nanoparticles (AlgMNP)	cationic dye methylene blue	Batch	<ul style="list-style-type: none"> • Adsorption was quick as 80 % occurred in 15 minutes and equilibrium was attained in 2 h. • Maximum adsorption capacity was 273 mg g⁻¹ for AlgMNP and MB.

S.No.	Reference	Adsorbent	Adsorbate / Object of study	Operating Mode	Inference								
					<ul style="list-style-type: none"> AlgMNP was found to be effective in removing cationic pollutants from water. 								
19	(Guesmi et al., 2018)	hydroxyapatite sodium alginate (CaHAp-Alg) hybrid materials	methylene Blue	Batch	<ul style="list-style-type: none"> XRD data confirms that the presence of alginate effected crystallinity. Following were the Surface area of adsorbents <table border="1"> <thead> <tr> <th><i>Adsorbent</i></th> <th><i>Surface area (m² g⁻¹)</i></th> </tr> </thead> <tbody> <tr> <td>Hydroxyapatite (CaHAp)</td> <td>21.640</td> </tr> <tr> <td>Hydroxyapatite sodium alginate CaHAp-(Alg)₅</td> <td>12.840</td> </tr> <tr> <td>CaHAp-(Alg)₁₀</td> <td>3.390</td> </tr> </tbody> </table> <ul style="list-style-type: none"> The monolary adsorption capacity of CaHAp-(Alg)₁₀ was 142.850 mg g⁻¹. Langmuir isotherm model was found fit with R² > 0.99 and dimensionless factor R_L value lies between 0.250 to 0.040 for CaHAp-(Alg)₁₀ 	<i>Adsorbent</i>	<i>Surface area (m² g⁻¹)</i>	Hydroxyapatite (CaHAp)	21.640	Hydroxyapatite sodium alginate CaHAp-(Alg) ₅	12.840	CaHAp-(Alg) ₁₀	3.390
<i>Adsorbent</i>	<i>Surface area (m² g⁻¹)</i>												
Hydroxyapatite (CaHAp)	21.640												
Hydroxyapatite sodium alginate CaHAp-(Alg) ₅	12.840												
CaHAp-(Alg) ₁₀	3.390												

S.No.	Reference	Adsorbent	Adsorbate / Object of study	Operating Mode	Inference
					<ul style="list-style-type: none"> Pseudo second order was most suitable model with $R^2 = 0.999$.
20	(Jayalakshmi and Jeyanthi, 2019)	cobalt ferrite-alginate nanocomposite	reactive red 195 (RR195) and Reactive yellow 145 (RY145) from binary component system	Batch/Column	<ul style="list-style-type: none"> The equilibrium time for binary adsorption was 60 minutes. Pseudo second order model was found to fit the kinetic data. The adsorbent was magnetically separable and reusable. The pH_{ZPC} of $CoFe_2O_4$-ANa was 7.5 ΔG° was negative which confirms spontaneous adsorption.
21	(Kurczewska et al., 2019)	alginate /PAMAM dendrimer – Halloysite beads	cationic methyl green (MG) and anionic sunset	Batch	<ul style="list-style-type: none"> Adsorption capacity of alginate composite was improved in comparison to alginate beads. Pseudo second order kinetic model was found fit to the kinetic data with $R^2 > 0.94$.

S.No.	Reference	Adsorbent	Adsorbate / Object of study	Operating Mode	Inference
			yellow FCF (SY)		<ul style="list-style-type: none"> Equilibrium data was presented by Freundlich isotherm model with $R^2 > 0.95$. Negative value of ΔG° indicates spontaneous adsorption. ΔS° was positive so it indicates increased adsorbate adsorbent interaction.
22	(Panão et al., 2019)	alginate was covalently gelled in the presence of SiO_2	methylene blue		<ul style="list-style-type: none"> Hydrogels were synthesized from alginate and silica (SiO_2), vinylated with vinyltrimethoxysilane using crosslinking chemistry. Hydrogel can absorb 889.76 ± 12.65 g of water per 1g of dry polymer. Kinetic data was best fitted by Pseudo second order kinetic model with $R^2 > 0.96$. Equilibrium adsorption data was represented by Langmuir model with $R^2 > 0.97$.
23	(Mohammadi et al., 2018)	ABSGO beads	methylene blue (MB)		<ul style="list-style-type: none"> Nano beads were made with alginate/ calix[4] arenes and graphene oxide.

S.No.	Reference	Adsorbent	Adsorbate / Object of study	Operating Mode	Inference
		(alginate /GO and alginate/C4As-GOs nanocomposite)			<ul style="list-style-type: none"> • p-tert butyl calix[4] arene and sodium p-sulfonatocalix [4] arene modified GO nanosheets (CGO and SGO) were prepared. • The alginate beads containing SGO nanosheets (ABSGO) had high porosity and thin layered structure. • Langmuir and Freundlich adsorption isotherm was found suitable for ABSGO. • Maximum monolayer adsorption capacity was 170.36 mg g^{-1} for ABSGO. • The kinetic data confirmed that pseudo second order model was obeyed with $R^2 = 0.998$. • Gibbs free energy showed that adsorption was spontaneous.
24	(Ladnorg et al., 2019)	alginate-like exopolysaccharide (ALE)	methylene blue	Batch	<ul style="list-style-type: none"> • A compound similar to alginate was prepared from aerobic granular sludge (AGS). • 69 % dye was removed at 35 °C in 60 minutes contact time. • Langmuir isotherm model was best fitted with $R^2 = 0.967$.

S.No.	Reference	Adsorbent	Adsorbate / Object of study	Operating Mode	Inference
					<ul style="list-style-type: none"> The kinetics of ALE adsorption was best described by Pseudo first order model. Maximum adsorption capacity of MB by alginate and ALE were 345 mg g^{-1} and 106 mg g^{-1} respectively.
25	(Nasrullah et al., 2018)	mangosteen fruit peel (MP) AC into calcium-alginate beads (MPAC-alginate beads)	methylene blue	Batch	<ul style="list-style-type: none"> Immobilized activated carbon was made by entrapping activated carbon obtained from mangosteen fruit peel MPAC into calcium alginate beads (MPAC-alginate beads). BET surface area of MP, AC, AC-alginate beads were 3.787, 1621.8, and 890 respectively. Maximum monolayer adsorption capacity was 287.35 mg g^{-1}. Freundlich adsorption isotherm best fitted the equilibrium data with $R^2 = 0.954$. Pseudo second order kinetic model was found fit for the kinetic data with $R^2 \geq 0.998$. The adsorption process was spontaneous due to the negative value of ΔG°.

S.No.	Reference	Adsorbent	Adsorbate / Object of study	Operating Mode	Inference
					<ul style="list-style-type: none"> Positive value of ΔS° confirms increased interaction between methylene blue and MPAC-alginate beads.
26	(Shao et al., 2018)	hydrogen bonds between SA and 2-acrylamido-2-methylpropanesulfonic acid (AMPS), and the AMPS was then post-cross-linked to manufacture SA/PAMPS beads.	methylene blue (MB)		<ul style="list-style-type: none"> The equilibrium adsorption capacity was 2977 mg g^{-1} for MB. Pseudo second order kinetic order was found fit to the kinetic data. Langmuir adsorption isotherm model described the isotherm data.
27	(Sharma et al., 2019)	Aca-NaAlg-cl-poly (Typical alginate composite)	auramine-O (AO), malachite green (MG) and		<ul style="list-style-type: none"> A novel material Aca-NaAlg-cl-poly(AA) was synthesized using polymerisation by gum acacia, sodium alginate, acrylic acid, N,N'-methylene bisacrylamide (MBA). Central composite design of response surface methodology was used for optimization.

S.No.	Reference	Adsorbent	Adsorbate / Object of study	Operating Mode	Inference
			crystal violet (CV)		<ul style="list-style-type: none"> • Experimental adsorption capacities of AO, MG and CV were 2.01 mg g⁻¹, 3.06 mg g⁻¹ and 7.55 mg g⁻¹. • Selective removal of cationic dye was observed to be 97.49 %, 95.39 % and 94.56 % for AO, MG and CV respectively. • Langmuir adsorption model was found best fit with R² > 0.94. • Negative value of ΔG° confirmed spontaneous adsorption. • Positive value of ΔS° confirms increased interaction between dye and typical alginate composite.



MATERIALS AND METHODS

3.0 INTRODUCTION

In the present chapter materials required and experimental procedure for adsorption of AY-36 and DB-86 dyes are described. The details of various equipment are given. Response surface methodology was used in optimizing different parameters for the adsorption of DB-86 dye through alginate coated immobilized activated carbon. Beside this, kinetic models, isotherm models and thermodynamic conditions used are also described.

3.1 EXPERIMENTAL STUDIES

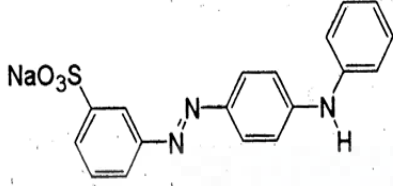
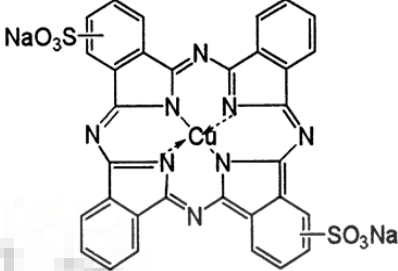

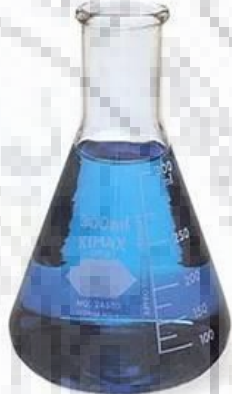
3.1.1 Materials

3.1.1.1 Dyes

Commercial grade dye, AY-36 was procured from Kashish colors Delhi and DB-86 from J C Dye Chem Industries, Gujarat, India and were used as an adsorbate without further purification. Properties of AY-36 and DB-86 dyes are shown in Table 3.1.

Table 3.1: Properties of dyes

Characteristics	AY-36	DB-86
Molecular formula	$C_{18}H_{14}N_3NaO_3S$	$C_{32}H_{14}CuN_8Na_2O_6S_2$
Molecular weight (g mol ⁻¹)	375.38 g mol ⁻¹	780.16 g mol ⁻¹
λ_{max}	434 nm	620 nm
CAS number	587-98-4	1330-38-7
Colour Index number	13065	74180

Characteristics	AY-36	DB-86
Molecular structure		
Pictorial view		

i. Calibration Curve for AY-36 Dye

A calibration curve as shown in Fig.3.1(a) was plotted for AY-36 dye at 434 nm after recording the standard concentration of dye. The absorbance of the AY-36 was measured and concentration was calculated from calibration curve.

ii. Calibration Curve for DB-86 Dye

A calibration curve for DB-86 dye as shown in Fig.3.1(b) was plotted at 620 nm after recording the standard concentration of dye. The absorbance of DB-86 was measured and concentration was calculated from calibration curve.

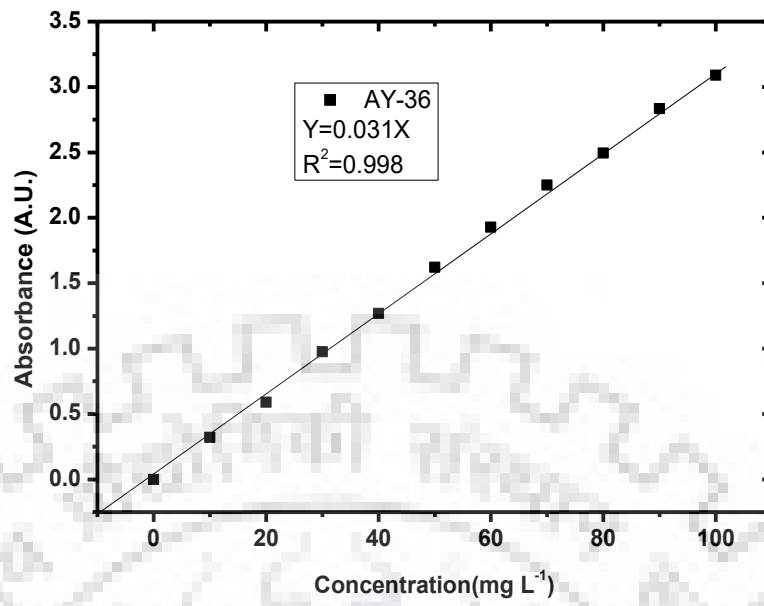


Fig.3.1 (a) : Calibration curve for AY-36 dye

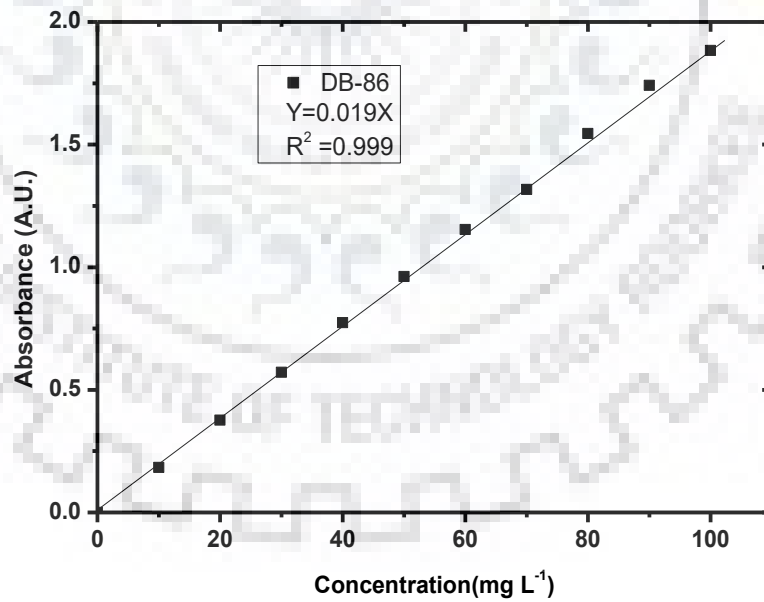


Fig.3.1 (b): Calibration curve for DB-86 dye

3.1.1.2 Raw Material for Adsorbent

i. Peanut Shells

Peanuts were purchased from local market of Roorkee, India. Peanut shells (Fig.3.2 (a)) are agricultural waste, available in abundance in India at almost no cost. Scientific classification of peanut is given in Table 3.2.

Table 3.2: Scientific Classification of Peanut

Kingdom	Plantae
Order	Fabales
Family	Fabaceae
Genus	Arachis
Species	Arachis hypogaea

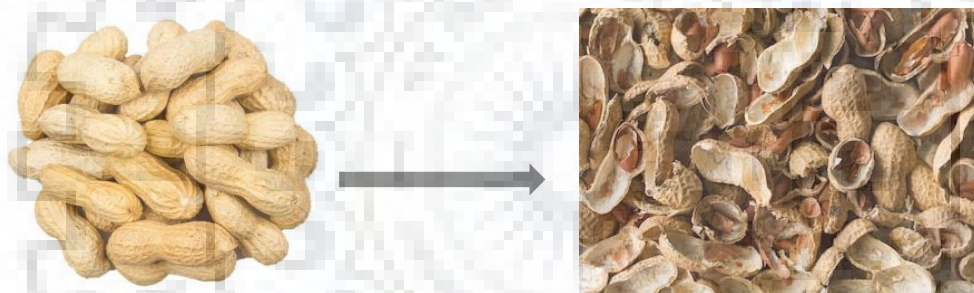


Fig.3.2 (a) : Peanuts and Peanut shells

ii. Sodium Alginate

Sodium alginate ($C_6H_9NaO_7$) (Fig.3.2(b)) was procured from SRL, India. It is a sodium salt of alginic acid.



Fig.3.2 (b) : Sodium Alginate

3.1.1.3 Chemicals

Chemicals used for experimentation namely, phosphoric acid of specific gravity 1.73, sodium bicarbonate, hydrochloric acid and sodium hydroxide were purchased from Merck, India. Fused calcium chloride was obtained from SRL, India. All the chemicals are of analytical grade and used without further purification. Double distilled water was used in the preparation of solutions.

3.1.1.4 Instruments

i. Analytical Instruments

Fig. 3.3(a) – (d) show the images of various analytical instruments which were used in the study:

Fourier Transform Infrared Spectrometer (FTIR),

EXSTAR TG /DTA 6300,

Surface Area analyser- ASAP 2010,

Scanning electron microscope (Scanning Electron Microscope model FEI Quanta 200F with Oxford-EDS system IE 250 X Max 80),

Scanning electron microscope (SEM, JEOL),

UV/Vis double beam spectrophotometer (model U-2900, Hitachi).

Scanning electron microscope (SEM) (Carl Zeiss, EVO-18),

EDX (Environmental Scanning Electron Microscope model FEI Quanta 200F with Oxford-EDS system IE 250 X Max 80),

Transmission electron microscopy (TECNAI G2 20 S-TWIN, FEI Netherlands),

X-ray diffraction (XRD) (Bruker D8 X-ray diffractometer),

BET surface area (Nova Touch Lx2 by Quantachrome, 2018, USA),

FTIR spectroscopy (Thermo Scientific, Nicolet, iS50 FTIR) with ATR mode.

ii. Auxiliary Equipment's

Fig. 3.4(a) – (g) shows the images of auxiliary equipment's used in the study namely: BOD orbital shaking incubator (Dewsil Scientific Private Limited), centrifuge (Remi, R-8C), hot air oven (Dewsil Scientific Private Limited), pH meter (U-tech), weighing balance (aczet), magnetic stirrer with hot plate, desiccator, double distillation water unit.



(a) X-ray diffraction (XRD)
(Bruker D8 X-ray diffractometer)



(b) Transmission electron microscopy
(TECNAI G2 20 S-TWIN, FEI Netherlands)



(c) UV/Vis double beam
spectrophotometer
(modelIU-2900, Hitachi)



(d) Scanning electron microscope (SEM)
(Carl Zeiss, EVO-18)

Fig.3.3 (a) – (d) : Analytical Instruments used in the study



**(a) BOD orbital shaking incubator
(Dewsil Scientific Private Limited)**



**(b) Hot air oven
(Dewsil Scientific Private Limited)**



**(c) Centrifuge
(RemiR-8C)**



(d) magnetic stirrer with hot plate

Fig.3.4 (a) – (d) : Auxiliary Equipment's used in the study



(e) weighing balance
(aczet)



(f) Desiccator



(g) pH meter
(U-tech)

Fig.3.4 (e) – (g) : Auxiliary Equipment's used in the study

3.1.2 Methods

3.1.2.1 Adsorbent Preparation

3.1.2.1.1 PnsAC Preparation

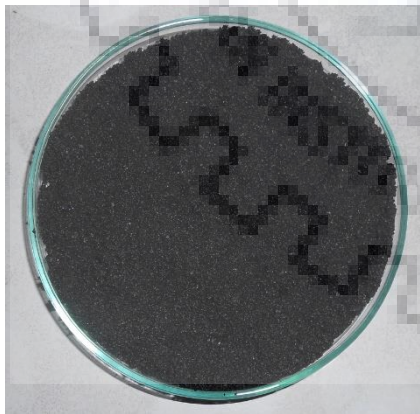
The shells were separated from peanuts and washed using distilled water to remove dust and dirt. After that, they were dried in an oven at 110 °C until a constant weight was obtained. The dried shells were crushed into smaller particles and then sieved through 10 –20 mesh screens (1.651-0.833 mm mesh opening size). Peanut shells and H₃PO₄ were mixed with a precursor ratio of 1:1.5 (peanut shell /acid = 1:1.5). The mixture was transferred to a cylindrical steel tube (2.54 cm ID x 60.96 in length), kept in a vertical furnace as shown in Fig.3.5 and heated up to 650 °C with a ramp of 10 °C min⁻¹ for pyrolysis. The mixture temperature was maintained at 650 °C for 2 h in the presence of nitrogen, supplied at the rate of 100 mL min⁻¹. While maintaining similar conditions, the temperature of the steel tube was then brought down to ambient temperature. The activated carbon thus obtained, was withdrawn from the steel tube and soaked overnight in 1 % solution of NaHCO₃. Later it was washed repeatedly to attain a pH of 7. Thereafter it was dried in an oven at 110 °C until its weight became constant. The resultant peanut shell activated carbon (PnsAC) was grounded and sieved to attain the particle size of less than 0.5mm. Fig.3.6 shows pictorial representation of prepared peanut shell activated carbon. Finally, the PnsAC was stored in a desiccator.

3.1.2.1.2 Alginate Coated Activated Carbon (PnsAC-alginate) Preparation

A 500 mL beaker filled with 200 mL distilled water was taken. 3 g of sodium alginate (pure) was added to the beaker and the beaker was kept on magnetic stirrer with hot plate for 1 hour at 800 rpm speed so that a homogenous mixture of sodium alginate is formed .The temperature of the mixture after 1 hour was maintained at 65 °C. Then 3 g of PnsAC was added to this mixture and stirred for 1hour at 800 rpm till a homogenous mixture was obtained. Then a 1 % solution of calcium chloride (fused) was prepared. The solution of activated carbon and sodium alginate was then poured drop by drop to calcium chloride solution using a dropper. PnsAC-alginate beads were thus formed. The beads were then allowed to settle down for about an hour in calcium chloride solution and later were washed with distilled water to remove excess calcium ion. Fig.3.7 shows pictorial representation of prepared alginate beads kept in a petri dish. Afterwards the beads were kept for drying in hot air oven at 100 °C, till constant weight was obtained.



Fig.3.5 : Experimental setup for preparation of PnsAC



**Fig.3.6 : Peanut Shell Activated Carbon
(PnsAC)**



Fig.3.7 : Alginate Beads

3.1.2.2 Adsorbate Preparation

AY-36 and DB-86 stock solution of concentration 1 g L^{-1} was prepared using double distilled water. To prevent photo-oxidation, brown glass bottles covered with aluminium foil were used for storing the stock solution. The pH of dye solution was adjusted by adding 0.1 N HCl or 0.1 N NaOH as required.

3.1.2.3 Characterization of PnsAC

Characterization was performed by using standard methods. In thermal analysis 10.32 mg mass of peanut shell was weighed and placed in the crucible then the crucible was kept on the microbalance. Nitrogen was taken as reactant gas at the flow of 100 mL min^{-1} and heated from $35 \text{ }^{\circ}\text{C}$ to $900 \text{ }^{\circ}\text{C}$ at the heating rate of $10 \text{ }^{\circ}\text{C min}^{-1}$. TG was recorded by using EXSTAR TG /DTA 6300, as the temperature increased.

Scanning electron microscope (SEM, JEOL) was used for the observation of surface morphology at the voltage of 15 KV. Gold sputtering was done before the sample observation. Field-emission scanning electron micrograph (FESEM) and energy-dispersive X-ray (EDS) spectrum were recorded using an environmental scanning electron microscope (model FEI Quanta 200 F with Oxford – EDS system IE 250X Max 80).

ASAP 2010 was used for the determination of N_2 adsorption –desorption isotherm at 77K. Brunauer-Emmett-Teller (BET) surface area (SBET) of activated carbon was calculated using BET equation. D-A equation was used in the calculation of micropore volume.

Surface properties of peanut shell and AC were analyzed using Perkin Elmer spectrum ES version 10.5.2, Fourier transform infrared (FTIR) spectro photometer. Sample was ground upto a particle size ($< 45\mu\text{m}$) and dried for 10 hrs at $150 \text{ }^{\circ}\text{C}$ and then for FTIR analysis pellets of 1mm thickness were made using sample to KBr ratio 1:100. The selected frequency range in the region of 400 to 4000 cm^{-1} .

The surface morphology of the PnsAC-alginate adsorbent was carried out using a scanning electron microscope (SEM) (Carl Zeiss, EVO-18) at an electron acceleration voltage of 20 kV with a magnification factor of 2 kX and 10 kX. The elemental characteristics of the adsorbent were carried out by EDX (Environmental Scanning Electron Microscope model FEI Quanta 200F with Oxford-EDS system IE 250 X Max 80). Transmission electron microscopy (TEM) was used to study the morphology with 25X-1100 kX magnification (TECNAI G2 20 S-TWIN, FEI Netherlands). X-ray diffraction (XRD) analysis of the adsorbent material was carried out using

Bruker D8 X-ray diffractometer equipment with a $\text{CuK}\alpha$ radiation source (used at 40 kV and 15 mA, diffraction angle ranged from 90° to 5° with continuous scanning mode). The PnsAC-alginate adsorbent was characterized in terms of specific surface area, pore volume and pore size distribution by N_2 adsorption–desorption (Nova Touch Lx2 by Quantachrome, 2018, USA) at 77 K. The surface area and pore size distribution were determined using the Brunauer–Emmett–Teller (BET) equation and Barrett–Joiner–Halenda (BJH) method, respectively. FTIR spectrum was observed for before and after adsorption of PnsAC-alginate using FTIR spectroscopy (Thermo Scientific, Nicolet, iS50 FTIR) with ATR mode in the range of $4000\text{--}400\text{ cm}^{-1}$ at 26°C . PnsAC-alginate samples ($<45\text{ }\mu\text{m}$) dried at 150°C for 10 h were used for preparation of pellet of 1 mm thickness by the KBr pellet method which was used for FTIR analysis. The Zero point charge (pH_{ZPC}) of PnsAC-alginate was measured by salt addition method (Dahri et al., 2014; Miyah et al., 2018) which was based on addition of 0.2 g of PnsAC-alginate into 50 mL of 50 mM NaCl solution taken in 250 mL reagent flask. The pH ($\text{pH}_{\text{initial}}$) of the solution was adjusted in the range of 2 to 9 by adding required volume of 0.1N HCl or 0.1N NaOH. The solution was stirred for 48 h at 120 rpm and the final pH of the solution (pH_{final}) was measured. The values of ($\text{pH}_{\text{final}} - \text{pH}_{\text{initial}}$) were plotted against $\text{pH}_{\text{initial}}$ and the pH_{ZPC} was determined from the point of intersection of the curve with the axis of $\text{pH}_{\text{initial}}$.

3.1.2.4 Batch Adsorption Studies

The adsorption potential of AY-36 and DB-86 on PnsAC was evaluated through batch experiments (Das et al., 2012). For each experiment, 100 mL of dye with different concentrations was poured in a 250-mL conical flask with stopper. Adsorbent doses varied from 2 g L^{-1} to 6 g L^{-1} for AY-36 and doses were 4 g L^{-1} to 12 g L^{-1} for DB-86 with an increment of 2 g. The temperature was maintained at 35°C . The mixture was shaken for an appropriate time interval in a BOD orbital shaking incubator. The mixture was centrifuged at 3500 rpm for 15 min in a 50 mL centrifuge tube. AY-36 concentration was determined at a wavelength of 434 nm and DB-86 was estimated at 620 nm by using UV/VIS double beam spectrophotometer. The plotted calibration curve was linear till 100 mg L^{-1} . To study the effect of pH, on the adsorption, experiments were conducted for the initial pH (pH_0) of range 2–11 at 35°C till the equilibrium was attained.

Adsorption studies of alginate coated AC were carried out to study the effect of pH, initial dye concentration and amount of alginate coated activated carbon. Batch adsorption experiments were conducted in 250 mL reagent bottle. 50 mL volume of different dye concentration were

taken with different amount of alginate coated AC for three hour at 120 rpm in BOD orbital incubator shaker. The optimization were carried out by varying the pH from 1.8 to 5.2, DB-86 concentration 65.91 to 234.09 mg L⁻¹ and alginate coated activated carbon from 11.591 g L⁻¹ to 28.408 g L⁻¹. % Removal is given by

$$\% \text{ Removal} = \frac{(C_0 - C_e)100}{C_0} \quad [3.1]$$

where C_0 is initial concentration and C_e is Equilibrium concentration.

Adsorption capacity is given by (mg g⁻¹) the amount of dye adsorbed per gram of alginate coated activated carbon. At equilibrium it is given by

$$q_e = \frac{(C_0 - C_e)V}{m} \quad [3.2]$$

At time $t = t$

$$q_t = \frac{(C_0 - C_t)V}{m} \quad [3.3]$$

where V = volume in litre and m = mass in gram of adsorbent.

3.2 KINETICS AND ADSORPTION ISOTHERM MODELS

3.2.1 Adsorption Kinetic Models

Adsorption kinetics plays a significant role in adsorption. It provides the information and mechanism of the process. Kinetic data were predicted using Pseudo first order model (Prola et al., 2013), Pseudo second order model (Mouni et al., 2018) and Intra particle diffusion model (Khani et al., 2018) for the adsorption of DB-86 dye.

Pseudo first order model is represented by:

$$\frac{dq_t}{dt} = k_1(q_e - q_t) \quad [3.4]$$

where k_1 is Pseudo first order rate constant (min⁻¹), on integration and applying boundary condition $t = 0$ to $t = t$ and $q_t = 0$ to $q_t = q_t$

$$\ln(q_e - q_t) = \ln q_e - k_1 t \quad [3.5]$$

For Pseudo first order model $\ln(q_e - q_t)$ is plotted with time. Slope gives k_1 value and q_e is calculated by intercept. If Pseudo first order is predicted, it is physical adsorption (physisorption).

The Pseudo second order model is represented by

$$\frac{dq_t}{dt} = k_2(q_e - q_t)^2 \quad [3.6]$$

where k_2 ($\text{g mg}^{-1} \text{ min}^{-1}$) Pseudo second order rate constant, on integration and applying $t = 0$ to $t = t$ and $q_t = 0$ to $q_t = q_t$ boundary condition

$$\frac{t}{q_t} = \frac{1}{k_2 q_e^2} + \frac{t}{q_e} \quad [3.7]$$

where q_e and q_t are amount of dye adsorbed per gram of adsorbent at equilibrium and time t respectively

For Pseudo second order model k_2 can be calculated by intercept of the linear plot of $\frac{t}{q_t}$ vs t . If

Pseudo second order is predicted its chemical adsorption (chemisorption).

Intra-particle diffusion model is given by

$$q_t = k_{id} t^{0.5} + C \quad [3.8]$$

k_{id} and C can be calculated by slope and intercept of the q_t vs $t^{0.5}$ plot. However if more than one distinct line was obtained, the adsorption process was controlled by two or more mechanism (Angela et al., 2018).

Boyd's diffusion model is given by

$$F = \frac{q_t}{q_e} = 1 - \frac{6}{\pi^2} \exp(-B_t) \quad \text{and} \quad [3.9]$$

$$B_t = -0.4977 - \ln(1 - F) \quad [3.10]$$

where F is the fraction of solute adsorbed at time t and B_t is mathematical function of F .

If in B_t Vs t curve, a straight line passing through origin is obtained then it is following intraparticle diffusion mechanism. Otherwise there exists film diffusion (Ai et al., 2011; Dahri et al., 2014). Various parameters of kinetic models were estimated utilizing linear regression by using MS-Excel.

3.2.2 Adsorption Isotherm Models

Adsorption isotherms provide crucial information regarding adsorption mechanisms and adsorption system design. The adsorption data of DB-86 was analysed for different adsorption models. The isotherm data q_e vs. C_e was observed to be concave downward.

Langmuir isotherm model (Foo and Hameed, 2010; Moideen, et al., 2015; Noorimotlagh et al., 2014; Reddy et al., 2014) is a two parameter model. Its equation is given by

$$q_e = \frac{q_m b C_e}{1 + b C_e} \quad [3.11]$$

where, b ($L \text{ mg}^{-1}$) is Langmuir isotherm constant and q_m (mg g^{-1}) is maximum monolayer coverage capacities. It has definite number of identical sites of equal affinity to adsorbing molecules. There is no lateral interaction and no hindrance even on neighbouring adsorbed molecules. According to Langmuir theory intermolecular force of attraction decreases with increase of distance. The another important separation factor (R_L) defined by

$$R_L = \frac{1}{1 + b C_0} \quad [3.12]$$

where b ($L \text{ mg}^{-1}$) is Langmuir constant and C_0 is adsorbate initial concentration (mg L^{-1}).

If ($R_L > 1$) then it is unfavourable, if ($R_L = 1$) it is linear, If ($0 < R_L < 1$) it is favourable and irreversible at ($R_L = 0$). Langmuir isotherm equation [3.11] can be linearized as

$$\frac{C_e}{q_e} = \frac{1}{b q_m} + \frac{C_e}{q_m} \quad [3.13]$$

Freundlich isotherm model (Cao et al., 2018; Nasri et al., 2019) is a two parameter model. Its equation is given by

$$q_e = K_F C_e^{\frac{1}{n}}, \quad [3.14]$$

where K_F [$(\text{mg g}^{-1})(L \text{ mg}^{-1})^{(1/n)}$] and n represent adsorption capacity and intensity, respectively.

This model can be applied to multilayer adsorption with non-uniform distribution of adsorption heat and affinities over the heterogeneous surface. It is widely applied for organic compounds. If the value of slope below unity implies chemisorption and if $1/n$ value is above one, it indicates cooperative adsorption. Equation [3.14] can be linearized in logarithmic form

$$\log q_e = \log K_F + \frac{1}{n} \log C_e \quad [3.15]$$

Temkin isotherm model (Khaled et al., 2009) is a two parameter model. Its equation is given by

$$q_e = \frac{R \times T}{b_o} \times \ln(\alpha \times C_e) \quad [3.16]$$

where T is the temperature in Kelvin (K), R is the universal gas constant whose value is $8.314 \text{ J mol}^{-1} \text{ K}^{-1}$ and $\beta_o = \frac{R \times T}{b_o}$. The constant b_o (J mole^{-1}) relates the heat of adsorption and α (L mg^{-1}) is Temkin isotherm equilibrium binding constant.

This model ignores extremely low as well as very large concentration. This model further assumes that heat of adsorption of all molecules in layer decreases linearly. It is further assumed that all the molecules have nearly uniform binding energies. If we are not having identical orientation this model is very good in prediction of gas phase equilibrium. Temkin model is simplified in linear form

$$q_e = \beta_o \ln \alpha + \beta_o \ln C_e \quad [3.17]$$

Redlich–Peterson model is a combination of Freundlich and Langmuir adsorption models. Redlich–Peterson isotherm follows the hybrid mechanism and does not assumes ideal monolayer adsorption (Rodríguez et al., 2009).

$$q_e = \frac{k_R C_e}{1 + a_R C_e^\beta} \quad [3.18]$$

The linear form of Equation [3.18] is

$$\ln \left[\frac{k_R C_e}{q_e} - 1 \right] = \ln a_R + \beta \ln C_e \quad [3.19]$$

where k_R (L g^{-1}) and a_R (L mg^{-1}) are Redlich–Peterson isotherm constants. Redlich–Peterson isotherm exponent is denoted by β (ranging from 0 to 1). For $\beta = 1$, Redlich–Peterson isotherm model converts to Langmuir isotherm model. If $a_R C_e^\beta \gg 1$ Redlich–Peterson isotherm model converts to Freundlich isotherm model and $a_R C_e^\beta \ll 1$ it follows Henry's law. Ratio $\frac{k_R C_e}{a_R C_e^\beta}$ represents adsorption capacity.

Sips isotherm is another mathematical model that describe adsorption equilibrium and is given by (Postai et al., 2016)

$$q_e = \frac{K_{LF} q_m C_e^n}{1 + K_{LF} C_e^n} \quad [3.20]$$

where K_{LF} and n are the Sips adsorption constant ($L \text{ mg}^{-1}$) and exponent, respectively. q_m is maximum adsorption capacity (mg g^{-1}).

The Toth isotherm mathematical model is used to describe adsorption on heterogeneous surfaces. This isotherm explains systems with sub-monolayer coverage and it reduces to Langmuir model when $t = 1$. The Toth isotherm equation can be given in the following form (Rodríguez et al., 2009):

$$q_e = \frac{k_T C_e}{[a_T + C_e^t]^{1/t}} \quad [3.21]$$

The linear form of eq. [3.21] is

$$\text{Ln} \left[\frac{q_e}{k_T} \right] = \text{Ln} C_e - \frac{1}{t} \text{Ln}(a_T + C_e^t) \quad [3.22]$$

Koble-Corrigan isotherm model (Khaled et al., 2009) is a three parameter model. Its equation is given by

$$q_e = \frac{AC_e^n}{1 + BC_e^n} \quad [3.23]$$

where A , B and n are isotherm constants. Koble-Corrigan isotherm incorporate Langmuir and Freundlich isotherm model. The value of B is nearly zero so this model favours Freundlich model over Langmuir model.

Radke-Prausnitz isotherm model (Singh et al., 2008) is a three parameter model. Its equation is given by

$$q_e = \frac{arC_e^n}{a + rC_e^{(n-1)}} \quad [3.24]$$

where n is model exponent and r and a are model constant. Radke-Prausnitz equation combines the Henry equation and Freundlich equation. This equation reduces to Henry's equation at lower concentration of adsorbate (Lataye et al., 2008).

Fritz-Schlunder isotherm model is a four parameter model applied for heterogeneous system and its equation is given by

$$q_e = \frac{\alpha_1 C_e^{\beta_1}}{1 + \alpha_2 C_e^{\beta_2}} \quad [3.25]$$

where β_1 and β_2 are isotherm exponent and α_1 and α_2 are model constant (Singh et al., 2008).

3.2.3 Optimization of feed conditions for adsorption of DB - 86

In the present study, RSM was used to obtain the optimal feed conditions of adsorption for maximum removal efficiency of DB-86 dye. A three-factor and five level (-1.68, -1, 0, +1, +1.68) full factorial central composite design was employed for design of experiments. The adsorption conditions were optimized using three independent variables: PnsAC-alginate dose (11.6-28.4 mg L⁻¹, X₁), concentration of DB-86 dye (65.9 -234 mg L⁻¹, X₂) and solution pH (1.82-5.2, X₃). The removal efficiency of DB-86 was considered as the response variable. Determination of zero point charge revealed that the PnsAC-alginate adsorbent was positively charged at pH less than 7.8. Several studies reported that the acidic condition (pH: 2-4) would be better in order to obtain higher removal efficiency of anionic dye while using adsorbent having positively charged surface (Maleki et al., 2016; Nemr et al., 2009; Temesgen et al., 2018). Thus in the present study, adsorption experiments were designed under acidic condition although typical textile effluent was generally alkaline (pH: 6.5-9.5) in nature (Khannous et al., 2015). A total of 20 experiments were performed in triplicate including six replicates of the centre points. Experimental data were fitted to the second order polynomial model (Montgomery, 2009):

$$Y = \beta_0 + \sum_{i=1}^3 \beta_i X_i + \sum_{i=1}^3 \beta_{ii} X_i^2 + \sum_{i=1}^2 \sum_{j=i+1}^3 \beta_{ij} X_i X_j \quad [3.26]$$

where, X and Y were independent variables and response variables, respectively. β_0 was the offset or constant term. β_i , β_{ii} and β_{ij} were the regression coefficients for linear effect, squared effect and interaction effect, respectively. The experimental results were expressed as means \pm standard deviation (n = 3). Results were analysed using the software Design- Expert 8.0.7.1 for

regression coefficients, regression equation and analysis of variance to determine any significant differences ($P < 0.05$).

3.2.4 Thermodynamic Study

It is necessary to analyse the system thermodynamically. Thermodynamic studies indicate the feasibility of the process. It was observed from the adsorption data, that there was no significant change in the adsorption with time at 35 °C and 45 °C. Therefore further studies had been carried out at maximum temp. of 35 °C.

Thermodynamic parameters like ΔS° , ΔH° and ΔG° were estimated by thermodynamic feasibility study (Leah et al., 2018).

Change in Gibbs free energy (ΔG°) is given by,

$$\Delta G^\circ = -RT \ln K_L^\circ \text{ and} \quad [3.27]$$

$$\Delta G^\circ = \Delta H^\circ - T\Delta S^\circ, \quad [3.28]$$

where $R = 8.314 \text{ J mol}^{-1} \text{ K}^{-1}$

A curve was plotted between Gibbs free energy (ΔG°) and absolute temperature (T), by slope and intercept we could find entropy (ΔS°) and enthalpy (ΔH°) respectively. Spontaneity of the process was judged by the (-ve) value of ΔG° (Mouni et al., 2018). As the value of ΔG° decreases with increase in temperature, rise in spontaneity was indicated.

3.2.5 Error analysis

The model that fits the data was judged by correlation coefficient (R^2), nonlinear regression coefficients like chi square test (χ^2) and Normalize standard deviation ($\Delta q_e\%$). The analysis equation are given by

$$\text{Chi square test } (\chi^2) = \sum_{i=1}^n \frac{(q_{e(\text{exp})} - q_{e(\text{pred})})^2}{q_{e(\text{exp})}} \quad [3.29]$$

$$\text{Normalized standard deviation } (\Delta q_e \%) = 100 \sqrt{\frac{\sum [(q_{e(\text{exp})} - q_{e(\text{pred})}) / q_{e(\text{exp})}]^2}{N}} \quad [3.30]$$

where $q_{e(\text{exp})}$ and $q_{e(\text{pred})}$ are the experimental q_e and predicted q_e , respectively. N is the number of measurements.

CHAPTER IV

ADSORPTION OF ACID YELLOW – 36 DYE USING PEANUT SHELL ACTIVATED CARBON

4.0 INTRODUCTION

In this chapter peanut shell activated carbon (PnsAC) was prepared using H_3PO_4 by pyrolysis. Isotherm, Kinetics and thermodynamic studies were also conducted to test its adsorption efficiency. The effect of operating parameters such as the initial pH, initial adsorbate concentration, adsorbent dose and contact time were also studied for dye removal using PnsAC from synthetic aqueous solution.

4.1 REMOVAL OF AY – 36 FROM AQUEOUS SOLUTION USING PnsAC

4.1.1 Characterization of PnsAC

Thermogravimetric analysis (TGA) is a technique to characterise the adsorbent in different environment. In this analysis mass of substance is observed as a function of temperature. In TGA exhibited three different zones, representing

- i. Removal of water
- ii. Decomposition of hemicellulose and cellulose
- iii. Decomposition of lignin

Thermogravimetric analysis of Peanut shell as shown in Fig.4.1, was conducted at a ramp of 10 °C. It showed that after attaining temperature of 600 °C, the loss of mass was almost negligible. Therefore, the pyrolysis temperature was considered as 650 °C.

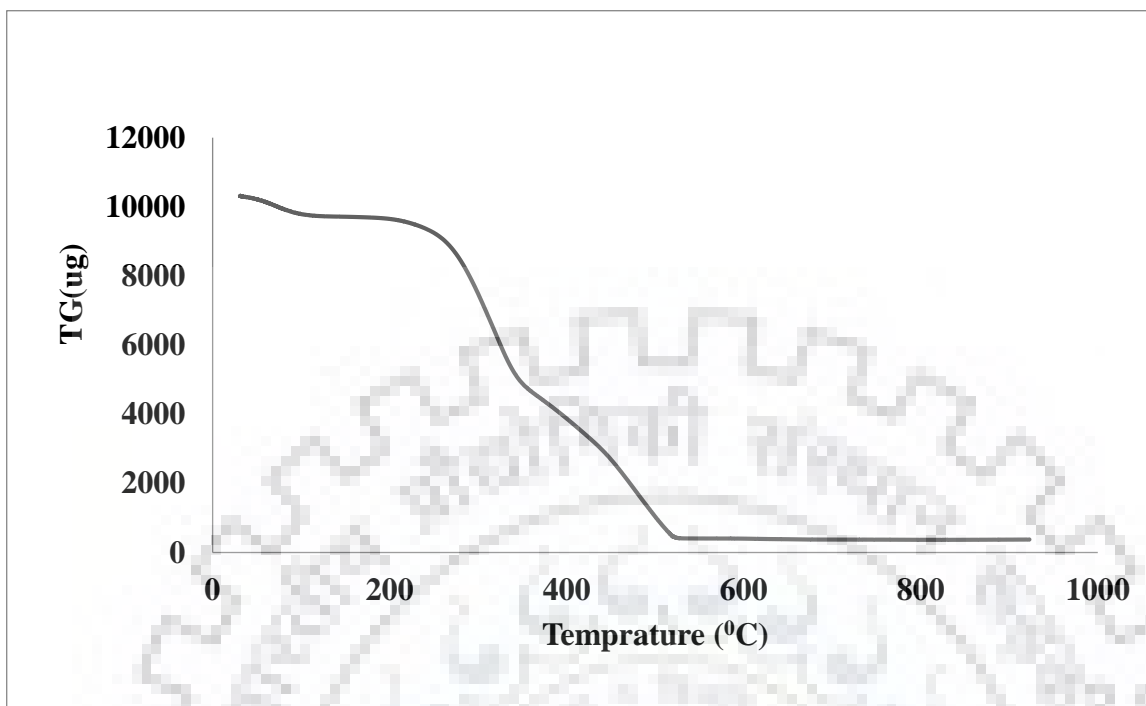


Fig.4.1 : Thermogravimetric analysis of Peanut shell at a heating rate of $10\text{ }^{\circ}\text{C min}^{-1}$

As shown in Fig.4.2 upon coating the nonconductive sample with platinum, surface morphology study showed the porous structure of PnsAC. Surface morphology of PnsAC was studied, before adsorption at 2500X magnification as shown in Fig.4.2 (a) and at 10000X as shown in Fig.4.2 (b). After adsorption surface morphology at 2500X is shown in Fig.4.2 (c) and at 10000X magnification is shown in Fig.4.2 (d).

Micropores and macropores were observed on the PnsAC surface. The pore structures of activated carbons are classified into micropore ($\leq 2\text{ nm}$) and macropore ($\geq 50\text{ nm}$) (Groen et al., 2003).

A high amount of cellulose in the Peanut shell was converted into porous carbon during the activation process. This conversion increased the size of the opening of pores (Saha et al., 2009).

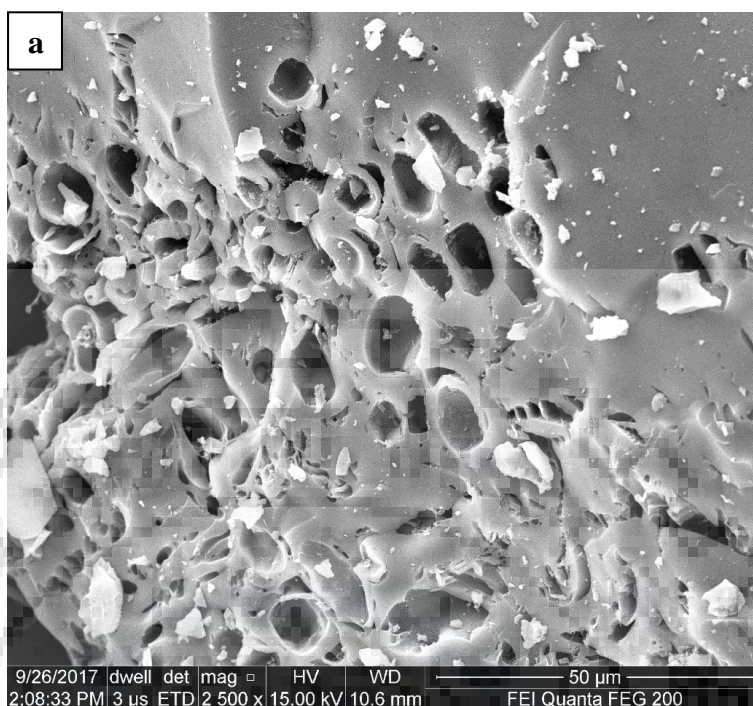


Fig. 4.2 (a) : Micrograph of PnsAC at 2500X, before adsorption

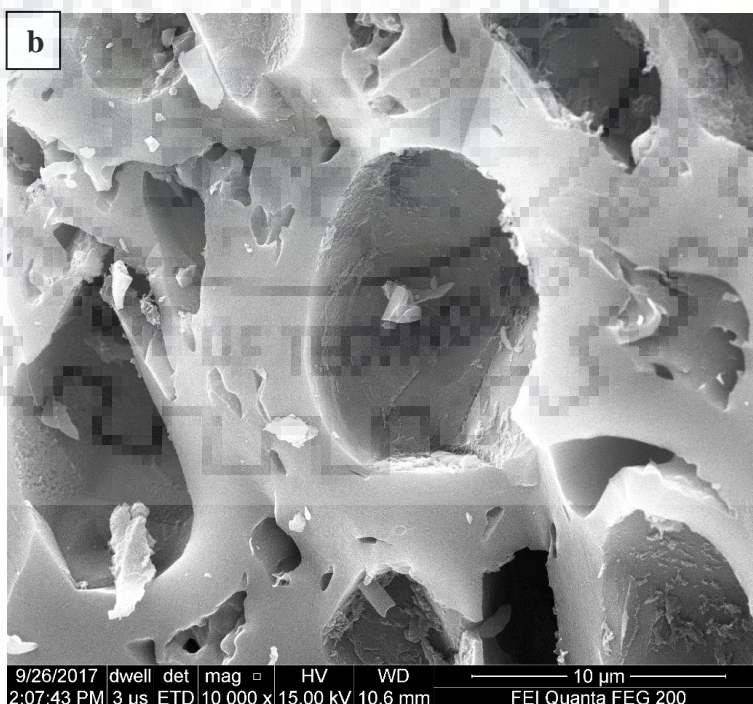


Fig. 4.2 (b) : Micrograph of PnsAC at 10000X, before adsorption

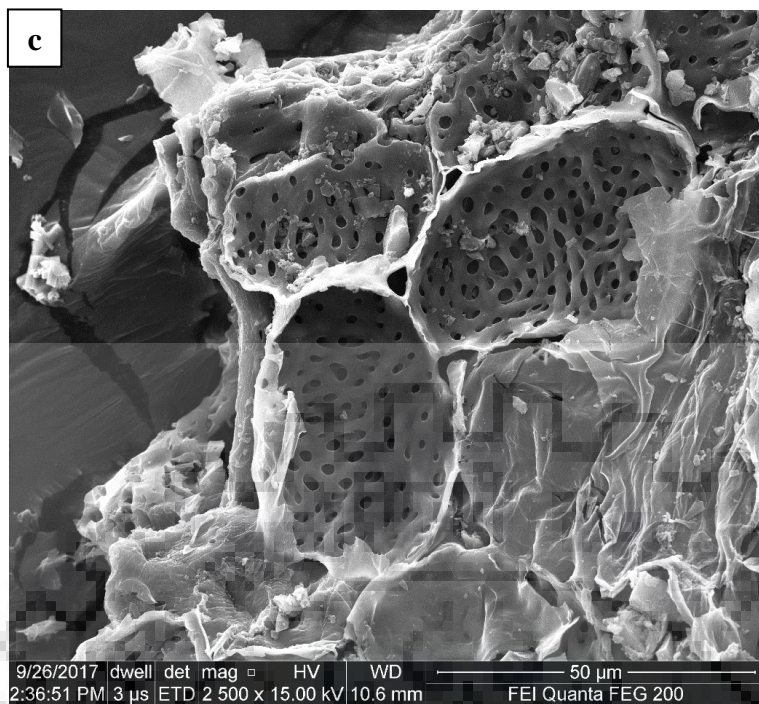


Fig. 4.2 (c) : Micrograph of PnsAC at 2500X, after adsorption of AY-36

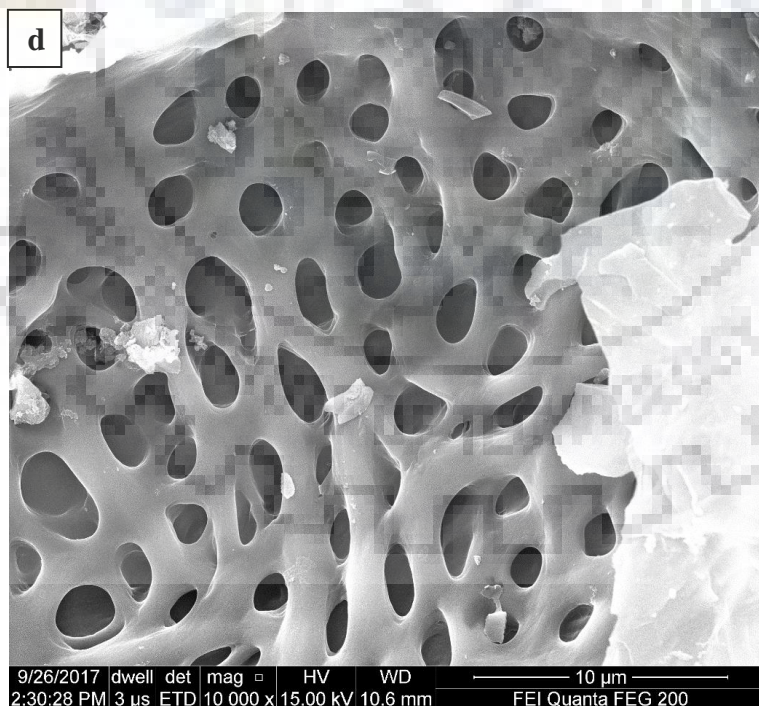


Fig. 4.2 (d) : Micrograph of PnsAC at 10000X, after adsorption of AY-36

The EDX spectra of PnsAC are shown in Fig. 4.3 (a) and 4.3 (b). A semi-quantitative analysis was carried out. Carbon, phosphorus, and oxygen were found before the adsorption of AY-36 dye, whereas after adsorption sulphur and nitrogen were found in addition to the aforementioned components. Fig.4.3 showed that nitrogen and sulphur are chemically associated with the dye molecule. Therefore, addition of nitrogen and sulphur indicates the adsorption of AY-36 dye on PnsAC.

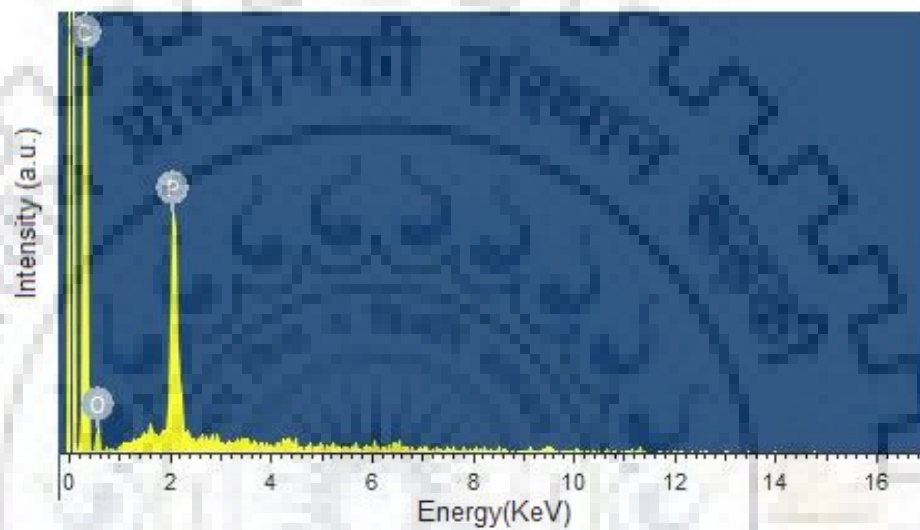


Fig. 4.3 (a) : EDX spectra of PnsAC before Adsorption

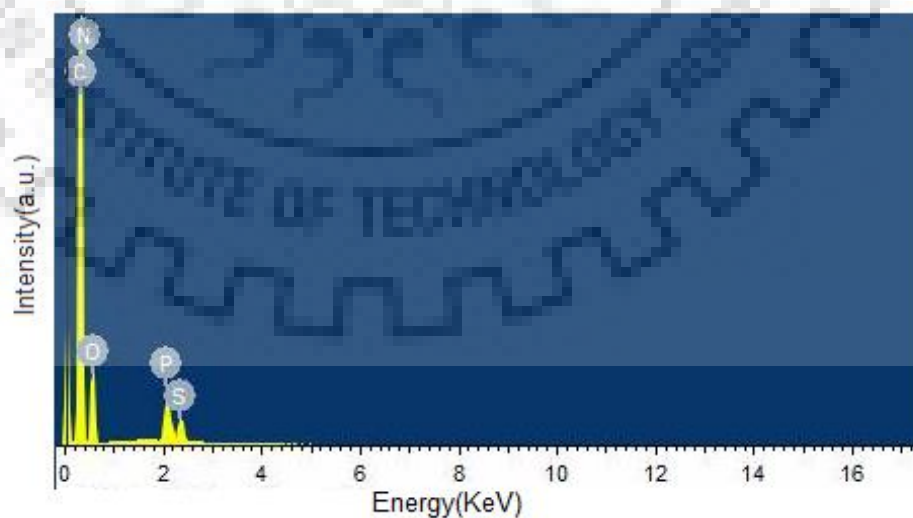


Fig. 4.3 (b) : EDX spectra of PnsAC after Adsorption of AY-36

FTIR analysis was conducted to detect the functional groups in PnsAC. The infrared vibrational spectrum is shown in Fig. 4.4 (a) and (b). The FTIR spectrum of PnsAC shows that the peak positions are at (2773, 2297, 1723, 1625, 1121, and 963) cm^{-1} . The band at 2773 cm^{-1} corresponds to C - H stretching, characteristic of aromatics, aliphatic and olefins in the lignocellulosic material. The band at 2297 cm^{-1} for peanut hull based activated carbon was attributed to the C - C stretching vibration while peak at 1723 attributed to (C = O) carbonyl compounds (Georgin et al., 2016). The absorption peak at 1625 cm^{-1} could be due to C = C present in structures such as olefins and aromatic rings (Wu et al., 2013a). The band at 1121 cm^{-1} indicated the presence of C - O bond in carboxylic group. 963 cm^{-1} is due to the presence of alcohol groups (R - OH). The evidence of hydroxyl groups in the peanut shells was mainly due to cellulosic components.

FTIR spectrum of PnsAC shows that the presence of above mentioned functional groups are ascribed to agricultural compounds of cellulose, hemicellulose and lignin (Zhong et al., 2012). The calculated BET surface area, Langmuir surface area, micropore area, and micropore volume of PnsAC were 965.678 $\text{m}^2 \text{g}^{-1}$, 1487.048 $\text{m}^2 \text{g}^{-1}$, 376.815 $\text{m}^2 \text{g}^{-1}$ and 0.204 $\text{cm}^3 \text{g}^{-1}$ respectively. The Langmuir isotherm based on assumption that the monolayer adsorption is the limit, whereas the BET isotherm equation ascribes partial and multilayer adsorption in terms of the monolayer. Therefore, the Langmuir surface area is always higher than the BET surface area (Gregg and Sing, 1982).

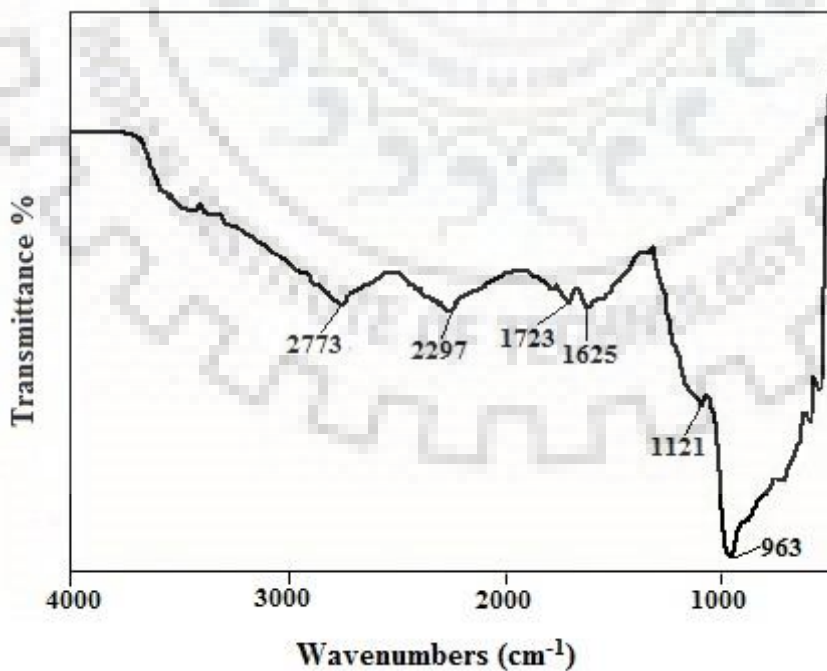


Fig. 4.4 (a) : FTIR image of PnsAC

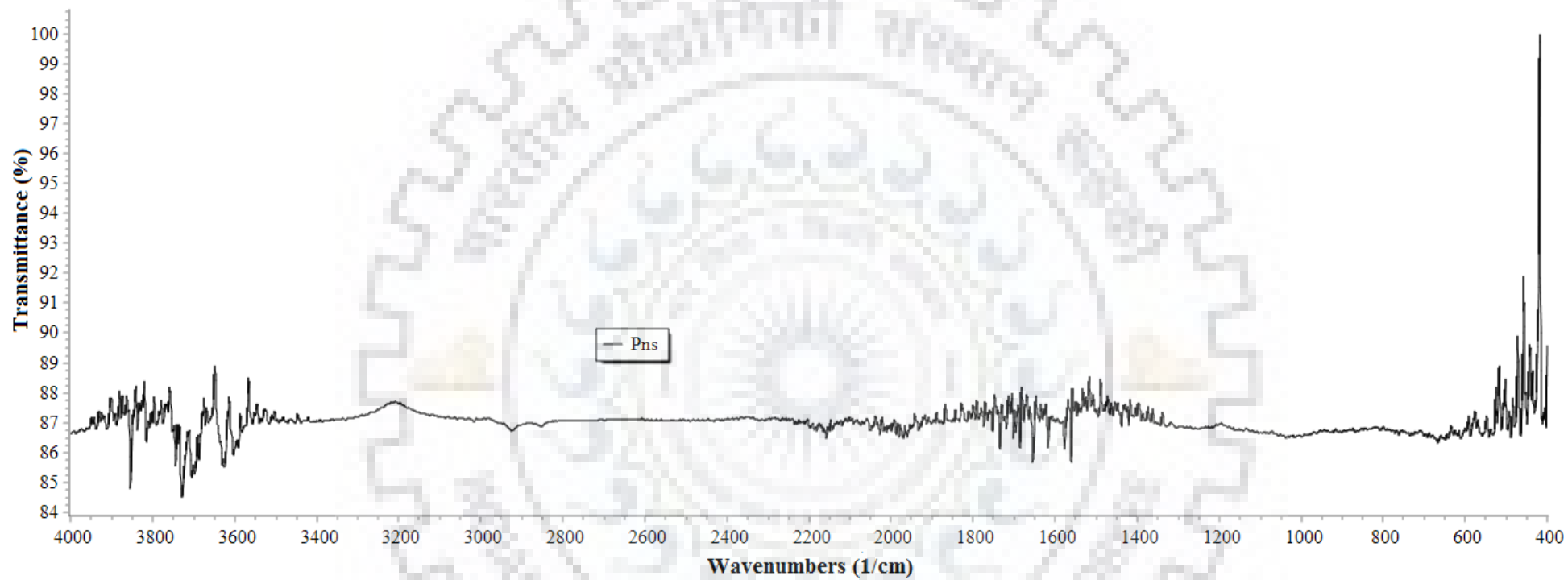


Fig. 4.4 (b) : FTIR image of Pns used as precursor

The Transmittance peak as shown in Fig. 4.4 (b) at 3624 cm^{-1} corresponds to stretching vibration of hydroxyl group (Zhong et al., 2012). The peak obtained at 1735 cm^{-1} was due to stretching of carbonyl group $\text{C} = \text{O}$, (Zhao et al., 2017) and this was shifted to 1723 cm^{-1} in activated carbon sample (PnsAC). The peak at 1654 cm^{-1} could be ascribed to $\text{C} = \text{C}$ stretching vibration of cyclic aromatic group (Yue et al., 2013) which was shifted to 1625 cm^{-1} in PnsAC. The band at 1561 cm^{-1} showed the presence of aromatic ring (Zhang et al., 2016). The peak at 1438 cm^{-1} corresponded to $\text{C} - \text{H}$ and CH_2 bending (Zhang et al., 2016) and carboxyl group, which originated from hemicellulose, lignin and cellulose existing in Pns (Zhao et al., 2017).

Peanut shells based activated carbon prepared in this study indicated relatively high surface area than reported earlier (Ahmad et al., 2012; Georgin et al., 2016) due to the additional chemical activation process of PnsAC. This showed that prepared PnsAC consists of porous structure.

4.1.2 Adsorption Studies

4.1.2.1 Effect of Initial pH

pH of adsorbate–adsorbent mixture affects the adsorption process. Adsorption of dye depends upon zero point charge and solution pH.

Zero point charge (pH_{ZPC}) is defined as the pH below which the total surface of the adsorbent particles is positively charged. Adsorption of anionic dye is favoured at $\text{pH} < \text{pH}_{\text{ZPC}}$ due to the net surface charge of the carbon material (Rodríguez et al., 2009). pH_{ZPC} of adsorbent developed from peanut shell, activated with phosphoric acid was found to be 2.3 (Fig. 4.5).

AY-36 is a negatively charged dye and when came into contact with PnsAC in the solution, an electrostatic force of attraction generated due to their opposite charges. The negative charge on the sorbent surface increased at high pH and thus, no attraction was observed among sorbent and dye molecules, resulting in decrease in adsorption.

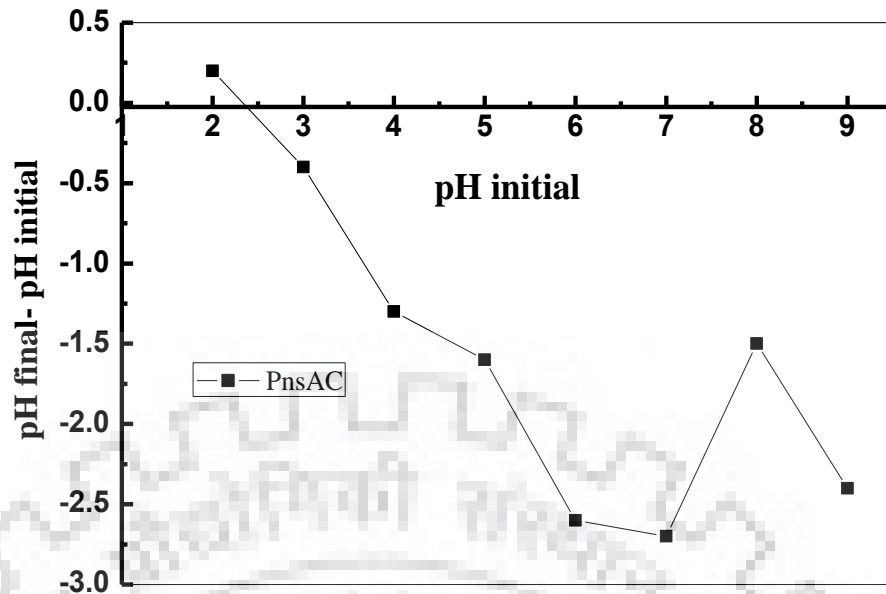


Fig. 4.5 : The zero point charge of PnsAC

The charge on the adsorbent surface, control the interaction of adsorbate ions on PnsAC surface. Fig. 4.6 illustrates the percent dye removal using PnsAC with time at different pH. The maximum adsorption was observed at a pH of 2. H^+ ion concentration on the adsorbent surface increased at low pH, and thus the surface was positively charged (Mittal et al., 2008; Nembr et al., 2009).

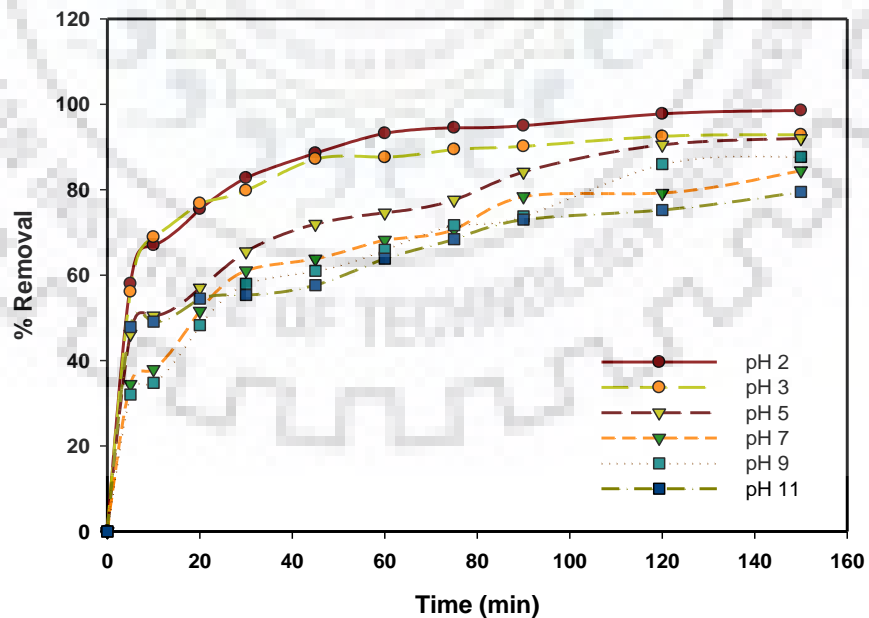


Fig. 4.6 : Effect of pH on dye removal using PnsAC at different time intervals (Temp: 35 °C; C_0 : 200 mg L⁻¹; PnsAC: 4 g L⁻¹)

When the pH was increased from 2 to 11, as shown in Fig. 4.6, for AY-36 with a concentration of 200 mg L^{-1} with a PnsAC dose of 4 g L^{-1} , the equilibrium adsorption capacity decreased from 49.275 mg g^{-1} to 39.75 mg g^{-1} , and the removal percentage decreased from 98.55 % to 79.5 %. Furthermore, it was observed that pH did not affect the adsorption equilibrium time.

4.1.2.2 Effect of Adsorbent Dose

The effect of adsorbent dose was studied by varying the dose from 2 to 6 g L^{-1} at optimized pH 2 and initial dye concentration of 200 mg L^{-1} . In the initial 30 minutes, 50 % removal was observed with an adsorbent dose of 2 g L^{-1} , and 82 % and 96 % removal were observed with adsorbent doses of 4 g L^{-1} and 6 g L^{-1} , respectively, as shown in Fig. 4.7. The percentage removal increased with an increase in the dose because more number of active sites were available. The increase in adsorbent dose from 4 g L^{-1} to 6 g L^{-1} was not that effective in terms of dye adsorptive removal in 150 minutes at constant initial dye concentration as most active sites of adsorbent remained vacant or unutilized due to concentration limitation (Singh et al., 2008). It could be interpreted from Fig.4.7 that, adsorbent dose of 4 g L^{-1} and 6 g L^{-1} resulted in almost same amount of adsorptive removal of dye in 150 minutes. Therefore, an optimum dose of 4 g L^{-1} PnsAC was chosen for AY-36 removal with initial concentration of 200 mg L^{-1} .

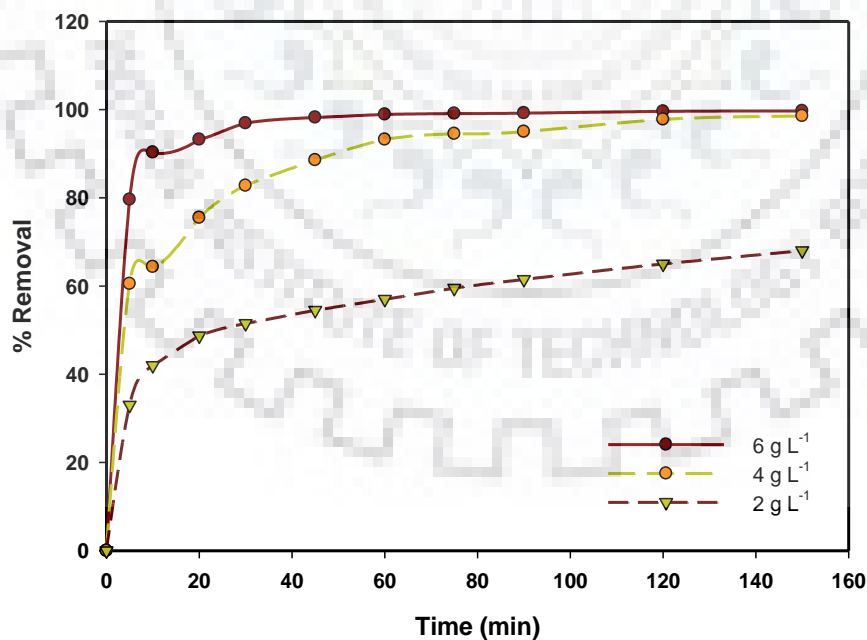


Fig. 4.7 : Effect of adsorbent dose on dye removal using PnsAC at different time intervals
(Temp: $35 \text{ }^{\circ}\text{C}$; C_0 : 200 mg L^{-1} ; pH: 2)

4.1.2.3 Effect of contact time and Initial Concentration

The amount of AY-36 adsorbed on PnsAC was studied as a function of shaking time at four different concentrations (100, 150, 200, and 250 mg L⁻¹) of AY-36 at 35 °C, 4 g L⁻¹ adsorbent dose, and pH of 2. The equilibrium was achieved in 150 minutes. It is evident from Fig. 4.8 that the dye sorption increased with increase in contact time in initial 20 minutes due to a strong driving force, then became slow up to 60 minutes and the saturation almost reached in 150 minutes. The removal was observed to be dependent on initial dye concentration. Initially, the sorption was fast and then, gradually it decreased and became constant after attaining equilibrium. An increase in the initial concentration results in the increased adsorption of AY-36. Higher initial concentrations resulted in increase in adsorptive removal because at higher concentrations; sorbate molecules occupied more sorption sites (AL-Othman et al., 2012; Georgin et al., 2016).

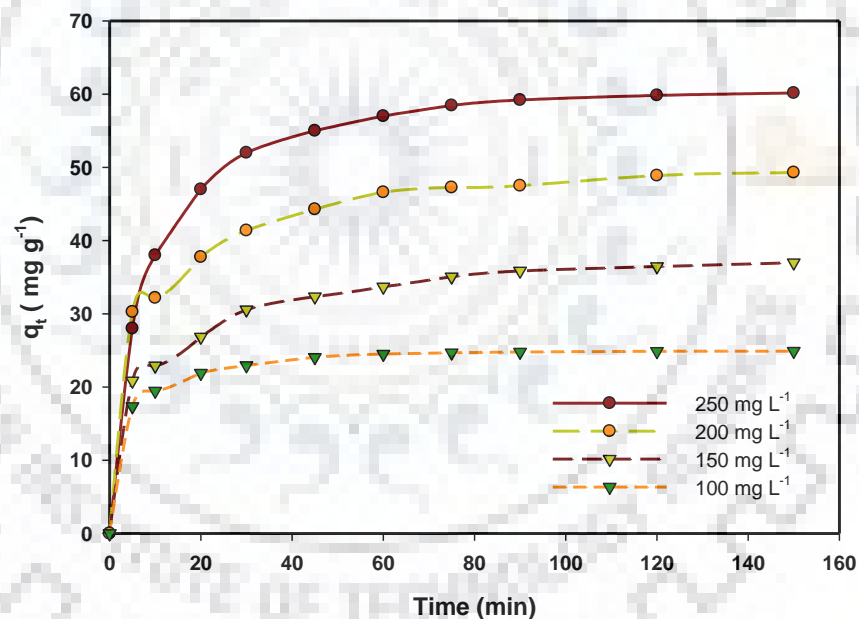


Fig. 4.8 : Effect of initial dye concentration on dye removal using PnsAC at different time intervals (Temp: 35 °C; PnsAC: 4 g L⁻¹; pH: 2)

4.1.3 Adsorption Equilibrium Isotherms

Calculated value of different parameters for various isotherm models were tabulated in Table 4.1.

Table 4.1: Adsorption equilibrium isotherm parameters of AY-36 on PnsAC

Isotherm Models	Parameters	Value
Langmuir	q_m (mg g ⁻¹)	66.7
	b (L mg ⁻¹)	0.94
	R^2	0.988
	$\Delta q_e\%$	16.7
Freundlich	K_F (L g ⁻¹)	32.5
	n	3.48
	R^2	0.954
	$\Delta q_e\%$	6.95
Redlich-Peterson	k_R (L g ⁻¹)	364.08
	a_R (L mg ⁻¹)	9.96
	β	0.77
	R^2	0.947
	$\Delta q_e\%$	7.23
Sip	K_{LF} (mg L ⁻¹)	0.35
	q_m (mg g ⁻¹)	128.07
	n	0.43
	R^2	0.949
	$\Delta q_e\%$	7.21
Toth	k_T (mg g ⁻¹)	600.0
	a_T (mg L ⁻¹)	0.43
	t	0.12
	R^2	0.948
	$\Delta q_e\%$	7.07

The dye uptake mechanism on adsorbent is therefore, likely to be complex due to wide range of adsorption sites and their corresponding energy considerations. Lower value of Δq_e % explained well the fitness of experimental data. Freundlich isotherm showed the minimum value of Δq_e %, therefore this model fitted the experimental data well. Though it was found that the experimental data are also in good agreement with Langmuir isotherm. The experimental data were in good agreement with the Freundlich isotherm with minimum value of Δq_e % showed that the surface of the PnsAC was non-uniform and heterogeneous. Fig. 4.9 presents the comparative study of experimental data with various isotherms model for the adsorption of AY-36 by PnsAC.

Furthermore, the data was found fit with the Langmuir isotherm (Rout et al., 2016). The interactions appeared to be driven by chemical forces as subsequently found from the kinetic and thermodynamic data. The Langmuir monolayer capacity of PnsAC for AY-36 dye adsorption was compared with other adsorbents (Table 4.2).

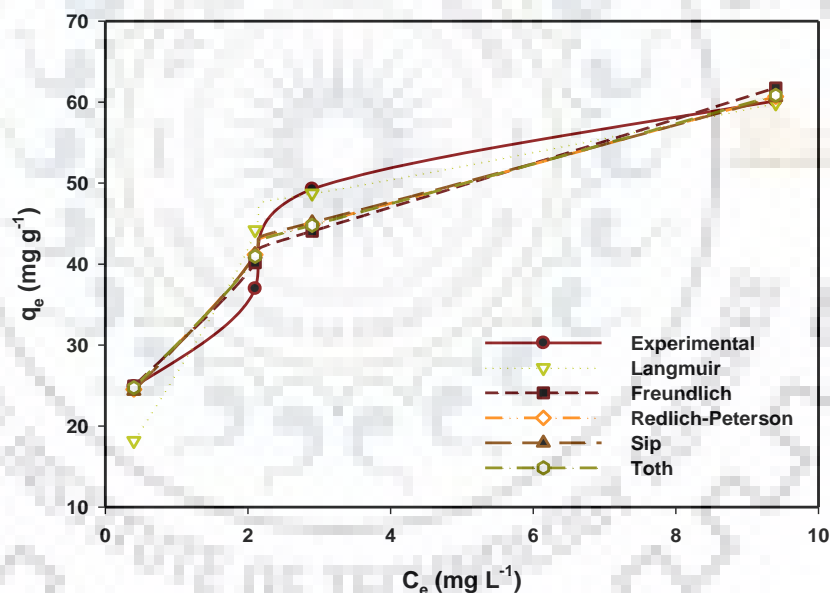


Fig. 4.9: Comparison of experimental and calculated equilibrium adsorption capacity using several isotherm models for the adsorption of AY – 36 on PnsAC (Temp: 35 °C; PnsAC: 4 g L⁻¹; pH: 2; C₀: 200 mg L⁻¹)

Table 4.2 : Comparison of monolayer adsorption capacities of AY-36 dye on various Adsorbents

Adsorbents	Maximum monolayer capacities (mg g ⁻¹)	References
Cross linked Chitosan beads	1334	(Chiou and Chuang, 2006)
Sawdust	1.310	(Pekkuz et al., 2008)
Cetyltrimethylammonium-bentonite	500	(Khenifi et al., 2007)
Graphene oxide	71.62	(Guo et al., 2013)
Grape industrial processing activated carbon	386	(Saygılı et al., 2015)
PnsAC	66.7	Present study

4.1.4 Adsorption Kinetics

A linear plot between (q_t) versus $t^{1/2}$ was used to predict the values of k_{id} and C . The value of constant, C in intra-particle diffusion model given in Table 4.3 suggested that the adsorption process was complex and involved more than one diffusional resistance (Rodríguez et al., 2009).

The values of correlation coefficient were found close to one and Δq_e % was found minimum for Pseudo second order kinetics, indicating that this model is more likely to predict the behaviour of the experimental data. Pseudo second order model (Fig. 4.10) is more likely to predict the kinetics, which indicated chemisorption mechanism as rate controlling during adsorption of AY-36 on PnsAC (Hameed et al., 2007; Zhong et al., 2012).

Table 4.3 : Kinetic parameters for AY-36 adsorption onto PnsAC

Kinetic models	Parameters	Value
Pseudo first order	$q_{e, \text{exp}} (\text{mg g}^{-1})$	49.3
	$q_{e, \text{calc}} (\text{mg g}^{-1})$	26.7
	$k_1 (\text{min}^{-1})$	0.035
	R^2	0.961
	$\Delta q_e \%$	22.9
Pseudo second order	$q_{e, \text{calc}} (\text{mg g}^{-1})$	52.6
	$k_2 (\text{g mg}^{-1} \text{min})$	0.003
	R^2	0.999
	$\Delta q_e \%$	3.41
Intra-particle diffusion	$C (\text{mg g}^{-1})$	28.46
	$k_{id} (\text{mg g}^{-1} \text{min}^{-0.5})$	1.977
	R^2	0.888
	$\Delta q_e \%$	3.45

In addition, the calculated q_e from Pseudo second order model as compared to the Pseudo first order kinetic model was found to be very close to the experimental q_e (Table 4.3) which further ensured suitability of this model. Suitability of Pseudo second order model possibly explains chemisorption mechanism as the rate controlling step for the sorption of AY-36 onto PnsAC (Hameed et al., 2007; Ma et al., 2012).

The intra-particle diffusion model consists of two phenomena, initial surface sorption and consequent intra-particle diffusion phenomena (Jo et al., 2016). The intra-particle diffusion model will be only limiting when the constant is zero in the plot of q_t versus $t^{1/2}$, (straight line pass through the origin). In the present study C is positive, which showed adsorption occurred right at the beginning of the process (Dalai et al., 2018; Ghaedi et al., 2014; Wu et al., 2009).

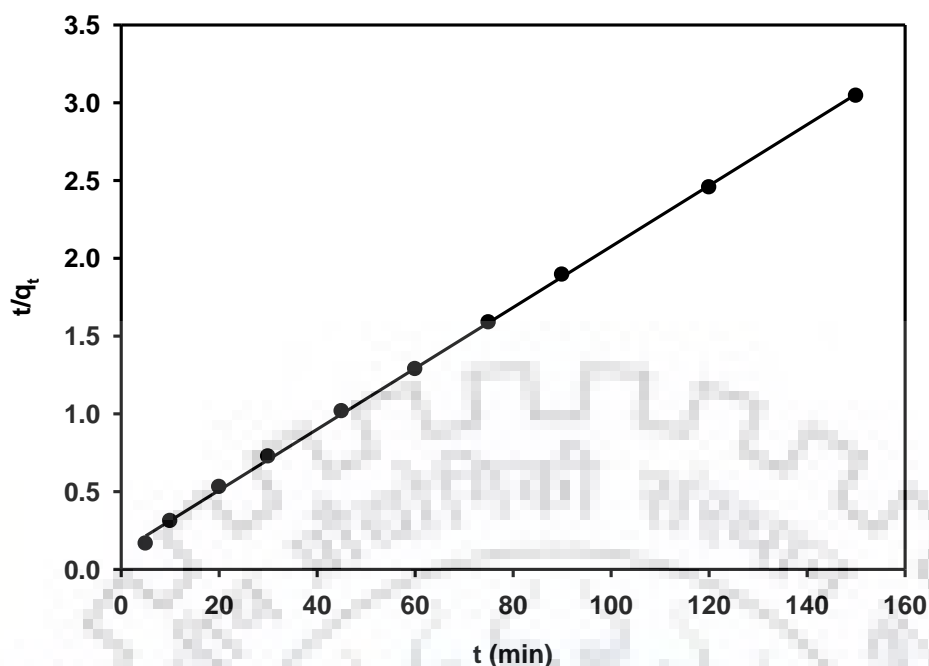


Fig. 4.10 : Pseudo second order kinetic plot (Temp: 35 °C; PnsAC : 4 g L⁻¹; pH : 2; C₀ : 200 mg L⁻¹)

Table 4.4 summarized the comparison of the Pseudo second order rate constants, using various adsorbate on peanut shell based activated carbon adsorbents.

Table 4.4 : Comparison of the Pseudo second order rate constant with various adsorbate on Peanut shell based activated carbon adsorbents

Adsorbates	Adsorbent preparation process	k_2 (g mg ⁻¹ min ⁻¹)	References
Direct Black 38	Microwave irradiation followed by pyrolysis	0.0607	(Georgin et al., 2016)
Cr(VI)	Chemical activation with KOH in N ₂ atmosphere – Oxidized	0.0069	(AL-Othman et al., 2012)
	Chemical activation with KOH in N ₂ atmosphere then heated in air – Unoxidized	0.0146	
Remazol Brilliant Blue R	Microwave induced phosphoric acid chemical activation	5.52×10^{-4}	(Zhong et al., 2012)

Adsorbates	Adsorbent preparation process	k_2 ($\text{g mg}^{-1} \text{min}^{-1}$)	References
Methylene blue	Activation by CO_2 in a high temperature fluidised bed reactor	5.15×10^{-5}	(Wu et al., 2013b)
AY-36	Activation by H_3PO_4 followed by pyrolysis at 650°C	0.0031	Present study

4.1.5 Adsorption Thermodynamics

Thermodynamic parameters including Gibbs free energy change (ΔG°), enthalpy change (ΔH°) and entropy change (ΔS°) were calculated for the adsorption process from the following equations (Hong et al., 2009; Karagoz et al., 2008);

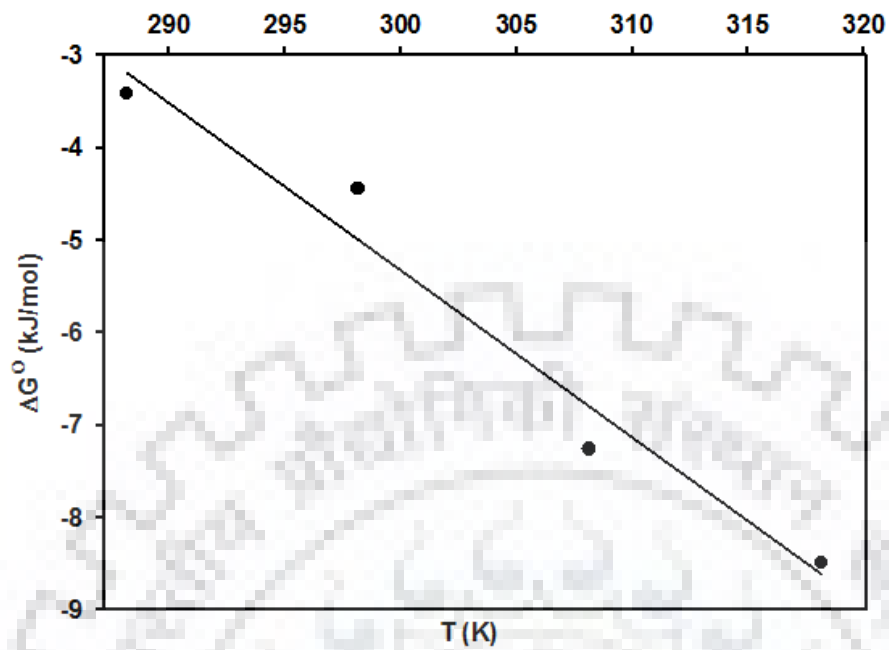
$$\Delta G^\circ = -RT \ln K_e \quad [4.1]$$

$$\Delta G^\circ = \Delta H^\circ - T\Delta S^\circ \quad [4.2]$$

The intercept and slope of a curve between ΔG° and T showed in Fig. 4.11 give ΔH° and ΔS° , respectively. Thermodynamic coordinates, namely ΔG° , ΔH° , and ΔS° (Lee and Sherif, 2001) are tabulated in Table 4.5. Negative values of ΔG° at all temperatures indicate that the process was spontaneous (Sharma et al., 2017). Values of ΔH° confirmed that the process was endothermic. Furthermore, ΔH° values in the range of 4 - 40 kJ mol^{-1} possess physisorption whereas chemical adsorption ranging from 40 to 800 kJ mol^{-1} . It can be inferred from ΔH° values in Table 4.5 that the interaction between AY-36 and PnsAC surface was may be due to chemical binding (Postai et al., 2016). Positive values of ΔS° indicated a natural attraction between the adsorbate and adsorbent (Kan et al., 2015).

Table 4.5 : Thermodynamic parameters for adsorption of AY-36 on PnsAC

T ($^\circ\text{C}$)	ΔG° (kJ mol^{-1})	ΔH° (kJ mol^{-1})	ΔS° ($\text{kJ mol}^{-1}\text{K}^{-1}$)
15	-3.42	48.689	0.18
25	-4.44		
35	-7.26		
45	-8.49		



**Fig. 4.11: Plot of ΔG° versus temperature for estimation of thermodynamic parameters
(Temp: 35 °C; PnsAC : 4 g L⁻¹; pH : 2; C₀ : 200 mg L⁻¹)**

ADSORPTION OF DIRECT BLUE – 86 DYE USING PEANUT SHELL ACTIVATED CARBON

5.0 INTRODUCTION

In this chapter ability of Peanut shell Activated Carbon (PnsAC) for the removal of DB-86 from aqueous solution is demonstrated. Batch experiments were performed to study the effect of initial pH, initial dye concentration, adsorbent concentration and temperature. Different kinetic models were utilized for fitting the experimental data. Isotherm models were applied to relate the dye adsorbed per unit mass of adsorbent to the adsorbate concentration at equilibrium. Thermodynamic analysis was done to assess the feasibility of the adsorption of DB-86 by PnsAC.

5.1 REMOVAL OF DB – 86 FROM AQUEOUS SOLUTION USING PnsAC

5.1.1 Characterization of PnsAC

PnsAC was analyzed by scanning electron microscope (SEM). Morphology and surface characterization such as particle shape and porosity of an adsorbent can be investigated using SEM. Higher the number of pores (size and shape), higher will be the adsorption. As presented in Fig.5.1, upon layering the nonconductive sample with gold, a surface morphology study presented the porous structure of PnsAC. In SEM pictures of PnsAC as shown in Fig.5.1 (a) – (d), significant mesopores were visualized. Fig.5.1 (a) – (b) presents the micrograph of PnsAC before adsorption at 10KX and 5KX respectively. After adsorption of DB-86 dye the micrograph images presented in Fig.5.1 (c) – (d) depicts, that the surface of adsorbent becomes smoother.

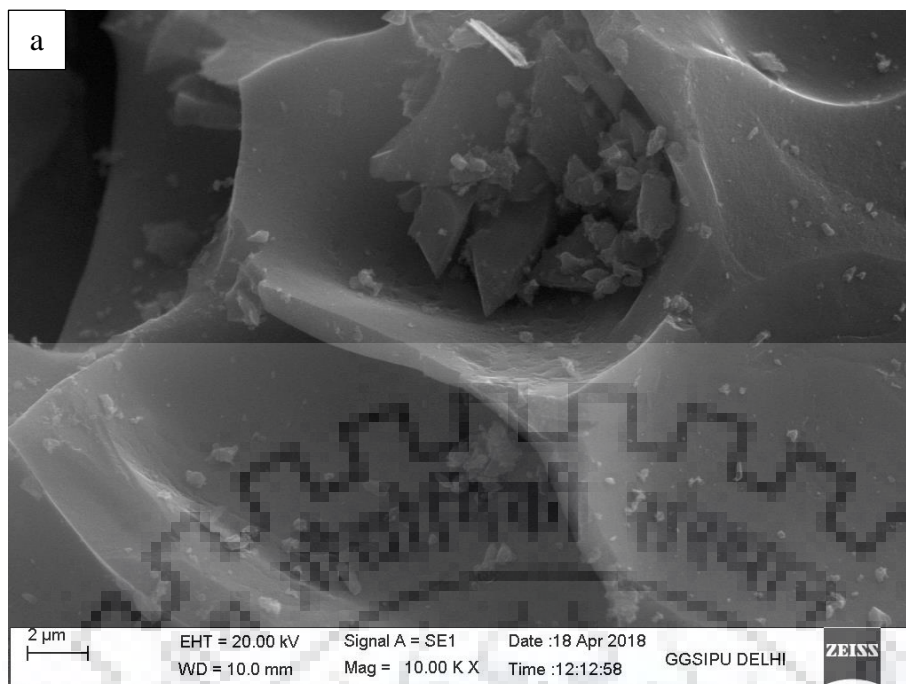


Fig.5.1 (a) : Micrograph of PnsAC before adsorption at 10KX

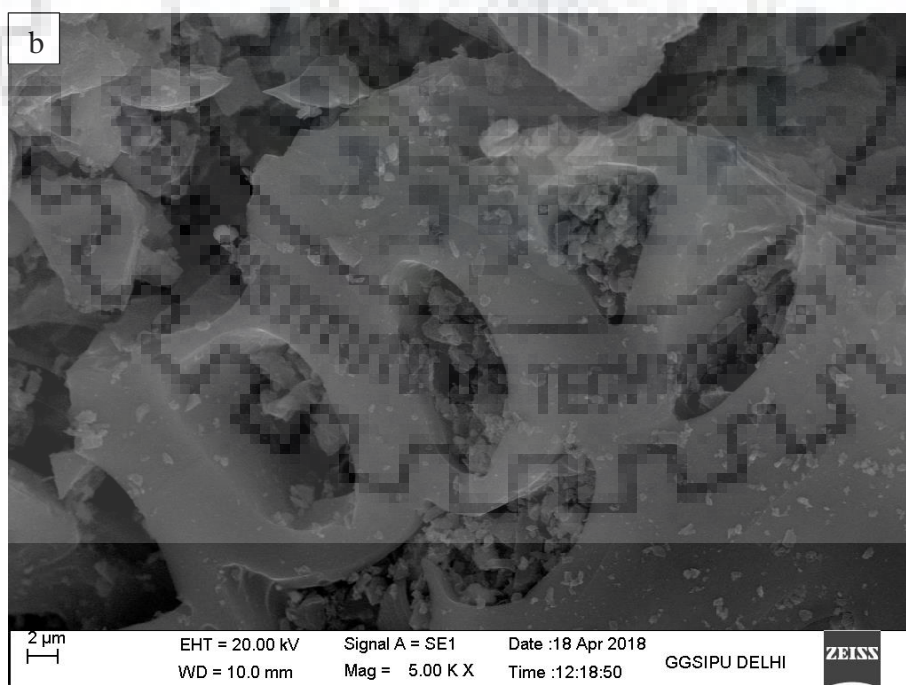


Fig.5.1 (b) : Micrograph of PnsAC before adsorption at 5KX

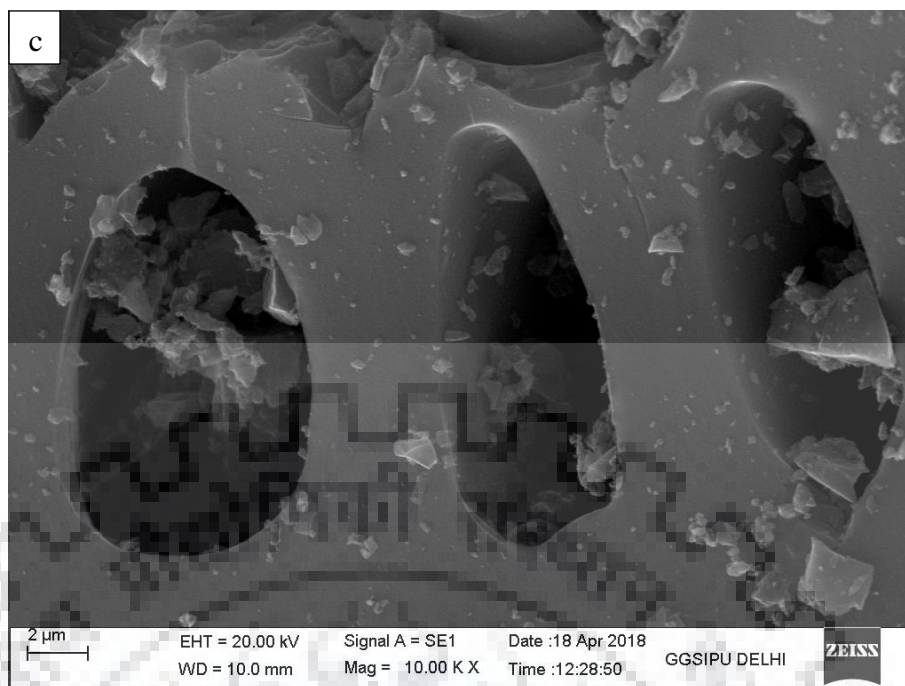


Fig.5.1 (c) : Micrograph of PnsAC after adsorption of DB-86 at 10KX

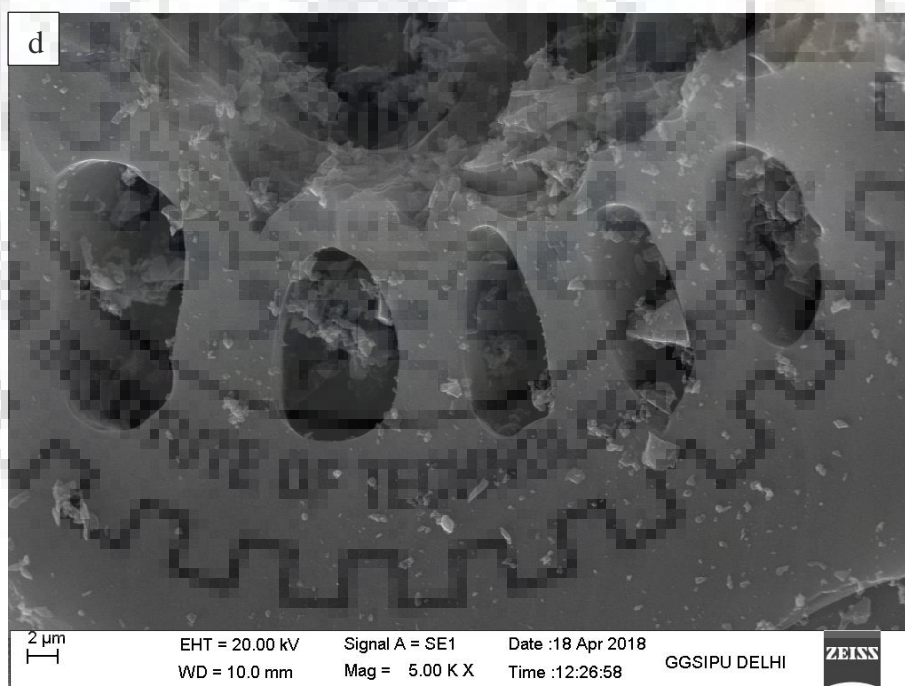


Fig.5.1 (d) : Micrograph of PnsAC after adsorption of DB-86 at 5KX

PnsAC samples were characterized by FTIR and EDX analysis, both before adsorption and after adsorption of DB-86 dye.

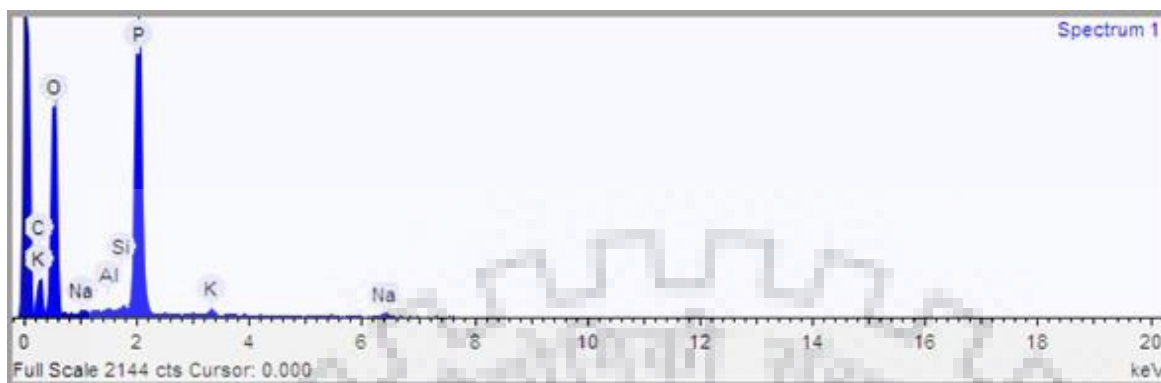


Fig. 5.2 (a) : EDX spectra before adsorption of DB-86

EDX spectrum as shown in Fig.5.2(a), revealed the presence of C, Na, O, P, K, Si, Al onto PnsAC adsorbent.

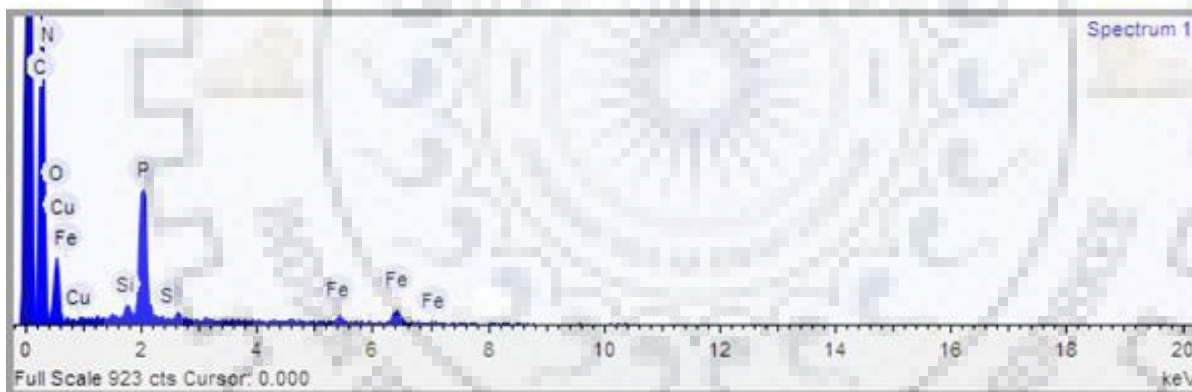


Fig. 5.2 (b) : EDX spectra after adsorption of DB-86

The presence of new elements S, Cu, N, Fe in the dye loaded PnsAC adsorbent indicated by EDX spectrum as shown in Fig.5.2 (b), confirmed the adsorption of DB-86 dye on the surface of PnsAC adsorbent.

FTIR spectra of PnsAC before and after adsorption of DB-86 dye are shown in Fig.5.2 (c). The Transmittance peak of PnsAC before adsorption of DB-86 dye at 3624 cm^{-1} corresponded to hydroxyl stretching vibration (Zhong et al., 2012). The peaks at 1654 cm^{-1} and 1561 cm^{-1} indicated the existence of aromatic ring (Yue et al., 2013; Zhang et al., 2016). The peak at 1438 cm^{-1} corresponded to C - H and CH_2 bending (Zhang et al., 2016) and carboxyl group, due to presence of lignin, cellulose and hemicellulose in the precursor (Zhao et al., 2017).

The transmittance peaks at 1654 cm^{-1} and 1438 cm^{-1} were not traceable in the FTIR spectra, after adsorption of DB-86 onto PnsAC. In addition to that, the new peaks found were at (2284, 2142, 911.1 and 596.7 cm^{-1}). The peak at 2284 cm^{-1} was due to $>\text{NH}_2^+$, $\equiv\text{NH}^+$, $=\text{NH}^+-$ group and 2142 cm^{-1} was showing $-\text{N}=\text{C}=\text{N}-$ group. So these peaks at 2284 cm^{-1} and 2142 cm^{-1} confirmed the adsorption of DB-86 dye.

The peak at 911.1 cm^{-1} showed $-\text{C}=\text{C}-$ group and 596.7 cm^{-1} showed alkyl-halide. The peaks at 911.1 cm^{-1} and 596.7 cm^{-1} falls under the category of fingerprint region.

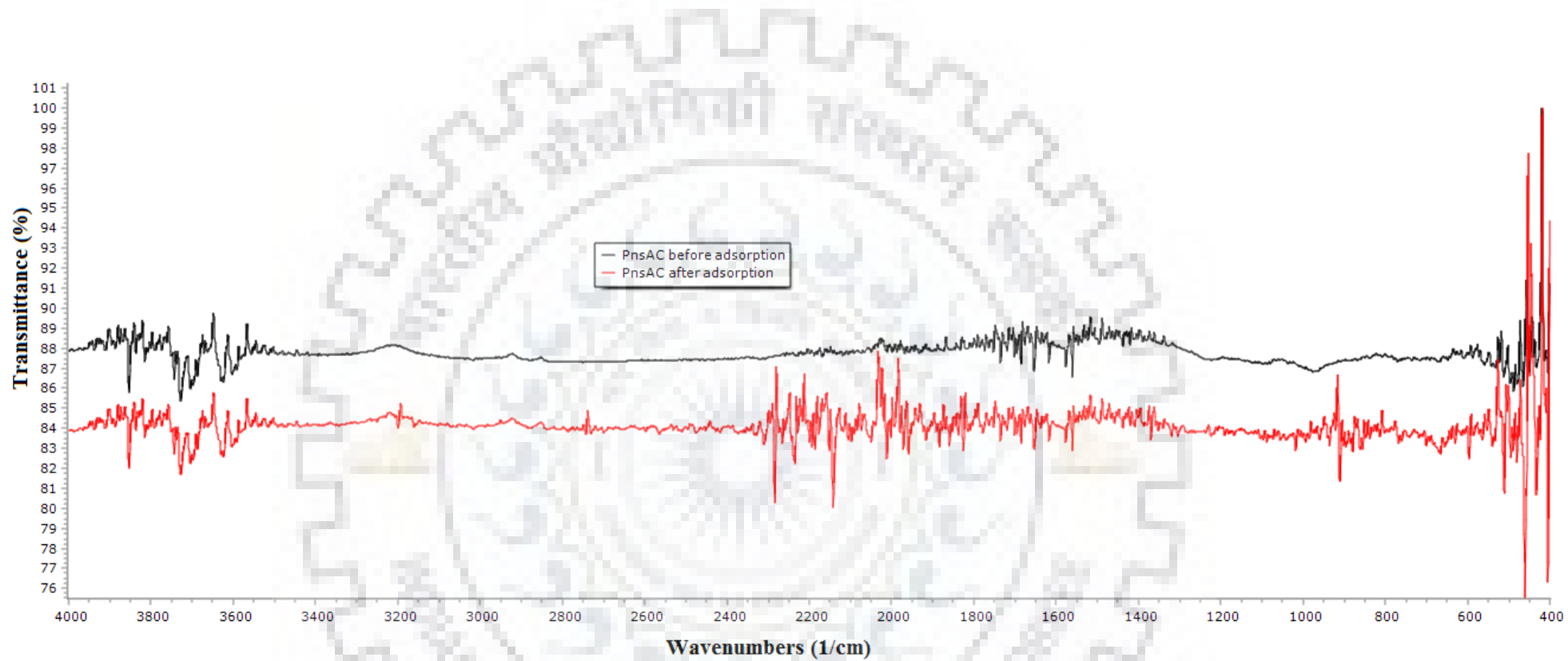


Fig. 5.2 (c) : FTIR of PnsAC before adsorption and after adsorption of DB-86

5.1.2 Effect of Initial pH

Effect of pH depends upon the charge present on the surface of adsorbent and is judged by zero point charge (pH_{ZPC}) (Singh et al., 2008). Zero point charge pH_{ZPC} was found to be 2.3 (Fig.4.5). If pH is less than pH_{ZPC} the surface of adsorbent is positively charged, so it will attract anionic dye DB-86 as there are opposite charges on adsorbent surface and dye. Furthermore, if pH is greater than pH_{ZPC} then the surface of adsorbent will be negatively charged. So there will be no electrostatic attraction between adsorbent and DB-86.

The effect of pH on DB-86 adsorption is shown in Fig.5.3. There is an attraction between dye molecules and PnsAC surface. For 100 mg L^{-1} dye concentration and 10 g L^{-1} PnsAC dose, equilibrium adsorption capacity is found to decrease from 7.86 mg g^{-1} to 2.29 mg g^{-1} , % removal decreased from 78.6 % to 22.9 % while pH is increased from 2 to 11. It can be said that maximum adsorption is at pH 2 and minimum adsorption is at pH 11. Maximum adsorption of anionic dye Direct Blue-53 was reported at pH 2, using multi-walled carbon nanotubes and activated carbon (Prola et al., 2013).

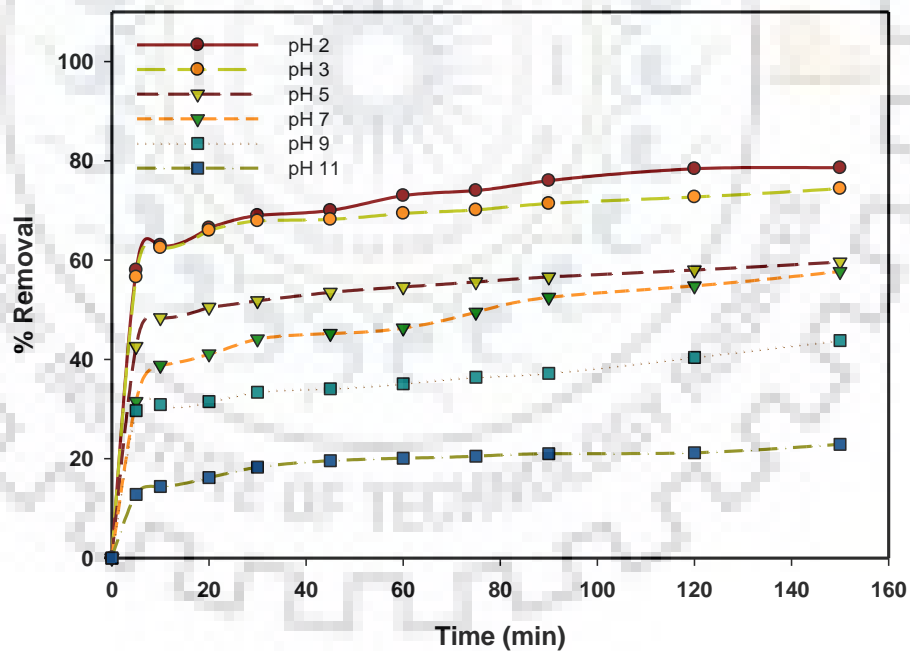


Fig.5.3 : Effect of pH on dye removal using PnsAC at different time intervals (Temp: $35 \text{ }^\circ\text{C}$; C_0 : 100 mg L^{-1} ; PnsAC: 10 g L^{-1})

5.1.3 Effect of Adsorbent dose

Effects of adsorbent dose were studied by varying the PnsAC dose from 4 g L^{-1} to 12 g L^{-1} at pH 2, 100 mg L^{-1} initial dye concentration, and temperature of $35 \text{ }^\circ\text{C}$. 40.6% removal was found in first 30 minutes with an adsorbent dose of 4 g L^{-1} . As evinced from Fig.5.4, 78.6% and 79.1% removal of DB-86 was observed at adsorbent dose of 10 g L^{-1} and 12 g L^{-1} , respectively. Percentage removal increases with the increase in adsorbent dose due to increase in available active sites (Othman et al., 2018).

It was observed from percentage removal versus time curve that 10 g L^{-1} and 12 g L^{-1} curves nearly overlap. Further there was no significant change with the adsorbent dose beyond 10 g L^{-1} . Therefore, the optimum dose for 100 mg L^{-1} solution of DB-86 was 10 g L^{-1} . The adsorption capacity of 100 mg L^{-1} DB-86 solution was found to decrease from 12.675 mg g^{-1} to 6.59 mg g^{-1} while the adsorbent dose was increased from 4 g L^{-1} to 12 g L^{-1} , respectively.

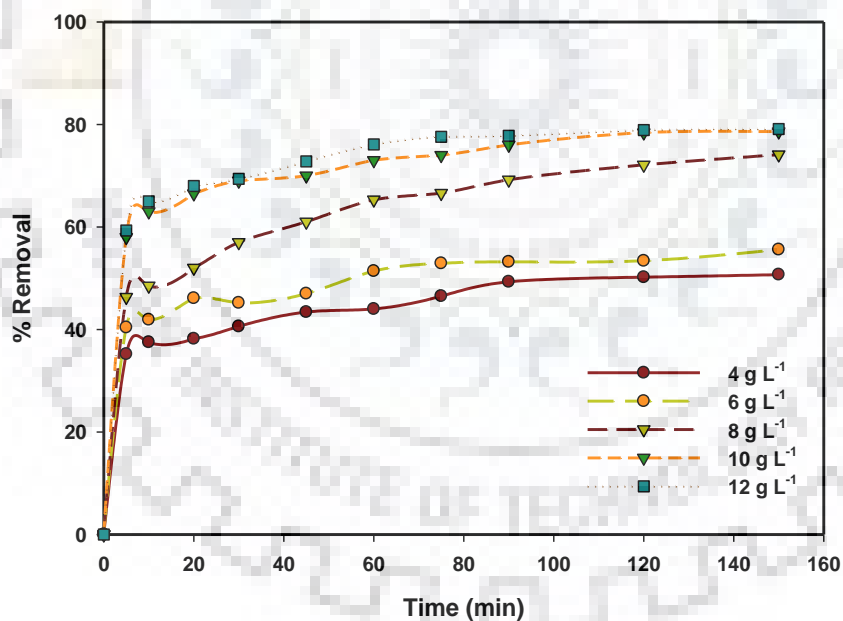


Fig.5.4 : Effect of adsorbent dose on dye removal using PnsAC at different time intervals (Temp: $35 \text{ }^\circ\text{C}$; C_0 : 100 mg L^{-1} ; pH: 2)

5.1.4 Effect of Initial DB – 86 Concentration

Various initial concentration of DB-86 dye (250 mg L^{-1} , 200 mg L^{-1} , 150 mg L^{-1} and 100 mg L^{-1}) were taken at 35°C , PnsAC dose 10 g L^{-1} , 120 rpm and pH of 2 as depicted in Fig.5.5. Initially the driving force is maximum so maximum adsorption was obtained in first half hour. The driving force is the difference in concentration between DB-86 solution and the concentration at adsorbent surface. Up to 15 minutes the dye adsorption was observed to be fast which decreased significantly and became almost constant as equilibrium was achieved. At higher initial dye concentration, adsorptive removal was decreased due to reduction in available adsorption sites for dye molecules (Singh et al., 2008).

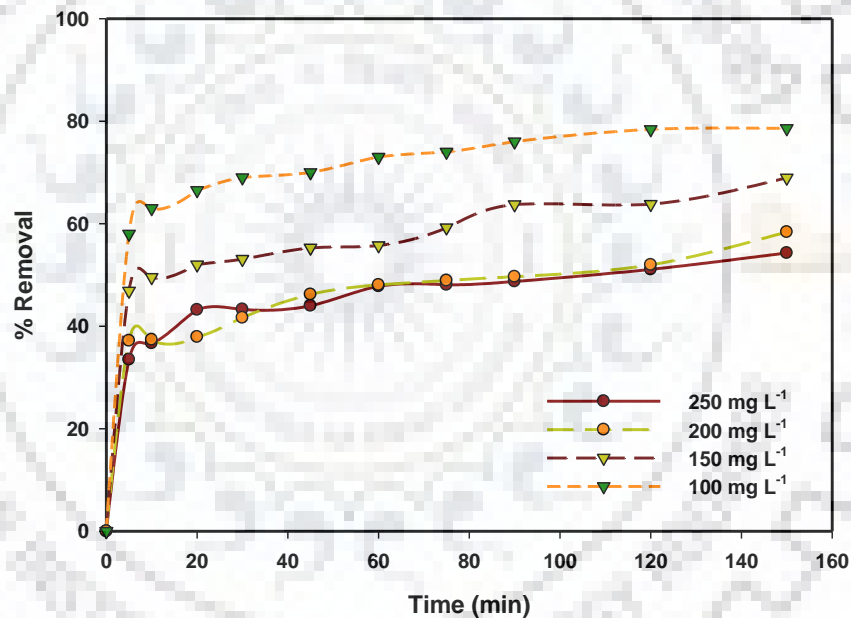


Fig.5.5 : Effect of initial dye concentration on dye removal using PnsAC at different time intervals (Temp: 35°C ; PnsAC: 10 g L^{-1} ; pH: 2)

5.1.5 Adsorption Equilibrium Isotherms

Adsorption isotherms provide crucial information regarding adsorption mechanisms and adsorption system design. The adsorption data of DB-86 was analysed for different adsorption models.

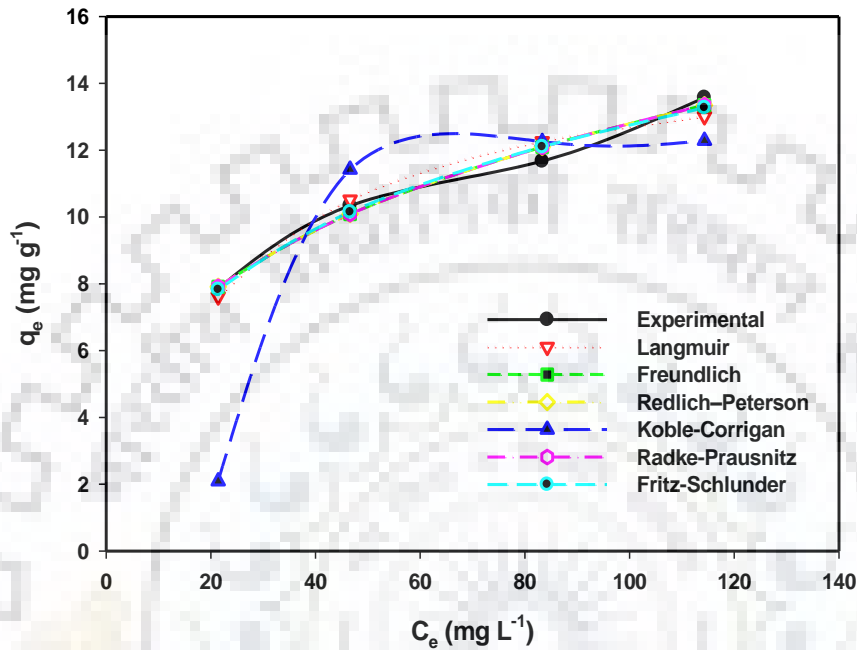


Fig.5.6 : Comparison of experimental and calculated equilibrium adsorption capacity using several isotherm models for the adsorption of DB-86 on PnsAC (Temp: 35 °C; PnsAC: 10 g L⁻¹; pH: 2)

Fig.5.6 shows plots between C_e versus q_e for different isotherm models. To compare the suitability isotherm, respective parameters, R^2 values, and normalized standard deviation (Δq_e %) of eight types of isotherm models are summarized in Table 5.1.

The minimum value of normalized standard deviation is found for Freundlich(Nasri et al., 2019), Redlich–Peterson, Sip, Radke–Prausnitz, Koble–Corrigan, and Fritz–Schlunder isotherm models. Contrarily, it is noteworthy that normalized standard deviation is comparatively high for Langmuir and Toth isotherm models, which shows that multilayer adsorption of DB-86 is mainly governing the adsorptive removal.

**Table 5.1 : Adsorption equilibrium isotherm parameters of Direct Blue-86 on PnsAC
(Temp: 35 °C; PnsAC: 10 g L⁻¹; pH: 2)**

Isotherm model		Parameters	Value
Langmuir	$q_e = q_m \frac{bC_e}{1+bC_e}$	q_m (mg g ⁻¹)	15.547
		b (L mg ⁻¹)	0.045
		R^2	0.956
		$\Delta q_e\%$	3.73
Freundlich	$q_e = K_F C_e^{1/n}$	K_F (L g ⁻¹)	3.039
		n	3.202
		R^2	0.983
		$\Delta q_e\%$	2.36
Redlich-Peterson	$q_e = \frac{k_R C_e}{1+a_R C_e^\beta}$	k_R (L g ⁻¹)	344.644
		a_R (L mg ⁻¹)	113.131
		B	0.688
		R^2	0.983
		$\Delta q_e\%$	2.36
Sips	$q_e = \frac{K_{LF} q_m C_e^n}{1+K_{LF} C_e^n}$	K_{LF} (mg L ⁻¹)	0.034
		q_m (mg g ⁻¹)	86.360
		N	0.355
		R^2	0.982
		$\Delta q_e\%$	2.36
Toth	$q_e = \frac{k_T C_e}{[a_T + C_e^t]^{1/t}}$	k_T (mg g ⁻¹)	614.013
		a_T (mg L ⁻¹)	0.554
		T	0.083
		R^2	0.982
		$\Delta q_e\%$	3.16
Koble-Corrigan		A	2.862
		B	0.044

Isotherm model		Parameters	Value
	$q_e = \frac{AC_e^n}{1+BC_e^n}$	N	0.372
		R ²	0.982
		Δq _e %	2.37
Radke-Prausnitz	$q_e = \frac{arC_e^n}{a+rC_e^{(n-1)}}$	A	319.895
		R	3.047
		N	0.312
		R ²	0.983
		Δq _e %	2.36
Fritz-Schlunder	$q_e = \frac{\alpha_1 C_e^{\beta_1}}{1 + \alpha_2 C_e^{\beta_2}}$	α ₁	1.708
		α ₂	0.458
		β ₁	1.299
		β ₂	1.027
		R ²	0.982
		Δq _e %	2.35

Freundlich, Redlich–Peterson, Sip, Radke–Prausnitz, Koble–Corrigan, and Fritz–Schlunder best fitted the equilibrium of experimental data with R² (≥ 0.982) and Δq_e % values (2.35 - 2.37), which shows that heterogeneous adsorption is dominating. Though, the aforementioned result of regression correlation coefficients (> 0.956) and Δq_e % values (< 4) shows good agreement in the case of all isotherms at different dye concentration ranges. The applicability of all the isotherm models to the DB-86 – PnsAC system implies that both monolayer adsorption and heterogeneous surface conditions exist simultaneously under existing experimental conditions. The adsorption of DB-86 on activated carbon is a complex process and involves more than one mechanism. Similar interpretation is reported by researchers for methylene blue adsorption onto silica adsorbent (Al-Qodah et al., 2007).

The value of Freundlich isotherm exponent *n* between 1 and 10 indicates favourability of adsorption (Singh et al., 2008). In the present investigation, *n* value was found to be 3.202, indicating that adsorption of DB-86 is favourable on PnsAC (Table 5.1). The Separation factor R_L of the Langmuir equation, indicates the nature of the adsorption process. This indicates the

nature of adsorption as $R_L > 1$ (unfavourable), $0 < R_L < 1$ (favourable), $R_L = 0$ (irreversible), and $R_L = 1$ (linear) (Sharma et al. 2017b). In the present study, the R_L values below 1.0 for adsorptive removal of DB-86 dye at prevailing operating condition.

5.1.6 Adsorption Kinetics

Adsorption kinetics plays a significant role in adsorption. It provides the information about the mechanism of the process. Kinetic data were predicted using Pseudo first order model (Prola et al., 2013), Pseudo second order model (Mouni et al., 2018) and intra-particle diffusion model (Khani et al., 2018) presented in Table 5.2 for the adsorption of DB-86 dye onto PnsAC.

In q_t vs $t^{0.5}$ plot, if the line passing through origin the diffusion is the rate controlling step and if the line is not passing through origin, shows that diffusional resistance is not only controlling mechanism and thickness of boundary layer is given by the constant C (Boukhalfa et al., 2019).

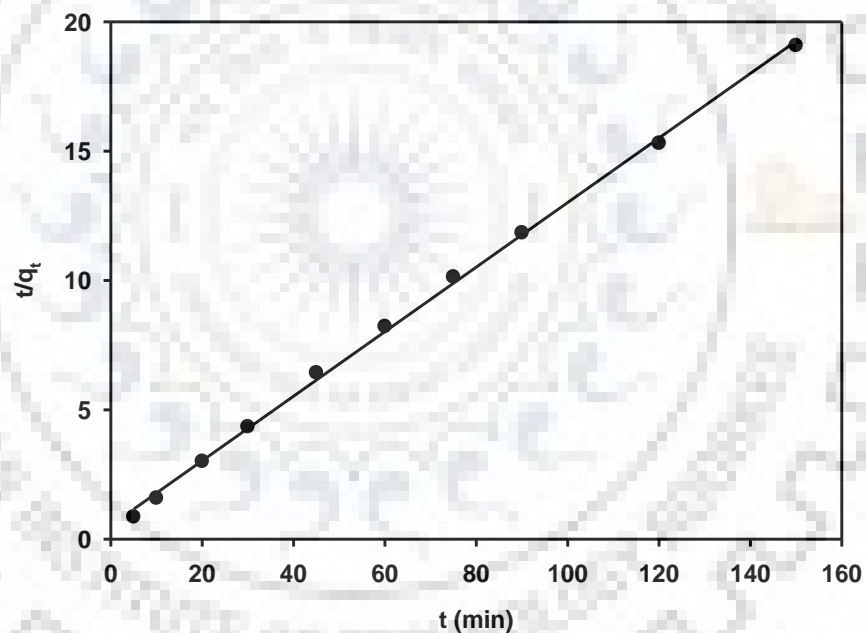


Fig.5.7: Pseudo second order kinetic plot (Temp: 35 °C; PnsAC: 10 g L⁻¹; pH: 2; C₀: 100 mg L⁻¹)

The correlation coefficient value of Pseudo second order kinetics model is maximum and (> 0.99), which shows that Pseudo second order model is best fit. Further it shows that chemisorption is dominating and the rate controlling (Fabryanty et al., 2017).

Table 5.2 : Kinetic parameters for DB-86 adsorption onto PnsAC at different initial dye concentration (Temp: 35 °C; PnsAC: 10 g L⁻¹; pH: 2)

		Pseudo first order model			Pseudo second order model			Intra-particle Diffusion Model		
C ₀ (mg l ⁻¹)	q _{e, exp} (mg g ⁻¹)	k ₁ (min)	q _e mg g ⁻¹	R ²	k ₂ (g mg ⁻¹ min ⁻¹)	q _e (mg g ⁻¹)	R ²	k _{id} (mg g ⁻¹ min ^{0.5})	C	R ²
100	7.86	0.083	3.721	0.870	0.029	8.065	0.998	0.198	5.654	0.952
150	10.34	0.037	4.572	0.790	0.012	10.417	0.991	0.311	6.303	0.965
200	11.67	0.032	5.703	0.797	0.009	11.628	0.987	0.418	6.167	0.957
250	13.57	0.041	6.038	0.824	0.010	13.699	0.995	0.464	7.961	0.937

5.1.7 Thermodynamic Study

It is necessary to analyse the system thermodynamically to understand the feasibility of the process. Percentage removal of DB-86 dye was studied at four different temperature (15 °C, 25 °C, 35 °C and 45 °C). The line of 45 °C nearly overlaps (Fig.5.8) the 35 °C curve. Since no significant variation in the removal of dye has been observed between 35 °C and 45 °C therefore further studies have been carried out at maximum temperature of 35 °C.

Thermodynamic parameters like ΔS° , ΔH° and ΔG° were estimated by thermodynamic study (Al-Qodah et al., 2007; Han et al., 2005).

$$\Delta G^\circ = -RT \ln K_d \quad [5.1]$$

$$\ln K_d = \frac{\Delta S^\circ}{R} - \frac{\Delta H^\circ}{RT} \quad [5.2]$$

where, R is the gas constant ($8.314 \text{ J mol}^{-1}\text{K}^{-1}$) and T is the absolute temperature. The values of change in entropy (ΔS°) and change in enthalpy (ΔH°) were obtained from the intercept and slope of plot $\ln K_d$ versus $1/T$ (Fig.5.9).

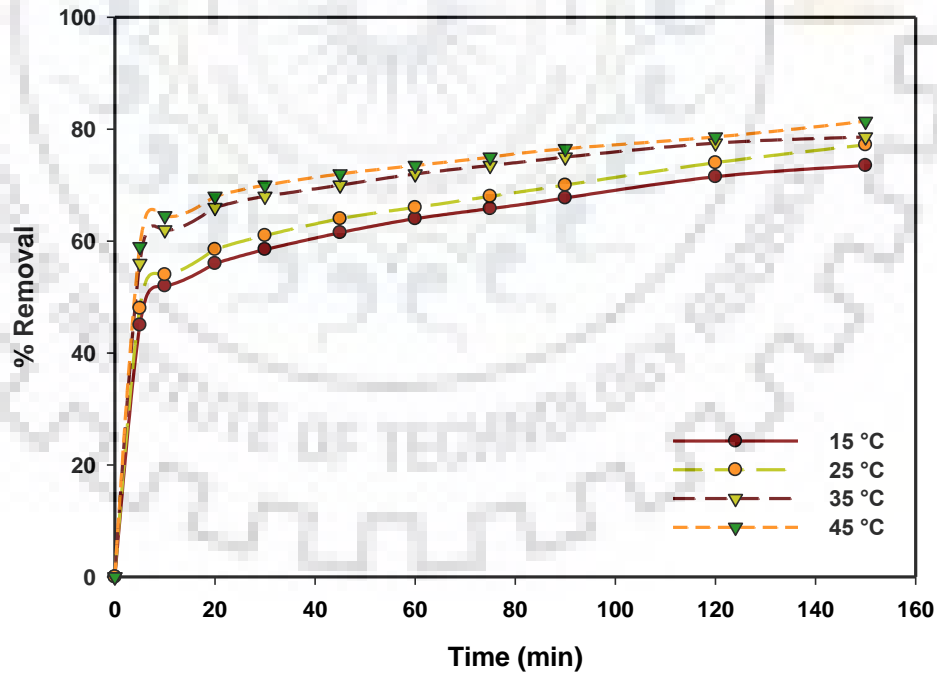


Fig.5.8 : Effect of temperature on dye removal using PnsAC at different time intervals (C₀: 100 mg L⁻¹; PnsAC: 10 g L⁻¹; pH: 2)

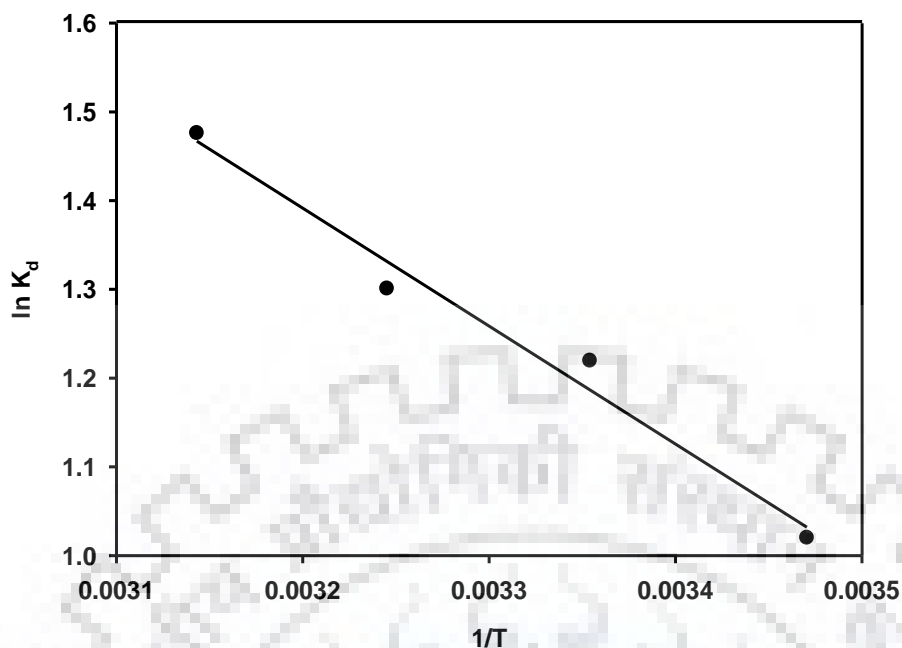


Fig. 5.9 : A thermodynamic plot of $\ln K_d$ against $1/T$ for adsorption of DB-86 onto PnsAC (PnsAC: 10 g L^{-1} ; pH: 2; C_0 : 100 mg L^{-1})

Table 5.3 : Thermodynamic parameters for adsorption of DB-86 on PnsAC

T (°C)	ΔG° (kJ mol ⁻¹)	ΔH° (kJ mol ⁻¹)	ΔS° (kJ mol ⁻¹ K ⁻¹)
15	-2.44	11.05	0.05
25	-3.02		
35	-3.33		
45	-3.90		

ΔG° value for decreases as temperature is increased from 15 °C to 45 °C. Spontaneity of the process is judged by the negative values of ΔG° (Mouni et al., 2018) . The value of ΔG° decreases with increase in temperature which indicates rise in spontaneity. Values of different thermodynamic parameters are tabulated in Table 5.3. ΔH° values show endothermic nature of the process (Postai et al. 2016). Positive value of ΔS° indicates that there exists natural attraction (Taşar et al. 2014) between dye and PnsAC. 4 - 40 kJ mol⁻¹ ΔH° values indicates physisorption whereas chemisorption range from 40 to 800 kJ mol⁻¹. ΔH° value from Table 5.3 inferred that sorption of DB-86 onto PnsAC is mainly due to physical adsorption (Postai et al., 2016).

ADSORPTION OF DIRECT BLUE – 86 DYE USING ALGINATE COATED PEANUT SHELL ACTIVATED CARBON

6.0 INTRODUCTION

In this chapter alginate (Arya and Srivastava, 2006) encapsulated activated carbon (PnsAC-alginate) prepared from waste peanut shell was utilized in adsorptive study of water soluble Direct Blue-86. Adsorption parameters such as solution pH, concentration of dye and adsorbent dose were optimized using RSM. Characterization of PnsAC-alginate adsorbent was carried out using SEM, EDS, TEM, XRD, BET surface area, FTIR and zero point charge analysis. Various adsorption isotherm models and kinetic models were examined to explain the adsorption process.

6.1 REMOVAL OF DB – 86 FROM AQUEOUS SOLUTION USING PnsAC - alginate

6.1.1 Characterization of PnsAC-alginate Adsorbent

Surface morphology of PnsAC-alginate adsorbent was observed from SEM analysis. Fig.6.1 show the SEM images of PnsAC-alginate adsorbent with and without adsorbed DB-86 dye. The SEM images showed porous texture surface morphology with cavities. Before adsorption, the cavities and pores on the surface of adsorbent were clearly visible, however, after adsorption, dye molecules adhered to surface of adsorbent and surface became smoother as evident from Fig.6.1(c). EDX spectrum as shown in Fig.6.1(e), revealed the presence of C, Na, Ca, Cl and O onto PnsAC-alginate adsorbent.

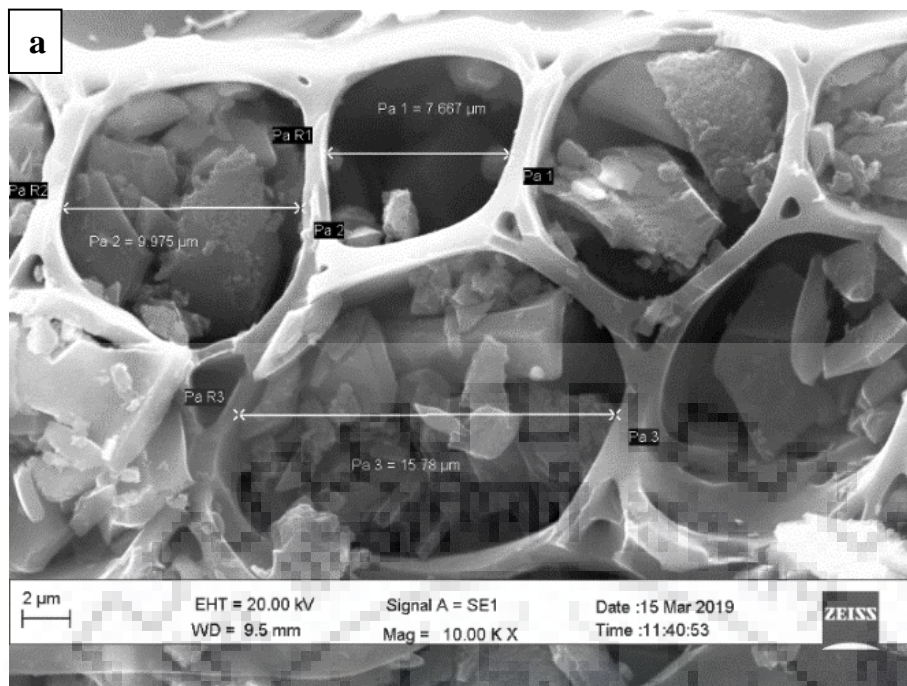


Fig.6.1 (a) : Scanning Electron Micrographs (SEM) image of PnsAC-alginate adsorbent at 10 KX before adsorption

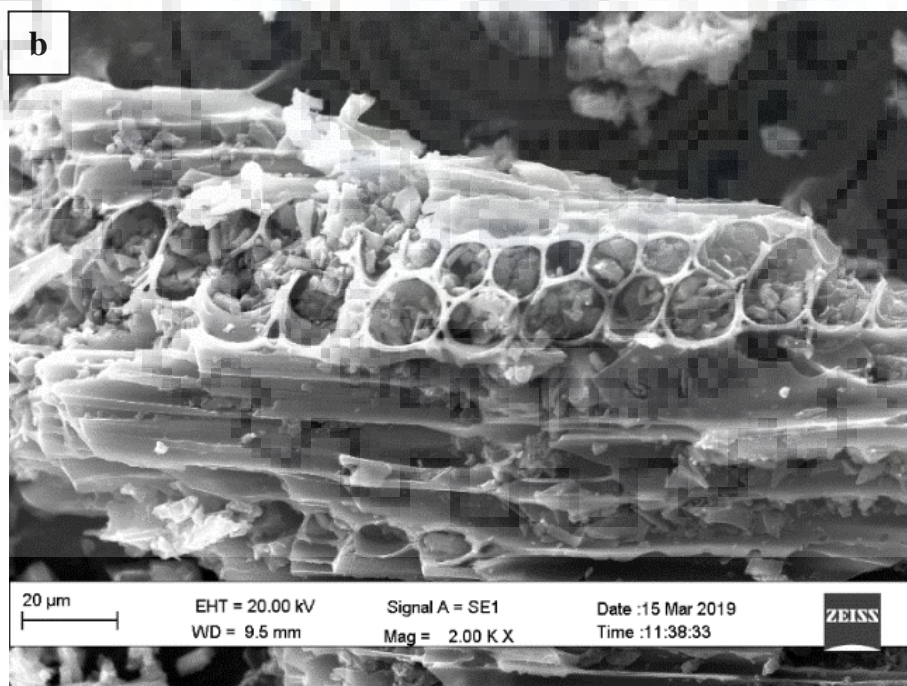


Fig.6.1 (b) : Scanning Electron Micrographs (SEM) image of PnsAC-alginate adsorbent at 2 KX before adsorption

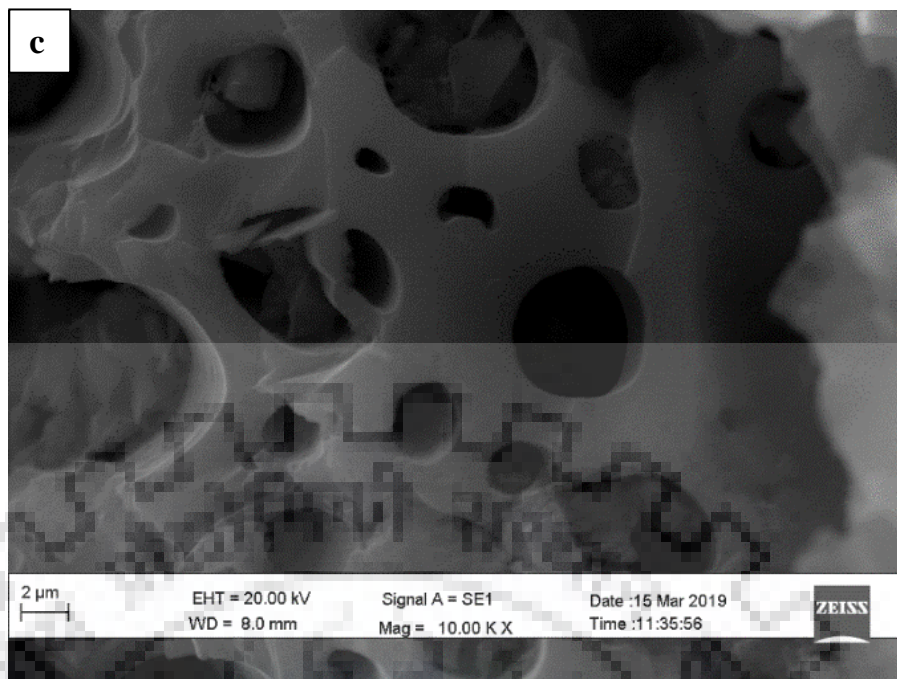


Fig.6.1 (c) : Scanning Electron Micrographs (SEM) image of PnsAC-alginate adsorbent at 10 KX after adsorption of DB-86

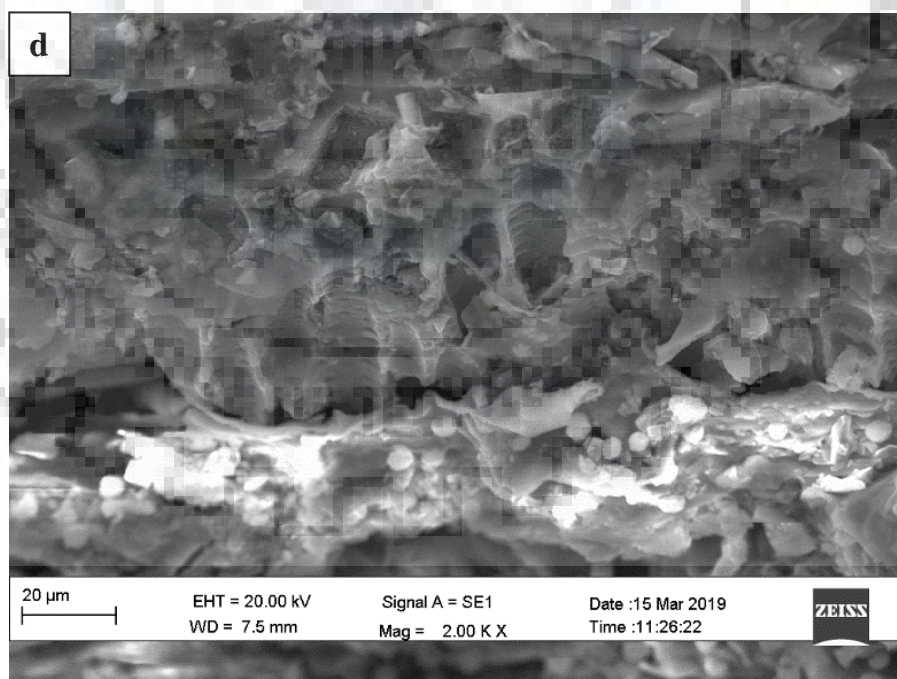


Fig.6.1 (d) : Scanning Electron Micrographs (SEM) image of PnsAC-alginate adsorbent at 2 KX after adsorption of DB-86

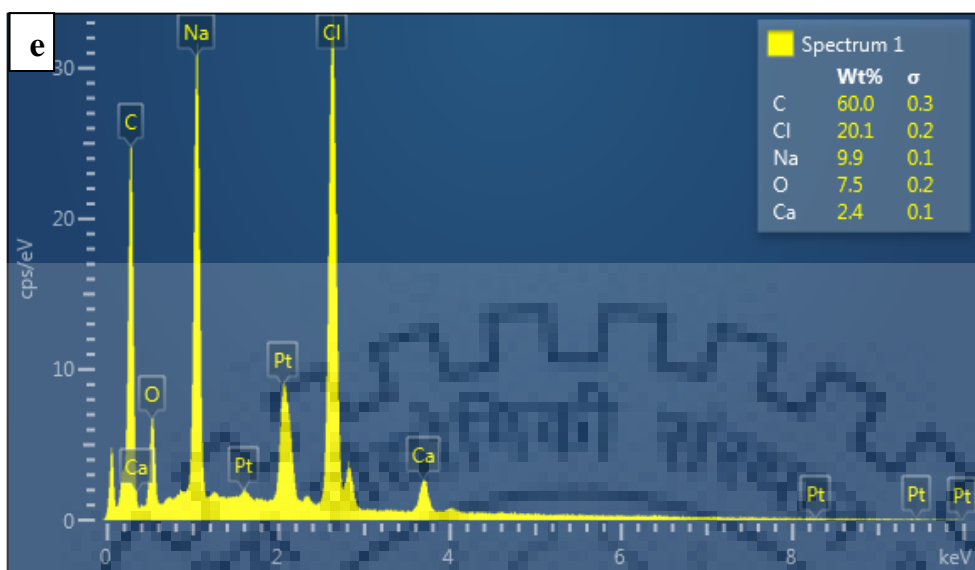


Fig.6.1 (e) : EDX spectra before adsorption of DB-86

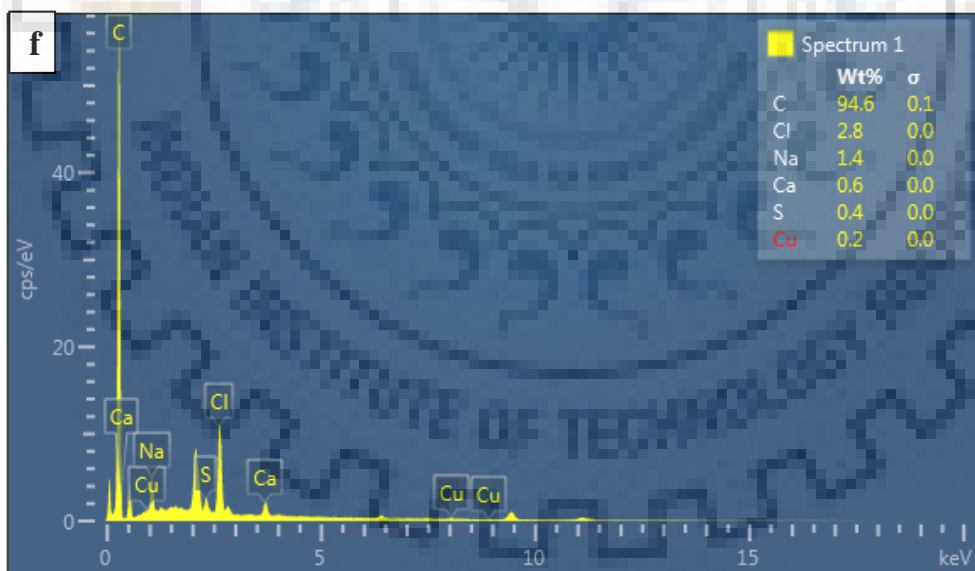


Fig.6.1 (f) : EDX spectra after adsorption of DB-86

The presence of two new elements S and Cu in the dye loaded PnsAC-alginate adsorbent was indicated by EDX spectrum shown in Fig.6.1 (f), which confirmed the adsorption of DB-86 dye on the surface of PnsAC-alginate adsorbent.

Fig.6.2 (a) showed the adsorption /desorption isotherms of PnsAC and PnsAC-alginate adsorbent. The nature of the isotherms were type I (IUPAC classification), indicating that both the adsorbents were mesoporous. The adsorption isotherms were used to calculate specific surface area and total pore volume. In addition, the pore size distribution was determined using BJH method for both types of PnsAC adsorbents. The pore size distribution were within the range of 2 to 30 nm, indicating the mesoporous region. Furthermore, similar type of pore size distributions were observed in both the adsorbents (Liang et al., 2016).

A narrow peak at a pore diameter of approximately 4 nm was present in Fig.6.2 (b), confirming that both the adsorbents had high mesoporosity. Various samples of PnsAC has been prepared several times and BET surface area was determined. It has been found that BET surface area varies between 802.6 to 965.6 m² g⁻¹. Average BET surface area is the order of 884 m² g⁻¹ with a variation of ± 9.2 %. The BET surface area for PnsAC-alginate was 142.5 m² g⁻¹. Total pore volume was found to be 0.040 mL g⁻¹ for PnsAC adsorbent and 0.043 mL g⁻¹ for PnsAC-alginate adsorbent. The values of surface area and pore size were consistent with the values reported in the literature (Benhouria et al., 2015; Kim et al., 2008; Nasrullah et al., 2018). Kim et al., (Kim et al., 2008) obtained 193.8 m² g⁻¹ surface area for mesoporous (2.65 nm) alginate-activated carbon. Benhouria et. al., (Benhouria et al., 2015) observed similar pore size distribution with surface area of 185.28 m² g⁻¹ and average pore size of 5.97 nm for activated carbon-bentonite-alginate bead. Nasrullah et al., (Nasrullah et al., 2018) also reported pore sizes of 4.43 nm and 3.43 nm for activated carbon and activated carbon-alginate beads, respectively. XRD patterns of PnsAC and PnsAC-alginate adsorbents were presented in Fig.6.2 (c). The diffraction peaks at 2θ = 26.3^o, 44.36^o, 77.18^o, and 83.17^o were attributed to the (0 0 2), (1 0 1), (1 1 0), and (1 1 2) lattice planes of carbon hexagonal structure (JCPDS), respectively, for both adsorbents. However, the intensity of the observed peaks in PnsAC-alginate adsorbent was decreased compared to PnsAC, suggesting the decreased crystallinity of carbon. The XRD peaks at 2θ = 45.5^o and 56.5^o; 2θ = 33.8^o, 36.0^o and 37.5^o for PnsAC-alginate indicated the presence of sodium chloride and of calcium chloride, respectively. TEM analysis of modified and unmodified PnsAC adsorbents shown in Fig. 6.2 (d), displayed the porous texture surface morphology, which was consistent with the SEM results.

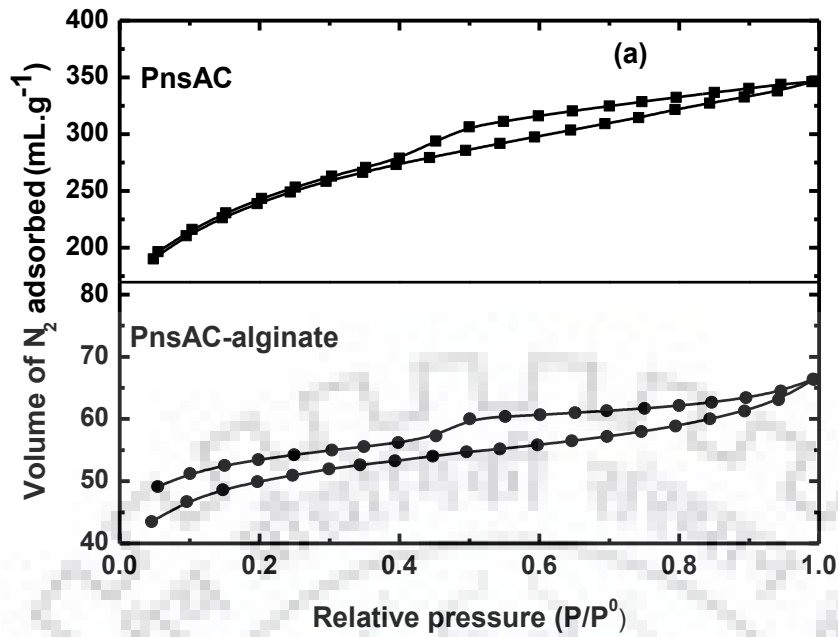


Fig.6.2 (a) : N₂ adsorption–desorption isotherm PnsAC and PnsAC-alginate

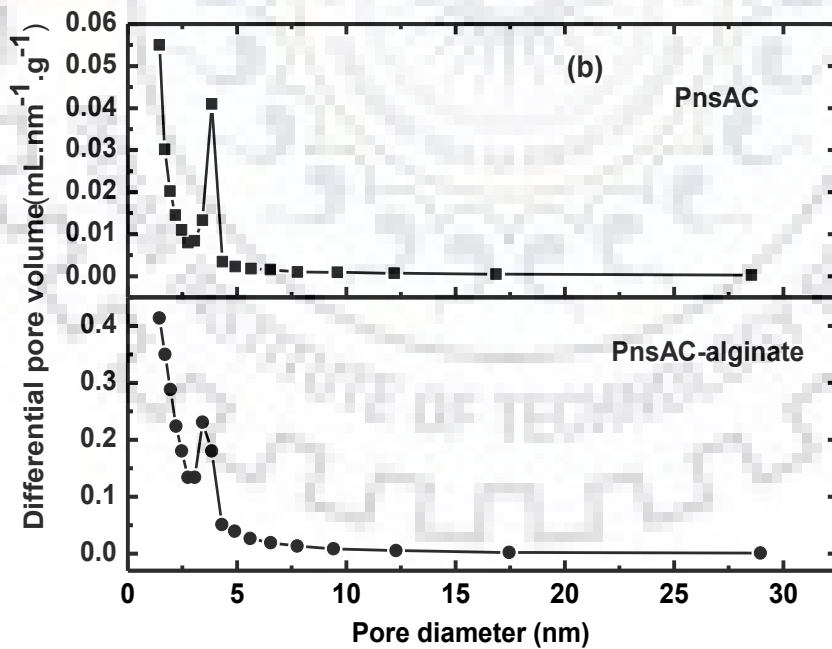


Fig.6.2 (b) : Pore size distribution (calculated using BJH method) of PnsAC and PnsAC-alginate

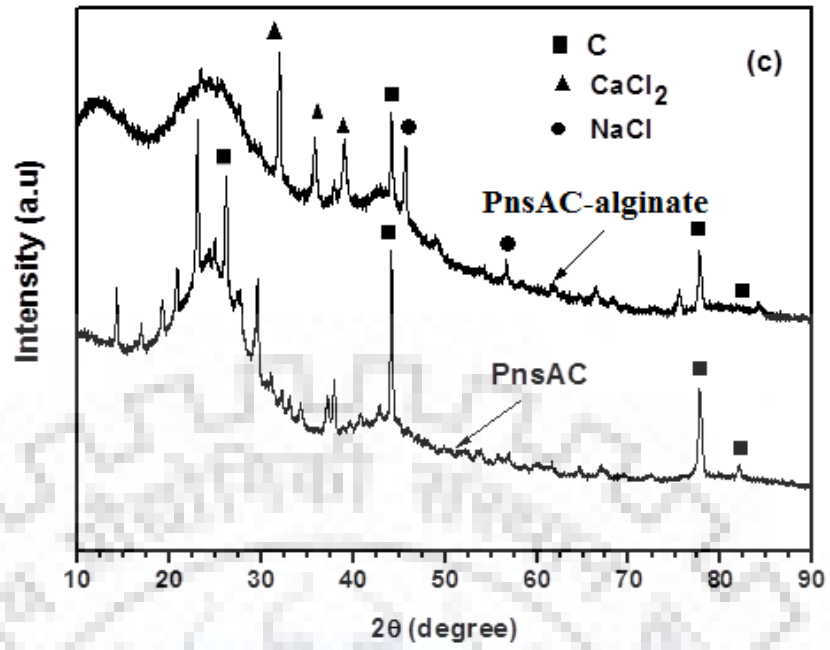
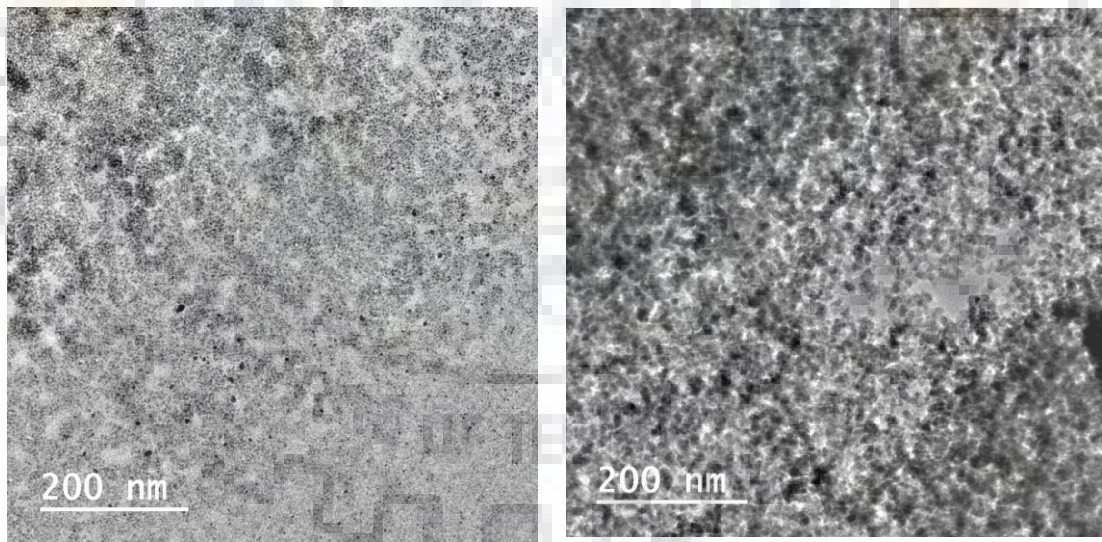


Fig.6.2 (c) : XRD patterns of PnsAC and PnsAC-alginate



PnsAC

PnsAC-alginate

Fig.6.2 (d) : HRTEM micrograph of PnsAC and PnsAC-alginate

The FTIR spectra of PnsAC-alginate adsorbent before adsorption and after adsorption of DB-86 were shown in Fig.6.3 (a). FTIR spectrum exhibited the characteristics of both dye as well as PnsAC-alginate, which was the result of the adsorption of DB-86 on the surface of PnsAC-alginate. In this spectrum, the appearance of the absorption band (3735 cm^{-1}) attributed to the stretching vibration of O – H bond of the sulfonic acid groups of DB-86 dye molecule (Villalobos et al., 2016).

The new peak appearing at 2109 cm^{-1} mainly on dye loaded adsorbent was due to C = N stretching vibration of dye molecule. A strong peak observed at 1592 cm^{-1} could be ascribed to C = O stretching vibration of carboxyl or carbonyl groups (Araujo et al., 2018; Saha et al., 2012) which was shifted from 1592 cm^{-1} to 1581 cm^{-1} after dye adsorption. The peak observed at 1006 cm^{-1} was due to the C - O bond of carboxylic groups (Daemi and Barikani, 2012) which was shifted to 1009 cm^{-1} after dye adsorption. The peak at 2324 cm^{-1} corresponded to C - C stretching (Georgin et al., 2016b). The band possibly attributed to C = C and CH₂ stretching vibrations, shifted from 1418 cm^{-1} to 1406 cm^{-1} and from 2657 to 2658 cm^{-1} , respectively, after dye adsorption (Mahmoodi et al., 2012). The peaks at 1981 cm^{-1} and 2051 cm^{-1} corresponded due to presence of olefinic C = C bond.

These suggested that the physisorption of DB-86 occurred on the positively charged surface of PnsAC-alginate. Thus, decolorization of the DB-86 dye was predominantly due to adsorption onto the PnsAC-alginate adsorbent.

The knowledge about pH_{ZPC} of adsorbent was very crucial in any adsorption process. It represented the pH value at which the surface of adsorbent contained zero charge. As observed in Fig.6.3 (b), the pH_{ZPC} of PnsAC and PnsAC-alginate were found to be 2.3 and 7.8, respectively. The pH_{ZPC} value of activated carbon prepared from peanut shell was reported as 10 (Villar da Gama et al., 2018). The surface of the adsorbent became negatively charged at the solution pH greater than pH_{ZPC} . However, the surface became positively charged at the solution pH less than pH_{ZPC} . Thus, the surface of PnsAC-alginate remained positively charged in the range of pH under the present investigation.

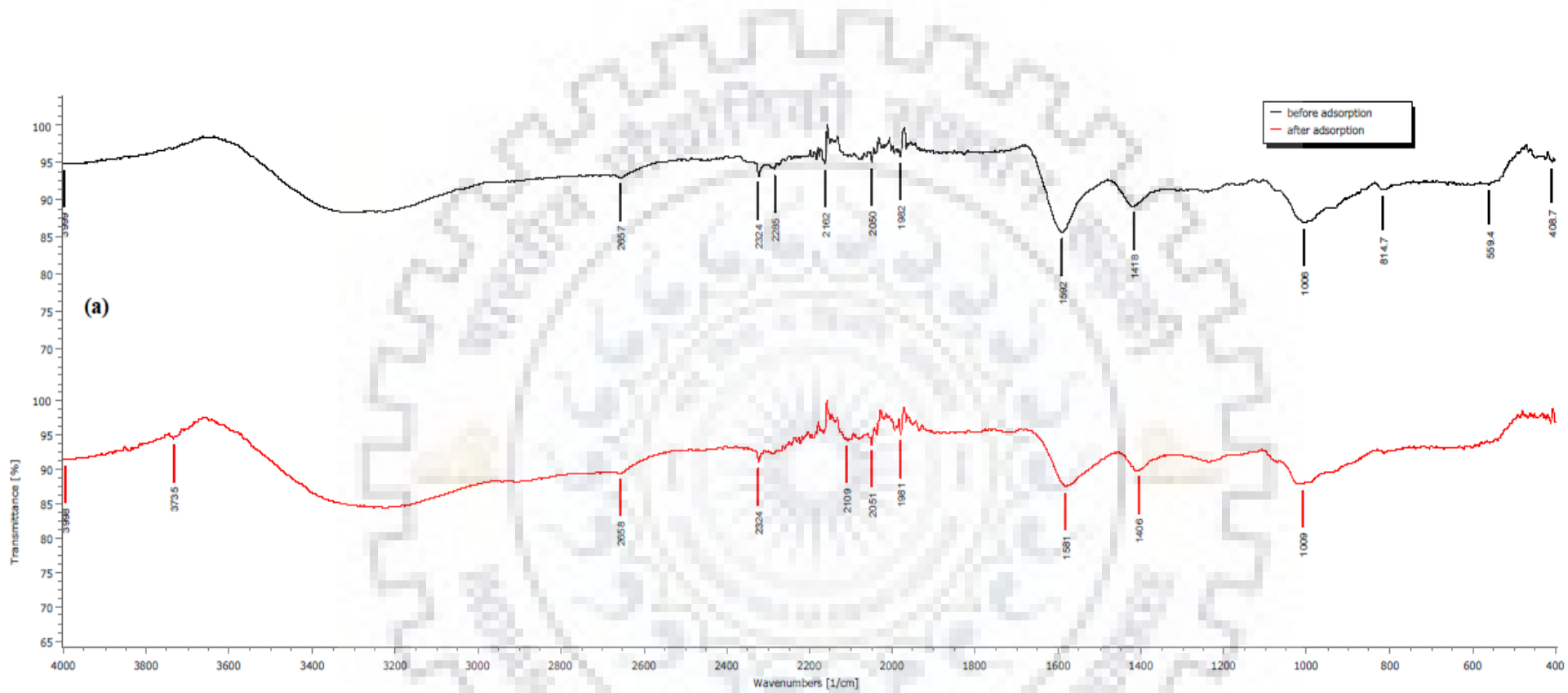


Fig 6.3 (a) : FTIR of PnsAC-alginate before adsorption and after adsorption of DB-86

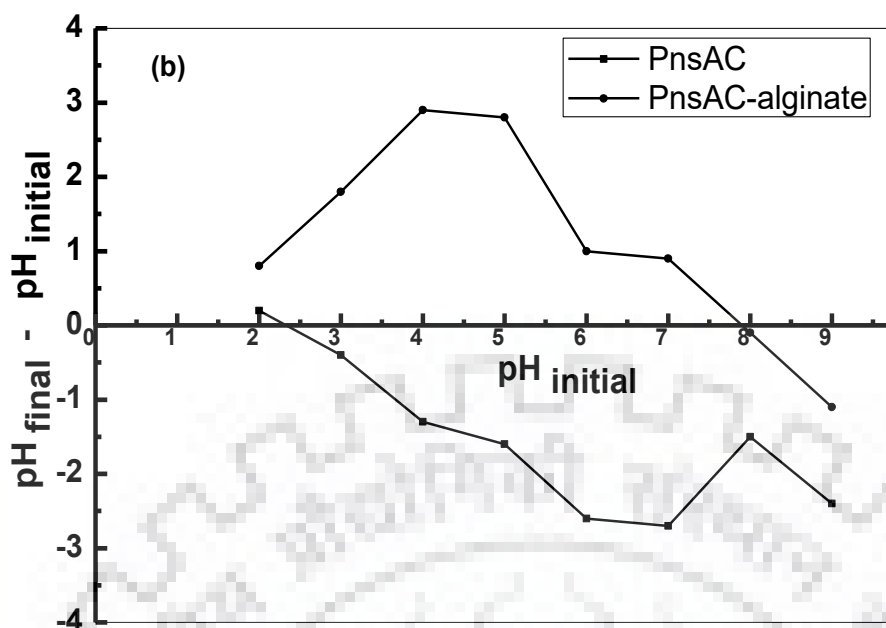


Fig 6.3 (b) : Zero point charge of PnsAC and PnsAC-alginate

6.1.2 Response Surface Methodology

ANOVA results revealed that the quadratic model equation derived by RSM could be satisfactorily used to describe the adsorption of DB-86 under a wide range of feed conditions. Central composite experimental design of five-levels and three-variables with their observed and predicted responses are showed in Table 6.1.

The significance of the model was determined by Fisher test. The F-statistic for the regression equation of all three responses showed that the calculated F values (F_{Model}) were greater than the tabulated F values ($F_{Tab.}$) at the 95 % confidence level, supporting the adequacy of the model. Also, the F-statistics for the lack-of-fit of all three responses showed that the calculated F values ($F_{Lack\ of\ fit}$) were greater than the tabulated F values at the 95 % confidence level, indicating the adequacy of goodness-of-fit (*Applied Mathematics in Chemical Engineering*, n.d.). The regression coefficients, the determination coefficient, the F-value, and the value of coefficient of variance for the model are presented in Table 6.2. The regression model for removal efficiency of DB-86 was found significant ($p < 0.0001$) with high R^2 values of 0.94, respectively. Furthermore, the low value of coefficient of variance (1.6 %) supported the good fit of the model, and thus, provided better precision and reliability of the experimental data. The coefficients of the model were statistically analysed with p-values.

Table 6.1 : Central composite experimental design of five-levels and three-variables with their observed and predicted responses

Run	pH	Initial DB-86 dye concentration (g L ⁻¹)	PnsAC-alginate (mg L ⁻¹)	Removal (%)	
				Experimental	Predicted
1	2.5	0.1	15	81	82.67
2	4.5	0.1	15	90	90.67
3	2.5	0.2	15	92	92.17
4	4.5	0.2	15	87	90.17
5	2.5	0.1	25	98	96.79
6	4.5	0.1	25	97	98.79
7	2.5	0.2	25	96	97.29
8	4.5	0.2	25	89	89.29
9	1.82	0.15	20	87	87.86
10	5.18	0.15	20	87	87.86
11	3.5	0.065	20	94	94.62
12	3.5	0.234	20	89	94.62
13	3.5	0.15	11.6	87	89.05
14	3.5	0.15	28.4	96	100.18
15	3.5	0.15	20	95	94.75
16	3.5	0.15	20	95	94.55
17	3.5	0.15	20	94	94.85
18	3.5	0.15	20	95	94.12
19	3.5	0.15	20	94	94.46
20	3.5	0.15	20	95	94.62

The statistical analysis of the coefficients of the regression model of dye removal efficiency revealed that interaction terms and quadratic terms of all the independent variables were significant ($p < 0.05$) as shown in Table 6.2. Linear terms of PnsAC-alginate concentration had highly significant influence ($p < 0.0001$) on dye removal efficiency while linear terms of initial dye concentration and solution pH were insignificant ($p > 0.05$). The insignificant terms ($p > 0.05$) were identified and eliminated from the initial model equation. The quadratic reduced

regression equation in terms of coded factors with only significant terms ($p < 0.05$) of three response variables was given expressed as follows.

$$Y_1 = 94.62 + 3.31X_3 - 2.5X_1X_2 - 1.5X_1X_3 - 2.25X_2X_3 - 2.39X_1^2 \quad [6.1]$$

Table 6.2 : Estimated regression coefficients for the polynomial model and the analysis of variance (ANOVA)

Coefficient	Estimate	Sum of squares	DF	Fvalue	p-value
Model		357.24	9	14.95	0.0001
β_0	94.62				
Linear					
β_1	-0.293	1.17	1	0.44	0.5216
β_2	-0.762	7.93	1	2.99	0.1146
β_3	3.31	149.18	1	56.17	< 0.0001
Interaction					
β_{12}	-2.5	50.0	1	18.83	0.0015
β_{13}	-1.5	18.0	1	6.78	0.0263
β_{23}	-2.25	40.5	1	15.25	0.0029
Quadratic					
β_{11}	-2.39	82.12	1	30.92	0.0002
β_{22}	-0.8	9.13	1	3.44	0.0934
β_{33}	-0.8	9.13	1	3.44	0.0934
Residual error		26.56	10		
Lack of fit		25.23	5	18.92	0.0029
Pure error		1.33	5		
Total					
R^2	0.94				
R^2_{adj}	0.87				
C.V%	1.77				

6.1.2.1 Effects of Independent Variables on DB – 86 Dye Removal Efficiency

The effects of PnsAC-alginate dosage, initial dye concentration and solution pH on removal efficiency of DB-86 were demonstrated using a response surface plot Fig.6.4 (a) – (b). A linear effect of adsorbent dose and quadratic effects of solution pH and initial dye concentration on the dye removal efficiency were observed. Fig.6.4 (a) showed the effect of adsorbent dose and initial dye concentration; while Fig.6.4 (b) depicted the influence of adsorbent dose and solution initial pH. As observed in Fig.6.4 (a) that the removal efficiency of DB-86 was strongly dependent on the initial dose of PnsAC-alginate. The increase in dye removal percent with increase in adsorbent doses might be due to the increase in the total available surface area of the PnsAC-alginate particles (Saeed et al., 2010), increasing the number of adsorption sites available for dye adsorption. The removal for DB-86 dye increased from 87 to 96 %, when the PnsAC-alginate dosage increased from 11.6 to 28.4 g L⁻¹ for fixed initial concentration of DB-86 dye (150 mg L⁻¹) and solution pH (3.5). This observation could also be described by the linear positive effect of PnsAC-alginate dose ($p < 0.0001$) on dye removal efficiency. The initial DB-86 dye concentration showed significant influence on its removal percent. It was observed that the percent removal of DB-86 dye increased with increase in dye concentration, however, at higher dye concentration the percent removal of dye declined. The initial increase in dye removal with increase in dye concentration is attributed to increase in the probability of contact between dye molecules and PnsAC-alginate (Khataee et al., 2011). At higher DB-86 dye initial concentration, the decline in dye removal might be due to nearly complete saturation of the binding sites of PnsAC-alginate. The effect of solution pH onto DB-86 dye adsorption was studied in the range of pH 1.8-5.2. As shown in Fig.6.3 (b), the pHzpc of the PnsAC-alginate adsorbent was found to be 7.8, indicating the presence of positive surface charges in the range of pH under investigation, thus favouring the adsorption of anionic DB-86 dye. The hydrophobic nature of the developed PnsAC-alginate adsorbent led to absorb hydrogen ions (H⁺) onto the surface when immersed in water and made it positively charged (Malik, 2004; Nemr et al., 2009; Senthil Kumar et al., 2010). Low pH led to an increase in H⁺ ion concentration in the system and the adsorbent surface acquired more positive charge by absorbing more H⁺ ions, which favoured the adsorption of anionic DB-86 dye molecules due to the strong electrostatic attraction resulting in an increase in dye removal efficiency. Lower dye removal efficiency at higher solution pH might be due to weak electrostatic attraction between anionic DB-86 dye molecules and comparatively less positively charged adsorbent surface.

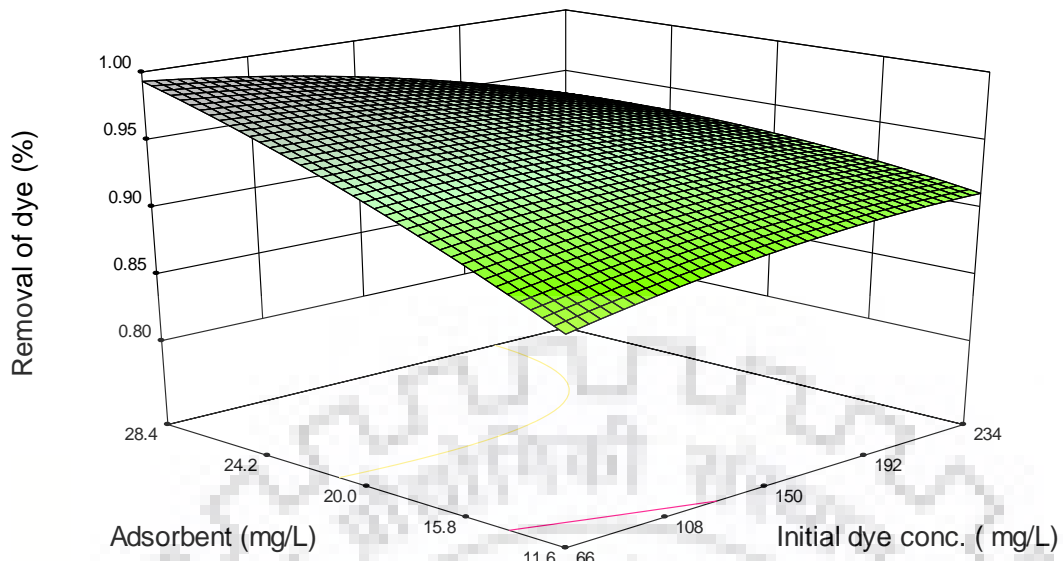


Fig.6.4 (a) : Three-dimensional response surface plot for the effect of adsorbent and initial DB-86 dye concentration during adsorption onto PnsAC-alginate

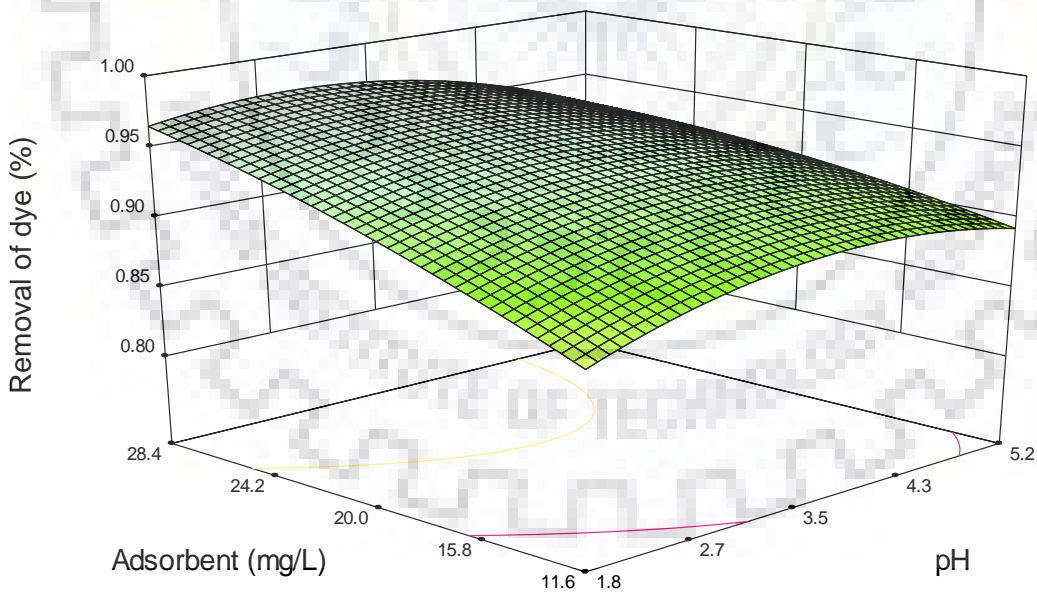


Fig.6.4 (b) : Three-dimensional response surface plot for the effect of adsorbent and solution pH on DB-86 dye removal efficiency during adsorption onto PnsAC-alginate

The combination of high adsorbent dose and high initial dye concentration resulted to decrease in dye removal efficiency.

Similarly the combined effect of high adsorbent dose and high solution pH also resulted to decrease in dye removal efficiency. This observation was in agreement with the results of ANOVA. The interactive effects of (i) PnsAC-alginate dose and initial dye concentration (β_{23}) and (ii) PnsAC-alginate dose and solution pH (β_{13}) were both found to be negative and statistically significant ($p < 0.05$). Maximum removal of the DB-86 dye (98.8 %) was observed at about 125 mg L⁻¹ initial DB-86 dye concentration; pH of 3.1 and PnsAC-alginate dose of 25 g L⁻¹.

6.1.2.2 Optimization of Feed Conditions and Validation of the Model

In this study, desirability function approach (Myers et al., 2016) was used for obtaining the optimal feed conditions of DB-86 adsorption by maximizing the removal efficiency of DB-86. The optimum values of the independent variables in actual terms were X_1 : 3.1, X_2 : 125.5 mg L⁻¹, and X_3 : 24.65 mg L⁻¹. Under the optimal feed conditions, the developed models predicted the DB-86 removal efficiency of 98.1 % with overall desirability function of 1.0. Validation experiments were performed in triplicate at predicted optimal feed conditions and resulted the DB-86 removal efficiency of (98.4 ± 0.1) %. Experimental results were matched well with the predicted results, which were validated by the RSM model with good correlation. Thus, it can be seen that the second-order model was adequate to explain the effect of selected variables of feed composition on the removal efficiency of DB-86. The maximum removal efficiency of 92 % was reported (Nemr et al., 2009) during adsorption of DB-86 at pH 2 with initial concentration of 100 mg L⁻¹ using activated carbon prepared from orange peel. In another study (Maleki et al., 2016), 90 % removal of DB-71 was reported using potato peel based adsorbent at pH 3.0 with initial dye concentration of 100 mg L⁻¹ and adsorbent dose of 20 g L⁻¹. Also, it appeared that unmodified PnsAC and Alginate adsorbents showed about 7 % and 12 %, respectively, less DB-86 dye removal efficiency as compared to PnsAC-alginate under the optimal conditions. This clearly indicated the superiority of PnsAC-alginate adsorbent in comparison to unmodified PnsAC adsorbent.

6.1.3 Kinetic Studies

Adsorption kinetic provided a valuable insight into controlling the adsorption mechanisms that was important for evaluating the efficiency of the process and further designing the adsorption system. The effect of the contact time on the adsorption of DB-86 by PnsAC-alginate beads was

illustrated in Fig.6.5 (a) – (d). The time dependence of the adsorption of DB-86 was observed by taking UV-visible absorbance spectra of DB-86 in the residual solution at different time intervals. The intensities of the absorption peaks decreased with time as shown in Fig.6.5 (d), thus confirming removal of DB-86 by adsorption, although the absorption spectrum appeared the same. As observed in Fig.6.5 (a) – (d), the adsorption capacity increased sharply at the initial stage of adsorption followed by gradual increase until reaching the equilibrium. Similar trends were observed at all experimental conditions. The rapid uptake of DB-86 on PnsAC-alginate beads was due to availability of large amount of surface area and readily accessible binding sites for interaction with DB-86, while the slow increase of adsorption capacity was mainly by the diffusion of DB-86 within the PnsAC-alginate particles. The equilibrium time for maximum adsorption capacity was found to be about 120 minutes for all the experimental conditions studied. After this equilibrium period, the adsorption capacity did not show any time dependent change. Thus, an optimum contact time of 120 minutes was considered for further equilibrium isotherms studies.

6.1.3.1 Effect of Adsorbent Dose on Adsorption

Adsorbent dose showed significant influences on the adsorption process by affecting adsorption capacity of the adsorbent. As seen in Fig.6.5 (a), the adsorption capacity decreased with increasing PnsAC-alginate dose. The decrease in adsorption capacity with increasing adsorbent dose at constant DB-86 dye concentration and volume might be attributed to the increasing number of binding sites available for adsorption. Also, overlapping or aggregation of adsorption sites led to decrease in total adsorbent surface area available for adsorption of dye molecule and an increase in diffusion path length. For instance, the equilibrium adsorption capacity decreased from 11.33 to 5.12 mg g⁻¹ with increase in adsorbent dose from 11.6 - 28.4 g L⁻¹.

6.1.3.2 Effect of Temperature on Adsorption

The effect of temperature on adsorption capacity was shown in Fig.6.5 (c). Increasing temperature led to increase the rate of diffusion of the DB-86 molecules across the external boundary layer and in the internal pores of the PnsAC-alginate particle, due to increase of kinetic energy of dye molecules. Thus, more number of dye molecules would undergo an interaction with binding sites of the adsorbent. Also, the increasing temperature might produce a swelling effect within the internal structure of the PnsAC-alginate, resulting in greater penetration of dye molecules and consequently increasing adsorption capacity. For instance, equilibrium adsorption capacity increased from 7.18 to 7.28 mg g⁻¹ with increase in temperature from 288 to 308 K,

indicating the process to be endothermic. The pH of the solution played an important role in the adsorption of DB-86 dye.

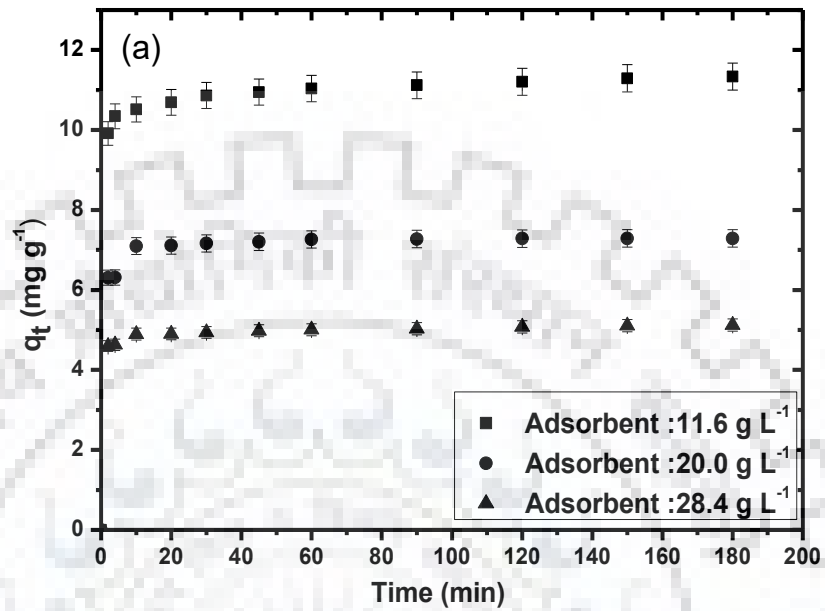


Fig.6.5 (a) : q_t vs t plot for different adsorbent dose at pH 3.5 and 308 K

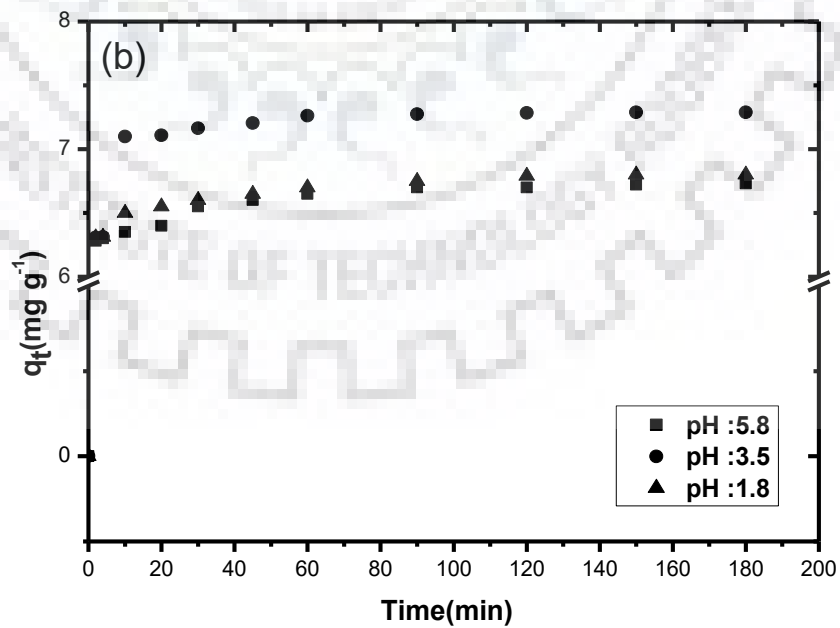


Fig.6.5 (b) : q_t vs t plot for different pH at 20 g L⁻¹ adsorbent dose and 308 K

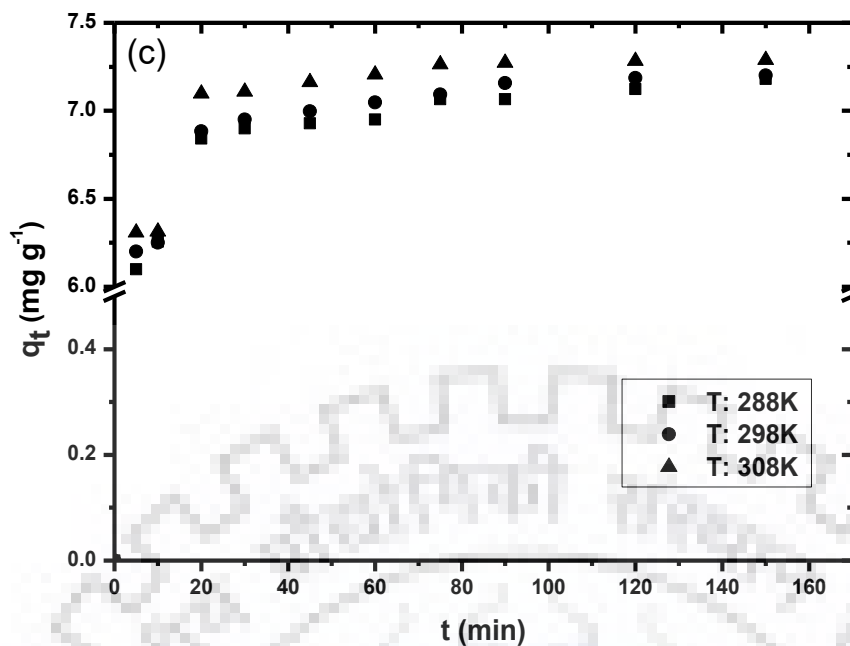


Fig.6.5 (c) : q_t vs t plot for different temperature at 20 g L^{-1} adsorbent dose and at pH 3.5

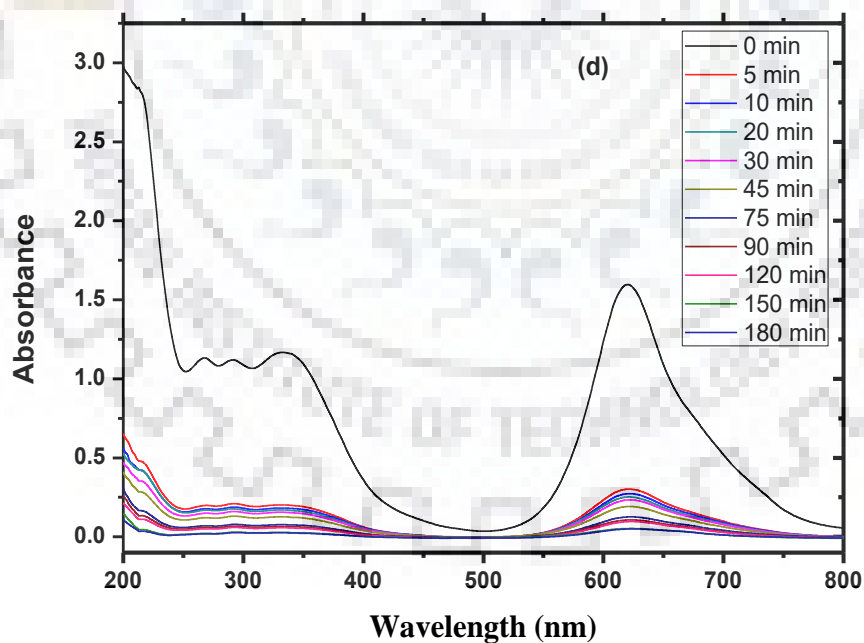


Fig.6.5 (d) : UV-visible absorbance spectra of DB-86 in the residual solution at different time intervals for optimum dose

6.1.3.3 Effect of Solution pH on Adsorption

As observed in Fig. 6.5(b), the equilibrium adsorption capacity increased with decrease in solution pH. This could be explained by the fact that decrease in solution pH led to increase in electrostatic attraction between the positively charged surface of the PnsAC-alginate, due to the positively charged functional groups and negatively charged anionic DB-86 dye molecules. Lower adsorption capacity at higher solution pH might be due to decrease in number of positively charged sites on PnsAC-alginate surface which might reduce the adsorption of anionic DB-86 dye molecules due to weak electrostatic attraction. In order to evaluate the performance of adsorbent under alkaline conditions, an adsorption experiment was also performed at solution pH of 8 ± 0.1 with optimal concentration of PnsAC-alginate and DB-86 dye, resulting in dye removal efficiency of $(82 \pm 0.5) \%$. This indicated that PnsAC-alginate adsorbent was not effective under alkaline conditions. The maximum equilibrium adsorption capacity was observed at pH 3.5. No further enhancement in equilibrium adsorption capacity was noticed on further decrease in solution pH.

6.1.3.4 Modelling of Adsorption Kinetics

The most widely used kinetic models such as the Lagergren first order (Lagergren, 1898) and Pseudo second order (Ho and McKay, 2002) were used in the present study to reveal the rate constants and equilibrium adsorption capacities. For Pseudo first order model, shown in Fig.6.6 (a), the values of K_1 and q_e were calculated from the slope and intercept, respectively, of plots of $\ln(q_e - q_t)$ versus t . For Pseudo second order model, shown in Fig.6.6 (b), the values of K_2 and q_e were determined from intercept and slope, respectively, from the plot between t/q_t and t . The results are summarized in Table 6.3. The values of the coefficient of determination (R^2) for the Pseudo first order model were relatively low, (0.05 - 0.35) and the calculated values of adsorption capacity were far from the corresponding experimental values, indicating that Pseudo first order model was not suitable to explain the adsorption kinetics of DB-86 onto the PnsAC-alginate beads.

On the other hand, high values of R^2 (0.999), low values of χ^2 , SD and the adequate fitting of predicted and experimental values of adsorption capacity for all experimental conditions suggested that Pseudo second order kinetic model was perfectly fit to explain the adsorption kinetics of DB-86. The Pseudo second order adsorption rate constant was used to estimate the initial adsorption rate (B , $\text{mg mL}^{-1} \text{ min}$) which was expressed:

$$B = \left(\frac{C_t}{t} \right)_{t \rightarrow 0} = K_2 C_e^2 \quad [6.2]$$

As observed in Table 6.3 that adsorption rate constant was strong increasing function of temperature and adsorbent dose, and weak function of solution pH. The relation between the rate constants and these variables could be described by an extended Arrhenius equation as (Zhao et al., 2014).

$$K_2 = K_0 e^{-E_a/RT} (SL)^m (pH)^n \quad [6.3]$$

where, K_0 , E_a , R and SL were pre-exponential factor, activation energy, molar gas constant, and PnsAC-alginate dose (mg L^{-1}), respectively. The m and n were parameters with respect to PnsAC-alginate dose and solution pH, respectively. By taking logarithm, Eq. [9] could be expressed as Eq. [6.4] :

$$\ln K_2 = \ln K_0 - E_a/RT + m \ln SL + n \ln pH \quad [6.4]$$

Therefore, the corresponding parameters could be fitted by plotting $\ln K_2$ versus $1/T$, SL and pH with multivariable regression. Thus, the Eq. [6.3] could be expressed in terms of fitted parameter:

$$K_2 = K_0 e^{-E_a/RT} (SL)^m (pH)^n \quad [6.5]$$

The high values of R^2 also suggested that this equation was significant and reliable to describe the relationship between adsorption rate constants and process parameters. Furthermore, it was worth mentioning that the above correlation was mainly valid in the studied experimental range. The proposed empirical correlations provided a simple and effective approach for estimation of rate constant which could be used for scaling-up and designing the adsorption equipment. The activation energy of DB-86 was estimated as $16.81 \text{ kJ mol}^{-1}$ under the optimal conditions. . Low activation energy ($< 40 \text{ kJ mol}^{-1}$) was characteristics for physisorption, while higher activation energy ($> 40 \text{ kJ mol}^{-1}$) suggested chemisorption (Chakraborty et al., 2011). The activation energy obtained for the adsorption of DB-86 onto PnsAC-alginate indicated physical adsorption involving weak interactions. The obtained value of activation energy was of the same order of magnitude as that obtained for adsorption of BG 4 onto sea shell powder (Chowdhury and Saha, 2010). The obtained value of activation energy was of the same order of magnitude as that obtained for adsorption of BG 4 onto sea shell powder (Chowdhury and Saha, 2010). In any adsorption study, it was very important to examine the controlling mechanism of sorption process. The rate of adsorption of DB-86 onto PnsAC-alginate beads could be controlled by film

diffusion or intra-particle diffusion or both. Pseudo first order and Pseudo second order models (Srivastava and Srivastava, 2006) could not be used for identifying the steps controlled during adsorption process.

Thus, the Intra-particle diffusion model, Boyd kinetic model and Liquid film diffusion model were used to test the experimental data for determining the rate controlling step. Intra-particle diffusion model was given by:

$$q_t = k_{id}t^{0.5} + C \quad [6.6]$$

where, k_{id} ($\text{mg g}^{-1}\text{min}^{-0.5}$) was the intra-particle diffusion rate and intercept (C) gave the idea about the boundary layer thickness, i.e. the higher the intercept value, the greater was the boundary layer effect on adsorption (Oubagaranadin et al., 2007). The values of k_{id} and C were determined experimentally from slope and intercept, respectively, of the plot of q_t versus $t^{0.5}$. The Boyd model was expressed:

$$F = \frac{q_t}{q_e} = 1 - \frac{6}{\pi^2} \exp(-B_t) \quad [6.7]$$

where, F is the fraction of DB-86 adsorbed at time t and the parameter B_t could be expressed as a function of F :

$$B_t = -0.4977 - \ln(1 - F) \quad [6.8]$$

It was suggested that if the plot of q_t versus $t^{0.5}$ or plot of B_t versus t yielded a straight line passing through the origin, the adsorption kinetics of DB-86 was controlled by intra-particle diffusion. Liquid film diffusion model was expressed:

$$\ln(1 - F) = -K_f t \quad [6.9]$$

where K_f was the film diffusion coefficient. A linear plot of $\ln(1 - F)$ versus t passing through origin suggests that adsorption kinetics is controlled film diffusion. As shown in Fig.6.6 (c) & (e), both the plots showed linearity with R^2 values of 0.96 and 0.86 respectively, but did not pass through the origin, indicating that intra-particle diffusion was not the rate determining step for adsorption of DB-86. Furthermore, the linear plot of $\ln(1 - F)$ versus t with non-zero intercept (Fig.6.6) suggested that adsorption of DB-86 was not controlled by only film diffusion. Thus, it was concluded that both film diffusion as well as intra-particle diffusion were important during adsorption of DB-86 onto the PnsAC-alginate beads.

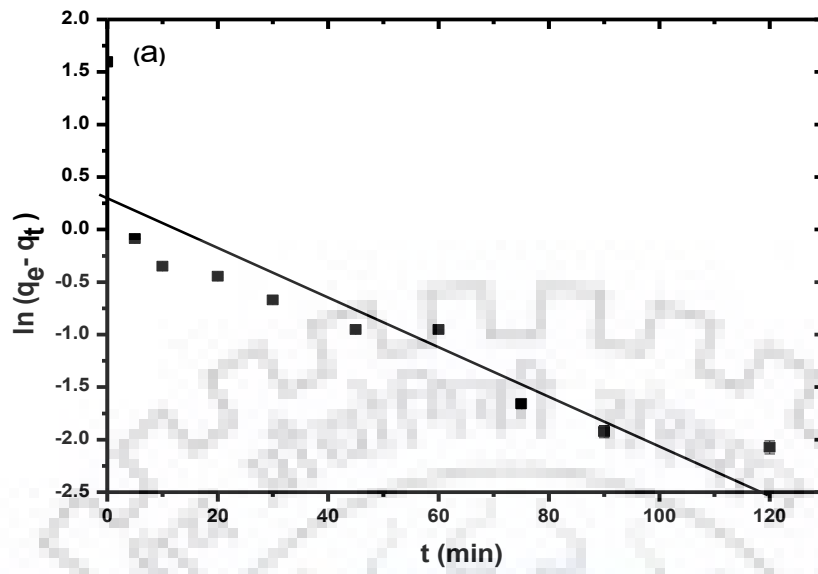


Fig.6.6 (a) : Pseudo first order kinetic model under optimal conditions

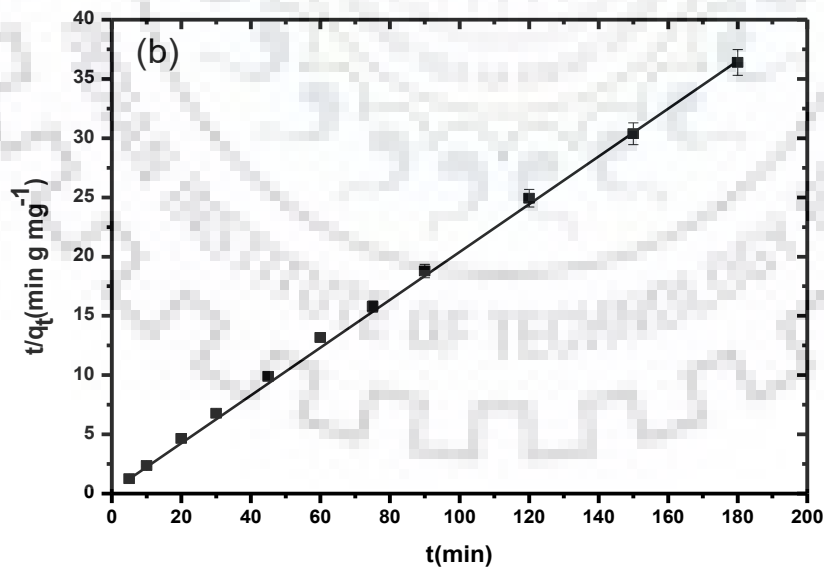


Fig.6.6 (b) : Pseudo Second order kinetic model under optimal conditions

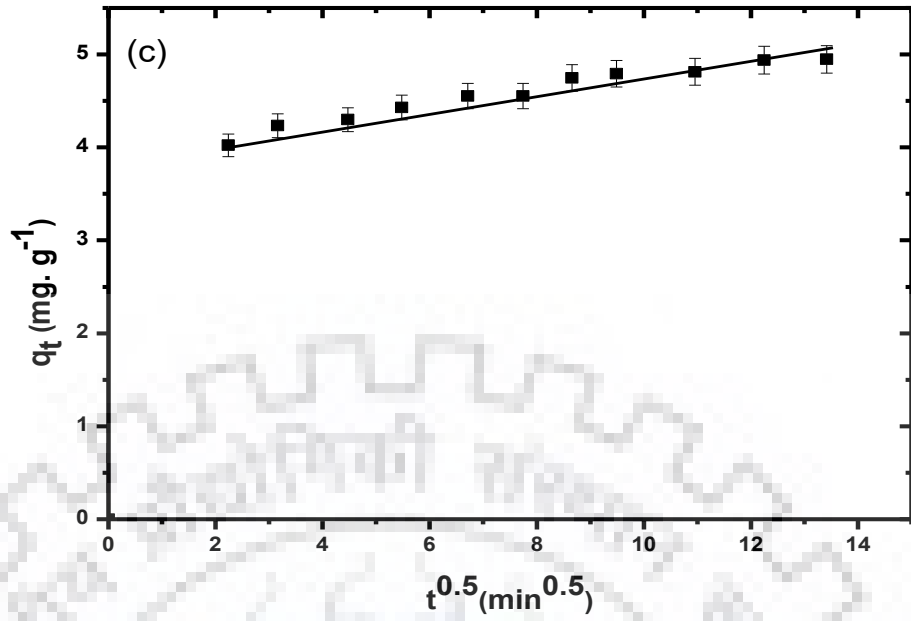


Fig.6.6 (c) : Intra-particle diffusion model under optimal conditions

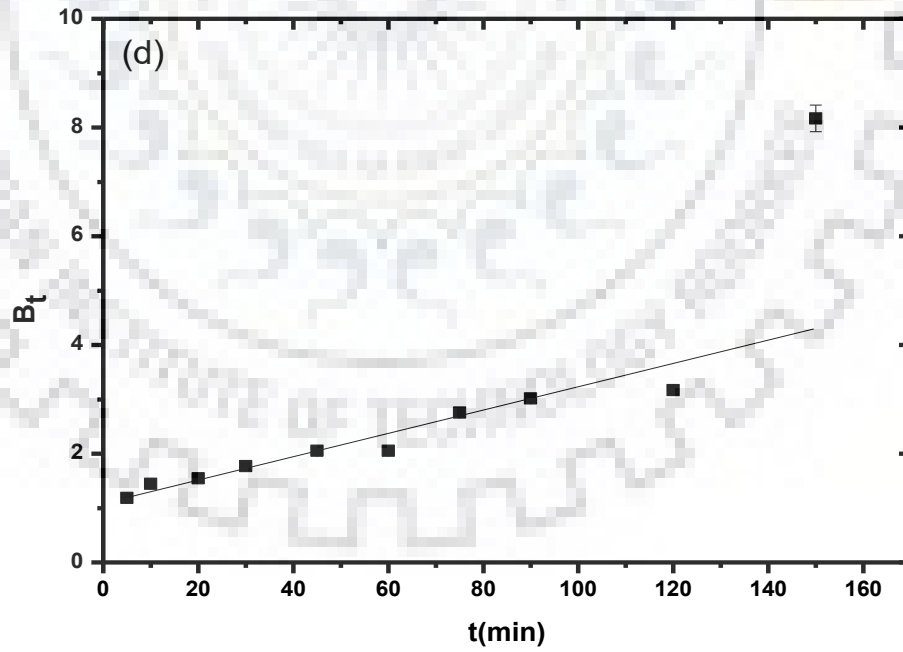


Fig.6.6 (d) : Boyd model under optimal conditions

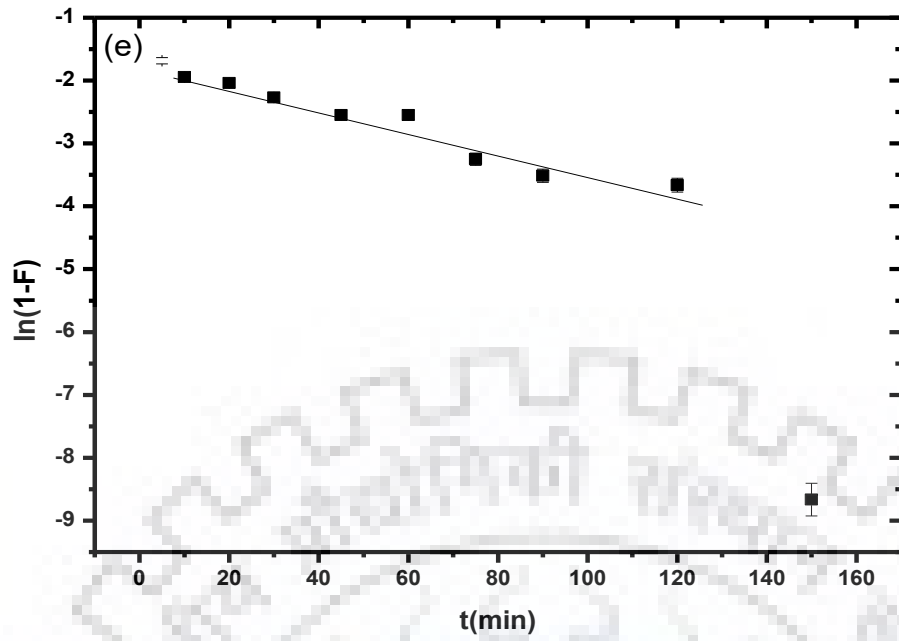


Fig.6.6 (e) : Liquid film diffusion model under optimal conditions

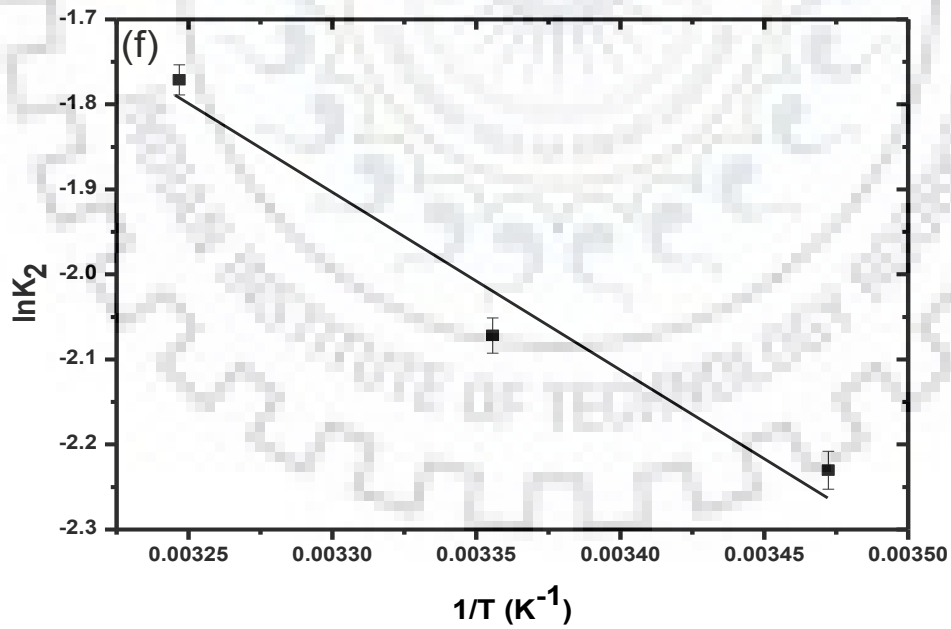


Fig.6.6 (f) : The plot of $\ln K_2$ Vs $1/T$

Table 6.3 : Kinetic data of DB-86 adsorption by PnsAC-alginate

			Pseudo first order kinetics						Pseudo second order kinetics						Intra-particle diffusion model		
PnsAC-alginate	pH	T (°C)	q_e^{exp} (mg g ⁻¹)	$k_1 \times 10^2$ (min ⁻¹)	q_e^{pred} (mg g ⁻¹)	R ²	SD (%)	χ^2	B (mg g ⁻¹ min ⁻¹)	$k_2 \times 10^2$ (g mg ⁻¹ min ⁻¹)	q_e^{pred} (mg g ⁻¹)	R ²	SD (%)	χ^2	$K_{id} \times 10^1$ (mg g ⁻¹ min ^{0.5})	C_i (mg g ⁻¹)	R ²
11.6	3.5	35	11.33	1.32	1.17	0.353	60.08	20.11	12.59	9.79	11.34	0.999	10.82	1.59	4.02	7.36	0.317
20.0	3.5	35	7.28	0.94	0.38	0.071	60.37	25.94	9.13	17.01	7.33	1	4.84	0.20	2.64	4.77	0.321
28.4	3.5	35	5.12	1.09	0.41	0.200	62.99	10.71	6.99	26.67	5.12	0.999	9.25	0.52	1.77	3.38	0.300
20.0	1.8	35	6.80	0.63	0.41	0.051	67.73	13.41	7.49	16.08	6.83	0.999	5.36	0.23	2.29	4.59	0.282
20.0	5.2	35	6.73	0.53	0.53	0.265	51.25	6.44	7.36	16.14	6.75	0.999	5.39	0.97	2.27	4.54	0.281
20.0	3.5	15	7.18	1.82	0.88	0.333	48.09	8.45	5.60	10.75	7.21	0.999	7.21	0.45	2.63	4.61	0.334
20.0	3.5	25	7.20	0.82	0.54	0.084	62.93	20.05	6.60	12.60	7.24	0.999	6.29	0.34	2.63	4.66	0.330
20.0*	3.1	35	4.95	0.48	0.73	0.081	72.38	13.12	1.46	5.84	5.00	0.999	15.24	1.38	0.87	3.92	0.963

*Under optimum conditions

6.1.4 Isotherm Studies

The equilibrium adsorption isotherm is fundamental in evaluating the adsorption mechanism, (Mohanty et al., 2008) explaining the interaction between adsorbates and adsorbent and also important in the design and scale up purposes. (Rout et al., 2016) Adsorption studies were performed using various concentrations of DB-86 ranging from 100 to 250 mg L⁻¹ under the optimized dose of PnsAC-alginate (24.65 g L⁻¹), solution pH (3.1) and temperature (35 °C). The Langmuir (Foo and Hameed, 2010; Noorimotlagh et al., 2014), Freundlich (Cao et al., 2018) and Temkin (Nemr et al., 2009) isotherm models were used to describe the equilibrium adsorption behavior of DB-86 on PnsAC-alginate beads as shown in Fig.6.7(a) – (d). Langmuir model assumed that:

- i. active sites were homogeneously distributed over the adsorbent surface which is energetically uniform,
- ii. all the sorbate molecules in solution competed for the same surface sites,
- iii. each active site adsorbed one sorbate molecules only and
- iv. there was no interaction between adsorbed molecules.

The linear form of the Langmuir isotherms was expressed:

$$\frac{C_e}{q_e} = \frac{1}{bq_m} + \frac{C_e}{q_m} \quad [6.10]$$

where, q_e (mg g⁻¹) was concentration of adsorbed DB-86 per gram of PnsAC-alginate, C_e (mg L⁻¹) was concentration of DB-86 in aqueous solution at equilibrium, q_m was maximum capacity of PnsAC-alginate (mg g⁻¹) to form a complete monolayer on the surface, and b was the Langmuir constant (L g⁻¹) related to binding energy, the affinity between the adsorbent and adsorbate. Both b and q_m were characteristics of adsorbate-adsorbent system. The Freundlich isotherm assumed that the amount adsorbed at equilibrium followed power law dependence on the concentration of sorbate. This represented the adsorption on an energetically non-uniform surface and can be used for heterogeneous systems with interactions between the adsorbed molecules. The linear form of the Freundlich isotherms was as follows:

$$\log q_e = \log K_F + \frac{1}{n} \log C_e \quad [6.11]$$

where, K_F ((mg g⁻¹)(L mg⁻¹)^(1/n)) and n (dimensionless) were the Freundlich constants that measured the adsorption capacity and adsorption intensity, respectively. Furthermore, the term $(1/n)$ was the heterogeneity factors related to binding strength. The values of $1/n < 1.0$ implied

the favourable adsorption conditions. Temkin isotherm model was used to determine the heat of the adsorption and the adsorbent-adsorbate interaction (Abbasi and Habibi, 2016).

Temkin model assumed that

- i. heat of adsorption of all molecules in layer decreased linearly with coverage of adsorbent surface (Gupta et al., 2014),
- ii. all the molecules have nearly uniform binding energies.

This model ignored extremely low as well as very large concentration. Temkin model was expressed:

$$q_e = \frac{R \times T}{b_o} \times \ln(\alpha \times C_e) \quad [6.12]$$

where T was the absolute temperature (K), R was the gas constant ($8.314 \text{ J mol}^{-1} \text{ K}^{-1}$). The constant b_o (J mol^{-1}) related the heat of adsorption and α (L mg^{-1}) was Temkin isotherm equilibrium binding constant, related to the maximum binding energy. The model was simplified in linear form:

$$q_e = \beta_o \ln \alpha + \beta_o \ln C_e \quad [6.13]$$

where, $\beta = \frac{R \times T}{b_o}$ The parameters of Langmuir, Freundlich and Temkin isotherms were obtained according to the intercept and slope from the plots between C_e/q_e versus C_e , $\log q_e$ versus $\log C_e$, and q_e versus $\ln C_e$, respectively, as shown in Fig.6.7. The estimated isotherm parameters for all the isotherms were presented in Table 6.4. The concordance between experimental data and calculated values was established by the coefficient of determination (R^2), normalize standard deviation (SD) and chi square test (χ^2).

As observed in Table 6.4, Temkin isotherm model represented a worse fit of experimental data with low R^2 values and high χ^2 and SD values to compare with the other two isotherm models. Both Langmuir and Freundlich isotherm models fitted equilibrium DB-86 adsorption data well. However, the Langmuir model with the highest value of R^2 , lowest values of χ^2 and SD exhibited better fit compared to Freundlich isotherm model at all experimental temperatures implying monolayer coverage of DB-86 molecules onto the PnsAC-alginate surface. Temperature was found to have significant effect on adsorption capacity. With increase in temperature from 288 to 318 K, the maximum monolayer adsorption capacity (q_m) decreased from 22.03 to 20.7 mg g^{-1} and Langmuir constant (b) values increased from 2.79×10^{-2} to $5.79 \times 10^{-2} \text{ L mg}^{-1}$.

Table 6.4 : Isotherm parameters for DB-86 adsorption at 35 °C

Statistical Parameter	Langmuir isotherm			Freundlich isotherm		Temkin isotherm		
	$q_m(\text{mg g}^{-1})$	$b (\text{L mg}^{-1})$	R_L	$K_F(\text{mg g}^{-1})$ $(\text{L mg}^{-1})^{(1/n)}$	$1/n$	$A (\text{L mg}^{-1})$	β	$b (\text{J mol}^{-1})$
	21.60 ± 0.92	0.041 ± 0.004	0.039-0.270	1.83 ± 0.31	1.96 ± 0.11	0.52 ± 0.04	4.33 ± 0.38	591.91
R^2	0.982			0.967		0.930		
SD (%)	13.74			11.93		30.62		
χ^2	1.20			2.67		4.16		

The maximum dye sorption capacity of various agricultural-based biosorbent materials reported in the literature including PnsAC-alginate were presented in Table 6.5. Under optimal conditions, the maximum adsorption capacity obtained from Langmuir isotherm model was found to be 21.6, mg g⁻¹ for DB-86 dyes. As evident from the Table 6.5 that the adsorption capacity of PnsAC-alginate was found to be comparable and in some cases the capacity was higher than that of many corresponding agricultural-based biosorbents. Differences in dye adsorption capacity were due to the differences in morphology, functional groups, surface area and porosity of each adsorbent material. The easy availability and cost effectiveness of PnsAC-alginate are main advantages, which made it better biosorbent for removal of DB-86 from aqueous solutions.

Table 6.5 : Adsorption capacity of different adsorbents

Adsorbent	Adsorption capacity (mg g⁻¹)	Reference
Chitin	6.9	(Cao et al., 2018)
Caulerpa racemosa var. cylindracea	5.23	(Cao et al., 2018)
BTST(base treated shorea dasyphylla sawdust	24.4	(Hanafiah et al., 2012)
Raw KT3B kaolin (Algeria)	52.76	(Mouni et al., 2018)
Mixture almond shells	22.42	(Doulati Ardejani et al., 2008)
Orange peel activated carbon	33.78	(Nemr et al., 2009)
Pine cone activated carbon rice	27.53	(Taşar et al., 2014)
Almond shell activated carbon	1.33	(Katheresan et al., 2018)
Walnut shell activated carbon	3.53	(Katheresan et al., 2018)
Apricot shell activated carbon	4.11	(Katheresan et al., 2018)
Peanut shell activated carbon	21.60	Present study

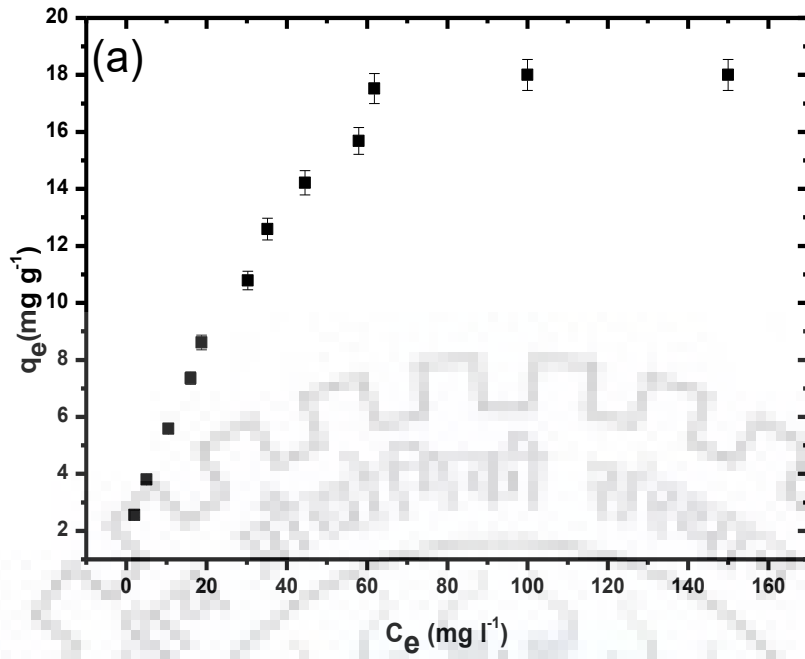


Fig.6.7 (a) : The plot of q_e Vs C_e , (Adsorption isotherm of DB-86 at 24.65 g L^{-1} adsorbent, 3.1 pH and 308 K)

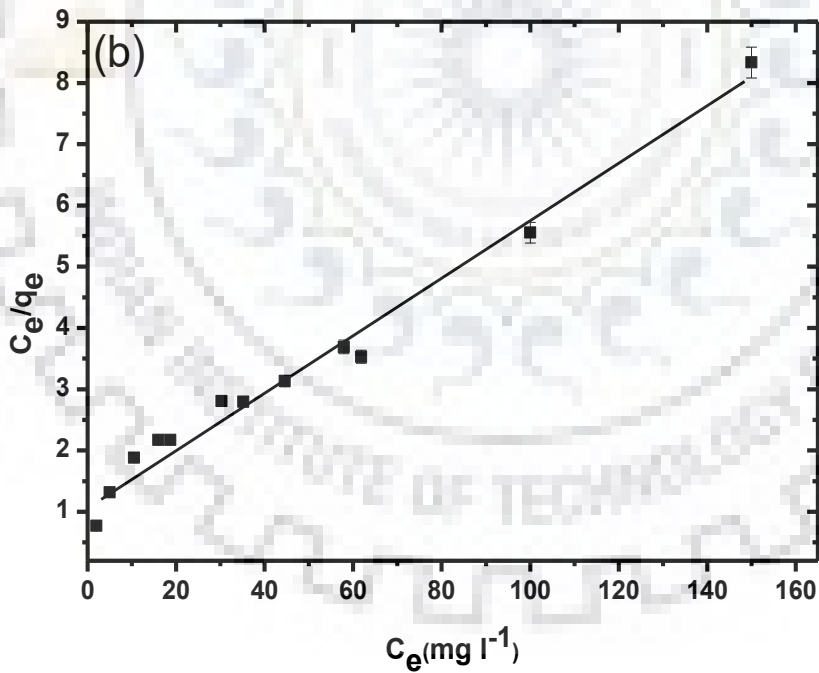


Fig.6.7 (b) : The linearized plot of Langmuir isotherm (Adsorption isotherm of DB-86 at 24.65 g L^{-1} adsorbent, 3.1 pH and 308 K)

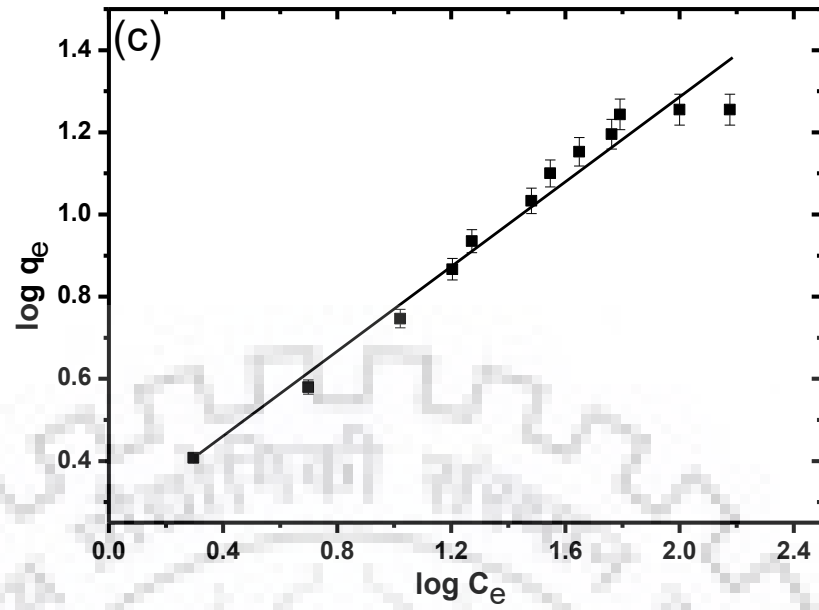


Fig.6.7 (c) : The linearized plot of Freundlich isotherm (Adsorption isotherm of DB-86 at 24.65 g L⁻¹ adsorbent, 3.1 pH and 308 K)

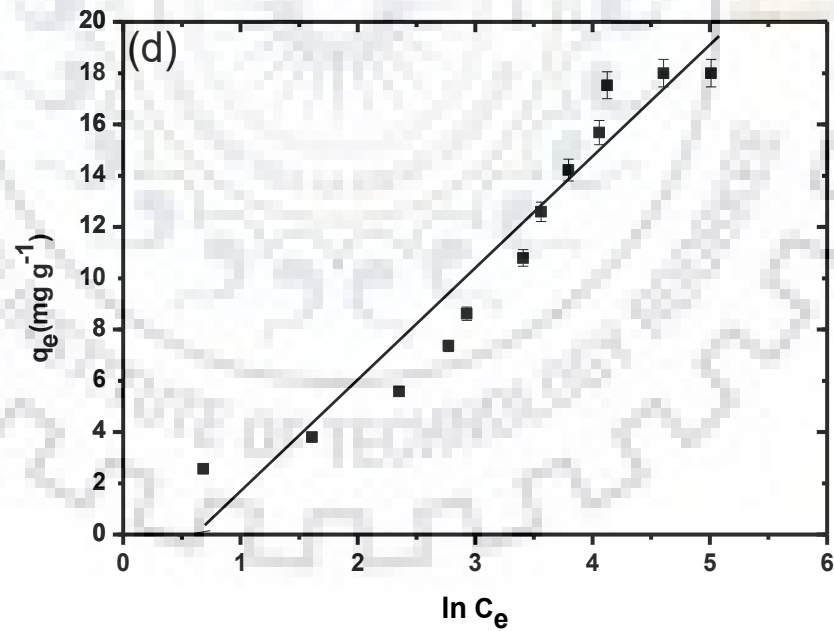


Fig.6.7 (d) : The linearized plot of Temkin isotherm (Adsorption isotherm of DB-86 at 4.65 g L⁻¹ adsorbent, 3.1 pH and 308 K)

6.1.5 Activation Energy and Thermodynamic Study

The activation energy was calculated by Arrhenius equation for the adsorption of DB-86 on PnsAC-alginate beads as:

$$\ln k_2 = \ln A - \frac{E_a}{RT} \quad [6.14]$$

where E_a is activation energy in J mol^{-1} , A is Arrhenius constant, R is universal gas constant $8.314 \text{ J mol}^{-1}\text{K}^{-1}$. Slope of the plot of $\ln k_2$ with $\frac{1}{T}$ gives activation energy.

In order to evaluate the thermodynamic feasibility and the nature of the adsorption process, thermodynamic parameters such as standard free energy change (ΔG°), enthalpy change (ΔH°) and entropy change (ΔS°) were estimated using the following equations:

$$\Delta G^\circ = -RT \ln K_L \quad [6.15]$$

$$\Delta G^\circ = \Delta H^\circ - T\Delta S^\circ \quad [6.16]$$

$$\text{where } K_L = b (\text{L mg}^{-1}) \times 1000 (\text{mg g}^{-1}) \times M_{\text{DB-86}} (\text{g mol}^{-1}) \times C^\circ (\text{mol L}^{-1}) \quad [6.17]$$

K_L in Eq.[6.15] was the (dimensionless) ‘thermodynamic’ Langmuir constant for the adsorption process. The value of K_L was obtained from the value of b (in L mg^{-1}), calculated from isotherm data using Eq.[6.10] with changing all concentration terms into molar form and taking into account the standard state $C^\circ = 1 \text{ mol L}^{-1}$ (Mouni et al., 2018). The values of ΔH° and ΔS° were obtained from the intercept and slope, respectively, of the linear plot of ΔG° vs T (Fig.6.8). Negative values of ΔG° (-23.9 to $-28.3 \text{ kJ mol}^{-1}$) estimated from Langmuir constant indicated the feasibility and spontaneity of adsorption of DB-86 on the PnsAC-alginate beads. Positive value of ΔH° (17 kJ mol^{-1}) indicated that the adsorption was endothermic in nature and increased with increase in temperature. Also, it indicated that the physical adsorption process played the significant role in the adsorption of DB-86 onto PnsAC-alginate. It was important to note that in several previous studies, the Pseudo second order kinetics with physical adsorption was reported such as adsorption of DB-86 on activated carbon prepared from orange peel (Nemr et al., 2009), adsorption of methylene blue onto natural clay (Bentahar et al., 2017) and kaolin (Mouni et al., 2018). The positive value of ΔS° ($14.23 \times 10^{-2} \text{ kJ mol}^{-1} \text{ K}^{-1}$) implied that the adsorption of DB-86 on the PnsAC-alginate beads was accompanied by increase in randomness at the solid/solution interface during the adsorption of DB-86 onto PnsAC-alginate adsorbent. Similar results were observed in the adsorption of methylene blue (Angela et al., 2018; Han et al., 2009; Mouni et al.,

2018). To check the favourability of the adsorption process, a dimensionless equilibrium parameter R_L , known as separation factor was calculated using the following equation:

$$R_L = \frac{1}{1 + bC_0} \quad [6.18]$$

For favourable adsorption process, the value of R_L varied in the range 0 – 1. The calculated R_L values for the adsorption of DB-86 onto PnsAC-alginate beads were 0.039 - 0.27 at temperatures 293 - 308 K, indicating favourable adsorption of DB-86 onto PnsAC-alginate. According to the experimental results and characterization of adsorbents in the present study, the adsorption mechanism of DB-86 onto PnsAC-alginate beads could be described by following steps in sequential:

- i. Transport of DB-86 from bulk solution to the exterior surface of PnsAC-alginate beads through a boundary layer (liquid film diffusion).
- ii. Adsorption of dye on the adsorbent surface, which might be due to the formation of weak hydrogen bonds between the positively charged PnsAC-alginate surface and the oxygen atoms of DB-86 molecules as shown in Fig.6.9

The following reactions possibly occurred at the solid / liquid interface:



(Formation of weak hydrogen bond due to electrostatic interaction)

- iii. Transport of DB-86 from the exterior surface to the pores of PnsAC-alginate beads (intraparticle diffusion).
- iv. Adsorption of DB-86 onto the active site in inner and outer surface of PnsAC-alginate beads.

Table 6.6 : Thermodynamic parameters for Adsorption of DB-86 dye

T (K)	$K_L \times 10^2$ (L mg ⁻¹)	ΔG° (kJ mol ⁻¹)	ΔH° (kJ mol ⁻¹)	$\Delta S^\circ \times 10^2$ (kJ mol ⁻¹ K ⁻¹)
288	2.79	-23.91	17.01	14.23
298	3.96	-25.61		
308	4.11	-26.56		
318	5.79	-28.33		

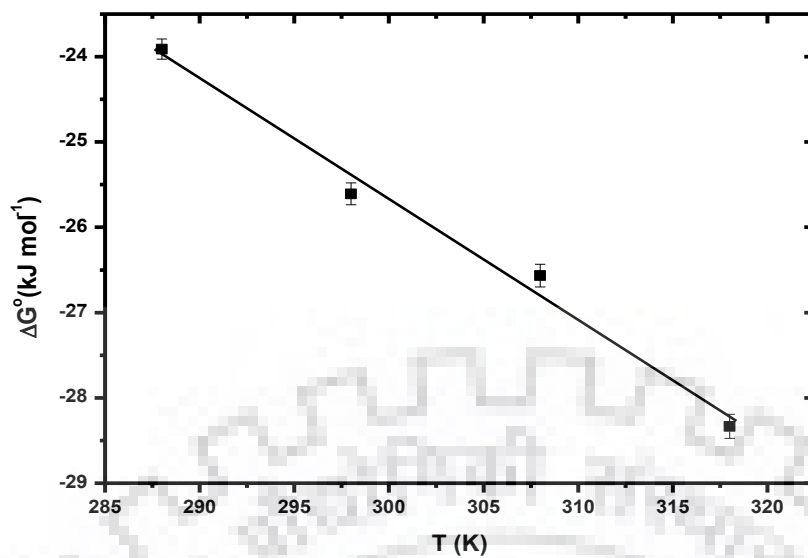


Fig.6.8 : The plot of ΔG° vs T for DB-86 adsorption

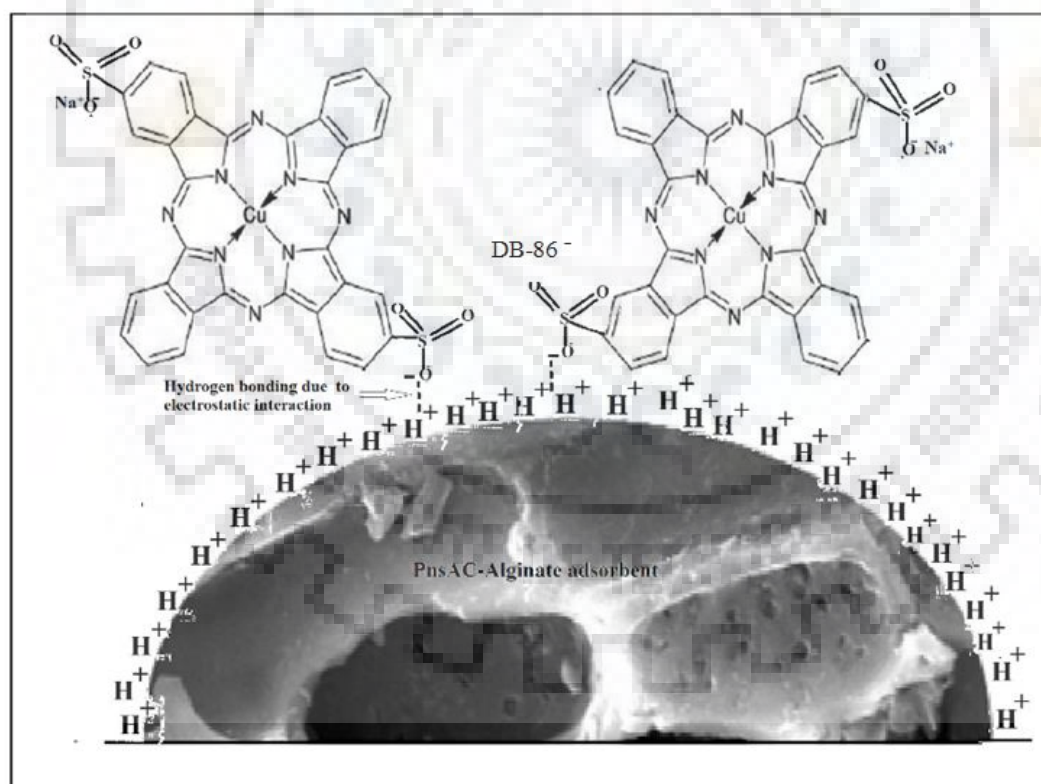


Fig.6.9 : Possible adsorption Mechanism of DB-86 by PnsAC-alginate

CHAPTER VII

CONCLUSIONS AND RECOMMENDATIONS

7.0 INTRODUCTION

The present study concerns with the removal of Acid Yellow-36 and Direct Blue-86 dyes, from synthetic wastewater using Peanut shell Activated Carbon (PnsAC) and alginate coated Peanut shell Activated Carbon (PnsAC-alginate). The results of adsorption studies of AY-36 and DB-86 dye on PnsAC and PnsAC-alginate have been presented separately. Conclusions are summarised (7.1) and compiled (7.2) according to the objectives given in the section 1.4 of Chapter I.

7.1 SUMMARY OF PRESENT WORK

7.1.1 REMOVAL OF AY – 36 FROM AQUEOUS SOLUTION USING PnsAC

- i. The low cost AC was prepared by acid treatment followed by pyrolysis at 650 °C of peanut shells, which is an agricultural waste.
- ii. Peanut shell based activated carbon was used to remove acidic dye Acid Yellow -36 (AY-36) from the aqueous solution.
- iii. Characterisation was done using TGA, FESEM with EDX, FTIR, BET surface area and Zero point charge, which confirmed that PnsAC was good adsorbent.
- iv. To test the efficacy of adsorbent, batch adsorption study was conducted at different operating conditions.
- v. The estimated optimum conditions were 4g L⁻¹ of PnsAC, 200 mg L⁻¹ AY-36 at 35 °C temperature. Adsorption was observed to be pH dependent and maximum dye removal was obtained at pH 2.
- vi. Among several isotherm models, Freundlich isotherm model explained well the adsorption equilibrium with minimum normalized standard deviation (Δq_e %) value.

Freundlich isotherm model:

$$q_e = 32.5 C_e^{1/3.48} \quad (\Delta q_e\% = 6.95) \quad [7.1]$$

Toth isotherm model:

$$q_e = \frac{600C_e}{[0.43 + C_e^{0.43}]^{1/0.43}} \quad (\Delta q_e\% = 7.07) \quad [7.2]$$

Sips isotherm model:

$$q_e = \frac{0.35 \times 128.07 C_e^{0.43}}{1 + 0.35 C_e^{0.43}} \quad (\Delta q_e\% = 7.21) \quad [7.3]$$

Redlich Peterson isotherm model:

$$q_e = \frac{364.08 C_e}{1 + 9.96 C_e^{0.77}} \quad (\Delta q_e\% = 7.23) \quad [7.4]$$

Langmuir isotherm model:

$$q_e = 66.7 \frac{0.94 C_e}{1 + 0.94 C_e} \quad (\Delta q_e\% = 16.7) \quad [7.5]$$

- vii. Kinetic data were analysed using Pseudo first order, Pseudo second order, and intra-particle diffusion models.
- viii. Pseudo second order fitted the kinetic data. Moreover, the interactions between dye and PnsAC were likely to be driven by chemical forces.
- ix. Negative value of ΔG° confirms the process to be feasible and spontaneous. Positive values of ΔH° indicates that the adsorption process is endothermic. Positive values of ΔS° increased disorderness in the adsorption of AY-36.
- x. These results indicate that the PnsAC is a potential adsorbent that can be successfully used commercially for the treatment of wastewater containing AY-36.

7.1.2 REMOVAL OF DB – 86 FROM AQUEOUS SOLUTION USING PnsAC

- i. The activated carbon was made from agricultural waste peanut shells using H_3PO_4 .
- ii. The BET surface area was found to be $965.67 \text{ m}^2 \text{ g}^{-1}$. Other characterization study reveals that PnsAC can be used as an efficient adsorbent to remove Direct Blue-86 (DB-86). Adsorption depends on pH and maximum adsorption was found at pH 2.

iii. Equilibrium time was observed at 150 minutes. Kinetic data was very well described by Pseudo second order model.

iv. Various isotherm model equations with their normal standard deviation are given below.

Freundlich isotherm model:

$$q_e = 3.039 C_e^{1/3.202} \quad (\Delta q_e\% = 2.36) \quad [7.6]$$

Redlich Peterson isotherm model:

$$q_e = \frac{344.644C_e}{1+113.131C_e^{0.688}} \quad (\Delta q_e\% = 2.36) \quad [7.7]$$

Sips isotherm model:

$$q_e = \frac{0.034 \times 86.36 C_e^{0.982}}{1+0.034 C_e^{0.982}} \quad (\Delta q_e\% = 2.36) \quad [7.8]$$

Fritz-Schlunder isotherm model:

$$q_e = \frac{1.708 C_e^{1.299}}{1+0.458 C_e^{1.027}} \quad (\Delta q_e\% = 2.35) \quad [7.9]$$

Radke-Prausnitz isotherm model:

$$q_e = \frac{319.895 \times 3.047 C_e^{0.312}}{319.895 + 3.047 C_e^{(0.312-1)}} \quad (\Delta q_e\% = 2.36) \quad [7.10]$$

Koble-Corrigan isotherm model:

$$q_e = \frac{2.862 C_e^{0.372}}{1+0.044 C_e^{0.372}} \quad (\Delta q_e\% = 2.37) \quad [7.11]$$

Toth isotherm model:

$$q_e = \frac{614.013 C_e}{[0.554 + C_e^{0.083}]^{1/0.083}} \quad (\Delta q_e\% = 3.16) \quad [7.12]$$

Langmuir isotherm model:

$$q_e = 15.547 \frac{0.045 C_e}{1+0.045 C_e} \quad (\Delta q_e\% = 3.73) \quad [7.13]$$

- v. The value of ΔG° and ΔH° indicates that process is spontaneous and endothermic. The positive value of ΔS° indicates the interaction between adsorbate and adsorbent.
- vi. From the present study we can say that Peanut shell Activated Carbon (PnsAC) can be utilized commercially in the removal of Direct Blue 86 dye, but its removal efficiency is not as good as it is for AY-36 dye.

7.1.3 REMOVAL OF DB – 86 FROM AQUEOUS SOLUTION USING PnsAC-ALGINATE

- i. The alginate encapsulated Activated Carbon (PnsAC-alginate), prepared from waste Peanut shell was used as an adsorbent for the removal of Direct Blue-86 (DB-86) from aqueous solutions.
- ii. Characterization of PnsAC-alginate was done by using SEM, EDX, XRD, TEM, S_{BET} , pH_{ZPC} and FTIR analysis. SEM – EDX study confirmed the adsorption of DB-86 dye onto PnsAC-alginate. XRD results suggested the decrease crystallinity of carbon in PnsAC-alginate. TEM analysis confirmed the porous texture surface morphology, which was consistent with the SEM. BET surface area of PnsAC-alginate was $142.5 \text{ m}^2 \text{ g}^{-1}$. The average pore size was 5.97 nm. The estimated value of pH_{ZPC} for PnsAC-alginate was 7.8.
- iii. FTIR analysis confirmed the adsorption of DB-86 onto PnsAC-alginate. The experimental results also showed that the dye removal efficiency was increased by 7 % as compared with Peanut shell Activated Carbon (PnsAC) as an adsorbent.
- iv. The effects of temperature, extraction time, adsorbent dose, dye concentration and solution pH on the adsorption of DB-86 onto PnsAC-alginate were studied.
- v. Central composite design coupled with response surface methodology (RSM) was used to optimize the adsorption feed conditions in order to achieve maximum dye removal efficiency.
- vi. The statistical analysis revealed that for maximum dye removal efficiency, the optimal conditions were adsorbent dose of 24.65 g L^{-1} , DB-86 dye concentration of 125.5 mg L^{-1} and pH of 3.1. Under the optimized conditions, experimental dye removal efficiency ($98.4 \pm 0.1\%$) agreed closely with the predicted results, thus indicating the suitability of RSM in optimizing the feed conditions.
- vii. The adsorption kinetics of DB-86 was well described by Pseudo second order kinetic model with intra-particle and film diffusion mechanisms.

- viii. Freundlich isotherm model provided the best fit to the adsorption equilibrium data. By Langmuir adsorption isotherm study, maximum monolayer adsorption capacity was found to be $21.6 \pm 0.9 \text{ mg g}^{-1}$.

Freundlich isotherm model:

$$q_e = 1.83 C_e^{0.967} \quad (\Delta q_e\% = 11.93) \quad [7.14]$$

Langmuir isotherm model:

$$q_e = 21.6 \frac{0.041C_e}{1+0.041C_e} \quad (\Delta q_e\% = 13.74) \quad [7.15]$$

- ix. Estimation of thermodynamic parameters revealed that the adsorption process was feasible, spontaneous and endothermic in nature.
- x. The present study demonstrated that PnsAC-alginate effectively removed anionic DB-86 dye from aqueous solution.

7.2 CONCLUSIONS

Present work has been taken with the objective of removing two dyes (AY-36 & DB-86) from wastewater. Following conclusions have been drawn from the present work:

- i. Adsorptive removal of dyes were carried out with indigenously made Activated Carbon from the agricultural waste, Peanut shell using H_3PO_4 .
- ii. 98 % removal of dye AY-36 was obtained at 200 mg L^{-1} dye concentration with PnsAC dose of 4 g L^{-1} at pH 2.
- iii. 78.6 % removal of dye DB-86 was attained at the concentration of 100 mg L^{-1} dye for 10 g L^{-1} of PnsAC dose at pH 2.
- iv. A novel adsorbent of PnsAC was made successfully by surface modification with alginate.
- v. 98.4 % removal of dye DB-86 was achieved by surface modified PnsAC (PnsAC-alginate).
- vi. RSM technique was utilized for optimization of dye concentration, PnsAC-alginate dose and pH of the process.
- vii. The optimum value of independent variables were 3.1 pH, 125.5 mg L^{-1} dye concentration and 24.65 mg L^{-1} PnsAC-alginate.

- viii. Various kinetic models and equilibrium isotherm models were studied.
- ix. Thermodynamic parameters revealed that the process was spontaneous and endothermic.

7.3 RECOMMENDATIONS FOR FUTURE WORK

On the basis of present studies, the following recommendations have been made for further studies:

- i. Since present investigations revealed the feasibility of PnsAC and PnsAC-alginate for the removal of AY-36 and DB-86, adsorption studies can be done with some other dyes eg Direct Violet-35.
- ii. The present work pertains to the batch adsorption study, so it would be desirable that the continuous adsorption study in fixed bed or fluidized bed systems may be conducted for their application on large industrial scale.
- iii. The adsorption capacity of adsorbents using various surface modification agent, can be examined.
- iv. In the present study we have conducted experiment only on synthetic wastewater containing the specified % of dye. The effect of inorganic and organic constituent present in wastewater of textile industry have not been planned in this research and so have not been studied. However these studies are interesting and highly desirable for the practical application of present research work. The industrial wastewater from textile industry contains many organic and inorganic compounds other than the dyes. These other constituents include (Pérez et al., 2016)

Acid $\text{Na}_2\text{SO}_4, \text{H}_2\text{SO}_4, \text{CH}_2\text{O}_2, \text{C}_2\text{H}_4\text{O}_2, \text{CH}_3\text{COONH}_4, (\text{NH}_4)_2\text{SO}_4$

Basic $\text{CH}_2\text{O}_2, \text{C}_2\text{H}_4\text{O}_2, \text{C}_2\text{H}_2\text{O}_4, \text{C}_{76}\text{H}_{52}\text{O}_{46}$

Direct $\text{NaCl}, \text{Na}_2\text{SO}_4, \text{NaNO}_2, \text{HCl}$

Reactive $\text{NaCl}, \text{CON}_2\text{H}_4, \text{Na}_2\text{CO}_3, \text{P}_2\text{O}_5, \text{Na}_3\text{P}_2\text{O}_7$

In the present work their effect on adsorption process has not been studied. It is suggested that these aspects related to industrial wastewater may be studied in future for its practical implementation in the industry.

REFERENCES

- Abbasi, M., Habibi, M.M., 2016. Journal of the Taiwan Institute of Chemical Engineers Optimization and characterization of Direct Blue 71 removal using nanocomposite of Chitosan-MWCNTs : Central composite design modeling. *J. Taiwan Inst. Chem. Eng.* 62, 112–121. doi:10.1016/j.jtice.2016.01.019
- Abd El-Rehim, H. a., Hegazy, E.S. a., Diao, D. a., 2012. Photo-catalytic degradation of metanil yellow dye using TiO₂ immobilized into polyvinyl alcohol/acrylic acid microgels prepared by ionizing radiation. *React. Funct. Polym.* 72, 823–831. doi:10.1016/j.reactfunctpolym.2012.07.009
- Abid, M.F., Zablouk, M.A., Abid-Alameer, A.M., 2012. Experimental study of dye removal from industrial wastewater by membrane technologies of reverse osmosis and nanofiltration. *Iranian J. Environ. Health Sci. Eng.* 9. doi:10.1186/1735-2746-9-17
- Adeosun, S., Taiwo, O., Akpan, E., Gbenebor, O., Gbagba, S., Olaleye, S., 2016. Mechanical characteristics of groundnut shell particle reinforced polylactide nano fibre. *REVISTAMATERIA* 482–491.
- Ahmad, M., Lee, S.S., Dou, X., Mohan, D., Sung, J.K., Yang, J.E., Ok, Y.S., 2012. Effects of pyrolysis temperature on soybean stover- and peanut shell-derived biochar properties and TCE adsorption in water. *Bioresour. Technol.* 118, 536–544. doi:10.1016/j.biortech.2012.05.042
- Ahmad, R., Mondal, P.K., Usmani, S.Q., 2010. Hybrid UASFB-aerobic bioreactor for biodegradation of acid yellow-36 in wastewater. *Bioresour. Technol.* 101, 3787–3790. doi:10.1016/j.biortech.2009.12.116
- Ahmida, K., Darmoon, M., Al-tohami, F., Erhayem, M., Zidan, M., 2015. Effect of Physical and Chemical Preparation on Characteristics of Activated Carbon from Agriculture Solid Waste and their Potential Application. *Int. Conf. Chem. Civ. Environ. Eng.* 83–87. doi:10.15242/iicbe.c0615015
- Ai, L., Li, M., Li, L., 2011. Adsorption of Methylene Blue from Aqueous Solution with Activated Carbon / Cobalt Ferrite / Alginate Composite Beads: Kinetics, Isotherms, and Thermodynamics. *J. Chem. Eng. Data* 56, 3475–3483.
- Aichour, A., Zaghouane-Boudiaf, H., Iborra, C.V., Polo, M.S., 2018. Bioadsorbent beads prepared from activated biomass/alginate for enhanced removal of cationic dye from water medium: Kinetics, equilibrium and thermodynamic studies. *J. Mol. Liq.* 256, 533–540. doi:10.1016/j.molliq.2018.02.073
- Ajmal, A., Majeed, I., Malik, R.N., Idriss, H., Nadeem, M.A., 2014. Principles and mechanisms of photocatalytic dye degradation on TiO₂ based photocatalysts: a comparative overview. *RSC Adv.* 4, 37003–37026. doi:10.1039/C4RA06658H
- Ali, I., Qureshi, A.A., Alothman, Z.A., Alwarthan, A., 2017. Dye Wastewater Treatment by Adsorption, in: Inc, J.W.& S. (Ed.), *Kirk-Othmer Encyclopedia of Chemical Technology*. John Wiley & Sons, Inc., Hoboken, NJ, USA, pp. 1–15.
- AL-Othman, Z.A., Ali, R., Naushad, M., 2012. Hexavalent chromium removal from aqueous

- medium by activated carbon prepared from peanut shell: Adsorption kinetics, equilibrium and thermodynamic studies. *Chem. Eng. J.* 184, 238–247. doi:10.1016/j.cej.2012.01.048
- Al-Qodah, Z., Lafi, W.K., Al-Anber, Z., Al-Shannag, M., Harahsheh, A., 2007. Adsorption of methylene blue by acid and heat treated diatomaceous silica. *Desalination* 217, 212–224. doi:10.1016/j.desal.2007.03.003
- Amin, N.K., 2009. Removal of direct blue-106 dye from aqueous solution using new activated carbons developed from pomegranate peel: Adsorption equilibrium and kinetics. *J. Hazard. Mater.* 165, 52–62. doi:10.1016/j.jhazmat.2008.09.067
- Anastopoulos, I., Kyzas, G.Z., 2014. Agricultural peels for dye adsorption : A review of recent literature. *J. Mol. Liq.* 200, 381–389. doi:10.1016/j.molliq.2014.11.006
- Angela, D., Sumalinog, G., Capareda, S.C., Daniel, M., Luna, G. De, 2018. Evaluation of the effectiveness and mechanisms of acetaminophen and methylene blue dye adsorption on activated biochar derived from municipal solid wastes. *J. Environ. Manage.* 210, 255–262.
- Anjaneya, O., Souche, S.Y., Santoshkumar, M., Karegoudar, T.B., 2011. Decolorization of sulfonated azo dye Metanil Yellow by newly isolated bacterial strains: *Bacillus* sp. strain AK1 and *Lysinibacillus* sp. strain AK2. *J. Hazard. Mater.* 190, 351–358. doi:10.1016/j.jhazmat.2011.03.044
- Applied Mathematics in Chemical Engineering, 2nd ed, n.d. . Tata McGraw-Hill Publishing Company New Delhi.
- Araujo, L.A., Bezerra, C.O., Cusioli, L.F., Silva, M.F., Nishi, L., Gomes, R.G., Bergamasco, R., 2018. Moringa oleifera biomass residue for the removal of pharmaceuticals from water. *J. Environ. Chem. Eng.* 6, 7192–7199. doi:10.1016/j.jece.2018.11.016
- Arumugam, N., Chelliapan, S., Kamyab, H., 2018. Treatment of Wastewater Using Seaweed : A Review 1–17. doi:10.3390/ijerph15122851
- Arya, S.K., Srivastava, S.K., 2006. Kinetics of immobilized cyclodextrin gluconotransferase produced by *Bacillus macerans* ATCC 8244. *Enzyme Microb. Technol.* 39, 507–510. doi:10.1016/j.enzmictec.2005.12.019
- Auta, M., Hameed, B.H., 2011. Preparation of waste tea activated carbon using potassium acetate as an activating agent for adsorption of Acid Blue 25 dye. *Chem. Eng. J.* 171, 502–509. doi:10.1016/j.cej.2011.04.017
- Bayat, M., Javanbakht, V., Esmaili, J., 2018. Synthesis of zeolite / nickel ferrite / sodium alginate bionanocomposite via a co-precipitation technique for efficient removal of water-soluble methylene blue dye. *Int. J. Biol. Macromol.* 116, 607–619. doi:10.1016/j.ijbiomac.2018.05.012
- Belaid, K.D., Kacha, S., Kameche, M., Derriche, Z., 2013. Adsorption kinetics of some textile dyes onto granular activated carbon. *J. Environ. Chem. Eng.* 1, 496–503. doi:10.1016/j.jece.2013.05.003
- Benhouria, A., Islam, M.A., Zaghouane-Boudiaf, H., Boutahala, M., Hameed, B.H., 2015. Calcium alginate–bentonite–activated carbon composite beads as highly effective adsorbent for methylene blue. *Chem. Eng. J.* 270, 621–630. doi:10.1016/j.cej.2015.02.030
- Bentahar, S., Dbik, A., Khomri, M. El, Messaoudi, Nouredine ElLacherai, A., 2017. Adsorption of methylene blue, crystal violet and congo red from binary and ternary systems with natural clay: Kinetic, isotherm, and thermodynamic. *J. Environ. Chem. Eng.* 5, 5921–5932.

doi:10.1016/j.jece.2017.11.003

- Boukhalfa, N., Boutahala, M., Djebri, N., Idris, A., 2019. International Journal of Biological Macromolecules Kinetics , thermodynamics , equilibrium isotherms , and reusability studies of cationic dye adsorption by magnetic alginate / oxidized multiwalled carbon nanotubes composites. *Int. J. Biol. Macromol.* 123, 539–548. doi:10.1016/j.ijbiomac.2018.11.102
- Cao, J.-S., Lin, J.-X., Fang, F., Zhang, M.-T., Hu, Z.-R., 2014. A new absorbent by modifying walnut shell for the removal of anionic dye: kinetic and thermodynamic studies. *Bioresour. Technol.* 163, 199–205. doi:10.1016/j.biortech.2014.04.046
- Cao, Y., Pan, Z., Shi, Q., Yu, J., 2018. Modification of chitin with high adsorption capacity for methylene blue removal. *Int. J. Biol. Macromol.* 114, 392–399.
- Chakraborty, S., Chowdhury, S., Das Saha, P., 2011. Adsorption of Crystal Violet from aqueous solution onto NaOH-modified rice husk. *Carbohydr. Polym.* 86, 1533–1541. doi:10.1016/j.carbpol.2011.06.058
- Chemical Economics Handbook [WWW Document], n.d. . IHS Markit. URL <https://ihsmarkit.com/products/dyes-chemical-economics-handbook.html>
- Chemistry of dyes [WWW Document], n.d. URL <http://www.chm.bris.ac.uk/webprojects2002/price/colour.htm> (accessed 5.31.19).
- Chiou, M.S., Chuang, G.S., 2006. Competitive adsorption of dye metanil yellow and RB15 in acid solutions on chemically cross-linked chitosan beads. *Chemosphere* 62, 731–740. doi:10.1016/j.chemosphere.2005.04.068
- Chowdhury, S., Saha, P., 2010. Sea shell powder as a new adsorbent to remove Basic Green 4 (Malachite Green) from aqueous solutions: Equilibrium, kinetic and thermodynamic studies. *Chem. Eng. J.* 164, 168–177. doi:10.1016/j.cej.2010.08.050
- Crittenden, Borchardt, Harza, M.W., 2012. *MWH’s water treatment: principles and design*, 3rd ed. ed. John Wiley & Sons, Hoboken, N.J.
- Daemi, H., Barikani, M., 2012. Synthesis and characterization of calcium alginate nanoparticles, sodium homopolymannuronate salt and its calcium nanoparticles. *Sci. Iran.* 19, 2023–2028. doi:10.1016/j.scient.2012.10.005
- Dahri, M.K., Kooh, M.R.R., Lim, L.B.L., 2014. Water remediation using low cost adsorbent walnut shell for removal of malachite green: Equilibrium, kinetics, thermodynamic and regeneration studies. *J. Environ. Chem. Eng.* 2, 1434–1444. doi:10.1016/j.jece.2014.07.008
- Dalai, A.K., Sharma, K., Vyas, R.K., Singh, K., 2018. Degradation of a synthetic binary dye mixture using reactive adsorption : Experimental and modeling studies. *J. Environ. Chem. Eng.* 6, 5732–5743. doi:10.1016/j.jece.2018.08.069
- Danish, M., Ahmad, T., 2018. A review on utilization of wood biomass as a sustainable precursor for activated carbon production and application. *Renew. Sustain. Energy Rev.* 87, 1–21. doi:10.1016/j.rser.2018.02.003
- Das, S., Mitra, K.S., Chakraborty, S., 2012. Magnetohydrodynamics in narrow fluidic channels in presence of spatially non-uniform magnetic fields: framework for combined magnetohydrodynamic and magnetophoretic particle transport. *Microfluid Nanofluid* 799–807. doi:10.1007/s10404-012-1001-z
- De Castro, M.L.F.A., Abad, M.L.B., Sumalinog, D.A.G., Abarca, R.R.M., Paoprasert, P., de

- Luna, M.D.G., 2018. Adsorption of Methylene Blue dye and Cu(II) ions on EDTA-modified bentonite: Isotherm, kinetic and thermodynamic studies. *Sustain. Environ. Res.* doi:10.1016/j.serj.2018.04.001
- Deniz, F., 2013. Dye removal by almond shell residues : Studies on biosorption performance and process design. *Mater. Sci. Eng. C* 33, 2821–2826. doi:10.1016/j.msec.2013.03.009
- Dias, J.M., Alvim-Ferraz, M.C.M., Almeida, M.F., Rivera-Utrilla, J., Sánchez-Polo, M., 2007. Waste materials for activated carbon preparation and its use in aqueous-phase treatment: A review. *J. Environ. Manage.* 85, 833–846. doi:10.1016/j.jenvman.2007.07.031
- Dias, J.M., Alvim-ferraz, M.C.M., Almeida, M.F., Sa, M., 2007. Waste materials for activated carbon preparation and its use in aqueous-phase treatment : A review. *J. Environ. Manage.* 85, 833–846. doi:10.1016/j.jenvman.2007.07.031
- Dil, E.A., Ghaedi, M., Asfaram, A., 2017. Ultrasonics Sonochemistry The performance of nanorods material as adsorbent for removal of azo dyes and heavy metal ions : Application of ultrasound wave , optimization and modeling. *Ultrason. Sonochemistry* J. 34, 792–802. doi:10.1016/j.ultsonch.2016.07.015
- Dogan, M., Ozdemir, Y., Alkan, M., 2007. Adsorption kinetics and mechanism of cationic methyl violet and methylene blue dyes onto sepiolite. *Dye. Pigment.* 75, 701–713. doi:10.1016/j.dyepig.2006.07.023
- Doulati Ardejani, F., Badii, K., Limaee, N.Y., Shafaei, S.Z., Mirhabibi, a R., 2008. Adsorption of Direct Red 80 dye from aqueous solution onto almond shells: effect of pH, initial concentration and shell type. *J. Hazard. Mater.* 151, 730–7. doi:10.1016/j.jhazmat.2007.06.048
- Draget, K.I., 2009. 29- Alginates, in: *Handbook of Hydrocolloids.* pp. 807–828. doi:10.1533/9781845695873.807
- Draget, K.I., Taylor, C., 2011. Chemical, physical and biological properties of alginates and their biomedical implications. *Food Hydrocoll.* 25, 251–256. doi:10.1016/j.foodhyd.2009.10.007
- Dutta, M., Basu, J.K., Faraz, H., Gautam, N., Kumar, A., 2012. Fixed-bed Column Study of Textile Dye Direct Blue 86 by using A Composite Adsorbent. *Arch. Appl. Sci. Res.* 4, 882–891.
- El Ashtoukhy, E.S.Z., 2009. Loofa *egyptiaca* as a novel adsorbent for removal of direct blue dye from aqueous solution. *J. Environ. Manage.* 90, 2755–2761. doi:10.1016/j.jenvman.2009.03.005
- El-Shafey, E.I., 2007. Removal of Se(IV) from aqueous solution using sulphuric acid-treated peanut shell. *J. Environ. Manage.* 84, 620–627. doi:10.1016/j.jenvman.2007.03.021
- Fabryanty, R., Valencia, C., Soetaredjo, F.E., Putro, J.N., Santoso, S.P., Kurniawan, A., Ju, Y.H., Ismadji, S., 2017. Removal of crystal violet dye by adsorption using bentonite – alginate composite. *J. Environ. Chem. Eng.* 5, 5677–5687. doi:10.1016/j.jece.2017.10.057
- Faria, P.C.C., Orfao, J.J.M., Pereira, M.F.R., 2009. Activated carbon and ceria catalysts applied to the catalytic ozonation of dyes and textile effluents. *Appl. Catal. B Environ.* 88, 341–350. doi:10.1016/j.apcatb.2008.11.002
- Fernandez, M.E., Nunell, G.V., Bonelli, P.R., Cukierman, A.L., 2014. Activated carbon developed from orange peels: Batch and dynamic competitive adsorption of basic dyes. *Ind. Crops Prod.* 62, 437–445. doi:10.1016/j.indcrop.2014.09.015

- Foo, K.Y., Hameed, B.H., 2010. Insights into the modeling of adsorption isotherm systems. *Chem. Eng. J.* 156, 2–10. doi:10.1016/j.cej.2009.09.013
- Freeman, H.S., Reife, A., 2003. Dyes, *Environmental Chemistry*, in: John Wiley & Sons, I. (Ed.), *Kirk-Othmer Encyclopedia of Chemical Technology*. John Wiley & Sons, Inc., Hoboken, NJ, USA.
- Garg, D., Kumar, S., Sharma, K., Majumder, C.B., 2019. Application of waste peanut shells to form activated carbon and its utilization for the removal of Acid Yellow 36 from wastewater. *Groundw. Sustain. Dev.* 8, 512–519. doi:10.1016/J.GSD.2019.01.010
- Georgin, J., Dotto, G.L., Mazutti, M.A., Foletto, E.L., 2016a. Preparation of activated carbon from peanut shell by conventional pyrolysis and microwave irradiation-pyrolysis to remove organic dyes from aqueous solutions. *J. Environ. Chem. Eng.* 4, 266–275. doi:10.1016/j.jece.2015.11.018
- Georgin, J., Luiz, G., Antonio, M., Luiz, E., 2016b. *Journal of Environmental Chemical Engineering* Preparation of activated carbon from peanut shell by conventional pyrolysis and microwave irradiation-pyrolysis to remove organic dyes from aqueous solutions. *Biochem. Pharmacol.* 4, 266–275. doi:10.1016/j.jece.2015.11.018
- Georgin, J., Marques, B.S., Peres, E.C., Allasia, D., Dotto, G.L., 2018. Biosorption of cationic dyes by Pará chestnut husk (*Bertholletia excelsa*). *Water Sci. Technol.* 1612–1621. doi:10.2166/wst.2018.041
- Ghaedi, M., Negintaji, G., Karimi, H., Marahel, F., 2013. Solid phase extraction and removal of brilliant green dye on zinc oxide nanoparticles loaded on activated carbon: New kinetic model and thermodynamic evaluation. *J. Ind. Eng. Chem.* 20, 1444–1452. doi:10.1016/j.jiec.2013.07.030
- Ghaedi, M., Pakniat, M., Mahmoudi, Z., Hajati, S., Sahraei, R., Daneshfar, A., 2014. Synthesis of nickel sulfide nanoparticles loaded on activated carbon as a novel adsorbent for the competitive removal of Methylene blue and Safranin-O. *Spectrochim. Acta - Part A Mol. Biomol. Spectrosc.* 123, 402–409. doi:10.1016/j.saa.2013.12.083
- Ghaly, A.E., Ananthashankar, R., Alhattab, M., Ramakrishnan, V. V., 2014. Production, Characterization and Treatment of Textile Effluents: A Critical Review. *J. Chem. Eng. Process Technol.* 5, 1–18. doi:10.4172/2157-7048.1000182
- Girgis, B.S., Yunis, S.S., Soliman, A.M., 2002. Characteristics of activated carbon from peanut hulls in relation to conditions of preparation 57, 164–172.
- Global Alginate Industry Trends [WWW Document], n.d. URL <https://www.grandviewresearch.com/industry-analysis/alginate-market> (accessed 8.18.19).
- Global Dyes Market [WWW Document], n.d. URL <https://www.businesswire.com/news/home/20190219005492/en/Global-Dyes-Market-Type-Application-Region-Country> (accessed 6.1.19).
- Gong, R., Ding, Y., Li, M., Yang, C., Liu, H., Sun, Y., 2005. Utilization of powdered peanut hull as biosorbent for removal of anionic dyes from aqueous solution 64, 187–192. doi:10.1016/j.dyepig.2004.05.005
- Gregg, S.J., Sing, K.S.W., 1982. *Adsorption, Surface Area and Porosity*. Academic press, New York. doi:10.1149/1.2426447
- Groen, J.C., Peffer, L.A.A., Perez-Ramirez, J., 2003. Pore size determination in modified micro-

- and mesoporous materials. Pitfalls and limitations in gas adsorption data analysis. *Microporous Mesoporous Mater.* 60, 1–17. doi:10.1016/S1387-1811(03)00339-1
- Guesmi, Y., Agougui, H., La, R., Jabli, M., Hafiane, A., 2018. Synthesis of hydroxyapatite-sodium alginate via a co-precipitation technique for efficient adsorption of Methylene Blue dye. *J. of Molecular Liq. J.* 249, 912–920. doi:10.1016/j.molliq.2017.11.113
- Guo, X., Wei, Q., Du, B., Zhang, Y., Xin, X., Yan, L., Yu, H., 2013. Removal of Metanil Yellow from water environment by amino functionalized graphenes (NH₂-G) – Influence of surface chemistry of NH₂-G. *Appl. Surf. Sci.* 284, 862–869. doi:10.1016/j.apsusc.2013.08.023
- Gupta, V.K., Pathania, D., Singh, P., Kumar, A., Rathore, B.S., 2014. Adsorptional removal of methylene blue by guar gum – cerium (IV) tungstate hybrid cationic exchanger. *Carbohydr. Polym.* 101, 684–691. doi:10.1016/j.carbpol.2013.09.092
- Hameed, B.H., Ahmad, A.L., Latiff, K.N. a, 2007. Adsorption of basic dye (methylene blue) onto activated carbon prepared from rattan sawdust. *Dye. Pigment.* 75, 143–149. doi:10.1016/j.dyepig.2006.05.039
- Han, R., Zhang, J., Han, P., Wang, Y., Zhao, Z., Tang, M., 2009. Study of equilibrium, kinetic and thermodynamic parameters about methylene blue adsorption onto natural zeolite. *Chem. Eng. J.* 145, 496–504. doi:10.1016/j.cej.2008.05.003
- Han, R., Zhang, J., Zou, W., Shi, J., Liu, H., 2005. Equilibrium biosorption isotherm for lead ion on chaff. *J. Hazard. Mater.* 125, 266–271. doi:10.1016/j.jhazmat.2005.05.031
- Han, Y., Cao, X., Ouyang, X., Sohi, S.P., Chen, J., 2016. Adsorption kinetics of magnetic biochar derived from peanut hull on removal of Cr (VI) from aqueous solution: Effects of production conditions and particle size. *Chemosphere* 145, 336–341. doi:10.1016/j.chemosphere.2015.11.050
- Hanafiah, M.A.K.M., Ngah, W.S.W., Zolkafly, S.H., Teong, L.C., Majid, Z.A.A., 2012. Acid Blue 25 adsorption on base treated Shorea dasyphylla sawdust: Kinetic, isotherm, thermodynamic and spectroscopic analysis. *J. Environ. Sci.* 24, 261–268. doi:10.1016/S1001-0742(11)60764-X
- Hassaan, M.A., El, A., Madkour, F.F., 2017. Testing the advanced oxidation processes on the degradation of Direct Blue 86 dye in wastewater. *Egypt. J. Aquat. Res.* 43, 11–19. doi:10.1016/j.ejar.2016.09.006
- Hassaan, M.A., Nemr, A. El, 2017. Health and Environmental Impacts of Dyes: Mini Review. *Am. J. Environ. Sci. Eng.* 1, 64–67. doi:10.11648/j.ajese.20170103.11
- He, J., Li, J., Du, W., Han, Q., Wang, Z., Li, M., 2018. A mesoporous metal-organic framework : Potential advances in selective dye adsorption. *J. Alloys Compd.* 750, 360–367.
- Heibati, B., Rodriguez-Couto, S., Amrane, A., Rafatullah, M., Hawari, A., Al-Ghouti, M. a., 2014. Uptake of Reactive Black 5 by pumice and walnut activated carbon: Chemistry and adsorption mechanisms. *J. Ind. Eng. Chem.* 20, 2939–2947. doi:10.1016/j.jiec.2013.10.063
- Ho, Y., Mckay, G., 2002. The kinetics of sorption of divalent metal ions onto sphagnum moss peat. *Water Res.* 34, 735–742. doi:10.1016/s0043-1354(99)00232-8
- Hong, S., Wen, C., He, J., Gan, F., Ho, Y.S., 2009. Adsorption thermodynamics of Methylene Blue onto bentonite. *J. Hazard. Mater.* 167, 630–633. doi:10.1016/j.jhazmat.2009.01.014
- Humelnicu, I., Adriana, B., Ignatc, M.-E., Dulmana, V., 2017. The removal of Basic Blue 41

- textile dye from aqueous solution by adsorption onto natural zeolitic tuff: Kinetics and thermodynamics. *Process Saf. Environ. Prot.* 5, 274–287.
- Hussain, I., Li, Y., Qi, J., Li, J., Wang, L., 2018. Nitrogen-enriched carbon sheet for Methyl blue dye adsorption. *J. Environ. Manage.* 215, 123–131.
- India - dyes and pigments production growth rate 2019 [WWW Document], n.d. URL <https://www.statista.com/statistics/757855/india-dyes-and-pigments-production-growth-rate/> (accessed 8.20.19).
- India - dyes and pigments production volume 2018 [WWW Document], n.d. URL <https://www.statista.com/statistics/726947/india-dyes-and-pigments-production-volume/> (accessed 8.20.19).
- Inyang, M., Gao, B., Zimmerman, A., Zhang, M., Chen, H., 2014. Synthesis, characterization, and dye sorption ability of carbon nanotube–biochar nanocomposites. *Chem. Eng. J.* 236, 39–46. doi:10.1016/j.cej.2013.09.074
- Isoda, N., Rodrigues, R., Silva, A., Gonçalves, M., Mandelli, D., Figueiredo, F.C.A., Carvalho, W.A., 2014. Optimization of preparation conditions of activated carbon from agriculture waste utilizing factorial design. *Powder Technol.* 256, 175–181. doi:10.1016/j.powtec.2014.02.029
- Jabli, M., Hassine, B. Ben, 2018. Improved removal of dyes by [sodium alginate/4-methyl-2-(naphthalen-2-yl)-N-propylpentanamide-functionalized ethoxy-silica] composite gel beads. *Int. J. Biol. Macromol.* 117, 247–255. doi:10.1016/j.ijbiomac.2018.04.194
- Jain, R., Gupta, V.K., Sikarwar, S., 2010. Adsorption and desorption studies on hazardous dye Naphthol Yellow S. *J. Hazard. Mater.* 182, 749–756. doi:10.1016/j.jhazmat.2010.06.098
- Jayalakshmi, R., Jeyanthi, J., 2019. Simultaneous removal of binary dye from textile effluent using cobalt ferrite-alginate nanocomposite: Performance and mechanism. *Microchem. J.* 145, 791–800. doi:10.1016/j.microc.2018.11.047
- Jo, S.W., Sheriff, S.A., Lear, W.E., 2016. Numerical Simulation of Saturated Flow Boiling Heat Transfer of Ammonia / Water Mixture in Bubble Pumps for Absorption – Diffusion Refrigerators. *J. Therm. Sci. Eng. Appl.* 6, 1–9. doi:10.1115/1.4025091
- Jung, K.W., Choi, B.H., Hwang, M.J., Jeong, T.U., Ahn, K.H., 2016. Fabrication of granular activated carbons derived from spent coffee grounds by entrapment in calcium alginate beads for adsorption of acid orange 7 and methylene blue. *Bioresour. Technol.* doi:10.1016/j.biortech.2016.07.098
- Kamboh, M.A., Bhatti, A.A., Solangi, I.B., Sherazi, S.T.H., Memon, S., 2014. Adsorption of direct black-38 azo dye on p-tert-butylcalix[6]arene immobilized material. *Arab. J. Chem.* 7, 125–131. doi:10.1016/j.arabjc.2013.06.033
- Kan, Y., Yue, Q., Kong, J., Gao, B., Li, Q., 2015. The application of activated carbon produced from waste printed circuit boards (PCBs) by H₃PO₄ and steam activation for the removal of malachite green. *Chem. Eng. J.* 260, 541–549. doi:https://doi.org/10.1016/j.cej.2014.09.047
- Karagoz, S., Tay, T., Ucar, S., Erdem, M., 2008. Activated carbons from waste biomass by sulfuric acid activation and their use on methylene blue adsorption. *Bioresour. Technol.* 99, 6214–6222. doi:10.1016/j.biortech.2007.12.019
- Katheresan, V., Kansedo, J., Lau, S.Y., 2018. Efficiency of various recent wastewater dye

- removal methods: A review. *J. Environ. Chem. Eng.* 6, 4676–4697. doi:<https://doi.org/10.1016/j.jece.2018.06.060>
- Khaled, A., Nemr, A. El, El-Sikaily, A., Abdelwahab, O., 2009. Removal of Direct N Blue-106 from artificial textile dye effluent using activated carbon from orange peel: Adsorption isotherm and kinetic studies. *J. Hazard. Mater.* 165, 100–110. doi:[10.1016/j.jhazmat.2008.09.122](https://doi.org/10.1016/j.jhazmat.2008.09.122)
- Khani, R., Sobhani, S., Hossein, M., Miri, S., 2018. Ecotoxicology and Environmental Safety Application of magnetic ionomer for development of very fast and highly efficient uptake of triazo dye Direct Blue 71 from different water samples 150, 54–61.
- Khannous, L., Elleuch, A., Fendri, I., Jebahi, N., Khlaf, H., Gharsallah, N., 2015. Treatment of printing wastewater by a combined process of coagulation and biosorption for a possible reuse in agriculture. *Desalin. Water Treat.* 57, 5723–5729. doi:[10.1080/19443994.2015.1005688](https://doi.org/10.1080/19443994.2015.1005688)
- Kharub, M., 2012. Use of various technologies, methods and adsorbents for the removal of dye. *J. Environemntal Res. Dev.* 6, 879–883.
- Khataee, A.R., Dehghan, G., Pourhassan, M., Zarei, M., Ebadi, E., 2011. Neural network modeling of biotreatment of triphenylmethane dye solution by a green macroalgae. *Chem. Eng. Res. Des.* 89, 172–178. doi:[10.1016/j.cherd.2010.05.009](https://doi.org/10.1016/j.cherd.2010.05.009)
- Khenifi, A., Bouberka, Z., Sekrane, F., Kameche, M., Derriche, Z., 2007. Adsorption study of an industrial dye by an organic clay. *Adsorption* 13, 149–158. doi:[10.1007/s10450-007-9016-6](https://doi.org/10.1007/s10450-007-9016-6)
- Kim, T.Y., Jin, H.J., Park, S.S., Kim, S.J., Cho, S.Y., 2008. Adsorption equilibrium of copper ion and phenol by powdered activated carbon, alginate bead and alginate-activated carbon bead. *J. Ind. Eng. Chem.* 14, 714–719. doi:[10.1016/j.jiec.2008.07.004](https://doi.org/10.1016/j.jiec.2008.07.004)
- kirk othmer, 2017. Removal of dyes from water by adsorption using nanoadsorbents, in: Kirk-Othmer Encyclopedia of Chemical Technology. doi:[10.1002/0471238961.koe00035](https://doi.org/10.1002/0471238961.koe00035)
- Kumar, R., Ahmad, R., 2011. Biosorption of hazardous crystal violet dye from aqueous solution onto treated ginger waste (TGW). *DES* 265, 112–118. doi:[10.1016/j.desal.2010.07.040](https://doi.org/10.1016/j.desal.2010.07.040)
- Kumari, S., Das, D., 2015. Improvement of gaseous energy recovery from sugarcane bagasse by dark fermentation followed by biomethanation process. *Bioresour. Technol.* 194, 354–363. doi:[10.1016/j.biortech.2015.07.038](https://doi.org/10.1016/j.biortech.2015.07.038)
- Kurczewska, J., Cegłowski, M., Schroeder, G., 2019. Alginate / PAMAM dendrimer – Halloysite beads for removal of cationic and anionic dyes. *Int. J. Biol.* 123, 398–408. doi:[10.1016/j.ijbiomac.2018.11.119](https://doi.org/10.1016/j.ijbiomac.2018.11.119)
- Kwak, H.W., Hong, Y., Lee, M.E., Jin, H.J., 2018. Sericin-derived activated carbon-loaded alginate bead: An effective and recyclable natural polymer-based adsorbent for methylene blue removal. *Int. J. Biol. Macromol.* 120, 906–914. doi:[10.1016/j.ijbiomac.2018.08.116](https://doi.org/10.1016/j.ijbiomac.2018.08.116)
- Kwiatkowski, J.F. (Ed.), 2012. Activated carbon : classifications, properties and applications. Nova Science Publishers, Inc. New York.
- Ladnorg, S., Junior, N.L., Agnol, P.D., Domingos, D.G., Magnus, B.S., Wichern, M., Gehring, T., Costa, H.R. da, 2019. Alginate-like exopolysaccharide extracted from aerobic granular sludge as biosorbent for methylene blue : Thermodynamic, kinetic and isotherm studies. *J. Environ. Chem. Eng.* 7, 103081. doi:[10.1016/j.jece.2019.103081](https://doi.org/10.1016/j.jece.2019.103081)

- Lagergren, S., 1898. Zur theorie der sogenannten adsorption geloster stoffe. K. Sven. Vetenskapsakademiens. Handlinger 24, 1–39.
- Lataye, D.H., Mishra, I.M., Mall, I.D., 2008. Pyridine sorption from aqueous solution by rice husk ash (RHA) and granular activated carbon (GAC): parametric, kinetic, equilibrium and thermodynamic aspects. *J. Hazard. Mater.* 154, 858–70. doi:10.1016/j.jhazmat.2007.10.111
- Leah, M., Castro, F.A. De, Love, M., Abad, B., Angela, D., Sumalinog, G., Ruffel, R., Abarca, M., Paoprasert, P., Daniel, M., Luna, G. De, 2018. Adsorption of Methylene Blue dye and Cu (II) ions on EDTA-modified bentonite : Isotherm , kinetic and thermodynamic studies. *Sustain. Environ. Res.* 1–9.
- Lee, S., Sherif, S.A.R., 2001. Thermodynamic analysis of a lithium bromide / water absorption system for cooling and heating applications. *J. Therm. Sci. Eng. Appl.* 1031, 1019–1031. doi:10.1002/er.738
- Li, D., Li, C., Tian, Y., Kong, L., Liu, L., 2015. Influences of impregnation ratio and activation time on ultramicropores of peanut shell active carbons. *Mater. Lett.* 141, 340–343. doi:10.1016/j.matlet.2014.11.042
- Liang, J., Liu, M., Zhang, Y., 2016. Cd (II) removal on surface-modified activated carbon : equilibrium , kinetics and mechanism. *Water Sci. Technol.* 1800–1808. doi:10.2166/wst.2016.338
- Liao, P., Malik, Z., Zhang, W., Yuan, S., Tong, M., Wang, K., 2012. Adsorption of dyes from aqueous solutions by microwave modified bamboo charcoal. *Chem. Eng. J.* 195–196, 339–346. doi:10.1016/j.cej.2012.04.092
- Liu, X., Wang, M., Zhang, S., Pan, B., 2013. Application potential of carbon nanotubes in water treatment: A review. *J. Environ. Sci.* 25, 1263–1280. doi:10.1016/S1001-0742(12)60161-2
- Lochananon, W., Chatsiriwech, D., 2008. Effect of phosphoric acid concentration on properties of peanut shell adsorbents. *J. Ind. Eng. Chem.* 14, 84–88. doi:10.1016/j.jiec.2007.09.001
- Luo, H., Huang, X., Luo, Y., Li, Z., Li, L., Gao, C., Xiong, J., Li, W., 2018. Spectrochimica Acta Part A : Molecular and Biomolecular Spectroscopy Adsorption behavior and mechanism of acidic blue 25 dye onto cucurbit [8] uril : A spectral and DFT study 193, 125–132.
- M. Saban Tanyildizi, 2011. Modeling of adsorption isotherms and kinetics of reactive dye from aqueous solution by peanut hull. *Chem. Eng. J.* 168, 1234–1240. doi:10.1016/j.cej.2011.02.021
- Ma, J., Jia, Y., Jing, Y., Yao, Y., Sun, J., 2012. Kinetics and thermodynamics of methylene blue adsorption by cobalt-hectorite composite. *Dye. Pigment.* 93, 1441–1446. doi:10.1016/j.dyepig.2011.08.010
- Ma, Y., Qi, P., Ju, J., Wang, Q., Hao, L., Wang, R., Sui, K., Tan, Y., 2019. Gelatin/alginate composite nanofiber membranes for effective and even adsorption of cationic dyes. *Compos. Part B Eng.* 162, 671–677. doi:10.1016/j.compositesb.2019.01.048
- Mahmoodi, N.M., Hayati, B., Arami, M., 2012. Kinetic, equilibrium and thermodynamic studies of ternary system dye removal using a biopolymer. *Ind. Crops Prod.* 35, 295–301. doi:10.1016/j.indcrop.2011.07.015
- Maleki, A., Daraei, H., Khodaei, F., Aghdam, K.B., Faez, E., 2016. Direct blue 71 dye removal probing by potato peel-based sorbent: applications of artificial intelligent systems. *Desalin. Water Treat.* 57, 12281–12286. doi:10.1080/19443994.2015.1048733

- Malik, P.K., 2004. Dye removal from wastewater using activated carbon developed from sawdust: Adsorption equilibrium and kinetics. *J. Hazard. Mater.* 113, 81–88. doi:10.1016/j.jhazmat.2004.05.022
- Malik, P.K., 2003. Use of activated carbons prepared from sawdust and rice-husk for adsorption of acid dyes: A case study of acid yellow 36. *Dye. Pigment.* 56, 239–249. doi:10.1016/S0143-7208(02)00159-6
- Mall, I.D., Srivastava, V.C., Kumar, G.V. a, Mishra, I.M., 2006. Characterization and utilization of mesoporous fertilizer plant waste carbon for adsorptive removal of dyes from aqueous solution. *Colloids Surfaces A Physicochem. Eng. Asp.* 278, 175–187. doi:10.1016/j.colsurfa.2005.12.017
- Markets, research and, n.d. Dyes & Pigments Market - Growth, Trends, and Forecast (2019 - 2024) [WWW Document]. Res. Mark. URL <https://www.researchandmarkets.com/reports/4515712/dyes-and-pigments-market-growth-trends-and> (accessed 5.31.19).
- McHugh, D.J., n.d. Chapter 2 production properties and uses of alginates by Dennis J McHugh Department of Chemistry University College University of New South Wales Australia.
- Mittal, A., Gupta, V.K., Malviya, A., Mittal, J., 2008. Process development for the batch and bulk removal and recovery of a hazardous, water-soluble azo dye (Metanil Yellow) by adsorption over waste materials (Bottom Ash and De-Oiled Soya). *J. Hazard. Mater.* 151, 821–832. doi:10.1016/j.jhazmat.2007.06.059
- Mittal, A., Mittal, J., Malviya, A., Kaur, D., Gupta, V.K., 2010. Journal of Colloid and Interface Science Adsorption of hazardous dye crystal violet from wastewater by waste materials. *J. Colloid Interface Sci.* 343, 463–473. doi:10.1016/j.jcis.2009.11.060
- Miyah, Y., Lahrichi, A., Idrissi, M., Khalil, A., Zerrouq, F., 2018. Adsorption of methylene blue dye from aqueous solutions onto walnut shells powder : Equilibrium and kinetic studies. *Surfaces and Interfaces* 11, 74–81.
- Mohammadi, A., Doctorsafaei, A.H., Zia, K.M., 2018. Alginate / calix [4] arenes modified graphene oxide nanocomposite beads : Preparation , characterization , and dye adsorption studies. *Int. J. Biol. Macromol.* 120, 1353–1361. doi:10.1016/j.ijbiomac.2018.09.136
- Mohammed, N., Grishkewich, N., Waeijen, H.A., Berry, R.M., Tam, K.C., 2016. Continuous flow adsorption of methylene blue by cellulose nanocrystal-alginate hydrogel beads in fixed bed columns. *Carbohydr. Polym.* 136, 1194–1202. doi:10.1016/j.carbpol.2015.09.099
- Mohanty, K., Das, D., Nath, M., 2008. Treatment of phenolic wastewater in a novel multi-stage external loop airlift reactor using activated carbon 58, 311–319. doi:10.1016/j.seppur.2007.05.005
- Moideen, Siti Nur Fatimah Shreeshivadasan, C., Din, M.F., Ponraj, M., Yusof, M.B.M., Ismail, Z., Songip, A.R., 2015. Wasted cockle shell (*Anadara granosa*) as a natural adsorbent for treating polluted river water in the fabricated column model (FCM). *Desalin. Water Treat.* ISSN 3994, 0–9. doi:10.1080/19443994.2015.1082939
- Montgomery, D., 2009. Introduction To Statistical Quality Control, Arizona State University. doi:10.1002/1521-3773(20010316)40:6<9823::AID-ANIE9823>3.3.CO;2-C
- Mouni, L., Belkhir, L., Bollinger, J., Bouzaza, A., Assadi, A., Tirri, A., Dahmoune, F., Madani, K., Remini, H., 2018. Removal of Methylene Blue from aqueous solutions by adsorption on

- Kaolin : Kinetic and equilibrium studies. *Appl. Clay Sci.* 153, 38–45.
- Muntean, S.G., Paska, O., Coseri, S., Simu, G.M., Grad, M.E., Iliu, G., 2012. Evaluation of a Functionalized Copolymer as Adsorbent on Direct Dyes Removal Process : Kinetics and Equilibrium Studies. *J. Appl. Polym.* 1–13. doi:10.1002/app.38017
- Myers, R.H., Montgomery, D.C., Anderson-Cook, C., 2016. Response surface methodology: process and product optimization using designed experiments, Fourth ed. ed, Wiley series in probability and statistics. Wiley, Hoboken, New Jersey.
- Nasri, N.S., Chelliapan, S., Umar, H., Abbas, M., Zaini, A., Rashid, N.M., Abdul, Z., Kumar, T., Mohd, H., Mohsin, R., Zaini, N., 2019. Kinetic Equilibrium and Isotherm Modeling Adsorbed Methane Assessment on Synthesized PEEK-Porous Sorbent Carbon of Sustainable Coconut Shell Kernel. *Chem. Eng. Trans.* 72, 247–252. doi:10.3303/CET1972042
- Nasrullah, A., Bhat, A.H., Naeem, A., Isa, M.H., Danish, M., 2018. High surface area mesoporous activated carbon-alginate beads for efficient removal of methylene blue. *Int. J. Biol. Macromol.* 107, 1792–1799. doi:10.1016/j.ijbiomac.2017.10.045
- Nations, U., 2019. The United Nations World Water Development Report 2019.
- Neill, C.O., Hawkes, F.R., Hawkes, D.L., Lourenc, N.D., 1999. Review Colour in textile effluents – sources , measurement , discharge consents and simulation : a review. *J. Chem. Technol. Biotechnol.* 1018, 1009–1018.
- Nemr, A. El, Abdelwahab, O., El-sikaily, A., Khaled, A., 2009. Removal of direct blue-86 from aqueous solution by new activated carbon developed from orange peel. *J. Hazard. Mater.* 161, 102–110. doi:10.1016/j.jhazmat.2008.03.060
- Noorimotlagh, Z., Darvishi Cheshmeh Soltani, R., Khataee, a. R., Shahriyar, S., Nourmoradi, H., 2014. Adsorption of a textile dye in aqueous phase using mesoporous activated carbon prepared from Iranian milk vetch. *J. Taiwan Inst. Chem. Eng.* 45, 1783–1791. doi:10.1016/j.jtice.2014.02.017
- Nuithitikul, K., Srikhun, S., Hirunpraditkoon, S., 2010. Kinetics and equilibrium adsorption of Basic Green 4 dye on activated carbon derived from durian peel: Effects of pyrolysis and post-treatment conditions. *J. Taiwan Inst. Chem. Eng.* 41, 591–598. doi:10.1016/j.jtice.2010.01.007
- Núñez, J., Yeber, M., Cisternas, N., Thibaut, R., Medina, P., Carrasco, C., 2019. Application of electrocoagulation for the efficient pollutants removal to reuse the treated wastewater in the dyeing process of the textile industry. *J. Hazard. Mater.* doi:10.1016/j.jhazmat.2019.03.030
- Othman, N.H., Alias, N.H., Shahrudin, M.Z., Bakar, N.F.A., Him, N.R.N., Lau, W.J., 2018. Adsorption kinetics of methylene blue dyes onto magnetic graphene oxide. *J. Environ. Chem. Eng.* 6, 2803–2811.
- Othmer, K., n.d. Dyes, azo 1.
- Oubagaranadin, J.U.K., Murthy, Z.V.P., 2012. Activated Carbons : Classifications ,Properties and Applications, in: *Activated Carbon Classification Properties and Application.* pp. 239–266.
- Oubagaranadin, J.U.K., Sathyamurthy, N., Murthy, Z.V.P., 2007. Evaluation of Fuller’s earth for the adsorption of mercury from aqueous solutions: A comparative study with activated carbon. *J. Hazard. Mater.* 142, 165–174. doi:10.1016/j.jhazmat.2006.08.001

- Oussalah, A., Boukerroui, A., Aichour, A., Djellouli, B., 2019. Cationic and anionic dyes removal by low-cost hybrid alginate / natural bentonite composite beads : Adsorption and reusability studies. *Int. J. Biol. Macromol.* 124, 854–862. doi:10.1016/j.ijbiomac.2018.11.197
- Outline, C., 2013. Water Treatment for Inorganic Pollutants by Adsorption Technology. doi:10.1016/B978-0-444-59399-3.00002-7
- Oxbow Activated Carbon [WWW Document], n.d. URL <http://www.oxbowactivatedcarbon.com/> (accessed 8.26.19).
- Panão, C.O., Campos, E.L.S., Lima, H.H.C., Rinaldi, A.W., Lima-tenório, M.K., Tenório-neto, E.T., Guilherme, M.R., Asefa, T., Rubira, A.F., 2019. Ultra-absorbent hybrid hydrogel based on alginate and SiO₂ microspheres : A high-water-content system for removal of methylene blue. *J. Mol. Liq.* 276, 204–213. doi:10.1016/j.molliq.2018.11.157
- Pawar, R.R., Lalmunsiam, Gupta, P., Sawant, S.Y., Shahmoradi, B., Lee, S.M., 2018. Porous synthetic hectorite clay-alginate composite beads for effective adsorption of methylene blue dye from aqueous solution. *Int. J. Biol. Macromol.* 114, 1315–1324. doi:10.1016/j.ijbiomac.2018.04.008
- Pekkuz, H., Uzun, I., Güzel, F., 2008. Kinetics and thermodynamics of the adsorption of some dyestuffs from aqueous solution by poplar sawdust. *Bioresour. Technol.* 99, 2009–2017. doi:10.1016/j.biortech.2007.03.014
- Pérez, A., Poznyak, T., Chairez, I., 2016. Effect of Inorganic Additives in the Textile Dyes Removal by Ozonation. *Textile Wastewater Treat.* doi:10.5772/62286
- Pirkarami, A., Olya, M.E., 2017. Removal of dye from industrial wastewater with an emphasis on improving economic efficiency and degradation mechanism. *J. Saudi Chem. Soc.* 21, S179–S186. doi:10.1016/j.jscs.2013.12.008
- Postai, D.L., Demarchi, C.A., Zanatta, F., Melo, D.C.C., Rodrigues, C.A., 2016. Adsorption of rhodamine B and methylene blue dyes using waste of seeds of *Aleurites Moluccana*, a low cost adsorbent. *Alexandria Eng. J.* doi:10.1016/j.aej.2016.03.017
- Prola, L.D.T., Machado, F.M., Bergmann, C.P., Souza, F.E. De, Gally, C.R., Lima, E.C., Adebayo, M.A., Dias, S.L.P., Calvete, T., 2013. Adsorption of Direct Blue 53 dye from aqueous solutions by multi-walled carbon nanotubes and activated carbon. *J. Environ. Manage.* 130, 166–175.
- Raja, A.S.M., Arputharaj, A., Saxena, S., Patil, P.G., 2019. 9 - Water requirement and sustainability of textile processing industries, *Water in Textiles and Apparel*. Elsevier Ltd. doi:10.1016/B978-0-08-102633-5.00009-9
- Ranjithkumar, V., Sangeetha, S., Vairam, S., 2014. Synthesis of magnetic activated carbon/ α -Fe₂O₃ nanocomposite and its application in the removal of acid yellow 17 dye from water. *J. Hazard. Mater.* 273C, 127–135. doi:10.1016/j.jhazmat.2014.03.034
- Rashed, M.N., 2013. Adsorption Technique for the Removal of Organic Pollutants from Water and Wastewater, in: *Organic Pollutants - Monitoring, Risk and Treatment*. InTech, pp. 167–194. doi:10.5772/54048
- Rashidi, N.A., Yusup, S., 2017. A review on recent technological advancement in the activated carbon production from oil palm wastes 314, 277–290.
- Ravi, Pandey, L.M., 2019. Enhanced adsorption capacity of designed bentonite and alginate

- beads for the effective removal of methylene blue. *Appl. Clay Sci.* 169, 102–111. doi:10.1016/j.clay.2018.12.019
- Reddy, K.R., 2008. Physical and Chemical Groundwater Remediation Technologies. *Overexploitation Contam. Shar. Groundw. Resour.* 257–274. doi:10.1007/978-1-4020-6985-7_12
- Reddy, K.R., Xie, T., Dastgheibi, S., 2014. Adsorption of mixtures of nutrients and heavy metals in simulated urban stormwater by different filter materials. *J. Environ. Sci. Heal. Part A* 49, 524–539. doi:10.1080/10934529.2014.859030
- Reviews, S.E., 2018. Activated carbon from lignocellulosics precursors: A review of the synthesis methods, characterization techniques and applications. *Renew. Sustain. Energy Rev.* 82, 1393–1414.
- Ricordel, S., Taha, S., Cisse, I., Dorange, G., 2001. Heavy metals removal by adsorption onto peanut husks carbon: Characterization, kinetic study and modeling. *Sep. Purif. Technol.* 24, 389–401. doi:10.1016/S1383-5866(01)00139-3
- Robinson, T., Chandran, B., Nigam, P., 2002. Removal of dyes from a synthetic textile dye effluent by biosorption on apple pomace and wheat straw 36, 2824–2830.
- Robinson, T., McMullan, G., Marchant, R., Nigam, P., 2001. Remediation of dyes in textile effluent: a critical review on current treatment technologies with a proposed alternative. *Bioresour. Technol.* 77, 247–255.
- Rodríguez, A., García, J., Ovejero, G., Mestanza, M., 2009. Adsorption of anionic and cationic dyes on activated carbon from aqueous solutions: Equilibrium and kinetics. *J. Hazard. Mater.* 172, 1311–1320. doi:10.1016/j.jhazmat.2009.07.138
- Rout, P.R., Dash, R.R., Bhunia, P., 2016. Nutrient removal from binary aqueous phase by dolochar: Highlighting optimization, single and binary adsorption isotherms and nutrient release, *Process Safety and Environmental Protection*. Institution of Chemical Engineers. doi:10.1016/j.psep.2016.01.001
- Ruiz, E.J., Arias, C., Brillas, E., Hernández-Ramírez, A., Peralta-Hernández, J.M., 2011. Mineralization of Acid Yellow 36azo dye by electro-Fenton and solar photoelectro-Fenton processes with a boron-doped diamond anode. *Chemosphere* 82, 495–501. doi:10.1016/j.chemosphere.2010.11.013
- Sadaf, S., Bhatti, H.N., 2014. Batch and fixed bed column studies for the removal of Indosol Yellow BG dye by peanut husk. *J. Taiwan Inst. Chem. Eng.* 45, 541–553. doi:10.1016/j.jtice.2013.05.004
- Saeed, A., Sharif, M., Iqbal, M., 2010. Application potential of grapefruit peel as dye sorbent: Kinetics, equilibrium and mechanism of crystal violet adsorption. *J. Hazard. Mater.* 179, 564–572. doi:10.1016/j.jhazmat.2010.03.041
- Saha, A.A., Mitra, K.S., Tweedie, M., Susanta Roy, McLaughlin, J., 2009. Experimental and numerical investigation of capillary flow in SU8 and PDMS microchannels with integrated pillars. *Micro fluid Nanofluid* 451–465. doi:10.1007/s10404-008-0395-0
- Saha, P. Das, Chakraborty, S., Chowdhury, S., 2012. Batch and continuous (fixed-bed column) biosorption of crystal violet by *Artocarpus heterophyllus* (jackfruit) leaf powder. *Colloids Surfaces B Biointerfaces* 92, 262–270. doi:10.1016/j.colsurfb.2011.11.057
- Sahu, O., Singh, N., 2019. Significance of bioadsorption process on textile industry wastewater,

The Impact and Prospects of Green Chemistry for Textile Technology. Elsevier Ltd.
doi:10.1016/B978-0-08-102491-1.00013-7

- Samal, K., Mohanty, K., Raj, N., 2018. Saponin extracted waste biomass of *Sapindus mukorossi* for adsorption of methyl violet dye in aqueous system. *Surfaces and Interfaces*. doi:10.1016/j.surfin.2018.12.009
- Sandoval, A., Hernández-ventura, C., Klimova, T.E., 2017. Titanate nanotubes for removal of methylene blue dye by combined adsorption and photocatalysis 198, 22–30.
- Sarkar, A.K., Pal, A., Ghorai, S., Mandre, N.R., Pal, S., 2014. Efficient removal of malachite green dye using biodegradable graft copolymer derived from amylopectin and poly(acrylic acid). *Carbohydr. Polym.* 111, 108–15. doi:10.1016/j.carbpol.2014.04.042
- Saygılı, H., Güzel, F., Önal, Y., 2015. Conversion of grape industrial processing waste to activated carbon sorbent and its performance in cationic and anionic dyes adsorption. *J. Clean. Prod.* 93, 84–93. doi:10.1016/j.jclepro.2015.01.009
- Scientific, F., 1997. "Silica Gel Dessiccant"[sic].
- Senthil Kumar, P., Ramalingam, S., Senthamarai, C., Niranjanaa, M., Vijayalakshmi, P., Sivanesan, S., 2010. Adsorption of dye from aqueous solution by cashew nut shell: Studies on equilibrium isotherm, kinetics and thermodynamics of interactions. *Desalination* 261, 52–60. doi:10.1016/j.desal.2010.05.032
- Sham, A.Y.W., Notley, S.M., 2018. Adsorption of organic dyes from aqueous solutions using surfactant exfoliated graphene. *J. Environ. Chem. Eng.* 6, 495–504.
- Shao, Z., Huang, X., Yang, F., Zhao, W., Zhou, X., Zhao, C., 2018. Engineering sodium alginate-based cross-linked beads with high removal ability of toxic metal ions and cationic dyes. *Carbohydr. Polym.* 187, 85–93. doi:10.1016/j.carbpol.2018.01.092
- Sharma, A.K., Priya, Kaith, B.S., Sharma, N., Bhatia, J.K., Tanwar, V., Panchal, S., Bajaj, S., 2019. Selective removal of cationic dyes using response surface methodology optimized gum acacia-sodium alginate blended superadsorbent. *Int. J. Biol. Macromol.* 124, 331–345. doi:10.1016/j.ijbiomac.2018.11.213
- Sharma, K., Dalai, A.K., Vyas, R.K., 2017a. Removal of synthetic dyes from multicomponent industrial wastewaters. *Rev. Chem. Eng.* 34, 107–134. doi:DOI 10.1515/revce-2016-0042
- Sharma, K., Vyas, R.K., Dalai, A.K., 2017b. Thermodynamic and Kinetic Studies of Methylene Blue Degradation Using Reactive Adsorption and Its Comparison with Adsorption. *J. Chem. Eng. Data* 62, 3651–3662. doi:10.1021/acs.jced.7b00379
- Shriram, B., Kanmani, S., 2014. Ozonation of Textile Dyeing Wastewater - A Review. *J. Institute Public Heal. Eng.* 2014–15, 46–50.
- Singh, R.K., Kumar, S., Kumar, S., Kumar, A., 2008. Development of parthenium based activated carbon and its utilization for adsorptive removal of p -cresol from aqueous solution. *J. Hazard. Mater.* 155, 523–535. doi:10.1016/j.jhazmat.2007.11.117
- Srivastava, S., Srivastava, A.K., 2006. Biological phosphate removal by model based continuous cultivation of *Acinetobacter calcoaceticus*. *Process Biochem.* 41 41, 624–630. doi:10.1016/j.procbio.2005.08.009
- Stothers, E.N.A.J.B., n.d. *ENCYCLOPÆDIA BRITANNICA* dye [WWW Document]. URL <https://www.britannica.com/technology/dye#ref277817> (accessed 5.31.19).

- Suteu, D., Bilba, D., Doroftei, F., Malutan, T., 2017. Sorption of Brilliant Red HE-3B Reactive Dye from Aqueous Solution onto Seashells Waste: Equilibrium and Kinetic Studies. *Sorption of Brilliant Red HE-3B Reactive Dye from Aqueous Solution onto Seashells Waste: Equilibrium and Kinetic Studies*. *Sep. Sci. Technol.* 6395, 1462–1471. doi:10.1080/01496395.2011.561514
- Talbot, D., Abramson, S., Gri, N., Bée, A., 2018. pH-sensitive magnetic alginate / γ -Fe₂O₃ nanoparticles for adsorption / desorption of a cationic dye from water. *J. Water Process Eng.* 25, 301–308. doi:10.1016/j.jwpe.2018.08.013
- Taşar, Ş., Kaya, F., Özer, A., 2014. Biosorption of lead(II) ions from aqueous solution by peanut shells: Equilibrium, thermodynamic and kinetic studies. *J. Environ. Chem. Eng.* 2, 1018–1026. doi:10.1016/j.jece.2014.03.015
- Temesgen, F., Gabbiye, N., Sahu, O., 2018. Biosorption of reactive red dye (RRD) on activated surface of banana and orange peels: Economical alternative for textile effluent. *Surfaces and Interfaces* 12, 151–159. doi:10.1016/j.surfin.2018.04.007
- Uyar, G., Kaygusuz, H., Erim, F.B., 2016. Methylene blue removal by alginate–clay quasi-cryogel beads. *React. Funct. Polym.* 106, 1–7. doi:10.1016/j.reactfunctpolym.2016.07.001
- Venugopal, V., Mohanty, K., 2011. Biosorptive uptake of Cr (VI) from aqueous solutions by Parthenium hysterophorus weed : Equilibrium , kinetics and thermodynamic studies. *Chem. Eng. J.* 174, 151–158. doi:10.1016/j.cej.2011.08.068
- Villalobos, M.C., Cid, A.A.P. aez, Herrera, A.M., 2016. Removal of textile dyes and metallic ions using polyelectrolytes and macroelectrolytes containing sulfonic acid groups. *J. Environ. Manag. J.* 177, 65–73. doi:10.1016/j.jenvman.2016.04.004
- Villar da Gama, B.M., Elisandra do Nascimento, G., Silva Sales, D.C., Rodríguez-Díaz, J.M., Bezerra de Menezes Barbosa, C.M., Menezes Bezerra Duarte, M.M., 2018. Mono and binary component adsorption of phenol and cadmium using adsorbent derived from peanut shells. *J. Clean. Prod.* 201, 219–228. doi:10.1016/j.jclepro.2018.07.291
- Wang, B., Gao, B., Zimmerman, A.R., Lee, X., 2018. Impregnation of multiwall carbon nanotubes in alginate beads dramatically enhances their adsorptive ability to aqueous methylene blue. *Chem. Eng. Res. Des.* 133, 235–242. doi:10.1016/j.cherd.2018.03.026
- Wang, Q., Ju, J., Tan, Y., Hao, L., Ma, Y., Wu, Y., Zhang, H., Xia, Y., Sui, K., 2019. Controlled synthesis of sodium alginate electrospun nanofiber membranes for multi-occasion adsorption and separation of methylene blue. *Carbohydr. Polym.* 205, 125–134. doi:10.1016/j.carbpol.2018.10.023
- Wang, S., Zhu, Z.H., 2006. Characterisation and environmental application of an Australian natural zeolite for basic dye removal from aqueous solution. *J. Hazard. Mater.* 136, 946–952. doi:10.1016/j.jhazmat.2006.01.038
- Wikipedia activated alumina, n.d. activated alumina [WWW Document].
- Wilson, K., Yang, H., Seo, C.W., Marshall, W.E., 2006. Select metal adsorption by activated carbon made from peanut shells. *Bioresour. Technol.* 97, 2266–2270. doi:10.1016/j.biortech.2005.10.043
- Wu, F.C., Tseng, R.L., Juang, R.S., 2009. Initial behavior of intraparticle diffusion model used in the description of adsorption kinetics. *Chem. Eng. J.* 153, 1–8. doi:10.1016/j.cej.2009.04.042

- Wu, M., Guo, Q., Fu, G., 2013. Preparation and characteristics of medicinal activated carbon powders by CO₂ activation of peanut shells. *Powder Technol.* 247, 188–196. doi:10.1016/j.powtec.2013.07.013
- Wu, M.B., Li, R.C., He, X.J., Zhang, H.B., Sui, W. Bin, Tan, M.H., 2015. Microwave-assisted preparation of peanut shell-based activated carbons and their use in electrochemical capacitors. *Xinxing Tan Cailiao/New Carbon Mater.* 30, 86–91. doi:10.1016/S1872-5805(15)60178-0
- Xu, T., Liu, X., 2008. Peanut Shell Activated Carbon: Characterization, Surface Modification and Adsorption of Pb²⁺ from Aqueous Solution. *Chinese J. Chem. Eng.* 16, 401–406. doi:10.1016/S1004-9541(08)60096-8
- Yang, R.T., 2003. *Adsorbents: Fundamentals and Applications*. John Wiley & Sons, Inc., Hoboken, NJ, USA.
- Year End Review 2018: Ministry of Textiles, n.d.
- Yue, M., Zhang, M., Liu, B., Xu, X., Li, X., Yue, Q., Ma, C., 2013. Characteristics of amine surfactant modified peanut shell and its sorption property for Cr(VI). *Chinese J. Chem. Eng.* 21, 1260–1268. doi:10.1016/S1004-9541(13)60621-7
- Zhang, R., Zhang, J., Zhang, X., Dou, C., Han, R., 2014. Adsorption of Congo red from aqueous solutions using cationic surfactant modified wheat straw in batch mode: Kinetic and equilibrium study. *J. Taiwan Inst. Chem. Eng.* 45, 2578–2583. doi:10.1016/j.jtice.2014.06.009
- Zhang, S., Tao, L., Jiang, M., Gou, G., Zhou, Z., 2015. Single-step synthesis of magnetic activated carbon from peanut shell. *Mater. Lett.* 157, 281–284. doi:10.1016/j.matlet.2015.05.117
- Zhang, S., Tao, L., Zhang, Y., Wang, Z., Gou, G., Jiang, M., Huang, C., Zhou, Z., 2016. The role and mechanism of K₂CO₃ and Fe₃O₄ in the preparation of magnetic peanut shell based activated carbon. *Powder Technol.* 295, 152–160. doi:10.1016/j.powtec.2016.03.034
- Zhang, Y., Li, J., Li, W., 2015. Effect of particle size on removal of sunset yellow from aqueous solution by chitosan modified diatomite in a fixed bed column. *RSC Adv.* 5, 85673–85681. doi:10.1039/c5ra13645h
- Zhao, B., Xiao, W., Shang, Y., Zhu, H., Han, R., 2017. Adsorption of light green anionic dye using cationic surfactant-modified peanut husk in batch mode. *Arab. J. Chem.* 10, S3595–S3602. doi:10.1016/j.arabjc.2014.03.010
- Zhao, X., Morikawa, Y., Qi, F., Zeng, J., Liu, D., 2014. A novel kinetic model for polysaccharide dissolution during atmospheric acetic acid pretreatment of sugarcane bagasse. *Bioresour. Technol.* 151, 128–136. doi:10.1016/j.biortech.2013.10.036
- Zhong, Z.Y., Yang, Q., Li, X.M., Luo, K., Liu, Y., Zeng, G.M., 2012. Preparation of peanut hull-based activated carbon by microwave-induced phosphoric acid activation and its application in Remazol Brilliant Blue R adsorption. *Ind. Crops Prod.* 37, 178–185. doi:10.1016/j.indcrop.2011.12.015
- Zou, X., Zhang, H., Chen, T., Li, H., Meng, C., Xia, Y., Guo, J., 2019. Preparation and characterization of polyacrylamide / sodium alginate microspheres and its adsorption of MB dye. *Colloids Surfaces A Physicochem. Eng. Asp.* 567, 184–192. doi:10.1016/j.colsurfa.2018.12.019